Resonances in Electron Impact on Atoms and Diatomic Molecules

George J. Schulz

Department of Engineering and Applied Science
Yale University
New Haven, Connecticut 06520

Reprinted from
Reviews of Modern Physics
Vol. 45, No. 3, pp. 378-486, July 1973

U.S. DEPARTMENT OF COMMERCE, Frederick B. Dent, *Secretary*
NATIONAL BUREAU OF STANDARDS, Richard W. Roberts, *Director*

Issued October 1973

Library of Congress Catalog Number: 73-600302

NSRDS-NBS 50

Nat. Stand. Ref. Data Ser., Nat. Bur. Stand. (U.S.), 50, 118 pages (Oct. 1973)

CODEN: NSRDAP

For sale by the Superintendent of Documents, U.S. Government Printing Office, Washington, D.C. 20402
(Order by SD Catalog No. C13.48:50). Price $1.35

Foreword

The National Standard Reference Data System provides access to the quantitative data of physical science, critically evaluated and compiled for convenience and readily accessible through a variety of distribution channels. The System was established in 1963 by action of the President's Office of Science and Technology and the Federal Council for Science and Technology, and responsibility to administer it was assigned to the National Bureau of Standards.

NSRDS receives advice and planning assistance from a Review Committee of the National Research Council of the National Academy of Sciences-National Academy of Engineering. A number of Advisory Panels, each concerned with a single technical area, meet regularly to examine major portions of the program, assign relative priorities, and identify specific key problems in need of further attention. For selected specific topics, the Advisory Panels sponsor subpanels which make detailed studies of users' needs, the present state of knowledge, and existing data resources as a basis for recommending one or more data compilation activities. This assembly of advisory services contributes greatly to the guidance of NSRDS activities.

The System now includes a complex of data centers and other activities in academic institutions and other laboratories. Components of the NSRDS produce compilations of critically evaluated data, reviews of the state of quantitative knowledge in specialized areas, and computations of useful functions derived from standard reference data. The centers and projects also establish criteria for evaluation and compilation of data and recommend improvements in experimental techniques. They are normally associated with research in the relevant field.

The technical scope of NSRDS is indicated by the categories of projects active or being planned: nuclear properties, atomic and molecular properties, solid state properties, thermodynamic and transport properties, chemical kinetics, and colloid and surface properties.

Reliable data on the properties of matter and materials is a major foundation of scientific and technical progress. Such important activities as basic scientific research, industrial quality control, development of new materials for building and other technologies, measuring and correcting environmental pollution depend on quality reference data. In NSRDS, the Bureau's responsibility to support American science, industry, and commerce is vitally fulfilled.

RICHARD W. ROBERTS, *Director*

Preface

The publication philosophy of the National Standard Reference Data System recognizes that data compilations will be most useful if all available channels of publishing and disseminating the information are employed. Selection of a specific channel—Government Printing Office, a scientific journal, or a commercial publishing house—is determined by the circumstances for the individual document concerned. The goal is to reach all of the appropriate audience most readily at minimum expense.

The two compilations which follow were first published in *Reviews of Modern Physics*. Since they represent a substantial collection of reference data, it appeared desirable to make them available in a form suitable for distribution to interested users of this type of information. With the generous permission of the editors of *Reviews of Modern Physics*, and the approval of the author, the Office of Standard Reference Data has undertaken to reprint the articles as a part of the National Standard Reference Data System-National Bureau of Standards series.

Contents

Resonances in Electron Impact on Atoms*

George J. Schulz

Department of Engineering and Applied Science, Mason Laboratory, Yale University, New Haven, Connecticut 06520

Electrons colliding with atoms can form, at well-defined energies, compound states consisting of the target atom plus the incident electron. The compound states, which are also called "resonances" or "temporary negative ions," often dominate electron collision processes. In this review we discuss the experimental methods which are useful for studying these resonances, and review the results obtained by various investigators. We list the energies and the widths of resonances for H, He, Ne, Ar, Kr, Xe, Li, Na, Hg, and O. The configurations and other properties of resonances in atoms are discussed. Whenever applicable, results are presented in the form of tables and energy level diagrams.

Key words: Atoms, H, He, Ne, Ar, Kr, Xe, Li, Na, Hg, O; compound states; cross-sections; electron impact; energy levels; resonances; temporary negative ions.

CONTENTS

I. INTRODUCTION

This paper and the paper following deal with a special topic in the field of electron impact on atoms and molecules. The object of interest are "resonances," also called "compound states" or "temporary negative ions." These three terms are synonyms and will be used interchangeably. "Resonances" occur at more or less well-defined energies when electrons scatter from atoms or molecules. The object can be considered as a "compound state," in that the incident electron attaches itself to the target atom (or molecule) for times which are longer than the normal transit time through the atom or molecule. Since the projectile is always a negatively charged electron, the "compound state" has a negative charge. Hence the term "temporary negative ion."

The "resonances" can be viewed as nonstationary (short-lived) states of an atom or molecule. In sharp contrast to stationary states of atoms, "resonances" decay by the emission of electrons, not by photons. Our definition of "resonances" in the present context excludes some types of nonstationary states which also can be viewed as resonances. For example, doubly excited states of atoms (e.g., the $2s^2$ and $2s2p$ states in helium) are nonstationary states which decay by electron emission, yielding positive ions. Nevertheless, such states are excited states of the *neutral* atom, and therefore do not meet our definition, namely that the states be temporary negative ions. This limitation of the review is rather arbitrary.

Resonances were discovered almost simultaneously by experiment and theory about 10 years ago, and great progress has been made in our understanding of these phenomena in the past decade. These two review papers represent an effort to discuss the spectroscopy of resonances in a more or less systematic fashion. The review is divided into two parts: In the present paper, we discuss resonances associated with atoms; in the second paper we discuss resonances associated with diatomic molecules. Resonances associated with more complex molecules also exist, but too little is known about them to justify inclusion in the present work.

In both parts of this review we present a concise discussion of the energy levels, the classification of resonances, and their decay. Comparison with theory is presented whenever such comparison is meaningful, but a full exposition of theory is not attempted. Energy level diagrams for resonances are constructed to aid the overview and the tables of values can be found in the appendixes. The discussion is organized by species.

A. Theory

In atoms, resonances are mostly associated with excited states ("core-excited resonances"). Resonances associated with the ground states of atoms have been established only for the alkalis. One can distinguish between two distinct types of resonances, namely those that lie energetically below the state from which they derive (i.e., below the "parent") and those that lie above. Thus we introduce what may be called the geneology of resonances, a concept actually introduced for a better understanding of resonances in molecules and discussed in more detail in the second paper of this review. A positive ion with a particular configuration of electrons is considered the grandparent. Adding a single electron to this positive ion configuration gives a Rydberg state of the neutral atom or molecule: this is the parent. Adding an extra electron to the parent, we have a particular "resonance."

Resonances which lie below their parent are interchangeably called "closed-channel resonances," "Feshbach resonances," or "Type I resonances" (Taylor *et al.*, 1966, Taylor, 1970). They arise when the interaction potential between the incident particle and the excited state of the target is strong enough to support a bound state. They usually lie approximately 0–0.5 eV below the parent. When the excitation takes place near the center of the resonance, decay into the parent is energetically forbidden, but decay into some other states (nonparents) is allowed. Because decay into nonparents involves a change in configuration of the atoms, Feshbach-type resonances are usually long-lived and their widths are narrow. When such resonances are excited in the high-energy wing, decay into the parent may become energetically possible (Taylor, 1970), and such decay is favored. The end-result of such a decay is often a sharp peak near threshold in the excitation function of the parent state. Such effects are known in both atoms and in molecules.

A special case of a Feshbach-type resonance occurs when the energy level lies near the very top of the potential well. Such a state is called "virtual" and an example is discussed in connection with the 2^1S state of helium in Sec. IIIB5.

Resonances which lie above their parents are called 'shape resonances" or "open-channel resonances," or "Type II" (Taylor *et al.*, 1966). In this case, the potential forms a penetrable barrier which traps the incident particle near the target. The barrier is formed by the angular momentum of the electron. Thus, we expect p-, d-, f-wave resonances but generally not s-wave resonances, since the latter have $l=0$ and thus produce no barrier.

Shape resonances show a preference for decay into their parents and very often dominate the excitation cross section of their parent. Thus shape resonances usually have a shorter lifetime (i.e., larger width) compared to Feshbach resonances. An exception occurs when a shape resonance exists barely above an inelastic threshold (Macek and Burke, 1967). In this case the barrier can be viewed as being very thick (Taylor, 1970) and the resonance becomes long-lived, i.e., the width is narrow; such a case exists in atomic hydrogen.

The presence of resonances is ascertained experimentally by measuring structure in the energy dependence of elastic or inelastic cross sections. Because the structure is often very sharp, monochromatic beams of electrons are needed for such studies and the techniques generally employed are briefly reviewed below. These techniques are also useful for the study of resonances in molecules.

A particular resonance can decay, by the emission of an electron, into many final states. We thus may speak of "channels of decay" for a given resonance. Therefore the existence of a resonance may be detected by measuring the structure in the energy dependence of the cross section of any state which lies energetically below or near the resonance. In fact, sometimes it is possible to detect the existence of a resonance even in a state which lies energetically above the center of resonance. This effect is caused by the "wings" or "tails" of the resonance (Taylor, 1970). Not all decay channels are equally useful for detecting a particular resonance. Often, the branching ratio favors a particular decay and then it is easier to detect structure in the final state which is favored, provided that the nonresonant portion of the cross section is of the same order in the two states. Such phenomena are particularly important in molecules.

The energy dependence of the elastic cross section in the neighborhood of an isolated resonance in the s wave with a single decay channel can be expressed by the Breit–Wigner formula (Blatt and Weisskopf, 1952), $\sigma(E)\sim\pi\lambda\!\!\!^{-2} \mid A+\{\Gamma/[(E-E_0)+(\frac{1}{2}i)\Gamma]\} \mid^2$. Here, A represents direct "potential" scattering which varies only slowly with energy; Γ is the "width" of the state, i.e., the range of energies over which the resonance has a large effect on scattering; E_0 determines the location of the resonance; E is the energy; and $\lambda\!\!\!^{-}$ is the reduced wavelength of the electron. The cross section off resonance becomes $\pi\lambda\!\!\!^{-2} \mid A \mid^2$. When direct scattering is small, the cross section near a resonance becomes $\pi\lambda\!\!\!^{-2}[\Gamma^2/(E-E_0)^2+(\frac{1}{2}\Gamma)^2]$. The maximum cross section then occurs at the resonance energy E_0 and the half-width is Γ. In general, however, interference occurs between direct scattering and resonance scattering so that the shape of the cross section becomes more complicated, leading to destructive and constructive inter-

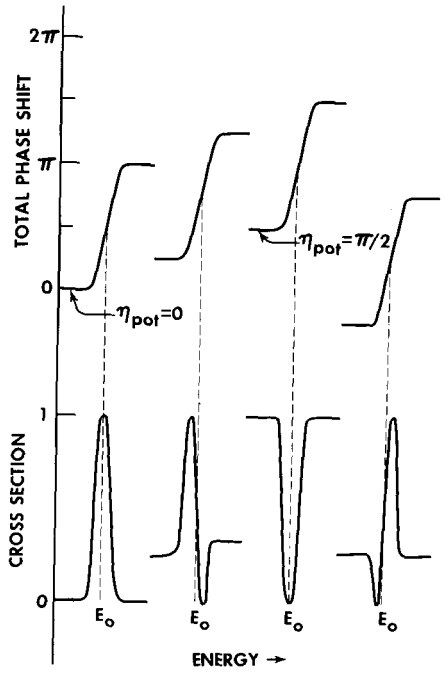

FIG. 1. Partial wave phase shift near a resonance (top portion) and resulting shape of the cross section near a resonance (bottom portion). The figure illustrates the interference between potential and resonance scattering. [After Smith (1966).]

ference. The phase shift η which always enters the expression for the elastic cross section [for s-wave scattering we can write $\sigma(E)=4\pi\lambda^2\sin^2\eta$], increases by π radians as the energy traverses each resonance. This can be seen from the expression for the resonant contribution to the phase shift, $\eta_{res}=-\cot^{-1}[(E-E_0)/\frac{1}{2}\Gamma]$. The smaller the width Γ, the more rapidly occurs the traversal of the phase shift by π radians. In Fig. 1 we plot the phase shift as a function of energy near a resonance for four arbitrary cases. The phase shift for potential scattering is different for each case, but in each case it increases by π radians as the energy traverses the resonant energy E_0. The shape of the resulting cross section, shown on the bottom of Fig. 1, shows the expected interference structure. The position of E_0 is defined to be the energy at which the *resonant portion* of the phase shift has increased by $\frac{1}{2}\pi$; i.e., $\eta_{res}=\frac{1}{2}(2n+1)\pi$. That is the position where the *total phase* shift (consisting of the sum of the phase shifts due to potential and resonant scattering) has increased by $\pi/2$ radians above the phase shift due to potential scattering which prevails just below the resonance.

When we are dealing with inelastic scattering, decay can take place to a state other than the ground state, and the resonant portion of the cross section becomes $\pi\lambda^2[\Gamma_{in}\Gamma_{out}/[(E-E_0)^2+(\frac{1}{2}\Gamma)^2]$. Here Γ_{in} is the width for decay into the ground state plus a free electron and Γ_{out} is the partial width for decay into the excited state plus a free electron. Then we have $\Gamma=\Gamma_{in}+\Gamma_{out}$.

It is often desirable to evaluate line profiles of resonances using the formula due to Fano (1961) and to Fano and Cooper (1965a):

$$\sigma(E)=\sigma_a[(q+\epsilon)^2/(1+\epsilon^2)]+\sigma_b.$$

Here, σ_a and σ_b are the resonant and nonresonant portions of the cross section, $\epsilon=(E-E_0)/\frac{1}{2}\Gamma$, and q is the "line profile index." Simpson *et al.* (1966) describe how one can evaluate the parameter q from experimental measurements. In fact, many authors extract this parameter from their experimentally observed line profiles. Figure 2 shows the line profiles plotted for various values of the parameter q.

If one wishes to analyze the line profile in terms of a symmetric and an asymmetric component, one can write (Shore, 1967)

$$\sigma(E)=C(E)+\tfrac{1}{2}\Gamma B[(E-E_0)^2+(\Gamma/2)^2]^{-1}$$
$$+D(E-E_0)[(E-E_0)^2+(\Gamma/2)^2]^{-1}.$$

The parameters B and D, specifying the symmetric and asymmetric components of the line, are constants. They are related to the Fano formula by the equation $B/D=(q^2-1)/(2q)$. Comer and Read (1972) have developed a simple method for obtaining resonance energies from broadened profiles using the formulation of Shore.

Recent reviews of the theory have been assembled by Smith (1966) and by Burke (1968).

B. Relationship of Theory to Experiment

The search for resonances in atoms by experimental methods consists of a search for structures in various cross sections. In circumstances when this structure is relatively narrow ($\lesssim$300 meV) and far removed from neighboring resonances, little ambiguity exists. In cases when the structure is broad, further verification is needed. Often, the angular distribution of scattered electrons can elucidate the process involved. In molecules, dissociative attachment and vibrational excitation provide extra evidence. This multiplicity of decay channels often makes the identification of resonances easier in molecules than it is in atoms.

There are many theoretical approaches to the calculation of resonances but a thorough review is beyond the scope of this paper. Nicolaides (1972), in reviewing the field recently, lists many of the pertinent theoretical references. One may rather arbitrarily divide the theories into the following classifications:

(a) Theories using the "scattering viewpoint."
(b) Theories treating resonances as a "decaying state."
(c) Theories treating resonances as special types of bound states using projection operators.
(d) Theories treating resonances as special types of bound states without use of projection operators.

The theories which use the scattering viewpoint, as exemplified by the close-coupling method, essentially simulate a scattering experiment and they calculate cross sections for various processes from the phase

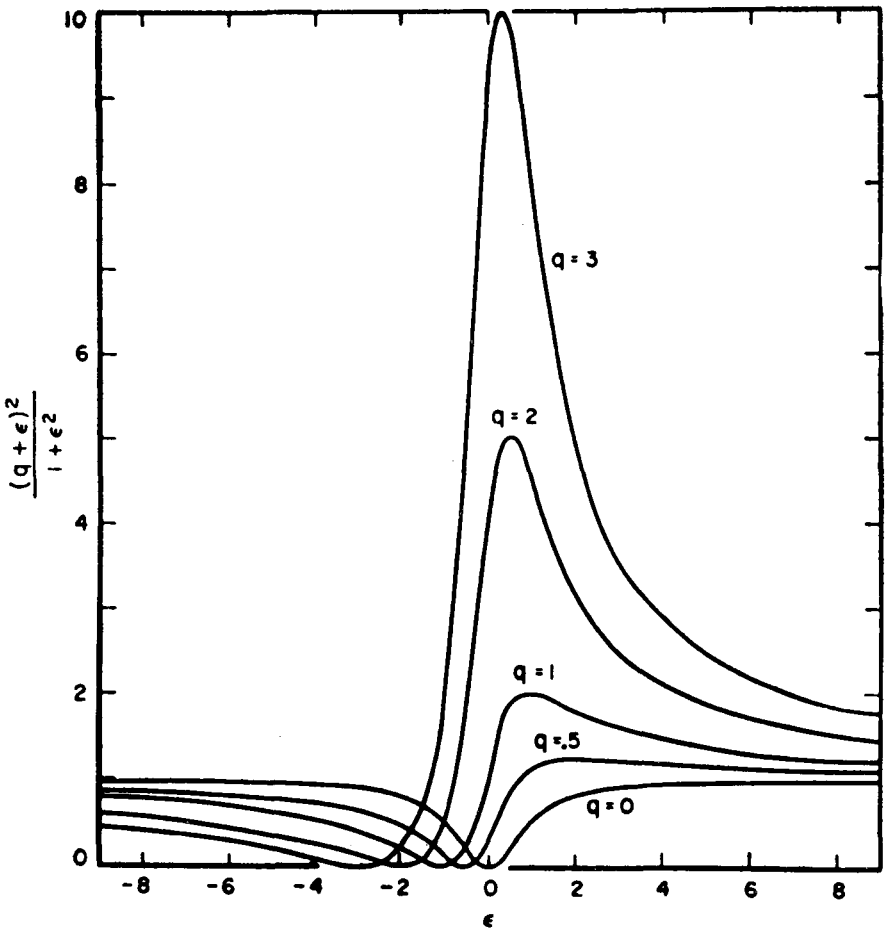

FIG. 2. Natural line shapes for different values of q. Reverse the scale of the abscissa for negative q. [From Fano (1961).]

shifts. When the phase shift rises rapidly by π radians, the resonance is located. The width is determined from the energy range over which the phase shift rises through π radians. This method appears to be very general and gives, in addition to the location and positions of resonances, cross sections for various processes. However, in all but the simplest systems, the computational needs become enormous. Therefore, considerable *a priori* judgement must be exercised as to which states to include to make a particular cross section meaningful. A great deal of relevant insight has been gained by the close-coupling calculations for various atoms and molecules. The frame-transformation theory also belongs in category (a). Here, an expansion is performed in the molecular frame of reference and the region around the molecule is divided into a "core region," and an outer region in which electron correlations are disregarded. This method has had good successes in recent years.

Theories treating resonances as decaying states (which they are) are based on the Kapur–Peierls theory. Here, a stationary value for a complex energy is obtained, which gives both the width and the energy of the resonance. Problems are the need for good wave functions and the need to define a definite radius of interaction. Both shape and Feshbach resonances can be treated in this manner.

Theories treating resonances by the use of projection operator techniques solve directly for the expectation value of the Hamiltonian, with the decay of the state ignored. The decay can be later introduced to give an estimate of the width of the state, but this is usually a difficult step. Only Feshbach-type resonances can be calculated in this manner.

Similar to the latter category are the techniques which search for locally stationary points of the expectation value of the Hamiltonian. A foremost example is the "stabilization method." Here, one takes a trial function which contains all the knowledge one has about the resonance. Both shape and Feshbach resonances can be calculated in this manner, but the width is again a difficult quantity to extricate.

When scattering amplitudes are calculated, structures in the cross section can be caused by poles, zeros, and branch points in the scattering amplitude. Only the poles should be associated with resonances. The zeros in the scattering amplitude for a single partial wave are associated with Ramsauer minima.

For simplicity of interpretation we assume in this

review that every resonance is characterized by a well-defined energy and width. Also, an attempt is made to associate resonances with one or two molecular orbitals of a negative ion state of the atom or molecule. Actually, a superposition of a few molecular orbitals must always be considered in order to describe a resonance properly. When only a single term is given, it is understood that this is the leading, i.e., dominant, term. Despite the fact that these assumptions oversimplify the problem, they seem to be applicable for most resonances discussed in this review. Exceptions are pointed out in the text. Thus, it is sometimes necessary to invoke the energy dependence of the resonance width and in other cases the resonance center cannot be located precisely from experimental information alone. Sometimes it does not appear to be possible to associate a dominant molecular orbital configuration with a particular resonance.

C. Isoelectronic and Isostate Comparisons

It is sometimes desirable to deduce the energy levels of resonances, especially those of the Feshbach type, from known energy levels of other atoms which exhibit some similarities with the resonances. This approach is of course only approximate but often the sequence of resonant states and the physical picture can be deduced from such comparisons.

A simple example is discussed by Herzenberg (1971): The lithium atom in its ground state has the approximate electronic structure $1s^2 2s$, and is known to be able to attach an electron with a binding energy of 0.6 eV to form a stable Li^- ion with the approximate structure $1s^2 2s^2$. The nucleus and the two $1s$ electrons in the ion form a small tightly bound core of charge $+|e|$ which provides an attractive potential to hold the two $2s$ electrons, whose wave functions extend far outside the core. A He^+ ion with its single $1s$ electron also constitutes a small tight core of charge $+|e|$ to which two electrons can be bound in an approximate configuration $2s^2$, as in Li^-. However, the resultant configuration $1s2s^2$ of He^- lies now nearly 20 eV above the configuration $1s^2$, and can therefore autoionize. It is the state $1s2s^2$ which shows up as a Feshbach resonance, with a binding energy of about 0.47 eV with respect to the $(1s2s)^3S$ state of He. This binding energy is somewhat smaller than the binding energy of 0.6 eV of the $1s^2 2s$ state of lithium. Using such an approach, one can apply this kind of numerology to other twinned atomic systems.

Kuyatt, Simpson, and Mielczarek (1965) use a somewhat different method of comparison: They consider the known energy levels of doubly excited states in helium ($2s^2$, $2s2p$, $2p^2$, $3s3p$, etc.). The two excited electrons are moving in a $Z=2$ field, whereas the two electrons in He^- ($1s2s^2$, $1s2s2p$, etc.) are moving in the $Z=1$ field of He^+. Kuyatt *et al.* take the energies of the doubly excited states of helium relative to the energy of He^{++} and divide this energy difference by $Z^2=4$ in order to obtain the corresponding energies of the He^- states relative to He^+. There is a fair resemblance between the He^- states thus obtained and the measured values.

Still another comparative method is used by Swanson, Cooper, and Kuyatt (1973). In order to interpret resonances in krypton, they compare the spectrum of resonances, i.e., Kr^-, with the isoelectronic atom, RbI. It appears that a fair comparison between these two sets of energy levels can be made if an arbitrary scaling constant is used.

D. Experimental Techniques

In this section we review briefly the particular experimental techniques which made possible the discovery and the analysis of resonances. The developments described here span a period of about ten years, but they are based on principles which have been known for a much longer period. Actually we are dealing here with a combination of methods which were brought to bear on the problem of resonances in electron collisions with atoms and molecules. Some of the techniques were borrowed from other fields of physics: ultra-high vacuum technology, low-current measurements, particle counting, and signal averaging. Also, progress was partially facilitated by the commercial availability of many of the necessary components. Parallel with these developments was an improved understanding of electron optics (see, e.g., Heddle, 1970; Read, 1970, 1971; Adams and Read, 1972) and the development of new types of electron monochromators (see, e.g., Kuyatt and Simpson, 1967; Klemperer, 1965; Kuyatt, 1968). Good electron monochromators and electron analyzers are a necessary prerequisite for the experimental studies described in this and the following review, since many of the phenomena of interest occur in a very narrow range of energies and thus the use of electron beams with a narrow energy resolution is a *sine qua non*.

Since all of the techniques have been described in the recent literature, in reviews (see, e.g., Bederson, 1968; Kuyatt, 1968) and in books (Hasted, 1964; McDaniel, 1964; Massey and Burhop, 1969) only a very brief outline of the techniques is given here. For details, the reader is referred to the above reviews.

Many combinations of electric and magnetic fields, using appropriate geometrical arrangements and suitable holes or slits, can give chromatic dispersion of electrons and can thus be used for producing monochromatic electron beams. Equally important is the use of metals with desirable surface properties. One wishes to have a surface with a uniform potential and high conductivity. The surface should not be affected by the gas which is being studied. Although many surfaces have been tried by different groups (e.g., gold, Advance, stainless steel, copper) it appears that molybdenum is a most desirable surface.

A variety of geometries are useful for producing monochromatic electrons: The parallel plate and the

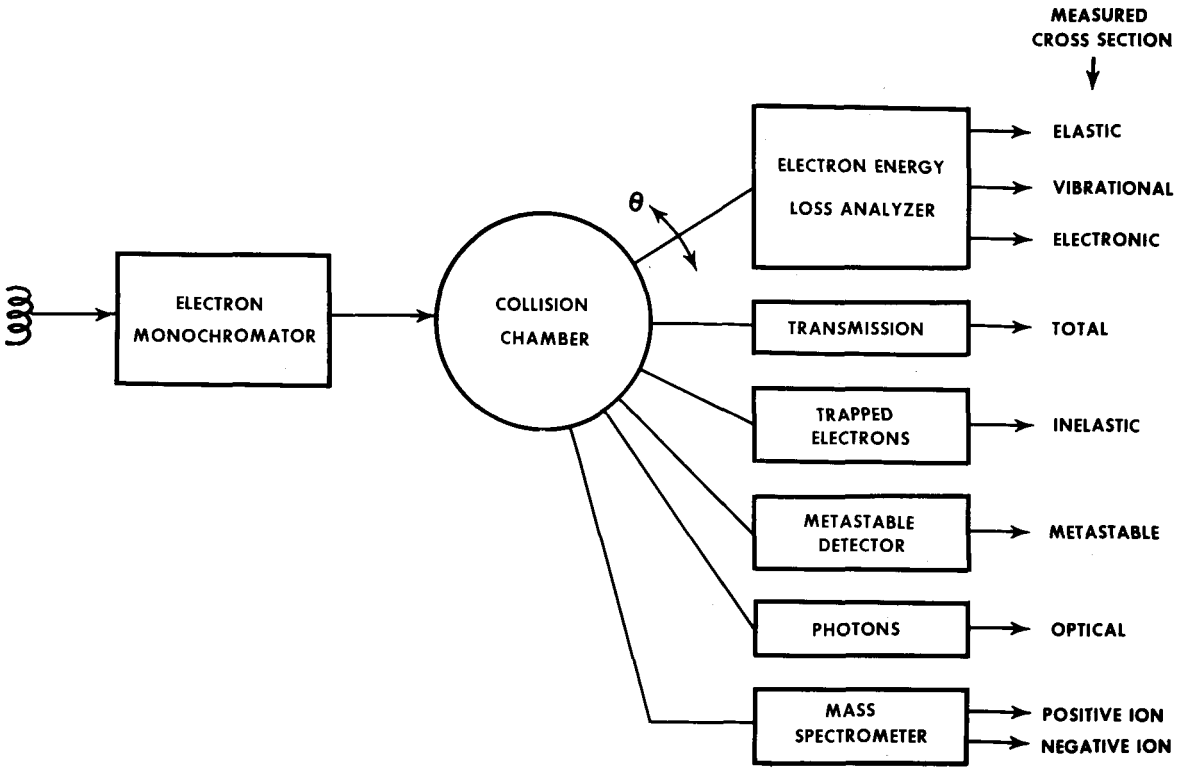

FIG. 3. Schematic overview of experiments which are useful for the study of resonances in atoms and molecules.

coaxial cylindrical "mirror" configurations, the 127° cylindrical electrostatic, and the 180° concentric spherical configurations. For production of very slow (<1 eV) monochromatic electrons, one can use the time-of-flight spectrometer. Monochromatic electrons can also be produced by ionization, using monochromatic photons. Electron monochromators can also be used in series to further improve the energy resolution. It appears that, at the present time, the most widely used monochromators for experiments in which a magnetically field-free region is desired are the 127° cylindrical and 180° concentric electrostatic configurations.

When an axial magnetic field is desired, one can use the retarding-potential difference method. The retarding-potential-difference method relies on the chopping of the electron distribution and thus is not a true monochromator. Although important advances have been made by use of this method, it has been made obsolete by the trochoidal monochromator. Also noteworthy are the 180° magnetic selector and the crossed electric and magnetic selector (Wien filter).

Figure 3 gives an overview of the experiments which are used for the measurement of resonances. The electron monochromator and the collision chamber are common to all experimental arrangements. The detection methods, however, differ widely, and are listed in Fig. 3. Below we discuss the various methods in slightly more detail, without giving credit to the inventors and users of the methods. Such credit would only duplicate the much more detailed credit given in the subsequent chapters (and in the following paper) when the actual accomplishments are discussed.

Differential Cross Section Measurements using Electrostatic Monochromators and Analyzers

A typical arrangement used for the measurement of structure in the differential elastic or inelastic cross section is shown in Fig. 4. This type of apparatus is typical of many instruments used in various laboratories to obtain the results discussed in subsequent sections. It is capable of measuring differential elastic or inelastic cross sections and usually it is possible to alter the angle between the monochromator and the analyzer, so that angular distributions of the scattered electrons can be obtained.

Electrons emitted from the filament are focussed, using electrostatic lenses (1–6) on a hole in plate 7, which serves as the input aperture for the monochromator. The monochromator itself may consist either of coaxial cylinders (127°) or concentric hemispheres (180°). Either of these devices should give an energy distribution with a full width at half-maximum of 0.02–0.06 eV. The electrons are focussed onto a molecular beam by the three-element lens system (10, 11, 12). Electrons scattered from the molecular beam pass through the electron optics of the analyzer, through the analyzer proper, and finally impinge on a multiplier and

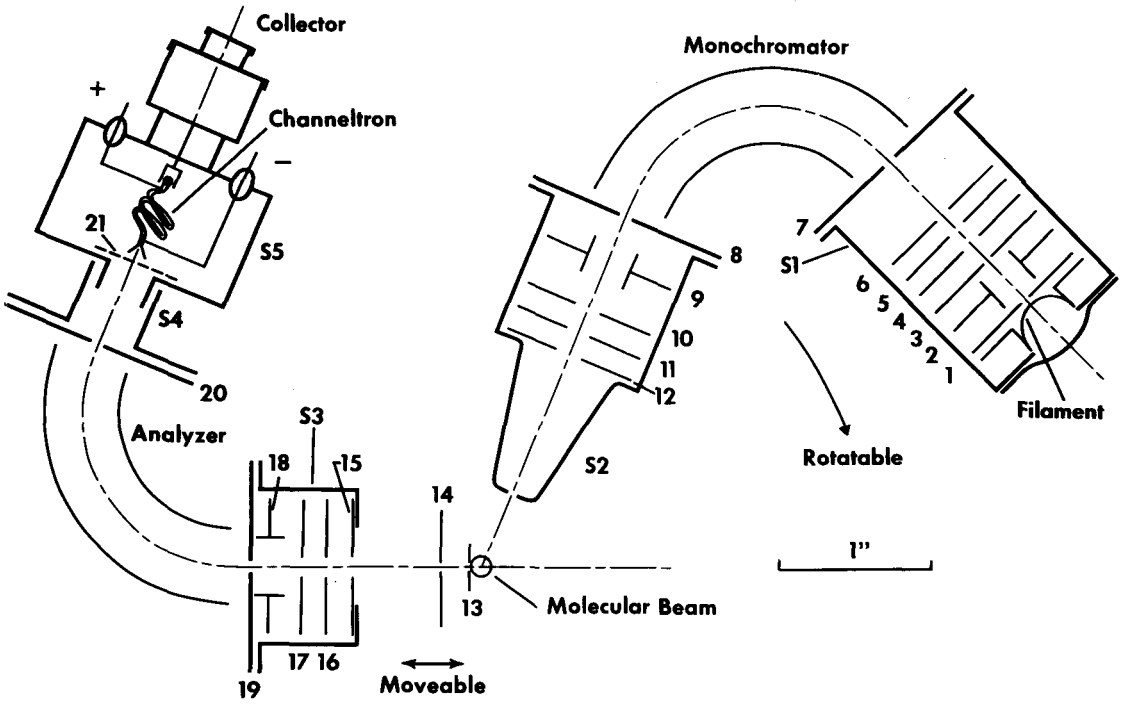

FIG. 4. Schematic diagram of a typical electrostatic monochromator with electrostatic analyzer. Angular distribution can be obtained by rotating the analyzer with respect to the monochromator. Elastic and inelastic differential cross sections can be obtained with such an instrument. [From Pavlovic, Boness, Herzenberg, and Schulz (1972).]

are counted. Use of a well-collimated molecular beam reduces Doppler broadening of the resonances. The electron optics is designed to maintain constant transmission characteristics throughout the spectrometer. Many shields are usually necessary (S_1–S_5) to restrict stray electrons from reaching the multiplier. One usually eliminates magnetic fields from the collision region, either by using a magnetic shield or by using Helmholtz coils.

Double electrostatic analyzers of the type shown in Fig. 4 have given a wealth of information on resonances. Usually, one obtains the energy dependence of the elastic or the specific inelastic cross section at a fixed angle of observation. Structure in such curves is analyzed and the position and the width of resonances can be deduced. Alternatively, one can obtain at a given incident energy the angular distribution of electrons. Such information is valuable for determining the configuration of particular resonances. The inelastic cross sections that have been studied are the vibrational and the electronic cross sections. Rotational cross sections have been studied only in the single case of H_2.

Measurement of Resonances in the Total Cross Section: The Transmission Method

The transmission method can also be used for studying resonances. In the appropriate geometry, the transmitted current I_t through a gas-filled chamber is related to the incident current I_0 by the relation $I_t = I_0 \exp(-NQ_tL)$, where N is the gas density, Q_t is the total cross section, and L is the length of the collision chamber. Small excursions in the cross section Q_t which often indicate the existence of resonances are exhibited by structures in the transmitted current. In fact, when $NQ_tL \gtrsim 1$, then some amplification of the structure takes place; i.e., the percentage change in the transmitted current is larger than the percentage excursion in the cross section. This fact can be utilized for a very sensitive measurement of resonances. A further refinement can be introduced by modulating the energy in the collision chamber and by observing essentially the derivative of the transmitted current.

An example of the arrangement for a transmission experiment is shown in Fig. 5. Here, a trochoidal monochromator is used for creating a monochromatic beam in an axial magnetic field. The electrons then enter the collision chamber region, maintained at a pressure of about 10^{-2} Torr, in which a cylindrical electrode M is mounted. A small modulation voltage (0.005–0.06 V) is applied to electrode M so that the electron energy in the collision chamber is modulated. The modulated transmitted signal is detected on the collector C. The retarding electrodes R are used to cut off all those electrons which have made collisions in the collision chamber, so that only the unscattered electrons are transmitted to the collector C. Only under such circumstances is the exponential relationship between the transmitted and the incident current valid.

Copious examples are given in the text showing the sensitivity of this method of measurement, both for

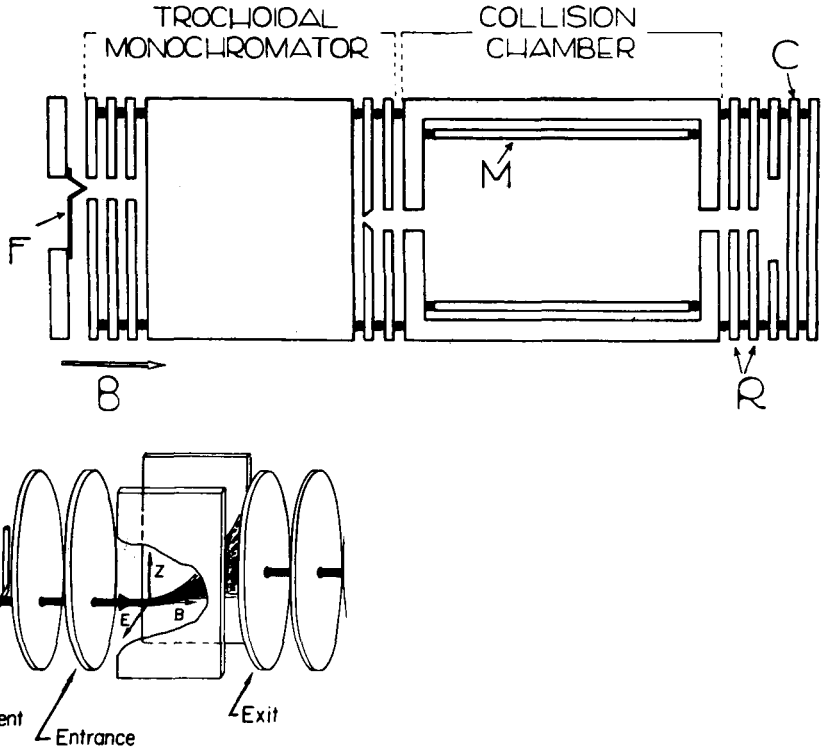

FIG. 5. Schematic diagram of a transmission experiment (top) and the details of the trochoidal monochromator (bottom). [From Sanche and Schulz (1972) and Stamatovic and Schulz (1970).]

atoms and for molecules. The high sensitivity for detecting resonances is thus established. However, since one cannot obtain information on the angular distribution of the electrons, one has great difficulty in establishing the configuration of the resonances. Also, it is difficult in this method to establish the final state to which a resonance has decayed. Thus, if one wishes to obtain more detailed information regarding the configuration and the channels of decay, one has to revert to the less sensitive but much more versatile double electrostatic analyzers.

It should be noted that the transmission method for detecting resonances need not use an axial magnetic field. Instead of a retarding electrode (R), one then can use a simple hole or slit for limiting the exit angle. Either method, with or without a magnetic field, should lead to an exponential dependence of the transmitted current with NQL. Optical focussing effects, i.e., the energy dependence of the transmitted current in the absence of gas, are inherently different in these two systems of measurement, but the optical focussing effects are probably easier to overcome in the presence of an axial magnetic field. And when one wishes to study resonances in a wide energy range, it is essential that optical focussing effects be small.

Total Cross Section Measurements using the Ramsauer Method

The measurement of resonances using the Ramsauer technique is a modern application of possibly the oldest quantitative approach to the measurement of cross sections, originated by Ramsauer and Kollath in the 1920's and 1930's. A review of the early work can be found, e.g., in Massey and Burhop (1969). A modern version of the apparatus is shown in Fig. 6. It is very similar to that used by Ramsauer and Kollath, the major modification being the provision here for differential pumping. Briefly, the electrons from an oxide-coated cathode, or a thoriated iridium filament, are momentum selected by the combination of the three slits, S_1, S_2, S_3, and a uniform magnetic field is applied perpendicular to the plane of the drawing. The electrons are then allowed to interact with the gas to be studied in the scattering cell, and the transmitted electron signal is studied as a function of gas density in the scattering region at a particular value of electron energy. If it is assumed that a current of electrons $I_{c0}+I_{s0}=I_0$ enters the scattering region, the current reaching the collector is given by $I_c(E)=I_{c0}(E)\exp[-\sigma_t(E)Nx]$, where I_{c0} is that part of the current entering the scattering region which would reach the collector in the absence of scattering, $\sigma_t(E)$ is the total cross section, N is the gas density, x is the path length of the electron beam through the scattering chamber, and E is the electron energy. The current reaching the scattering chamber walls is given by $I_s=I_{s0}+I_{c0}[1-\exp(-\sigma_t Nx)]$, where I_{s0} is that part of the current entering the scattering chamber which would reach the scattering chamber walls in the absence of scattering. Then we have $\ln[(I_c+I_s)/I_c]=\ln[(I_{c0}+I_{s0})/I_{c0}]+\sigma_t Nx$. The total cross section is directly determined by measuring the slope of a plot of the left-hand side of this equation vs N,

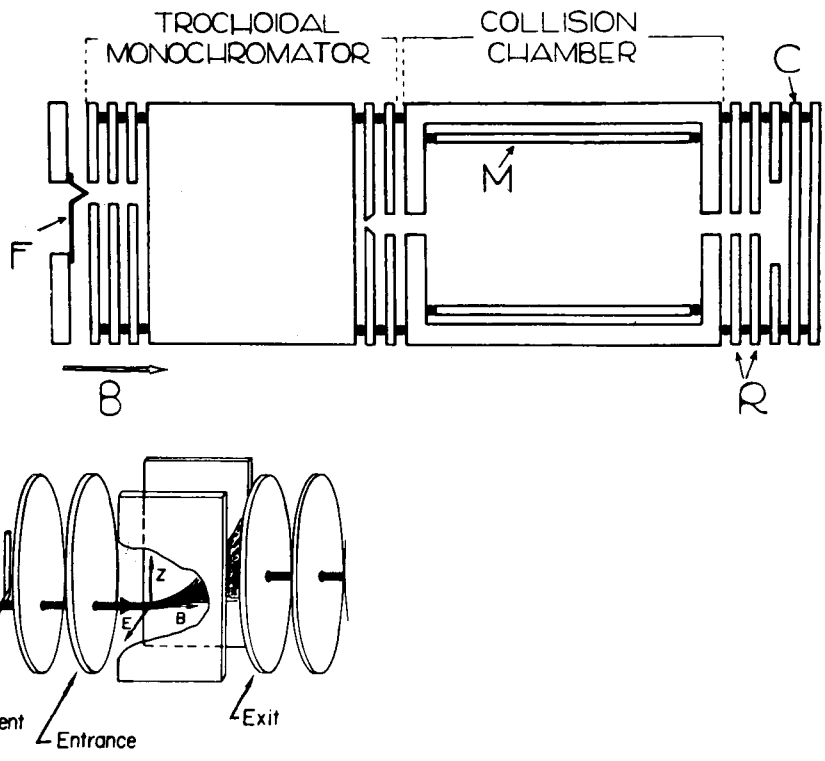

FIG. 5. Schematic diagram of a transmission experiment (top) and the details of the trochoidal monochromator (bottom). [From Sanche and Schulz (1972) and Stamatovic and Schulz (1970).]

atoms and for molecules. The high sensitivity for detecting resonances is thus established. However, since one cannot obtain information on the angular distribution of the electrons, one has great difficulty in establishing the configuration of the resonances. Also, it is difficult in this method to establish the final state to which a resonance has decayed. Thus, if one wishes to obtain more detailed information regarding the configuration and the channels of decay, one has to revert to the less sensitive but much more versatile double electrostatic analyzers.

It should be noted that the transmission method for detecting resonances need not use an axial magnetic field. Instead of a retarding electrode (R), one then can use a simple hole or slit for limiting the exit angle. Either method, with or without a magnetic field, should lead to an exponential dependence of the transmitted current with NQL. Optical focussing effects, i.e., the energy dependence of the transmitted current in the absence of gas, are inherently different in these two systems of measurement, but the optical focussing effects are probably easier to overcome in the presence of an axial magnetic field. And when one wishes to study resonances in a wide energy range, it is essential that optical focussing effects be small.

Total Cross Section Measurements using the Ramsauer Method

The measurement of resonances using the Ramsauer technique is a modern application of possibly the oldest quantitative approach to the measurement of cross sections, originated by Ramsauer and Kollath in the 1920's and 1930's. A review of the early work can be found, e.g., in Massey and Burhop (1969). A modern version of the apparatus is shown in Fig. 6. It is very similar to that used by Ramsauer and Kollath, the major modification being the provision here for differential pumping. Briefly, the electrons from an oxide-coated cathode, or a thoriated iridium filament, are momentum selected by the combination of the three slits, S_1, S_2, S_3, and a uniform magnetic field is applied perpendicular to the plane of the drawing. The electrons are then allowed to interact with the gas to be studied in the scattering cell, and the transmitted electron signal is studied as a function of gas density in the scattering region at a particular value of electron energy. If it is assumed that a current of electrons $I_{c0}+I_{s0}=I_0$ enters the scattering region, the current reaching the collector is given by $I_c(E)=I_{c0}(E)\exp[-\sigma_t(E)Nx]$, where I_{c0} is that part of the current entering the scattering region which would reach the collector in the absence of scattering, $\sigma_t(E)$ is the total cross section, N is the gas density, x is the path length of the electron beam through the scattering chamber, and E is the electron energy. The current reaching the scattering chamber walls is given by $I_s=I_{s0}+I_{c0}[1-\exp(-\sigma_t Nx)]$, where I_{s0} is that part of the current entering the scattering chamber which would reach the scattering chamber walls in the absence of scattering. Then we have $\ln[(I_c+I_s)/I_c]=\ln[(I_{c0}+I_{s0})/I_{c0}]+\sigma_t Nx$. The total cross section is directly determined by measuring the slope of a plot of the left-hand side of this equation vs N,

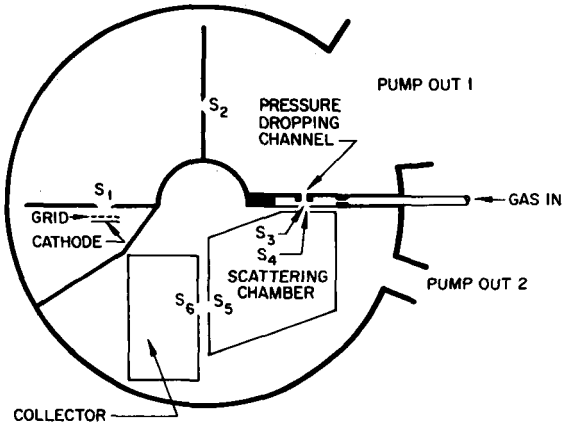

FIG. 6. Schematic arrangement of a modified Ramsauer apparatus for the measurement of total scattering cross section. [From Golden and Bandel (1965).]

at a constant energy. In this kind of selector, two parameters define the electron energy. One is the magnetic field strength and the other is the accelerating voltage. This coupling of the energy to two experimental parameters leads to the fact that the electron energy is usually not continuously variable. Since the energy spread is a function of the electron energy, the study of resonance effects is quite tedious, but resonances have been measured using this method. The advantage of this method lies in the fact that it yields the absolute magnitude of the total cross section at and near the resonance.

Inelastic Cross Section Measurements using the Trapped-Electron Method

The trapped-electron method has been used for the past 15 years for the measurement of inelastic cross sections, particularly near the threshold of excitation. Basically, the method consists of establishing an electrostatic potential well in which low-energy electrons, resulting from inelastic collisions, are trapped and subsequently collected with a very high efficiency.

Figure 7 shows a schematic diagram of the tube and the variation of potential along the axis. An electron beam collimated by a magnetic field is accelerated into the collision chamber with voltage V_A. The collision chamber consists of two end plates and a grid. A cylindrical (or parallel plane) outer collector surrounds the collision chamber. By applying a positive voltage to this collector, with respect to the collision chamber, an electrostatic well, having a depth W (in volts), can be produced along the axis of the tube.

An electron making an inelastic collision just above the threshold for an inelastic process loses most of its energy and is trapped in the well. It spirals back and forth following the magnetic field lines and eventually makes enough elastic collisions to diffuse across the magnetic field to the trapped-electron collector. At an electron energy that exceeds the threshold of an inelastic process by the amount W, the electrons have enough energy remaining to escape over the potential barrier at the end of the collision chamber, and the trapped-electron current vanishes. Therefore, as a function of accelerating voltage, the trapped-electron current is zero below an inelastic threshold, and then grows to a peak which is proportional to the magnitude of the cross section at an electron energy that exceeds the threshold by W.

The well depth can be determined by applying a negative voltage to the trapped-electron collector relative to the collision chamber, thus creating a potential barrier in the path of the electron beam.

The shift in the electron-beam retarding curve for different values of the applied voltage measures the size of the barrier, which is the well depth with reversed polarity. Other methods for establishing the well depth also exist.

Using the trapped-electron method, sometimes in conjunction with a modulation of the well depth, it is possible to measure an excitation function for several eV above the onset.

A method very similar in concept to the trapped-electron method is the "SF_6 scavenger technique." This technique takes advantage of the fact that SF_6 has a very large attachment cross section for zero-energy electrons, and a very small cross section for all other energies. Thus one admixes a small amount of SF_6 to the gas under study and whenever an inelastic collision takes place, it leads, near threshold, to zero-energy electrons which promptly attach to SF_6. By

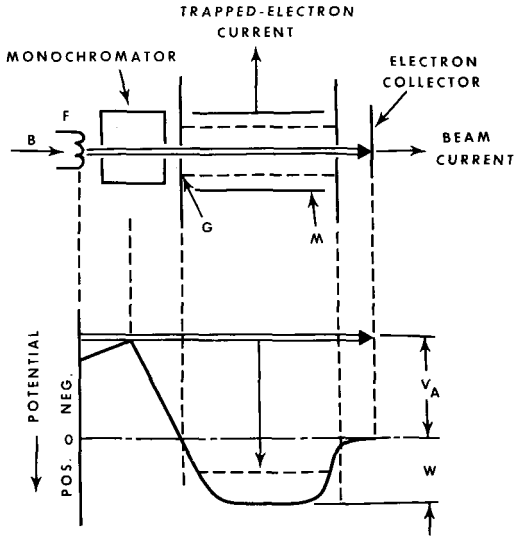

FIG. 7. Schematic diagram of a trapped-electron experiment and potential distribution at the axis of the tube. F is the filament, P_2 is the retarding electrode, G is the cylindrical grid forming the collision chamber, M is the cylinder for collection of trapped electrons, E is the electron beam collector, V_A is the accelerating voltage, and W is the depth of the well. The double line in (b) indicates the energy of the electron beam and the arrow indicates the energy lost by an electron in an inelastic collision. The electron energy in the collision chamber is (V_A+W). [From Schulz (1959).]

observing the SF_6^- current using a mass spectrometer, one can obtain information regarding the threshold behavior of inelastic cross sections. Often, the threshold region of inelastic cross sections shows resonance structures.

Measurement of Cross Sections for Metastable States using Surface Ejection

Measurements of the cross section for production of metastable states can be accomplished with high efficiency if the metastable state to be measured has an internal energy higher than about 10 eV. In this case, one can use for signal detection the ejection of electrons resulting from metastables impinging on a metal surface. Any kind of electron monochromator, magnetic or electrostatic, can be used for producing the monochromatic electron beam. Figure 8 shows a sketch of such an apparatus. If a single metastable state is involved, the current measured on the metastable detector i_M is given by $i_M = i_0 NQL\gamma\alpha$, where N is the gas density, i_0 is the current incident on the collision chamber, L is the path length, γ is the number of electrons ejected per metastable incident, α is the solid angle subtended by the metastable detector, and Q is the cross section for the particular metastable state. Since atoms may have more than one metastable state (e.g., 2^3S and 2^1S states for He), and since each metastable state leads to a different γ, the total curve is not easy to interpret. However, structure in the total metastable cross section is often very pronounced. Examples of such curves are shown in the text.

Measurement of Optical Excitation Cross Sections

Since resonances can be detected in any decay channel it is obvious that the excitation cross sections to any of the radiating states of atoms should also exhibit structure resulting from resonances. Any kind of monochromator which gives a sufficiently narrow electron energy distribution in conjunction with a sufficiently high electron current is acceptable for such experiments. This type of measurement is particularly suitable for detecting resonances at higher energies, e.g., a few eV below the ionization potential.

Measurements of the optical excitation functions using narrow electron energy distributions are just now receiving attention and a complete analysis of the observed structures is not yet available. Thus this review cannot do justice to this interesting experimental field, but one can anticipate interesting results in the near future.

Measurement of Positive Ions

Resonances can lie above the ionization potential of the atom. Such resonances can be studied by the methods previously outlined. However, it is now known that such resonances can decay by two-electron emission, yielding a positive ion. It was actually the use of

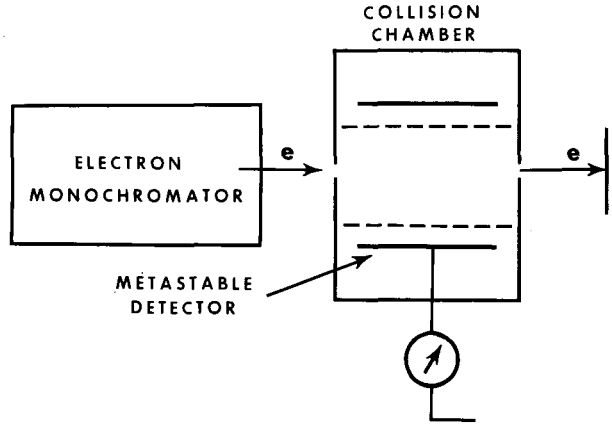

FIG. 8. Schematic diagram of an apparatus for study of metastable excitation by surface ejection of electrons.

the trapped-electron method which established this type of decay (see Sec. IIIC). If one examines the positive ion cross section very carefully, one can observe the resonances lying above the ionization threshold. As described in Sec. IIIC, such measurement must use sophisticated signal accumulation techniques, since the structure in the positive ion cross section is superimposed on a large monotonically varying background resulting from "direct" ionization. This background signal can be subtracted by use of electronic methods.

When measuring structure in positive ion cross sections, one must be careful to distinguish between "resonances", i.e., temporary negative ions and states of the neutral atom which lie above the ionization potential ("autoionizing states"). Both of these types of states can cause structure in the positive ion cross section.

Electron-Energy Distributions in Fast Neutral–Neutral Collisions

It has been pointed out by Barker and Berry (1966) that the electron energy distribution of the electrons resulting from collisions of fast neutral atoms could be used for detecting "resonances." The reaction leading to the detection of resonances is of the type

$$\mathrm{He}(1s^2)+\mathrm{He}(1s^2)\rightarrow\mathrm{He}^-(1s2s^2)+\mathrm{He}^+(1s)$$
$$\rightarrow\mathrm{He}(1s^2)+\mathrm{He}^+(1s)+e.$$

The electrons in the above reaction result from the decay of the $1s2s^2$ resonance and cause interference with electrons produced directly. Thus, structure in the electron energy distribution can be observed.

Actually, pronounced peaks consistent with the above reaction have been observed by Barker and Berry (1966) and by Schowengerdt, Smart, and Rudd (1973), in the energy range up to 150 keV.

However, no new information regarding the location or width of resonances has been generated with this method up to the present time, and thus no further use

can yet be made of this phenomenon. Nevertheless, the reaction itself appears to be of interest to the understanding of electron exchange in neutral–neutral collisions.

Electron-Energy Distribution in Fast Ion–Neutral Collisions

Fast ion–neutral collisions also lead to electron ejection which can be associated with resonances. When a stable negative ion collides with a neutral atom, the outer electron in the negative ion can be promoted to a resonance state. A peak in the energy distribution of ejected electrons occurs at the energy of the resonance. The results of such an experiment, involving O^- ions, are discussed in Sec. VII.

It is conceivable that the impact of fast positive ions on neutral atoms also could yield electrons associated with resonances. This process would involve electron-exchange, similar to that in neutral–neutral collisions.

Calibration of Energy Scales

Any discussion of new methods of measurement in the field of electron impact on atoms and molecules must point out the really significant progress which has been made in the past ten years or so in our ability to calibrate the electron energy scale accurately. Usually, the "primary" standard is a known ionization potential or an excitation potential. Important resonances are calibrated against such a standard. The resonances, in turn, can be used as "secondary" standards if they have a natural width which is narrow compared to the electron energy spread. Such a calibration can be performed to an accuracy of ± 0.03 or ± 0.05 eV, although in some cases even lower values are quoted.

II. HYDROGEN

From the theoretical viewpoint atomic hydrogen is obviously the simplest system for the calculation of resonances, but measurements in atomic hydrogen are difficult. The combination of establishing a monochromatic electron beam and a source of atomic hydrogen in an experiment proved to be elusive for many years. Thus, it is not surprising that the first indication of resonances in the scattering of electrons by atomic hydrogen came from theoretical work (Burke and Schey, 1962) and the lowest state was identified as ^1S, lying about 0.6 eV below the $n=2$ state of hydrogen. Since that discovery many determinations using a variety of theoretical methods have been made of the resonant energies.

The position of resonant energies can be evaluated by variational methods as eigenvalues of the Hamiltonian with the open channel projected out. The results thus obtained are approximations to the actual physical resonances in that the shift resulting from the coupling to the neighboring continuum is not included, and the finite width of the state is not considered. It turns out, however, that the actual shifts are small so that the variational calculations give a close indication of the position of the compound-state energy levels. This can be ascertained from Appendix I, where the results of the variational calculations are indicated by the appropriate symbol.

The position of resonant energies can also be determined by calculating the elastic or inelastic cross section for scattering of electrons with a very fine mesh of incident energies. In such a calculation, the existence of the resonance is exhibited by rapid transit of the phase shift through π radians in the vicinity of the compound state. From the variation of the phase shift, one can determine the position and width of the resonance and thus obtain a more complete description of the resonant behavior. The rapid transit of the phase shift through π radians is reflected in the behavior of the cross section by the appearance of sharp structure. To calculate the cross section, one must include several states of the target atom. For low-lying levels in hydrogen, it has been shown that it is sufficient to include the three lowest states of the atom in the close-coupling calculation (cc). As a next step, one can do close-coupling calculations with correlations included (ccc). For some calculations it has been found desirable to include six states of the target atom in the calculations (6-state).

Appendix I lists the results of various calculations for the energy and the width of resonances below the $n=2$ threshold. An energy level diagram is shown in Fig. 9. Here, only a single set of energy levels is shown, extending up to the $n=3$ threshold. Of the values listed in Appendix I, it is expected that the most accurate ones are those using an expansion of the wave function in terms of the $1s$, $2s$, $2p$ states of the target, together with up to 20 correlation terms. The results thus obtained are marked (ccc) in Appendix I, following the notation of Burke (1968). The values marked (cc) in Appendix I are obtained by Burke using the $1S$, $2S$, $2P$ states of the target atom in a close coupling expansion. The agreement between the values obtained (cc and ccc) gives confidence that the three-state close-coupling results are reliable. In fact, the good agreement between Burke's values and the values obtained by other investigators is remarkable.

Alternately, one can use the pseudo-state method (ps. st.) developed by Burke, Gallaher, and Geltman (1969) in which the first few states included are atomic eigenstates while higher bound and continuum states are represented by pseudo-states chosen to be orthogonal. The results of these calculations are marked (ps. st.) in Appendix I.

The theoretical values shown in Fig. 9 are those obtained by Burke using the close coupling plus correlation method (ccc). Above the lowest two levels, ^1S and ^3P, and below the $n=2$ threshold of H, there are shown a number of states which converge to the $n=2$ limit. It has been pointed out by Gailitis and Damburg (1963) that the degenerate dipole coupling between the $2S$ and

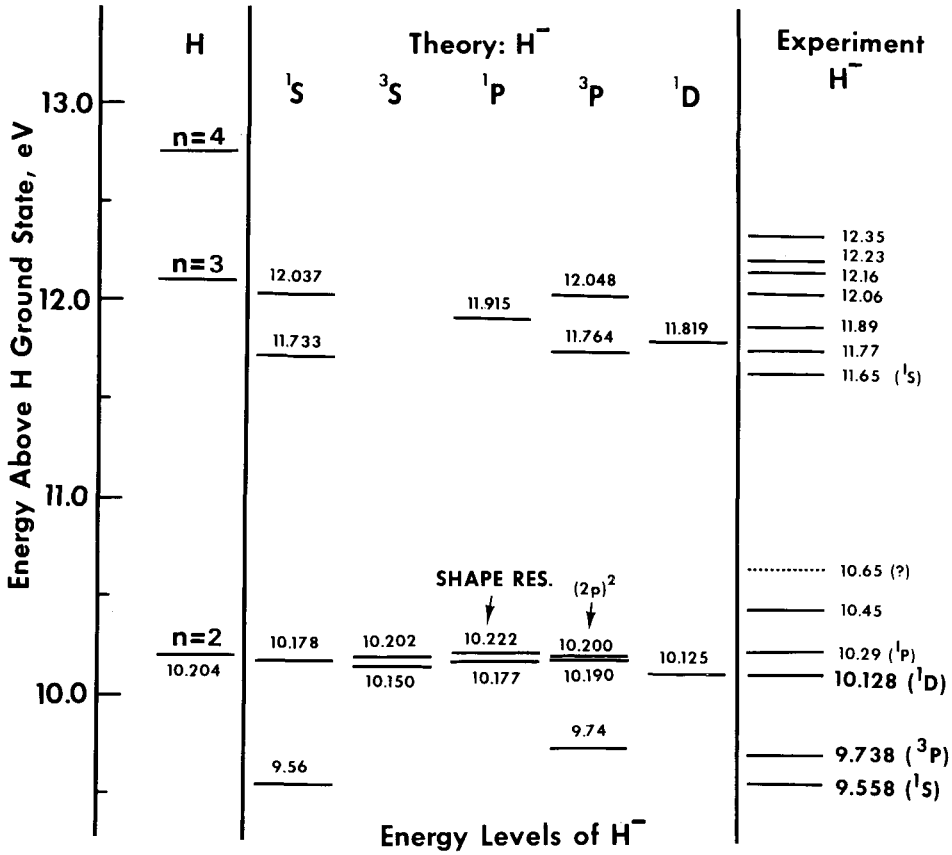

FIG. 9. Energy level diagram for compound states in atomic hydrogen, constructed from the results of theory and experiment. The theoretical values are taken from Burke (1968). Values below the $n=2$ level are also listed in Appendix I (marked ccc) in comparison with other results. The experimental values listed in the figure are those of Sanche and Burrow (1972) for the lowest three resonances and of McGowan *et al.* (1965, 1969) for the remainder.

$2P$ states of hydrogen produces, at large distances, an r^{-2} potential. This potential is sufficiently attractive to support an infinite number of bound states (S, P, D) in the absence of coupling to the ground state of hydrogen.

The state marked $(2p)^2$ in Fig. 9 is a ^3P state, but with even parity whereas all the other states in the ^3P column are of odd parity. If LS coupling is a good approximation, the $(2p)^2$ state does not participate in elastic scattering, nor does it decay to the ground state. The value quoted for the $(2p)^2$ state has been calculated by Drake (1970) by Holøien (1960).

Just above the $n=2$ state of hydrogen, Taylor and Burke (1967) find a core-excited shape resonance ^1P. Using a three-state plus twenty correlation term approximation, the energy is found to be 10.22204 eV and the width $\Gamma=0.0151$ eV. This width is unusually narrow for a shape resonance. As is common for shape resonances, the mechanism for the ^1P resonance is provided by the angular momentum barrier, together with the short-range nuclear attraction. Because the resonance lies so close to the $n=2$ state, the barrier is very thick, and the penetrability very low. As pointed out in Sec. I, such circumstances lead to a narrow width. The existence of such a resonance close to the threshold of an inelastic process dominates the behavior of the inelastic cross section near threshold.

The tabulated data of Taylor and Burke (1967) show that the ^1P resonance exhibits itself by a peak in the elastic cross section near 10.222 eV. This peak, being only 1.3% of the elastic cross section would be difficult to observe experimentally. Nevertheless, this peak in the elastic cross section provides an example of the decay of a core-excited shape resonance into the elastic decay channel.

The six higher states of H^- (near $n=3$) shown in Fig. 9 are the result of a close-coupling calculation involving the $1s$, $2s$, $2p$, $3s$, $3p$, and $3d$ states (Burke *et al.*, 1966, 1967). The energies and the widths for these states have been obtained by Macek and Burke (1967) and are also discussed by Burke (1968).

A. Resonances in the Elastic Cross Section

As previously mentioned, experiments with monochromatic electrons in atomic hydrogen are among the most difficult. The first confirmation of the theoretical considerations was the experiment of Schulz (1964a) who found a peak in the unscattered electron current transmitted through atomic hydrogen at an electron energy of 9.70 ± 0.15 eV. For various technical reasons, the electron energy distribution in this early experiment was insufficient to resolve the ^1S and the ^3P resonances. Very recently, Sanche and Burrow (1972) succeeded in resolving these states in a transmission experiment which uses many improvements developed

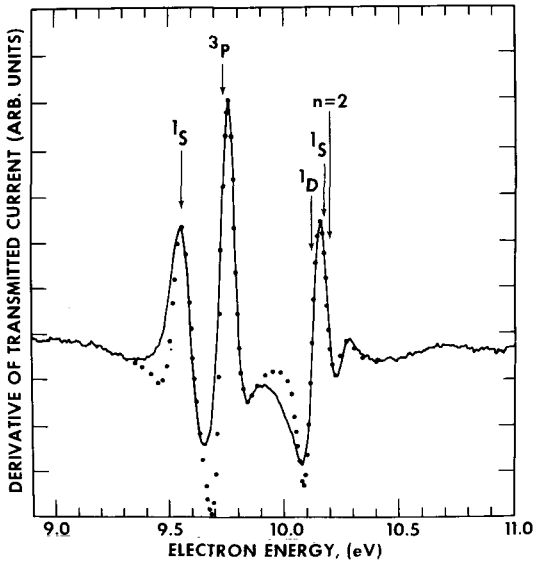

FIG. 10. Derivative of the transmitted current vs electron energy in atomic hydrogen. The experimental results are shown by the solid line. The points are the best fit that can be obtained from the theoretical shape of the cross section, but leaving the energies and the widths of the resonances as parameters. The computer program which is used for obtaining these points includes Doppler broadening and approximates the electron energy distribution by a Gaussian function with a half-width of 70 meV. The energies and widths which give the best fit to the experiment are listed in Appendix I. The arrows point to the energies of the major resonances obtained using close coupling plus correlation. [From Sanche and Burrow (1972).]

over the past few years: A trochoidal monochromator is used and the electron energy in the collision chamber modulated in a manner similar to that introduced by Sanche and Schulz (1972). A plot of the derivative of the transmitted current (which is the primary measurement in this type of experiment) vs electron energy is shown by the solid line in Fig. 10. The energies of several compound states (taken from the theoretical calculations cited in Fig. 9) are also shown in Fig. 10. The points in Fig. 10 are calculated from theory in the following manner: Sanche and Burrow (1972) take the theoretical values of the nonresonant phase shifts which are believed to be "exact" and use the energies and widths of the resonances in single-level Breit–Wigner formulas as parameters. They fold these results with a Gaussian electron energy distribution of appropriate width (70 meV), and include Doppler broadening. Then they calculate the derivative of the transmitted current. The values for energies and widths of the resonances which give the best agreement with experiment are listed in Appendix I and the derivative of the transmitted current vs electron energy which is obtained when these optimum values are used is shown by the points in Fig. 10. This experiment therefore shows that the theory using close-coupling plus correlation (ccc) is in agreement with experiment.

Kleinpoppen and Raible (1965) performed a crossed-beam experiment and found a decrease in the cross section (which corresponds to an increase in transmitted current) at an electron energy of 9.73±0.12 eV, as shown in Fig. 11. In addition, less pronounced structure around 10.1 eV was observed by Kleinpoppen and Raible, but was not discussed in their paper, probably because the authors did not consider it a sufficiently reliable observation. However, it is clear from Fig. 10 that such structure around 10.1 eV is expected to be visible.

The third experiment bearing on the subject of experimental observation of resonances below the $n=2$ threshold of hydrogen was performed by McGowan, Clarke, and Curley (1965) and their results are shown in Fig. 12. At first sight, this experiment shows little resemblance to the results of Kleinpoppen and Raible. However, McGowan (1966, 1967) points out that there is a strong variation of the differential cross section with angle: The interference between the potential and the resonant scattering causes the structure of the differential elastic cross section to depend strongly on the angle of observation. In order to demonstrate this effect, McGowan (1966) calculated the differential elastic scattering cross section in the region of the resonances, at selected angles of observation. Figure 13 shows the results of these calculations in comparison with some experiments. The experimental results of Kleinpoppen and Raible (taken at 94°) resemble the shape of the theoretical curve for $\theta=100°$. The experimental data of McGowan, Clarke, and Curley resemble the theoretical curve at 90°, as shown on the bottom left-hand portion of Fig. 13. A more detailed comparison is shown in Fig. 14. Here, the width of the ^1S resonance is left as a parameter. The best fit to experiment is obtained when the width of the ^1S resonance is taken to be 0.043±0.006 eV, in good agreement with the value of 0.0475 eV given by Burke.

The sharp hump observed just below the $n=2$ level of hydrogen in Fig. 12 can be ascribed to the effect of the ^1D state (Ormonde, McEwen, and McGowan, 1969). Figure 15 shows a detailed comparison between theory and experiment in the region 9.9–10.2 eV,

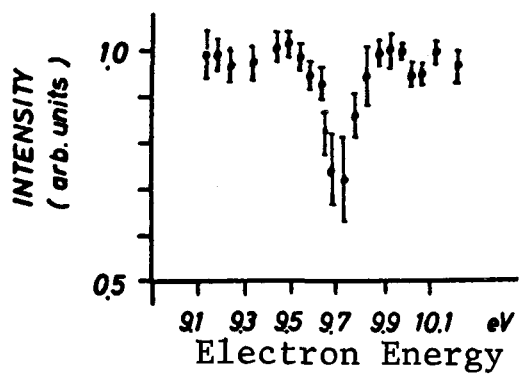

FIG. 11. Elastic cross section for electrons on atomic hydrogen. The angle of observation was 94°, and the width of the energy distribution about 0.1 eV. [From Kleinpoppen and Raible (1965).]

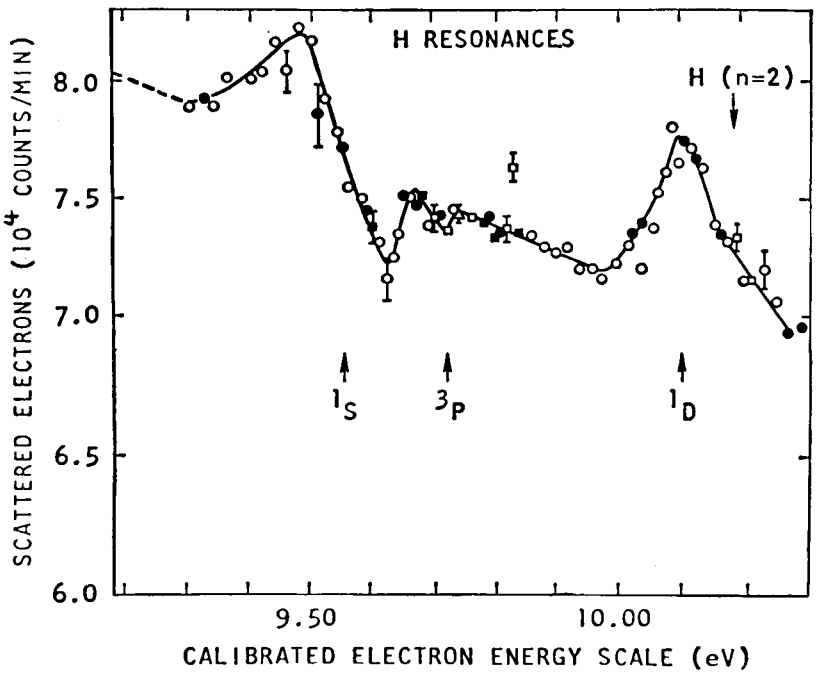

FIG. 12. Differential scattering cross section in hydrogen. The angle of observation is 90° with respect to the bombarding electrons. The position of the three lowest resonances, ^1S, ^3P, and ^1D, are shown. [From McGowan, Clarke, and Curley (1965) and McGowan (1970).]

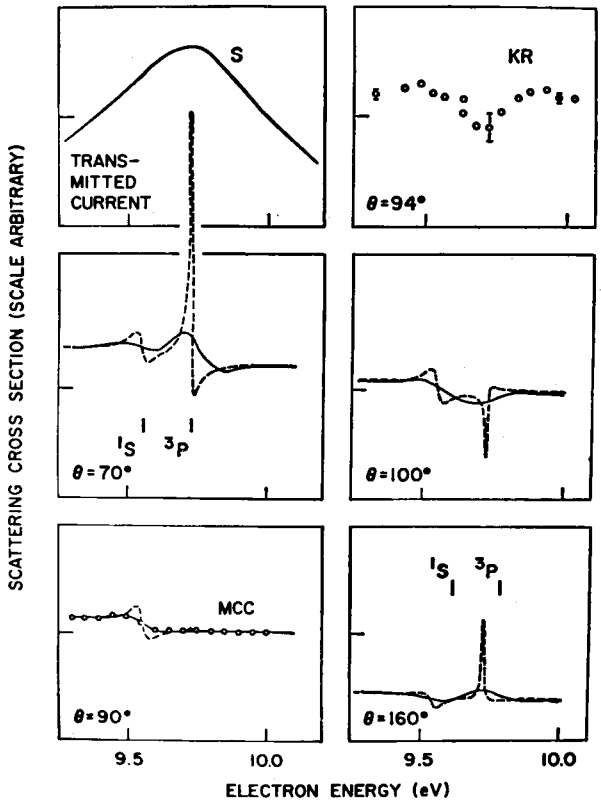

FIG. 13. The experimental results of Schulz (S), Kleinpoppen and Raible (KR), and McGowan, Clarke, and Curley (MCC) compared with the differential scattering calculations of McGowan (1966, 1967) for different scattering angles θ. The dashed line corresponds to the calculated cross section for an angular window of 15°. The position of the ^1S resonance is taken to be 9.56 eV and its width 0.04 eV. The ^3P resonance is taken to be at 9.73 eV with a width of 0.01 eV. The solid line represents the same calculation with the experimental value of the electron energy distribution (0.06 eV) folded in. [From McGowan (1966).]

when the ^1D state alone is considered. The agreement in Fig. 15 must be, presumably, considered fortuitous because a valid comparison between theory and experiment must also include the S, P, and ^3D contributions. For a comparison at 90°, such as is the case for McGowan's experiment, the P-wave contribution to the cross section should be zero. Figure 16 shows the valid comparison between theory and experiment. The ^1D compound state of H^- seems to be the dominant contribution near 10.1 eV.

It is clear from the work of McGowan that experiments on the angular distribution of electrons in the neighborhood of the ^1S and ^3P resonances in hydrogen are strongly dependent on the angle of observation and on the acceptance angle of the apparatus. Further work with much better angular resolution will be necessary before a really satisfactory check of the very elaborate theory can be made.

B. Resonances in the Inelastic Cross Sections

Resonances lying above the $n=2$ state of hydrogen seem to be most pronounced in the inelastic cross section. Figure 17 shows the cross section in the $2p$ excitation from threshold to about 3 eV above threshold. Structure in the cross section is evident and the location of this structure is transposed onto the energy level diagram, Fig. 9. Also shown in Fig. 17 are the theoretical curves. The sharp onset of the $2p$ excitation cross section results from the proximity of the ^1P shape resonance, which is almost coincident with the $n=2$ level. This sharp peak near threshold seems to be consistent with the earlier experimental results of Chamberlain, Smith, and Heddle (1964) which were obtained

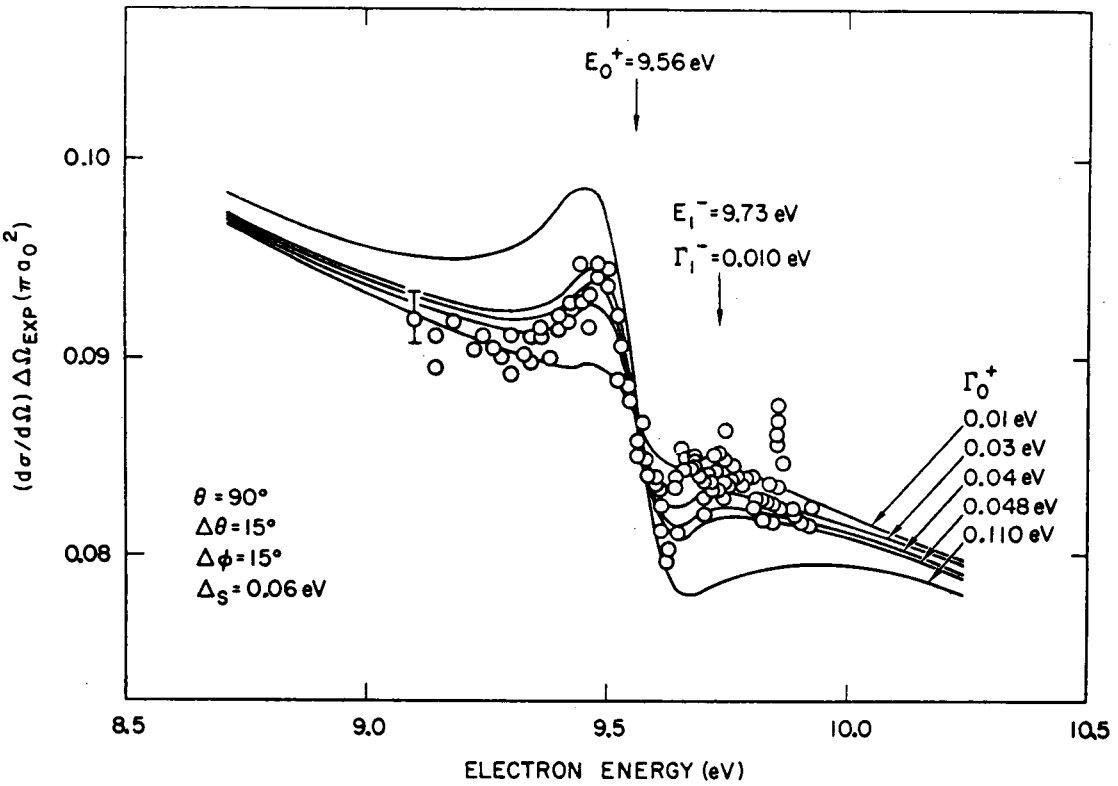

FIG. 14. Comparison between experimental and calculated cross sections in the region of the ^1S and ^3P resonances in hydrogen. The positions of the two resonances are fixed at 9.56 and 9.73 eV, respectively, and the width, Γ_0^+ of the ^1S resonance is varied from 0.01 to 0.110 eV. The best fit to the experimental data, indicated by the circles, is obtained when $\Gamma_0^+ = 0.043 \pm 0.006$ eV. [From McGowan (1967).]

with a broader electron energy spread. Also, the sharp peak near threshold is consistent with theory.

Two subsidiary peaks in the experimental curve shown in Fig. 17 occur at 10.45±0.03 eV and at 10.65± 0.03 eV, i.e., just above the $n=2$ state of hydrogen. According to McGowan *et al.* (1969), the first of these is statistically real and the second is not. McGowan *et al.* argue that the 10.45-eV peak may be an interference effect of the first resonance, as calculated by Marriott and Rotenberg (1968), or another shape resonance. Geltman and Burke (1970) used the pseudo-state expansion theory in an attempt to confirm the experimental structure near 10.45 and 10.65 eV. Their theory, however, shows no signs of the experimental structures and shows a smooth behavior in this energy range. It should be remarked that the pseudo-state expansion theory has achieved measures of success, notably in calculating the ratio of excitation cross sections $\sigma(1s-2s)/\sigma(1s-2p)$ in remarkably good agreement with the experiment of Ott, Kauppila, and Fite (1970).

Below the $n=3$ state of hydrogen, a number of resonances appear in both the experimental and theoretical curves of Fig. 17. For the lowest ^1S resonance, agreement exists between theory and experiment as to position and width. The dominant feature of the theory below the $n=3$ threshold is the ^1D resonance near 11.8 eV, but the dominant feature of the experimental curve appears about 0.1 eV higher. McGowan *et al.* (1969) argue that the theory is insufficient to predict the position of the ^1D resonance accurately and that more states need to be included in the theory to give the proper position for the ^1D resonance. Thus it may be more desirable to correlate the "dominant" features of experiment and theory.

The broad maximum in Fig. 17 just above the $n=3$ threshold appears to be a core-excited shape resonance (McGowan *et al.*, 1969).

C. A Resonance Involving H^{--}

Electron impact experiments on neutral atoms cannot give information on the possibility of the existence of resonances which involve doubly charged negative ions, e.g., H^{--}. In order to gain such evidence, one has to perform experiments in which electrons collide with negative ions. Such an experiment has recently been reported by Walton, Peart, and Dolder (1970). They studied the reaction $e+H^- \rightarrow H+2e$ in a beam experiment; their results are shown in Fig. 18. Noteworthy is the sharp structure appearing near 14.5 eV, which Walton *et al.* (1970) attribute to a state of H^{--}, with a lifetime of about 10^{-15} sec.

Taylor and Thomas (1972) calculated the position and designation of the state responsible for the experimental structure, using the stabilization method which is described in detail by Taylor (1970) and by Hazi and Taylor (1970). Taylor and Thomas (1972) find that a short-lived resonant state, H^{--}, with a configuration principally $(2s)^2 2p\ ^2P^0$ and an admixture of $(2p)^3$, exists at an energy of 14.8 eV and that its width can be estimated to be about 1 eV. The calculated energy and the lifetime are in good agreement with the experiment of Walton *et al.* (1970). Taylor and Thomas further point out that they find another resonance with a largely $(2p)^3$ wave function at some higher, unspecified energy.

The geometric structure of the H^{--} ion has been studied by Herzenberg and Ton-That (1973). They suggest that the only geometry which can lead to a quasistationary state must have all three electrons located at about the *same distance from the proton*, near the corners of an equilateral triangle. Then all three electrons comprising the H^{--} ion are attracted to the proton. By minimizing the expectation value of the Hamiltonian with respect to parameter controlling the radial distance of the electrons from the proton and the angles between the electrons, they find a quasistationary state. Their value for the energy of this state is 11.9 eV (compared to 14.5 eV for the experimental value quoted above) and a lower limit for the width is $\Gamma > 0.3$ eV. The contribution of the s^2p configuration is 87%, that of the p^3 configuration is 10%.

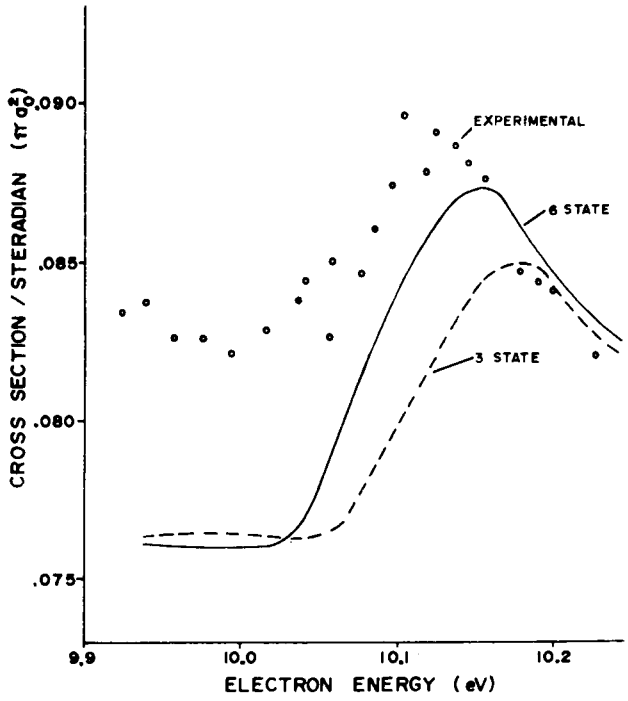

FIG. 16. Comparison of experimental and theoretical cross sections in the energy range 10.0–10.2 eV, for 90° scattering in atomic hydrogen. The theory (close-coupling) includes the ^1D and ^1S resonances as well as the $^{1,3}S$ and $^{1,3}D$ background phase shifts. The theoretical results are averaged over a 15° cone and folded with the experimental beam width. The absolute scale for the experimental points is obtained by normalizing the measured differential cross section in the region below the lowest ^1S resonance to the calculated cross section in that region. [From Ormonde, McEwen, and McGowan (1969).]

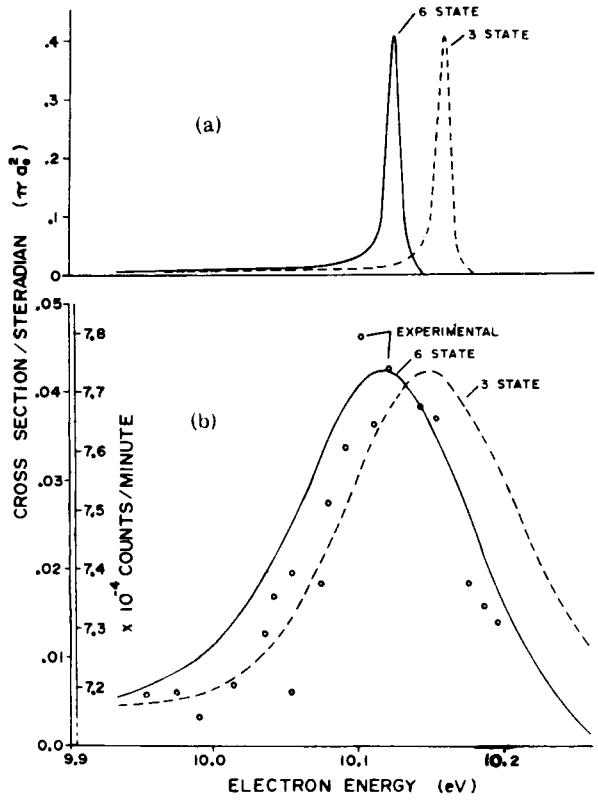

FIG. 15. (a) Close-coupling ^1D cross sections over the resonance region. (b) ^1D cross sections folded with the resolution of the experimental electron beam. The theoretical calculations correspond to the left-most scale, and the experimental points to the scale on the right. Because the measurements are relative, the results are displayed as shown in order to emphasize the agreement in shape between theory and experiment. [From Ormonde, McEwen, and McGowan (1969).]

Herzenberg and Ton-That also find an analogous state in He^-, at an energy of 45.9 eV, with all three electrons equidistant from the nucleus. This state could provide an interpretation for the broad resonance around 50 eV (see Sec. IIIC) observed in helium by Crooks *et al.* (1972).

Other doubly charged negatives have recently been observed using mass spectrometry (Baumann *et al.*, 1971). In this experiment, negative ions are formed in a Penning source. Electric and magnetic deflection experiments confirm that doubly charged negative ions are present in the beam. The ions which have been identified are O^{--}, Te^{--}, Bi^{--}, F^{--}, Cl^{--}, Br^{--}, and I^{--}. The lifetime of the above ions must be relatively long in order for them to survive their trip through the mass spectrometer ($\sim 10^{-6}$–10^{-7} sec). This is in contrast to H^{--}, for which the lifetime is about 10^{-15} sec. Fano (private communication) suggests that a plausible

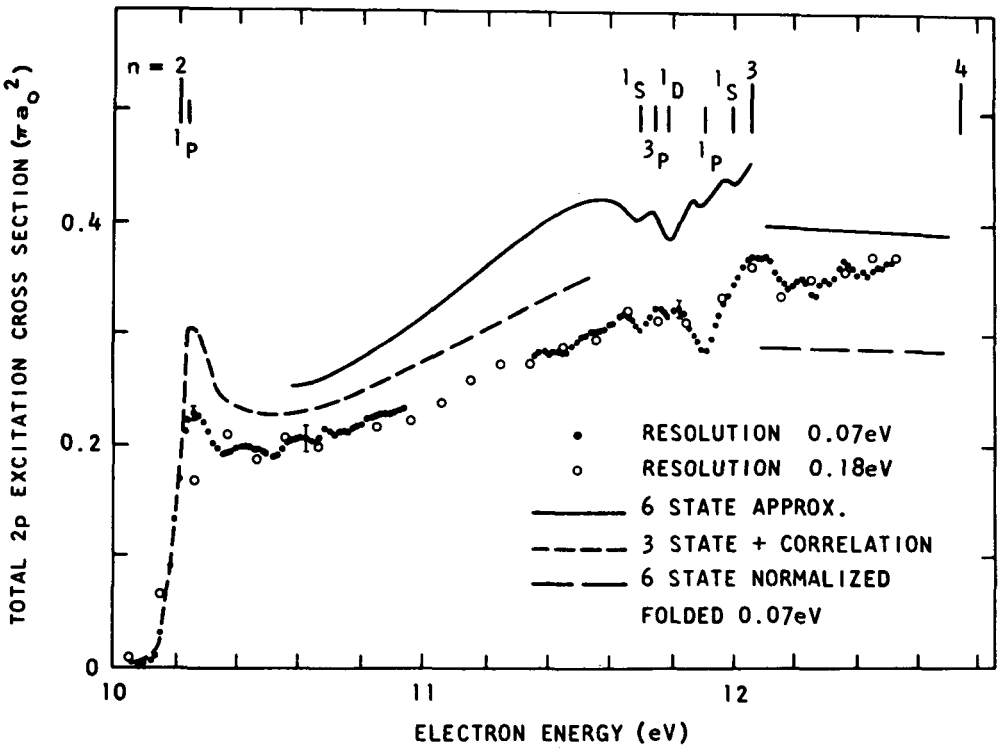

FIG. 17. Total $2p$ excitation cross section in hydrogen. The high-resolution experimental data indicated by the closed points were obtained with an energy spread of 70 meV and the low-resolution data, indicated by the open circles, were obtained with an energy spread of 180 meV. The experimental data are from McGowan, Williams, and Curley (1969). The cross section is plotted on an absolute scale, referenced to the values of Long, Cox, and Smith (1968). Also shown is the "six-state close-coupling" theory of Burke *et al.* (1967) and the "three-state close-coupling plus electron correlation" theory of Taylor and Burke (1967), into which the experimental resolution (70 meV) has been folded. [From McGowan, Williams, and Curley (1969).]

explanation for these long-lived negative ions could be a sextet of the type $3p^4(^3P)4s4p^2$ for Cl^{--} and a configuration $2p^3(^4S)3s3p^2$ for O^{--}. The energy of these levels is not known.

III. HELIUM

As we review the field of resonances and go from atomic hydrogen to helium, the most striking effect is the decrease in theoretical effort and the increase in experimental effort. Thus the guidance for classifying the structures found by experimentalists is not too extensive, and experiments usually precede theory. In fact, much of the classification has been obtained from experimentally measured angular distribution. The experiments performed to date have analyzed structures in the 2^3S, 2^1S, 2^3P, and 2^1P cross sections as well as in the total elastic and total metastable cross section.

The discovery of resonances in atoms came from measurements of the structure in the elastic cross section, as shown in Fig. 19. This type of experiment, especially when it is coupled with a measurement of angular distributions (Fig. 20), gives a great deal of information regarding the width, symmetry, and shape of the resonance, especially for resonances lying below the first electronically excited state of the atom.

For resonances lying above the first electronically excited state, as in the case of core-excited shape resonances associated with $n=2$ and higher-lying states, it is advantageous to study structures in the electronically excited states, such as 2^3S, 2^1S, 2^3P, 2^1P, etc. The decay into these final states is usually preferred.

For an overview of all the sharp resonances occurring by electron impact, it is advantageous to use a transmission experiment. These types of experiments, pioneered by Kuyatt, Simpson, and Mielczarek (1965), can be made very sensitive to sharp structures in the cross section by modulating the electron energy and thus performing a differentiation of the transmitted electron current with respect to energy. Such experiments have been performed for all rare gases by Sanche and Schulz (1972). A sample of their data for helium is shown in Fig. 21. The advantage of this type of experiment is the overview of the location of resonances on the energy scale. The disadvantage lies in the limited information: One generally cannot deduce the symmetry, the width, or the exact shape. Nor is it possible to observe broad resonances (e.g., shape resonances) very clearly. Various elastic and inelastic cross sections must be measured at different angles of observation to fill out the picture.

As an aid to the subsequent discussion, Fig. 22 shows an energy level diagram of the lowest states of neutral He and the position of resonances, as observed by

various investigators, both experimentally and theoretically. The solid horizontal lines indicate those resonances which seem well established at the present time.

A. Classification of Energy Levels in He

It has already been pointed out that the levels of the compound states in helium and other gases arise from the addition of an electron to a particular excited state

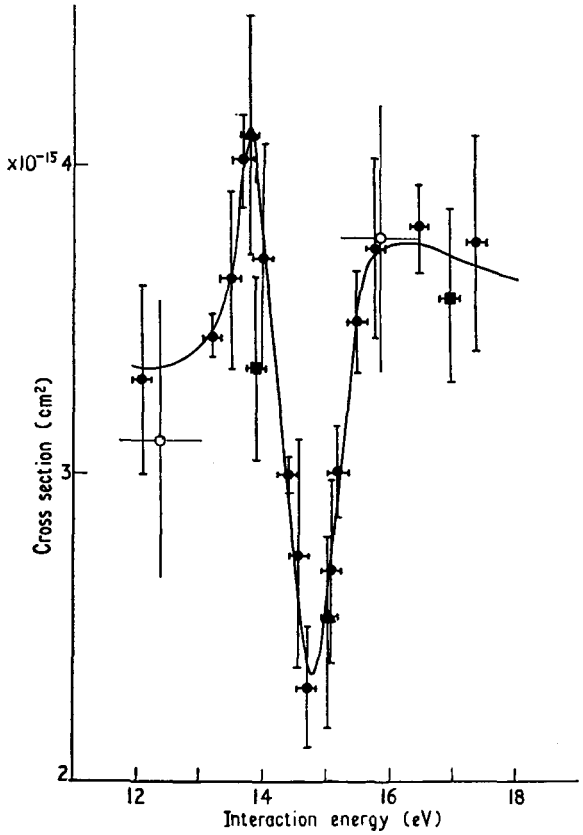

FIG. 18. Cross sections for detachment from H^- by electron impact. The symbols ■, ●, and ▲, respectively, refer to measurements with inclined beams in which the ion beam laboratory energies were 7, 8, and 10 keV. The open circles denote earlier measurements by Peart *et al.* (1970). Estimates of energy resolution and 90% confidence limits of random error are shown for each point. [From Walton, Peart, and Dolder (1970).]

of the atom. The resulting state lies, for the case of Feshbach resonances (also called "closed channel" and core-excited resonances), below the energy level of the parent. Thus one can think of these states as negative ions with a definite electron affinity, in the range of about 1/2 eV. It is also possible for the compound state to lie *at* the energy of the parent state ("virtual states") or *above* the parent state, by up to 3 eV. Thus one can list all the relevant configurations which can be derived from an excited state of helium, plus an additional electron. From the lowest states of helium, $1s2s$ and $1s2p$, we can write the states listed in

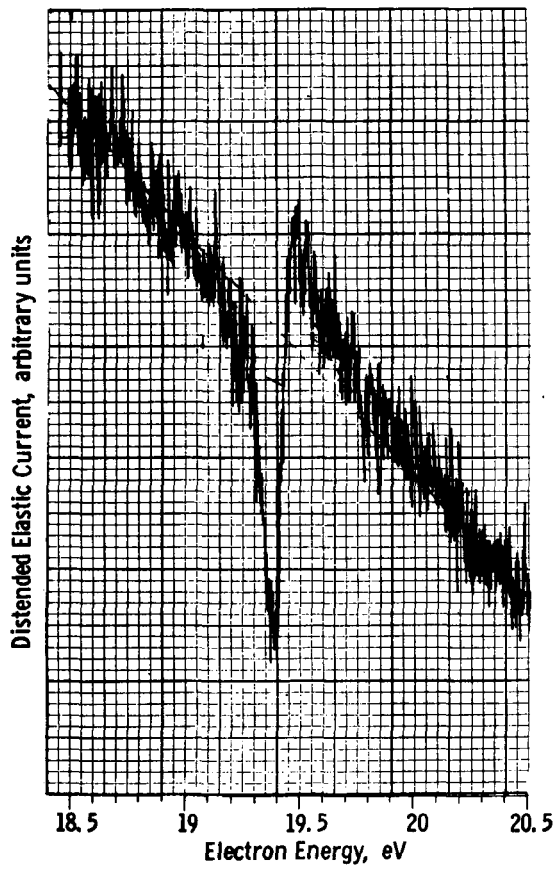

FIG. 19. The original observation of the $(1s2s^2)\ ^2S$ resonance in helium. The angle of observation is 72° and the elastic cross section is measured. The decrease in the cross section near 19.3 eV is approximately 14%. [From Schulz (1963).]

Table I. The superscripts designate states of odd and even parity. The $2s2p$ configuration can lead to ^3P and ^1P states. The addition of a $1s$ electron to this term results in two distinct ^2P states of different energy for the $1s2s2p$ configuration. One of these states has spins of the outer electrons parallel ($^2P_{\uparrow\uparrow}$), the other antiparallel ($^2P_{\uparrow\downarrow}$). The "parents" of these two states are the $(2s2p)^3P$ and $(2s2p)^1P$ states, respectively.

The $(2p)^2$ configuration, being composed of two equivalent electrons, results in ^1S, ^3P, and ^1D states.

TABLE I. Possible states of He^-.

	Outer electrons equivalent	Additional states for nonequivalent electrons (unlikely)
$1s2s^2$	$^2S^e_{\uparrow\downarrow}$	$^2S^e_{\uparrow\uparrow}$
$1s2s2p$	$^2P^o_{\uparrow\uparrow}$, $^2P^o_{\uparrow\downarrow}$, ~~$^4P^o$~~	...
$1s2p^2$	$^2S^e_{\uparrow\downarrow}$, $^2D_{\uparrow\downarrow}$, ~~$^2P^e$~~, ~~^4P~~	$^2S^e_{\uparrow\uparrow}$, $^2P^e$, $^2D^e_{\uparrow\uparrow}$

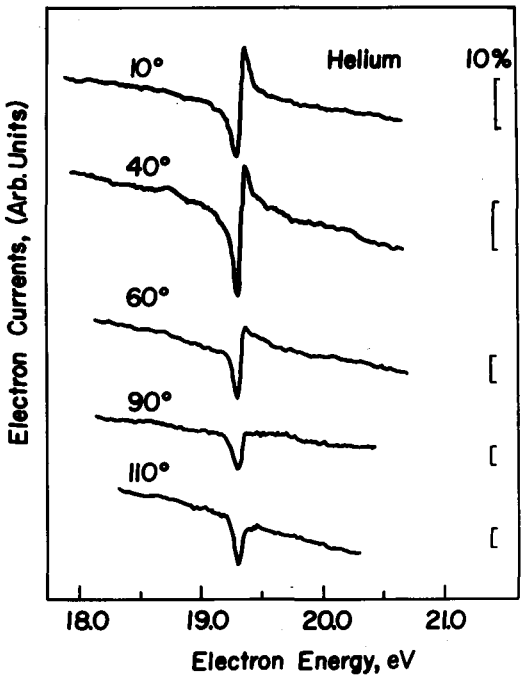

FIG. 20. The appearance of the $(1s2s^2)\ ^2S$ resonance in helium at different angles of observation. The vertical lines indicate a 10% change in the differential elastic cross section. [From Andrick and Ehrhardt (1966).]

Adding a $1s$ electron, we obtain ^2S, ^2P, ^4P, and ^2D states. These are the only allowed states within the LS coupling scheme, which is expected to be applicable for the case of He^-.

It was first pointed out by Fano and Cooper (1965) that there are restrictions on the quantum numbers of the compound states that can be reached by the collision of an electron with a ground-state helium atom (^1S). The *parity* and the *total angular momentum quantum* number J of the input channel must be invariant in the collision. They must be conserved for the system $e+\mathrm{He}(^1S)$ and for the system He^-. The spin quantum number S and the orbital angular momentum quantum number are each individually conserved only insofar as LS coupling is applicable. This should be the case for helium.

We can eliminate all the quartet states in Table I because these would require a spin–flip. Also, we can eliminate, as pointed out by Kuyatt *et al.* (1965) the state $^2P^e$ resulting from the $1s(2p)^2$ configuration. The parity of this state is necessarily *even*. In order to produce this state from ^1S state of helium (parity even), the electron must have a parity $(-1)^l$, where l is the orbital angular momentum. In order to produce a P state from an S state, we must have $l=1$, e.g., odd parity. Thus we cannot conserve parity and must

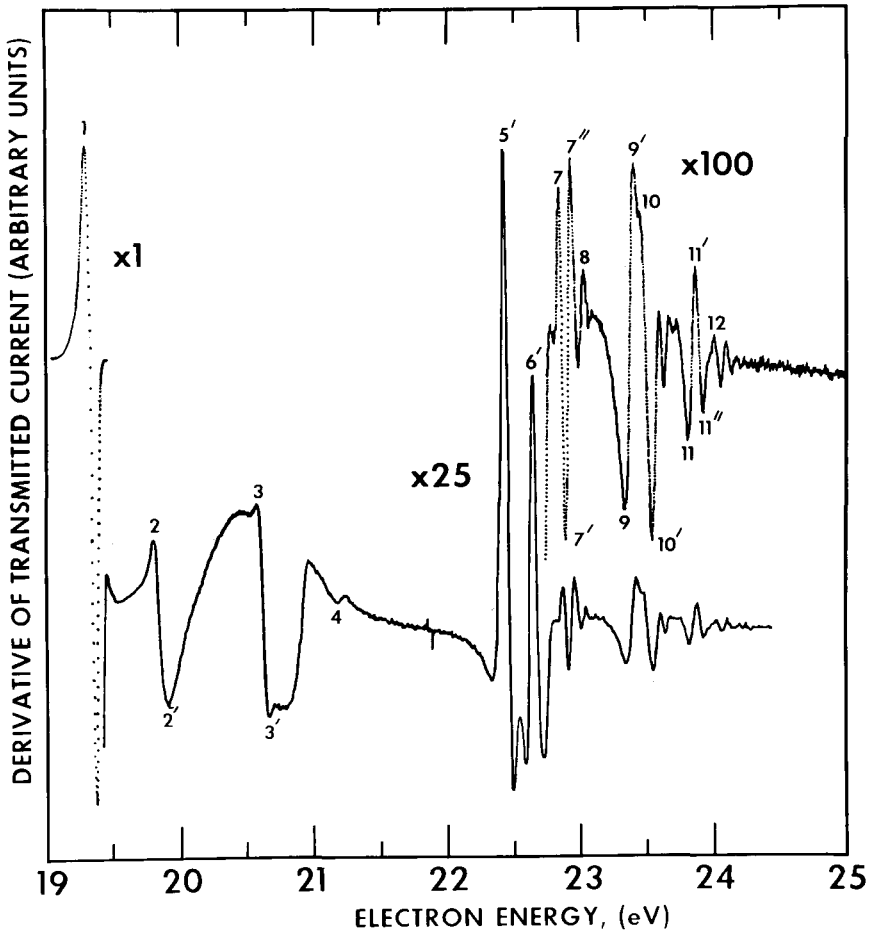

FIG. 21. Derivative of transmitted current vs electron energy in helium, below ionization. The gain of the amplifier is increased by a factor of 25 for the lower portion of the curve and by a factor of 100 for the inset in the upper right, compared to the region around 19.3 eV. The excursion around 19.3 eV corresponds to a change in transmitted current of about 10%. The smaller excursions (e.g., #12) thus correspond to a change in transmitted current of about 0.01%, which is the limit of this transmission experiment. [From Sanche and Schulz (1972).]

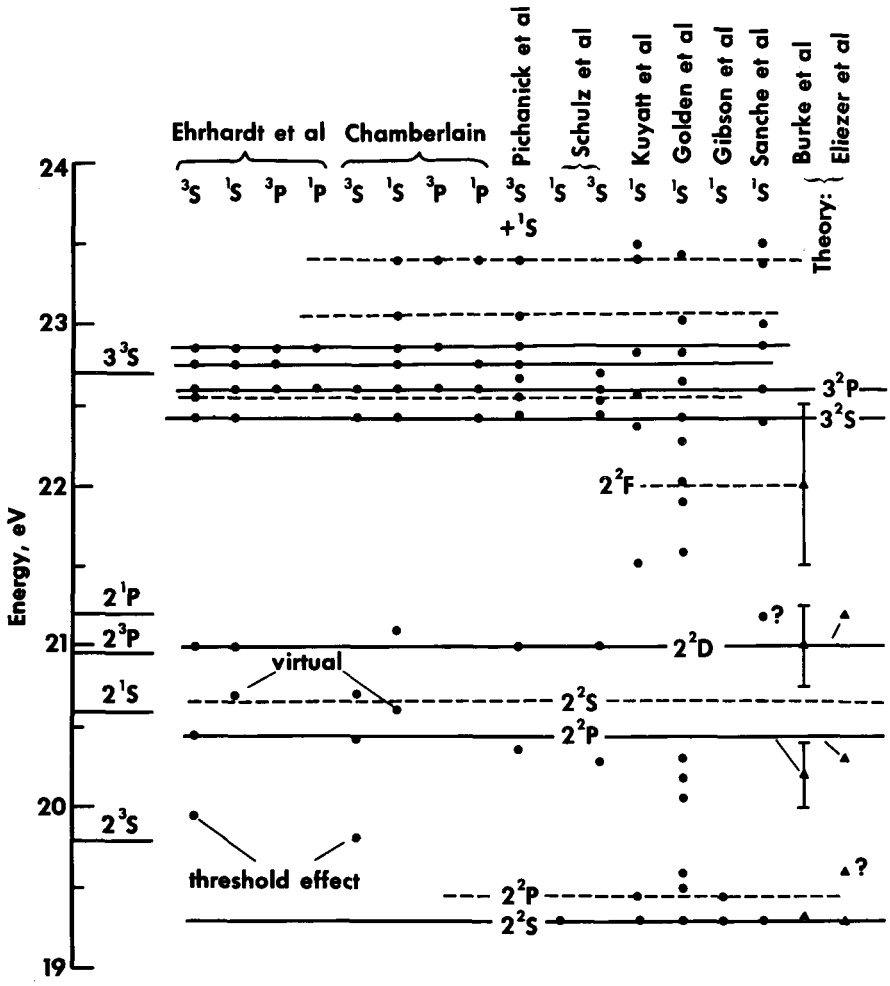

FIG. 22. Survey of energy values for resonances in helium. On the left-hand side of the diagram we show the lowest energy levels in He. The names of the authors are indicated above; just below the names we indicate the decay channels in which the resonances are observed. The dots indicate the position at which structures have been observed. Two theoretical columns are also included. Burke *et al.* (1969) calculate the widths of the ^2P, ^2D, and ^2F resonances and these are indicated by the vertical lines. The full horizontal lines indicate those resonances which seem firmly established. The many extra resonances found by Golden *et al.* (1970), as well as the resonance at 19.45 eV (dashed horizontal line), have been put in doubt by the results of Sanche and Schulz (1972) and must be seriously questioned at the present time. [From Sanche and Schulz (1972).]

cross out the $^2P^e$ state in Table I. This leaves us with one state from the $1s2s^2$ configuration, $^2S^e$, two states from the $1s2s2p(^2P^0)$ configuration (one with spins in the outer shell parallel, one antiparallel), and two states from the $1s2p^2$ configuration ^2S and ^2D. The total number is 5.

If the electrons in the outer shell are not equivalent, then we have to write $1s2p2p'$, where $2p'$ stands for electrons in an np orbital ($n=2\rightarrow\infty$) and additional states are possible, as postulated by Golden and Zecca (1970). These additional states are also listed in Table I, although they may not be real possibilities.

B. Resonances from 19.3 eV to the Ionization Potential

In this section we discuss resonances above the lowest 2^2S at 19.34 eV, and list them in a sequence of increasing energy. An attempt is made to establish the reliability of each determination. At the outset it must be stressed that differences in energy which are *less than* the observed width of these resonances (i.e., about 0.05 eV) must be ignored. Resonances can exhibit a different shape, depending on the angle of observation, or the acceptance angle at a fixed angle, or depending on the decay channel in which they are observed. Only a complete analysis involving phase shifts could establish a reliable guide to such differences.

1. 19.34 eV ($1s2s^2$, ^2S)

The resonance occurring near 19.3 eV was the first to be measured experimentally for an atomic system. Although some discrepancies as to the exact energy and width emerged initially, all the experimental values have converged to the region 19.30–19.35 eV. Appendix II lists some of the recent values obtained by experiment and by theory. Figure 19 reproduces the original measurement of this resonance obtained by observation of elastic scattering at an angle of 72 degrees, in a double electrostatic analyzer. Simpson and Fano (1963) confirmed the existence of this resonance and classified it as the $1s(2s)^2\,^2S$ state. Further experimental confirmation came from a Maier-Leibnitz type experiment of Fleming and Higginson (1963). Andrick and Ehrhardt (1966) obtained the angular dependence in the region of 19.3 eV and confirmed that the resonance appears in the s-wave. Figure 20 shows that the

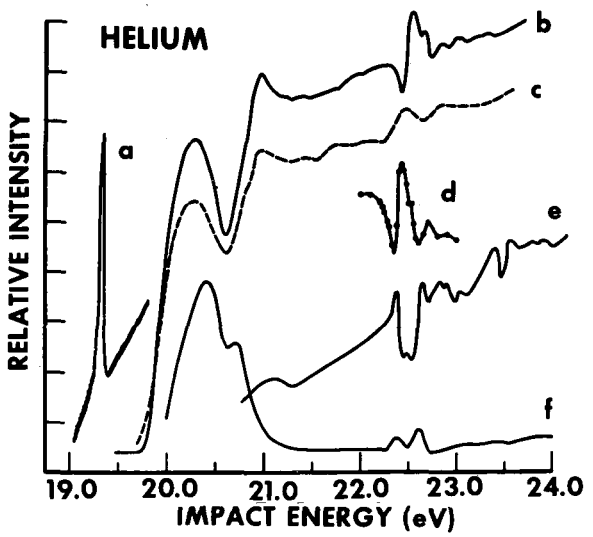

FIG. 23. Comparison of cross sections for production of metastables in helium. (experiments) a—resonance at 19.3 eV observed in a transmission experiment; b—total metastable cross section (Pichanick and Simpson, 1968); c—total metastable cross section (Schulz and Fox, 1957); d—2^3S differential cross section at 72° (Schulz and Philbrick, 1964); e—2^1S differential cross section at 0° (Chamberlain, 1967); f—2^3S differential cross section at 0° (Chamberlain, 1967). [From Pichanick and Simpson (1968).]

resonance can be clearly observed at 90°, at which angle the p wave disappears. An analysis of the phase shift shows that the phase shift of the s wave for potential scattering is 100 degrees, for the p wave 25 degrees, and for the d wave 4 degrees. These phase shifts can be compared with a subsequent study of Gibson and Dolder (1969) who obtained $\eta_0 = 110°$, $\eta_1 = 17°$, and $\eta_2 = 3°$. The agreement with the theory of LaBahn and Callaway (1964) is satisfactory. The variation of the resonance shape with angle is attributed to the interference of the s-wave with the other partial curves. Whereas the width of the resonance was estimated by Andrick and Ehrhardt (1966) to be 15–20 meV, more detailed analysis by Gibson and Dolder gives a value of 8 meV for the natural width at half-height, in good agreement with previous estimates. The value of 8 meV for the width of the resonance at 19.3 eV is probably the best experimental value available at this time. Appendix II compares the widths deduced from experiment and from theory. The latest calculations of this width, due to Temkin *et al.* (1972) and Sinfailam *et al.* (1972) give values of 14 and 15 meV, respectively.

2. 19.45 eV (?)

A small structure was observed by Gibson and Dolder (1969) in the differential elastic cross section just above the 2^2S resonance. This structure is most pronounced at an angle of observation of 54.5° and disappears at 90°. The angular distribution is indicative of a resonance in the p wave and we would deduce that the designation of the state is $(1s2s2p)\ ^2P^0$. The signal-to-noise ratio with which the 19.45 resonance was observed at 54.5° was only unity, and thus this observation alone cannot be considered to be conclusive. However, this resonance was observed at the identical energy in the transmission experiment of Kuyatt, Simpson, and Mielczarek ("peak" at 19.43±0.01 eV, "dip" at 19.47±0.01 eV), but was visible only on the runs with the highest energy resolution. Also, Golden and Zecca (1970) observed structure in their transmission experiment ("peak" at 19.47 eV, "dip" at 19.52 eV). Andrick and Ehrhardt (1966), whose experiment is similar to the experiment of Gibson and Dolder, did not observe the structure at 19.45 eV. Neither did Pavlovic (private communication) observe this resonance in an experiment which was specifically performed to study this resonance. Sanche and Schulz (1972) consider the 19.45 eV resonance a spurious effect resulting from the replication of the $(1s2s^2)\ ^2S$ resonance by electrons which have lost energy on collision with slits.

In their theoretical study, Eliezer and Pan (1970) found a ^2P root at 19.6 eV, but it "stabilized rather poorly." The latter authors consider the evidence unconvincing. Burke did not obtain such a state. Neither did Temkin, Bhatia, and Bardsley (1972), who made a purposeful attempt, using their quasi-projection theory, to find states below 19.8 eV. Similarly, Sinfailam and Nesbet (1972) searched for resonances below the 2^3S state with a fine mesh using a variational technique which takes polarization and correlation effects into account. They, too, find no evidence for resonances apart from the ^2S resonance. Thus we must conclude that the existence of a resonance at 19.45 eV is uncertain and in serious doubt.

3. 19.5–20.3 eV

Between 19.5 and 20.3 eV only Golden and Zecca (1970) have observed resonances. These authors observe 4 structures, each exhibiting a peak and a dip. The assignment given to these structures and the energies (in eV) of the peak and the dip are: $(1s2p^2)^2D_{\uparrow\uparrow}$: 19.58/19.62; $(1s2p^2)^2D_{\uparrow\downarrow}$: 20.04/20.10; $(1s2s2p)^2P_{\uparrow\downarrow}{}^0$: 20.17/20.21; $(1s2p^2)^2S_{\uparrow\uparrow}$: 20.3/20.35. No one else has observed structure attributable to resonances in this energy range (19.5–20.35 eV), although other transmission experiments in fact had a higher sensitivity for observing resonant structures. One would have to invoke some special features of Golden and Zecca's apparatus which would make this particular apparatus more sensitive to the particular resonances in the energy range under discussion. The angular acceptance angle for forward-scattered electrons could possibly be such a feature, but up to now very little attention has been given to such considerations.

Until the structure in this energy range is reproduced by other experiments, one must retain a skeptical attitude regarding the reality of the 4 structures in the

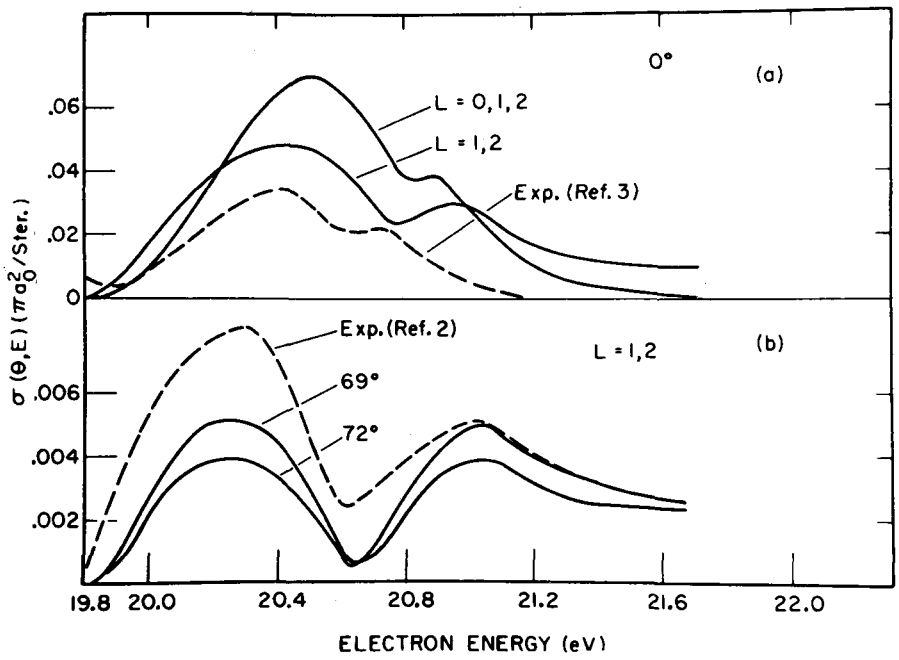

FIG. 24. Energy dependence of 2^3S cross section at 0° and 72°. The solid lines are from the close-coupling theory of Burke, Cooper, and Ormonde (1966). The dashed curves are experimental: The 72° data are from Schulz and Philbrick (1964) and the 0° data from Chamberlain and Heideman (1965). The first peak in the cross section curves is attributed to the ^3P resonance and the second to the ^3D resonance. [From Burke, Cooper, and Ormonde (1966).]

energy range 19.5–20.3 eV. We should note that the last of these structures coincides in energy with the broad 2^2P shape resonance discussed in the following section.

4. 20.3–20.45 eV (2^2P)

The total cross section for excitation of the 2^3S state exhibits a maximum at about 0.5 eV above threshold as shown in Fig. 23. It has been pointed out by Baranger and Gerjuoy (1957) that such behavior can best be explained by considering that the inelastic process proceeds via a compound state. By fitting the total 2^3S cross section with a Breit–Wigner one-level formula, they obtained a very good fit to the experimental cross section for metastable production (2^3S+2^1S) of Schulz and Fox (1957). The parameters that resulted in the best fit located the position of the resonance at 20.2 eV with a width of about 1.0 eV. More detailed theoretical considerations by Burke, Cooper, and Ormonde (1966), using the close-coupling approach, confirmed these ideas. Burke *et al.* found that the major peak of the 2^3S cross section occurs within the range of the p-wave resonance, which they calculate to occur at 20.2 eV with a width of 0.52 eV. Another smaller peak at the ^3D resonance (21.0 eV) is also found in this calculation. These considerations then lead us to associate experimentally determined maxima of the 2^3S cross section with the existence of compound states.

If the width of the p-wave resonance is anywhere near the value quoted by Burke *et al.* (0.52 eV), it is not surprising that the observed location of this maximum varies depending on angle and the mode of observation. Whereas the total 2^3S cross section peaks at 20.3–20.35 eV, (see, for example, Schulz and Fox, 1957; Pichanick and Simpson, 1968) the differential cross section peaks near 20.45 eV (Chamberlain, 1967; Ehrhardt and Willmann, 1967; Ehrhardt, Langhans, and Linder, 1968). It is doubtful that this discrepancy, of the order of 100 meV, is instrumental. In fact, the "shifting" of the peak is dramatically demonstrated in Fig. 24, due to Burke *et al.*, which shows a shift in the location of the peak in the 2^3S cross section by almost 200 meV between an angle of observation of 0° and 72°. Thus it is impossible to define, without a detailed analysis, the exact center of this resonance.

Ehrhardt and Willmann (1967) find that the angular distribution of the scattered electrons which have excited the 2^3S state around 20.45 eV (see Fig. 25) exhibits a p-wave character, so that the designation of this resonance as 2^2P seems established.

5. Effects near the Thresholds of the 2^3S and 2^1S Excitation Cross Section

The differential cross sections for both the 2^3S and the 2^1S states exhibit a small peak within 150 meV of threshold. This behavior has been observed in two independent experiments, one performed by Chamberlain and Heideman (1965), who analyzed the inelastically scattered electrons in the forward direction, and the other by Ehrhardt and Willmann (1967) and by Ehrhardt, Langhans, and Linder (1968), who observed inelastically scattered electrons at 10–90°. The latter experiments show that the angular dependences of the structures near both the 2^3S and the 2^1S thresholds are isotropic, indicating an s wave. The peaks occur at 19.95 eV (140 meV above the 2^3S threshold) and just above 20.6 eV, respectively.

The results of Ehrhardt *et al.* (1968) are shown in

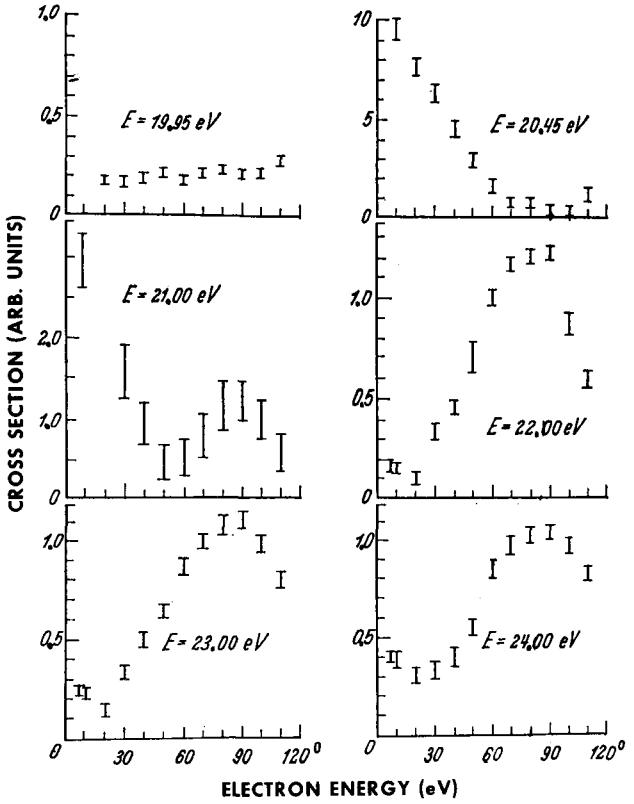

FIG. 25. Angular distribution of electrons having excited the 2^3S state in helium. The incident electron energy E, is indicated. The angular dependence at 19.95 eV corresponds to an s wave, at 20.45 eV to a p wave and at 21.00 eV to a d wave. All curves are experimental. [From Ehrhardt and Willmann (1967).]

Fig. 26. However, it seems that a note of caution is appropriate in analyzing the behavior of these excitation curves within the first 0.5 eV of threshold. This regime involves electrons which possess only 0–0.5 eV of energy after the collisions and which must be accepted by the electron analyzer. For the curves of Fig. 26 to be meaningful, it is desirable that no energy discrimination be present in this energy range. This requirement imposes a very severe demand on the electron optics which must exhibit a complete absence of chromatic aberration in the range 0–0.5 eV. This problem has not yet been solved. Also, there should be a complete absence of stray electric and magnetic fields, which could cause severe discrimination problems. It is probable that the curves of Fig. 26 are afflicted, within 0.5 eV of their thresholds, by an error of unknown magnitude, i.e., a correction factor of unknown shape should be applied to these curves.

One can obtain an indication of the seriousness of the problem outlined in the previous paragraph by taking the ratio of cross sections for the 2^3S excitation at two different energies, e.g., the ratio $\sigma(20.45\text{ eV})/\sigma(19.95\text{ eV})$. This is the ratio of cross sections near the center of the ^2P resonance to the peak near threshold. For the curve of Fig. 26, this ratio is about unity (at 70°), whereas it is about three (at 60°) in the older work of Ehrhardt and Willmann (1967). One should prefer, at the present time, the data shown in Fig. 26, due to Ehrhardt, Langhans, and Linder (1968) in preference to the older data of Ehrhardt and Willmann since the former authors have made a study of the energy discrimination in their apparatus and have come to the conclusion that the error is less than 50% in the energy range within 300 meV of the 2^3S threshold.

The experimentally measured width of the threshold structure near the onset of the 2^3S state is about 150 meV and thus should have been noticed in measurements of the total cross section for the 2^3S state. Although the resolution of many of the experiments on the total excitation of the 2^3S state had sufficient resolution, such a structure was not observed (see, e.g., Schulz and Fox, 1957) and the total 2^3S cross section rises to a broad maximum near 20.3 eV. Pichanick and Simpson (1968) made a careful examination of the threshold region with the purpose of examining the threshold structure (see Fig. 23), but failed to find any indication of its existence. If one integrates the theoretical differential cross section over all angles to obtain the total cross section, the threshold structure becomes almost invisible [Burke *et al.* (1967) and Linder, private communication] and thus the threshold structure near 19.95 eV cannot be observed in the total cross section for exciting the 2^3S state.

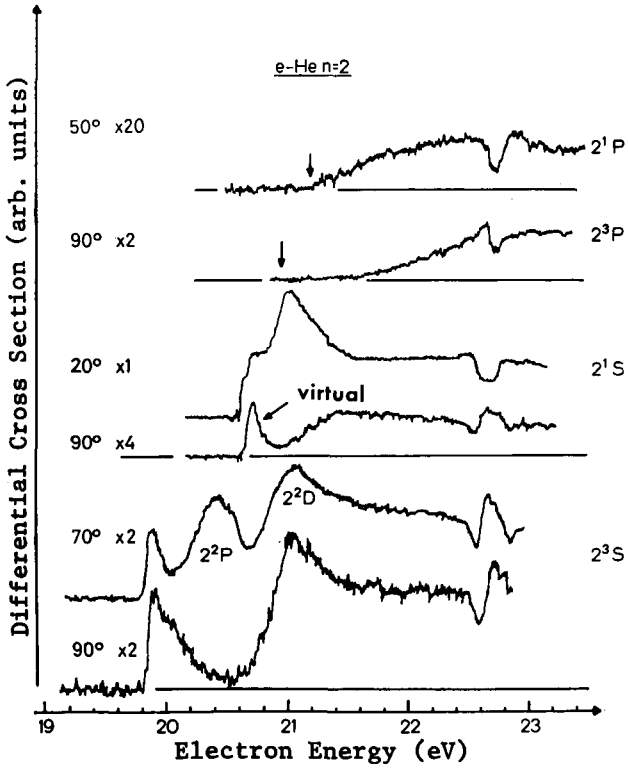

FIG. 26. Energy dependence of the differential cross sections for the excitation of 2^3S, 2^1S, 2^3P, and 2^1P levels of helium near threshold, at selected angles of scattering. The angle of observation is indicated, for each curve, on the left-hand side. The number following the designation of angle indicates the enlargement of the particular curve with respect to the 2^1S curve at 20°. Experimental. [From Ehrhardt, Langhans, and Linder (1968).]

Although the structures near the thresholds of the 2^3S and 2^1S states have a similar appearance, the interpretation advanced by Ehrhardt (1969) for the two effects is very different.

Ehrhardt and Willmann (1967) find that the threshold peak at 19.95 eV in the 2^3S differential excitation cross section is independent of angle. Thus they deduce that the threshold peak appears in the s-wave. In a number of publications, Ehrhardt *et al.* (1967, 1968, 1969) point out that the threshold effect is caused by the *tail* (i.e., the wings) of the 2^2S resonance, whose center is located at 19.34 eV. This conclusion relies heavily on the fact that the theoretical work of Burke and of Taylor could not account for other ^2S resonances in this energy range. In his review, Taylor (1970) further discusses the qualitative aspects of threshold peaks in inelastic cross sections caused by core-excited resonances lying below the inelastic threshold.

It is pointed out by Herzenberg (private communication), that very *sharp* peaks in inelastic cross sections near threshold can not be explained *quantitatively* in such a simple fashion. Rather, one has to realize that the decay width for a Feshbach resonance (e.g., 2^2S in helium) shows an abrupt increase in a narrow energy range starting at the inelastic threshold. Thus, in the case of helium, one can understand how a narrow width (~8 meV) below the threshold of the 2^3S state can be reconciled with a width considerably broader (~1 eV) above the 2^3S state. This argument should

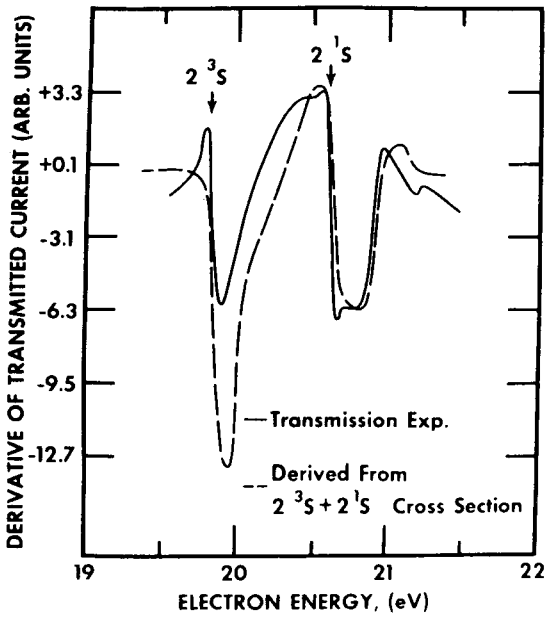

FIG. 27. An expanded view of the derivative of the transmitted current in the neighborhood of the lowest inelastic thresholds in helium. The solid line shows the experiment of Sanche and Schulz (1972) and the dashed line is obtained from the total metastable cross section. The two curves are normalized to each other in the region of the 2^1S excitation. The rise in the transmission curve just below the threshold for the 2^3S and 2^1S states is interpreted as a Wigner cusp in the elastic cross section. [From Sanche and Schulz (1972).]

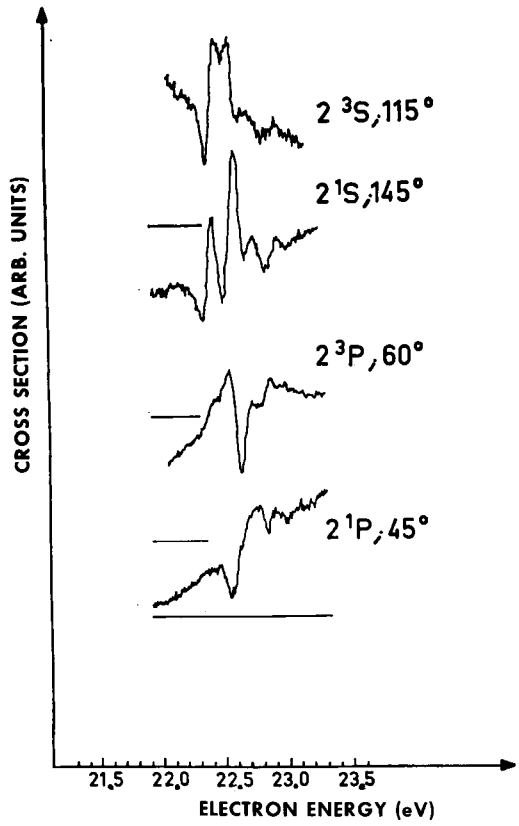

FIG. 28. Differential inelastic cross sections in the energy range 22.4–23.5 eV for helium. The structures are due to the $n=3$ compound states. The final state and the angle of observation are indicated for each curve. [From Andrick, Ehrhardt, and Eyb (1968).]

be applicable generally to the threshold excitation of those states which are parents of Feshbach resonances.

It would be satisfying if the threshold structure in the 2^1S state could be explained along similar lines. However, there seem to be good reasons to invoke a different explanation. This explanation is based on the work of Burke *et al.* (1967) and of Burke, Cooper, and Ormonde (1969) who calculated, using close-coupling methods, the cross section for the transition $e+\mathrm{He}(2^3S)\rightarrow \mathrm{He}(2^1S)+e$. They found a sharp peak at the threshold of the 2^1S state, which they attributed to a ^2S resonance close to the threshold of the 2^1S state. The existence of such a resonance would, of course, also affect the cross section $e+\mathrm{He}(1^1S)\rightarrow\mathrm{He}(2^1S)+e$.

The elastic cross section for scattering of electrons from the 2^1S state has a very large value ($1430\pi a_0^2$) near the 2^1S threshold, in the $l=0$ partial wave, again indicating the existence of a ^2S resonance near the 2^1S state. The threshold behavior of the elastic cross section for scattering from the 2^3S state is markedly different. Thus Ehrhardt *et al.* (1968) attribute the threshold structure near the 2^1S onset to a ^2S state existing near the 2^1S state and designate the ^2S resonance as a "virtual" state. On this model, the electron is captured just at the upper plateau of the potential well and experiences a phase shift. Taylor (1970) describes this

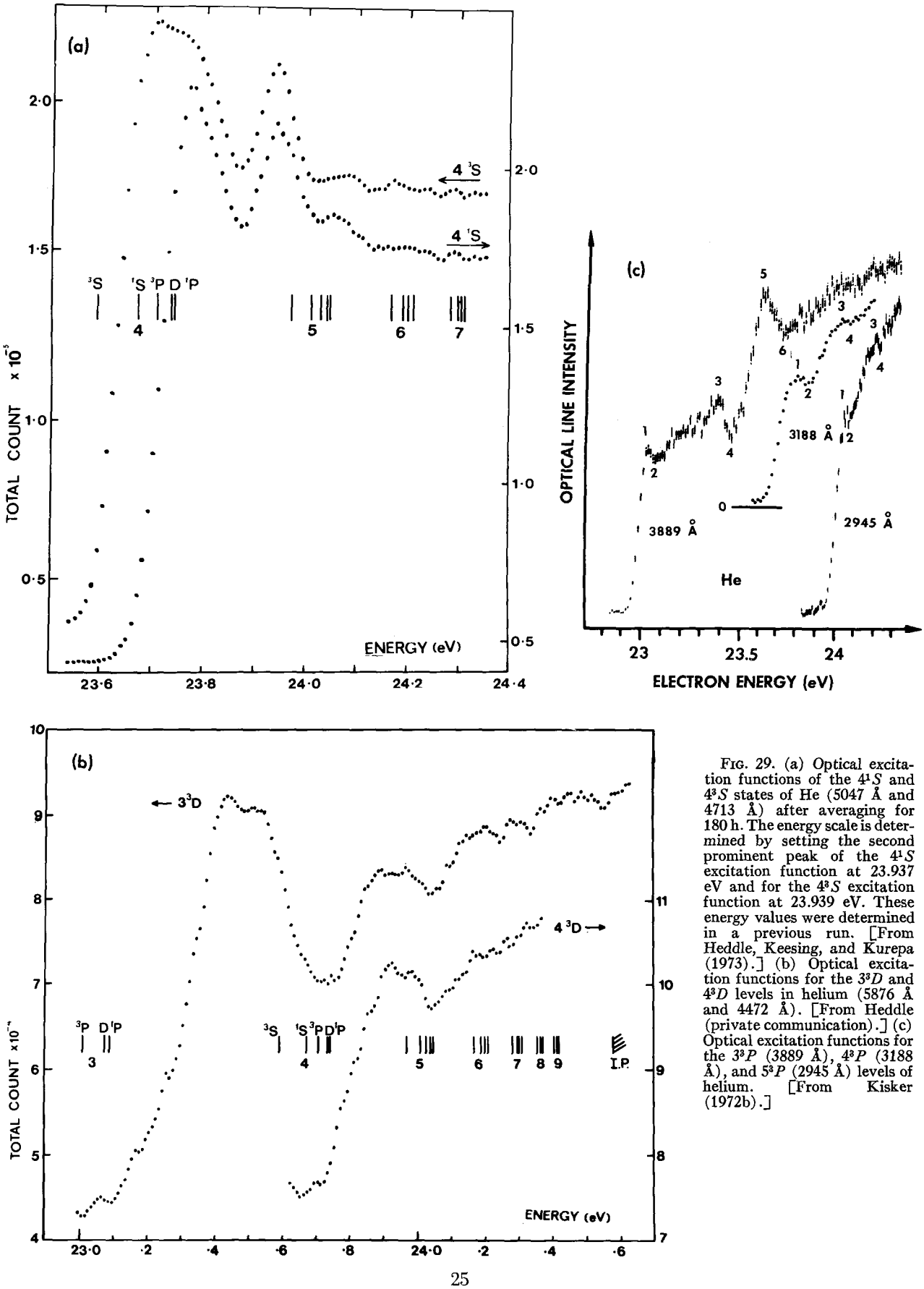

FIG. 29. (a) Optical excitation functions of the 4^1S and 4^3S states of He (5047 Å and 4713 Å) after averaging for 180 h. The energy scale is determined by setting the second prominent peak of the 4^1S excitation function at 23.937 eV and for the 4^3S excitation function at 23.939 eV. These energy values were determined in a previous run. [From Heddle, Keesing, and Kurepa (1973).] (b) Optical excitation functions for the 3^3D and 4^3D levels in helium (5876 Å and 4472 Å). [From Heddle (private communication).] (c) Optical excitation functions for the 3^3P (3889 Å), 4^3P (3188 Å), and 5^3P (2945 Å) levels of helium. [From Kisker (1972b).]

virtual state as a "bound" state that just slipped out of the potential well.

Taylor (private communication) describes the formation of the two 2^2S states as follows: The 2^3S state mixes with the 2^3P state, thus forming a polarization potential which combines with the low screening in excited states to form a well. The electron binds in this well and we get a resonance below the 2^3S state. Similarly, the 2^1S and 2^1P states mix to give a resonance below the 2^1S state. Both resonances have a ^2S character. As the two ^2S channels mix, the two states split apart. The lower ^2S state moves down to 19.3 eV and the upper ^2S moves up and slips out of the well, to become virtual. This approach, if substantiated by calculations, provides a very picturesque way to visualize the two low-lying s-wave resonances in He. In fact, experiments in other rare gases seem to indicate that such a picture is applicable there too.

The designation of the virtual state in terms of orbitals is by no means clear. Table I indicates that the only ^2S state which is not accounted for has the $1s2p^2$ configuration. However it is not suggested that this is the proper answer, since the $1s2p^2$ may have a very large width, and may lie at higher energies.

The resonance near the 2^1S threshold also strongly influences the superelastic cross section $e+\mathrm{He}(2^1S)\rightarrow \mathrm{He}(2^3S)+e$. This cross section exhibits a strong peak near zero energy. A very large average cross section for this process ($\sim 3\times 10^{-14}$ cm^2) for 300°K electrons had been previously measured by Phelps (1955) and the theory of Burke *et al.* (1969) shows agreement with this large value, which was not completely understood until the resonance process was invoked.

6. *Structure in the Elastic Cross Section near the 2^3S and 2^1S Thresholds (Wigner Cusps)*

The opening of an inelastic channel should be accompanied by the appearance of a cusp in the elastic cross section (Wigner, 1948; Baz 1958). Such a cusp has been observed recently in a transmission experiment in helium (Sanche and Schulz, 1972) as a sharp increase in the transmitted current and its derivative just below the threshold for the 2^3S and 2^1S states. The results are shown in Fig. 27. In the differential elastic cross section at 90°, the Wigner threshold cusp appears as a downward step which causes the cross section to decrease by about 1% (Cvejanovic, Comer, and Read, 1973).

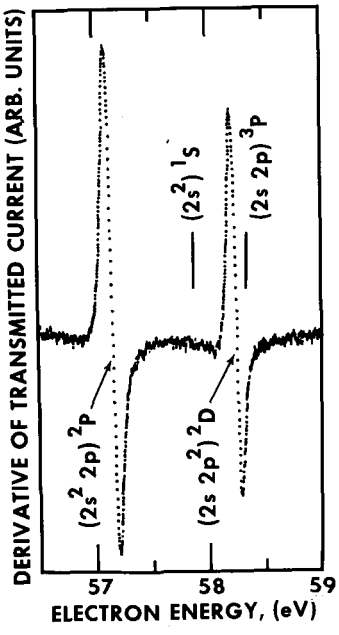

FIG. 30. Derivative of the transmitted current in helium in the region of doubly excited states. The vertical lines show the positions of the $2s^2$ and $2s2p$ excited states of helium. [From Sanche and Schulz (1972).]

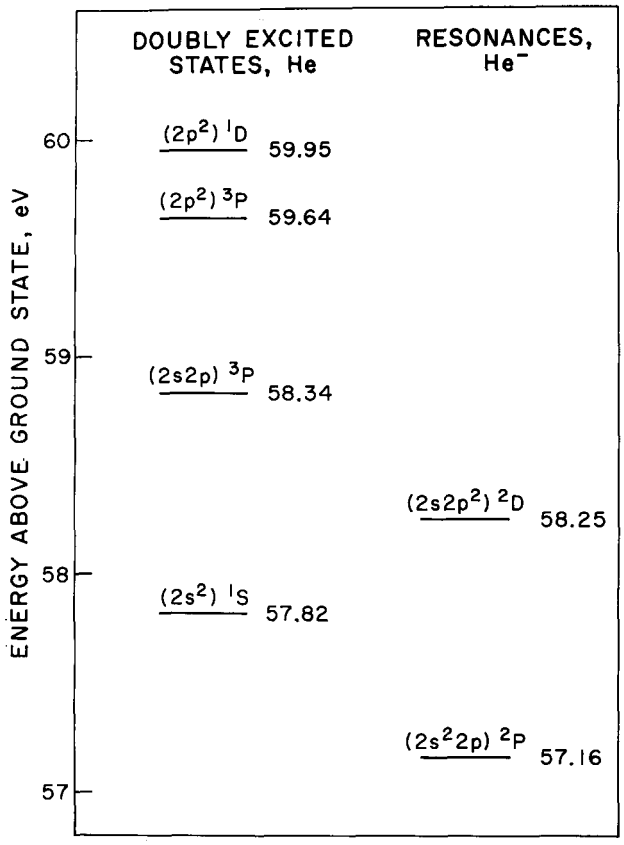

FIG. 31. Energy level diagram for the lowest doubly excited states of helium and the two associated compound states, He^-.

7. *21.0 eV (2^2D)*

The experimental determination of the location of the 2^2D resonance comes from the observation of a well-pronounced peak in the 2^3S and 2^1S cross sections at various angles of observation as shown in Fig. 26. The decay into the elastic channel has not yet been observed. The designation as ^2D comes from the angular distribution and from theoretical considerations. The experimental observations are as follows:

2^3S excitation: Schulz and Philbrick (1964) observed a peak, at 21.0 eV with a width of about 0.4 eV, at an angle of 72°. Ehrhardt and Willmann (1967) extended the angle of observation to include the range 7–110°. The angular distribution at 21.0 eV is found to be characteristic of a d wave, as can be seen in Fig. 25. Chamberlain (1967) studied forward-scattered electrons having excited the 2^3S state and finds structure at

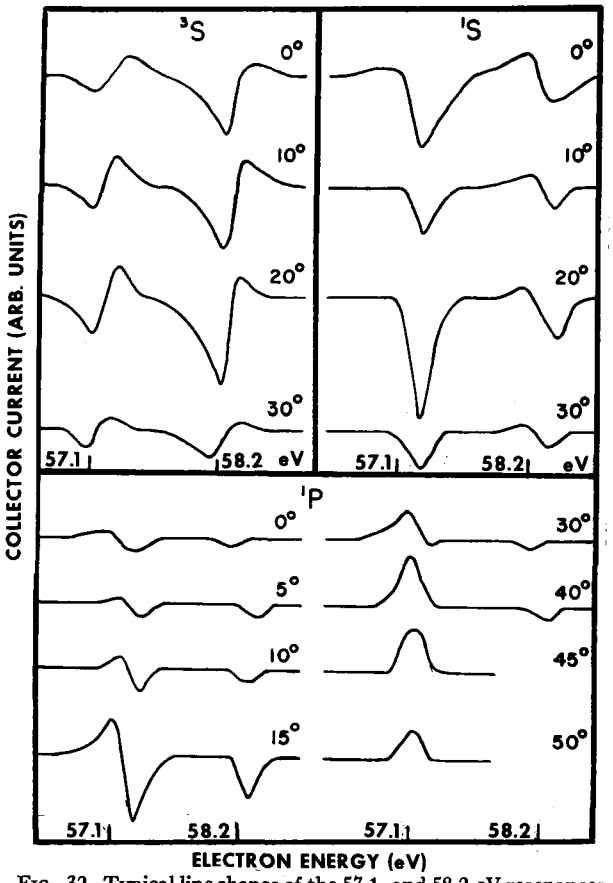

FIG. 32. Typical line shapes of the 57.1- and 58.2-eV resonances ($2s^22p$ and $2s2p^2$), as observed in ^3S, ^1S, and ^1P inelastic channels. The angles of observation are indicated on the figure. The ordinate is in arbitrary units and the zeros are displaced. The energy scale is accurate to about 0.2 eV. [From Simpson, Menendez, and Mielczarek (1966).]

20.7 eV, which probably results from the ^2D resonance. The position of the peak resulting from the ^2D resonance shifts to lower energies (i.e., from 21.0 eV to 20.7 eV) as the angle of observation is decreased (Linder, private communication). In view of the large width of this resonance and the possibility for interference, such a shift is not unusual.

2^1S excitation: The ^2D resonance at 21.0 eV is also prominent in the 2^1S excitation, as reported by Ehrhardt, Langhans, and Linder (1968) particularly at small angles of observation (10°~50°) and in forward scattering (Chamberlain, 1967).

In the total metastable excitation, which measures the sum of the 2^3S and 2^1S excitation, a peak occurs at 21.0 eV. This peak can be attributed, in retrospect, to the ^2D state.

The *theoretical work* on the ^2D state appears fairly consistent. Burke *et al.* place the ^2D state at 21.0 eV, and ascribe to it a width of 0.4 eV. The stabilization technique of Taylor gives a value of 20.3 eV (Eliezer and Pan, 1970). Also, the ^2D state is prominent in the calculated cross section for electron excitation of the 2^1S state from the 2^3S state (Burke *et al.*, 1967). The theory of Burke *et al.* (1969) shows that both the elastic and inelastic cross sections for electron impact on the low-lying metastable states in helium are dominated by the presence of the ^2P and ^2D resonances.

8. 22.42–24 eV (3^2S, 3^2P, etc.) Optical Excitation Functions

The data of Fig. 21 show many partially overlapping structures starting near 22.42 eV and extending to the ionization potential of helium. The lowest of these structures have been studied in the differential inelastic cross sections and are shown in Fig. 28. The values of the energies are listed, together with the suggested designations, in Appendix IIIa.

Very recently optical excitation functions have been studied using monochromatic electrons. Kurepa and Heddle (1972) have studied the following excitation functions: $4^3S\rightarrow2^3P$ (4713 Å); 4^1S-2^1P (5047 Å); 3^3S-2^3P (7065 Å); 4^1D-2^1P (4922 Å); 4^3D-2^3P (4472 Å); 3^3D-2^3P (5876 Å). Heddle, Keesing, and Kurepa (1973) have further analyzed the 4^1S and 4^3S excitations. Kisker (1972) has reported data on the $3^3P\rightarrow2^3S$ (3889 Å) and the $4^3P\rightarrow2^3S$ (3188 Å) lines.

Kurepa and Heddle (1972) detected seventeen structures, many of which appeared rather small, in the energy range 22.80–24.08 eV. Appendix IIIa lists the more prominent structures observed in this work. Also, Appendix IIIa lists large structures observed by Kisker (1972) in the 3^3P excitation and 4^3P excitation functions.

Most of the observations on structures in the optical excitation functions have not yet been analyzed in sufficient detail, so that any assignment is preliminary.

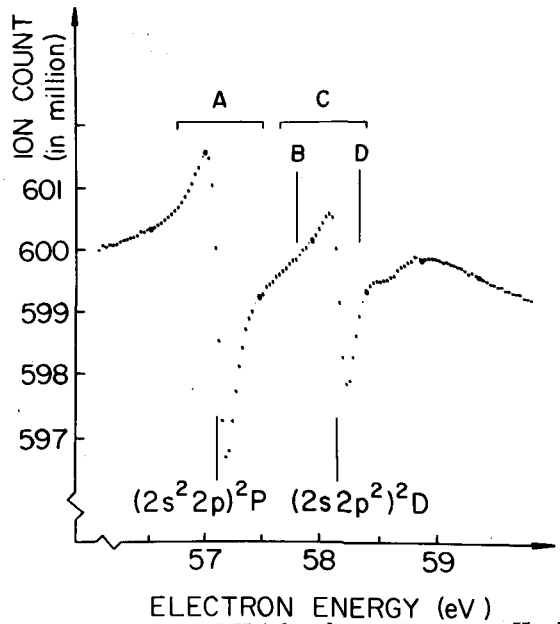

FIG. 33. Formation of He^+ by electron impact on He. The background ion formation is subtracted so that only the structure remains, representing ~0.8% of the total He^+ signal. The count rate is indicated. The structure results from the decay of the ($2s^22p$) and ($2s2p^2$) resonances by two-electron emission. [From Quémenér, Paquet, and Marmet (1971).]

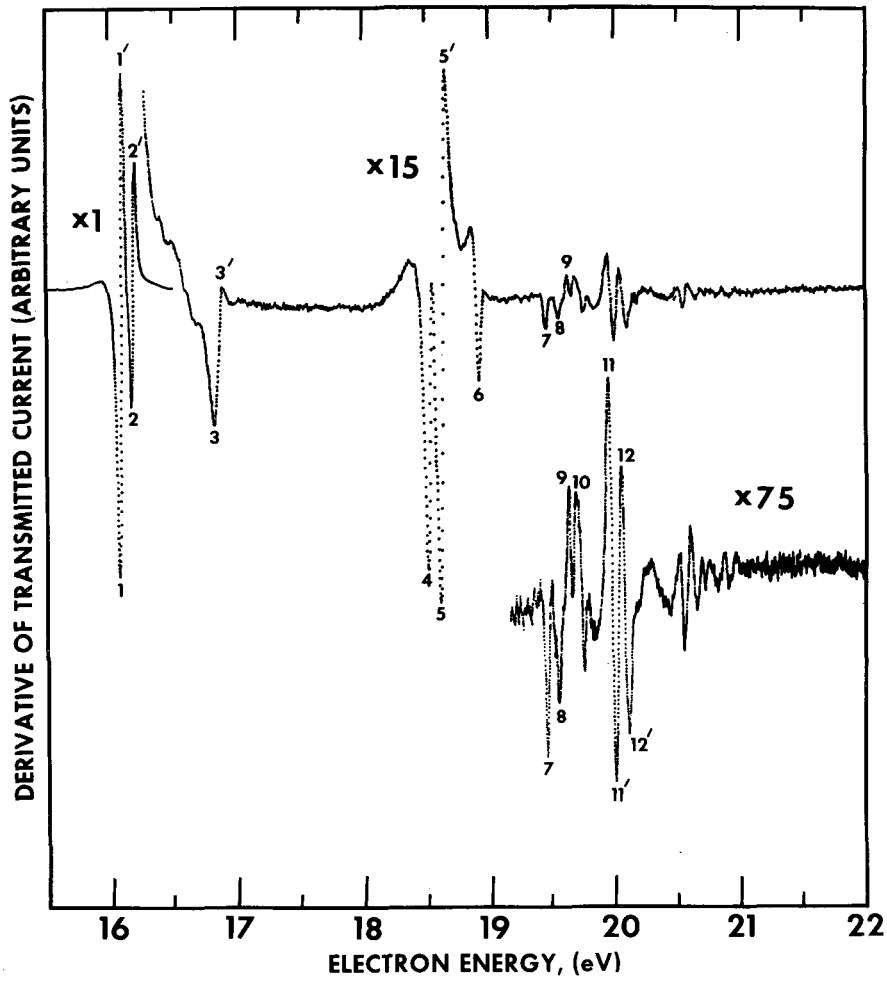

FIG. 34. Derivative of transmitted current vs electron energy in neon. [From Sanche and Schulz (1972).]

Nevertheless, Kurepa and Heddle (1972) propose that the large feature at 22.95±0.02 eV which appears in many of the excitation functions, be assigned to the $1s4s^2$ state of He^-. Similarly, the feature at 23.94±0.02 eV is assigned to the $5s^2$ configuration. It is, of course, understood that the above orbitals represent the dominant wavefunctions and that admixtures of other states are expected to contribute.

Figure 29(a) shows the results of Kurepa and Heddle (1972), as analyzed by Heddle *et al.* (1973) who have added all data from all their runs to aid in the distinction of real features from small fluctuations. The peak near 23.94±0.02 eV is very clearly exhibited in Fig. 29(a).

Figure 29(b) shows the optical excitation functions to two D states, and Fig. 29(c) the excitation functions to three P states, obtained by observing the wavelength indicated in the appropriate figure caption.

TABLE II. Values of the splitting between the $^2P_{3/2}$ and $^2P_{1/2}$ levels in the positive ion and in the compound state for Ne, Ar, Kr, and Xe.

Gas	Compound state: Sanche and Schulz (1972)	Compound state: Kuyatt, Simpson, Mielczarek (1965)	Positive ion
Ne	0.095	0.095	0.097
Ar	0.172	0.172	0.177
Kr	0.66	0.64	0.666
Xe	~1.2	1.25	1.306

C. Resonances above the Ionization Potential: $(2s^22p)^2P$ and $(2s2p^2)^2D$

The lowest doubly excited states of helium are the $(2s^2)^1S$ state at 57.82 eV, and the $(2s2p)^3P$ state at 58.34 eV (Rudd, 1964, 1965). Kuyatt, Simpson, and Mielczarek (1965) discovered, using a transmission experiment, that resonances of the Feshbach type are associated with these states. Golden and Zecca (1970), as well as Sanche and Schulz (1972), confirmed the position of these resonances using the transmission method (Fig. 30). Appendix IV lists the values for these resonances, as found by different experiments. Fano and Cooper (1965) classified these resonances as $(2s^22p)^2P$ for the lowest (~57.16 eV) and $(2s2p^2)^2D$ for the second (~58.25 eV). Various theoretical

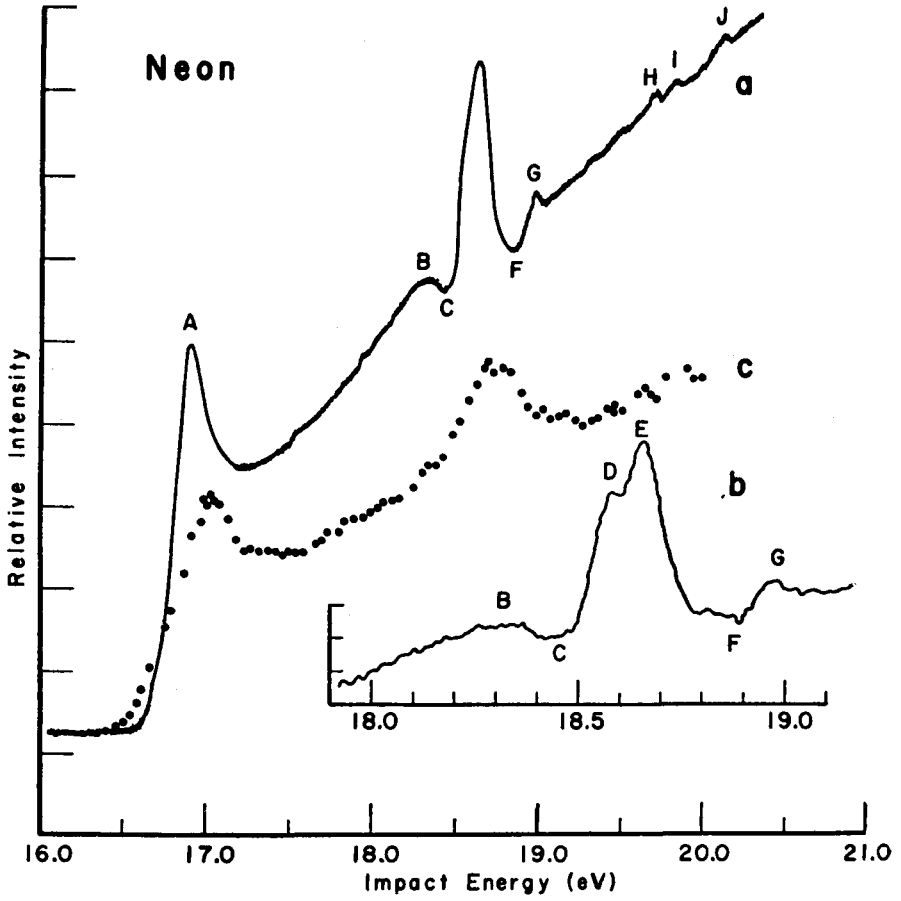

FIG. 35. Total metastable cross section for neon vs electron energy. Curve (a) is from Pichanick and Simpson (1968) with 50-meV resolution; curve (b) is the detail in the 18–19-eV range by the same authors, with 35-meV resolution; curve (c) is from Olmsted *et al.* (1965). [From Pichanick and Simpson (1968).]

approaches confirm the above assignment. Eliezer and Pan (1970) use the stabilization method to calculate the position of the $2s^22p$ and $2s2p^2$ states and Nicolaides (1972) uses a variational principle applied to the projection method with correlation included. Both theoretical methods give good agreement with the energies observed experimentally (see Appendix IV) and thus the assignment of the leading term ($2s^22p$ and $2s2p^2$) for the two resonances seems well established. In fact, Nicolaides (private communication) finds that the $2s^22p$ configuration contributes 73% to the square of the wave function of the ^2P resonance, with the remainder in terms like $2p^3$ and $2s2pnd$. For the ^2D resonance, the leading term, $2s2p^2$, contributes 83%, with the remainder in terms such as $2s^2nd$ and $2p^2nd$.

Figure 31 shows an energy level diagram in the region 57–60 eV. The ^2P and ^2D resonances can decay by the emission of a single electron into various excited states of helium. Decay into the 2^3S, 2^1S, and 2^1P states has been studied by Simpson, Menendez, and Mielczarek (1966) whose data are shown in Fig. 32.

The same resonances can also decay by the emission of two electrons, yielding $He^+ + 2e$. This type of decay has been found by Burrow and Schulz (1969) by studying the interference of zero-energy electrons produced in the two-electron decay. The trapped-electron method was used for these studies. This two-electron decay also causes structure when one observes the energy dependence of the formation of He^+, as was done by Grissom, Compton, and Garrett (1969). Quéméner, Paquet, and Marmet (1971) have improved the sensitivity for the detection of structure in positive ion curves by several orders of magnitude. Their results are shown in Fig. 33. An analysis of the peak shapes yields, for the ^2P state, $\Gamma = 0.045 \pm 0.007$ eV ($q = -0.75 \pm 0.12$) and, for the ^2D state, $\Gamma = 0.025 \pm 0.010$ eV ($q = -0.95 \pm 0.25$). Here, Γ is the width of the state and q is the "line profile index" (see Sec. I).

An unusual feature has been recently observed in the 2^3S excitation cross section near 50 eV by Crooks *et al.* (1972). When the energy dependence of the differential cross section for the electrons having excited the 2^3S state is examined around 90 degrees, a precipitous dip in the cross section is observed near 50 eV. Such behavior is reminiscent of interference phenomena, and calculations show (Macek and Wooten, unpublished) that the s and d waves exhibit interference. When the differential cross sections for excitation to the 2^3S state are integrated, the resulting total cross section exhibits a peak near 50 eV, which is 15 eV wide. Crooks *et al.* interpret this peak in terms of a p-wave resonance. It therefore appears that near 50 eV in helium, there is interference of partial waves and, in addition, a broad resonance.

The resonance itself could be understood by con-

sidering a state of He^- in which the three electrons comprising He^- are equidistant from the nucleus. Such a quasistationary state was calculated by Herzenberg and Ton-That (1973) to exist around 45.9 eV. It is of a similar nature as the state of H^{--} discussed in Sec. IIC, with the wave function having no radial nodes. The $2s^22p$ state at 57.16 eV, which has the same ^2P symmetry, has a radial node in each of the $2s$ factors.

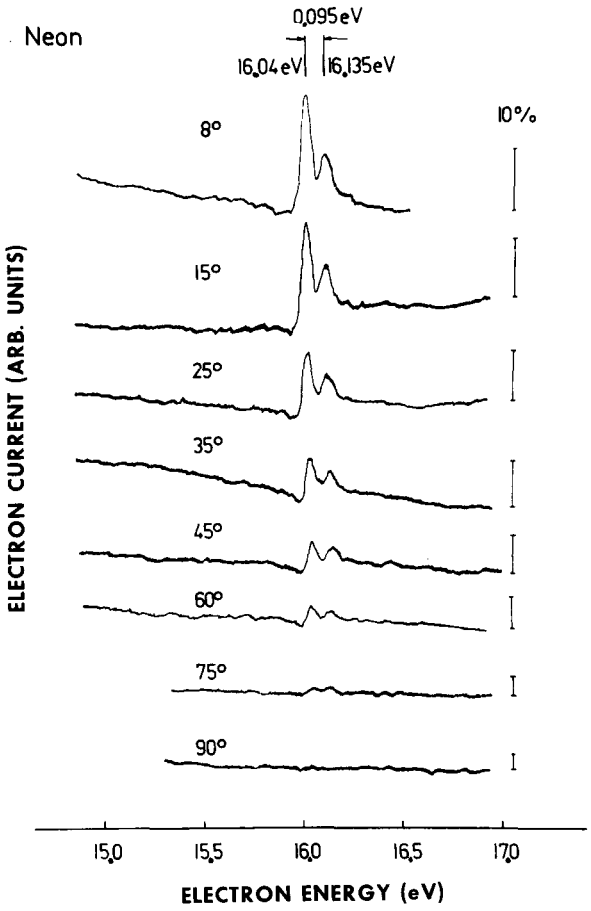

FIG. 36. Elastic cross section vs electron energy at designated angles of observation in neon. The vertical bars designate a 10% change in cross sections. The angular dependence of the resonances is characteristic of the p wave. [From Andrick and Ehrhardt (1966).]

IV. NEON, ARGON, KRYPTON, AND XENON

The rare gases Ne, Ar, Kr, and Xe exhibit marked similarities in terms of their resonances so that it is appropriate to consider them under a single heading.

A. Resonances Below the Ionization Potential

The first resonances in all the rare gases discussed in this section consist of two s electrons attached to the positive ion core (Simpson and Fano, 1963). Since the positive ion core is a doublet ($J=\frac{1}{2}$ and $J=\frac{3}{2}$), the resonances are also split. In fact, the splitting of the resonances is in very good agreement with the splitting

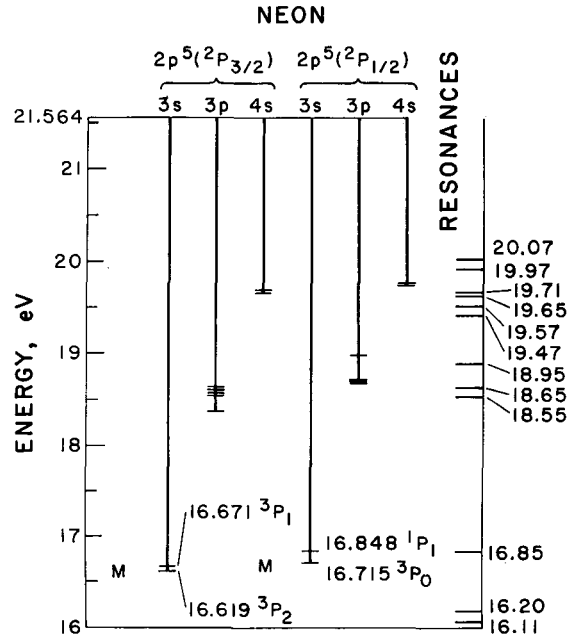

FIG. 37. Energy level diagram for neon, showing states of neon and the associated resonances. The values for the resonances are taken from Sanche and Schulz (1972) and a comparison with other values is shown in Appendix V. Metastable states are denoted by the letter M.

of the ion core, as shown in Table II, where comparison is made between the two available experiments on resonances and the known splitting of the ion core. The agreement between the splitting of the resonances and the positive ion core assures that the designations advanced by Simpson and Fano (1963) are correct. Thus, the lowest resonances in Ne, Ar, Kr, and Xe have

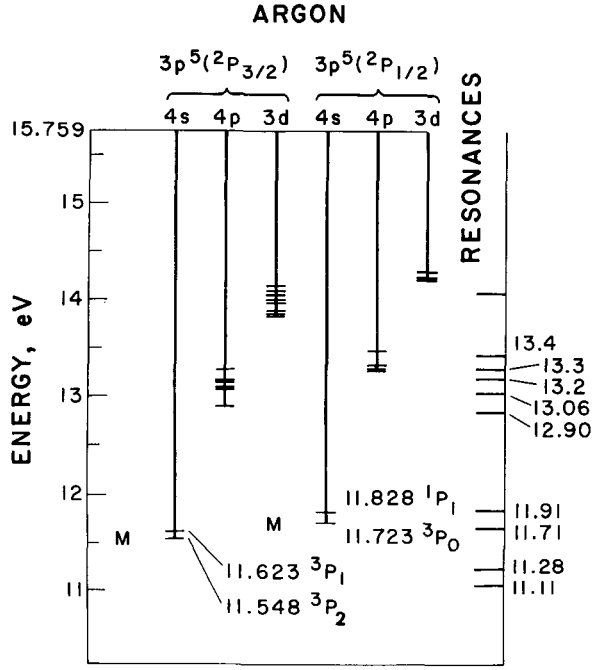

FIG. 38. Energy level diagram for argon. Numerical values are listed in Appendix VI.

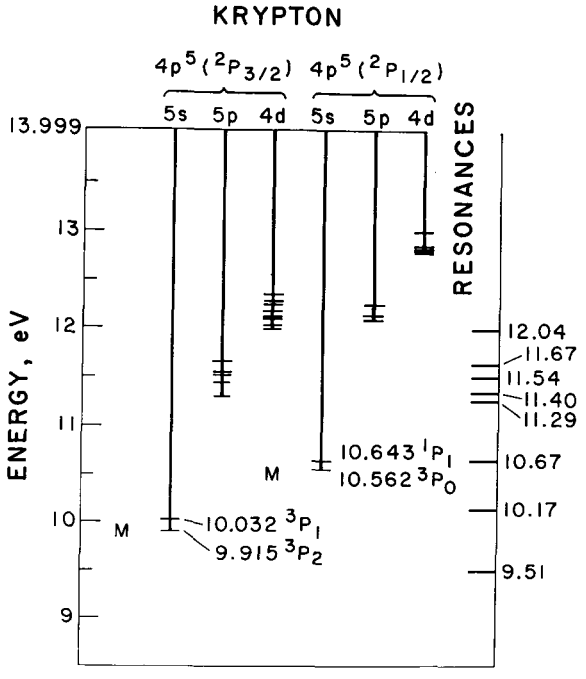

FIG. 39. Energy level diagram for krypton. Numerical values are listed in Appendix VII.

the form $(2p^53s^2)$, $(3p^54s^2)$, $(4p^55s^2)$, and $(5p^56s^2)$, respectively, each resonance being split by the amount indicated in Table II into a $^2P_{3/2}$ and a $^2P_{1/2}$ component.

Just as in the case of helium, our knowledge of resonances in Ne, Ar, Kr, and Xe comes from transmission experiments (Kuyatt *et al.*, 1965; Sanche and Schulz, 1972), from experiments on total metastable production (Olmsted *et al.*, 1965; Pichanick and Simpson, 1968) and from differential elastic scattering ex-

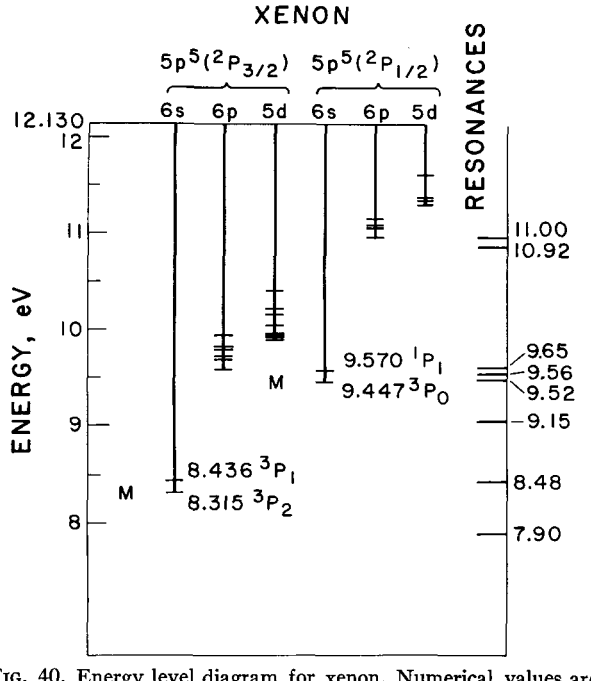

FIG. 40. Energy level diagram for xenon. Numerical values are listed in Appendix VIII.

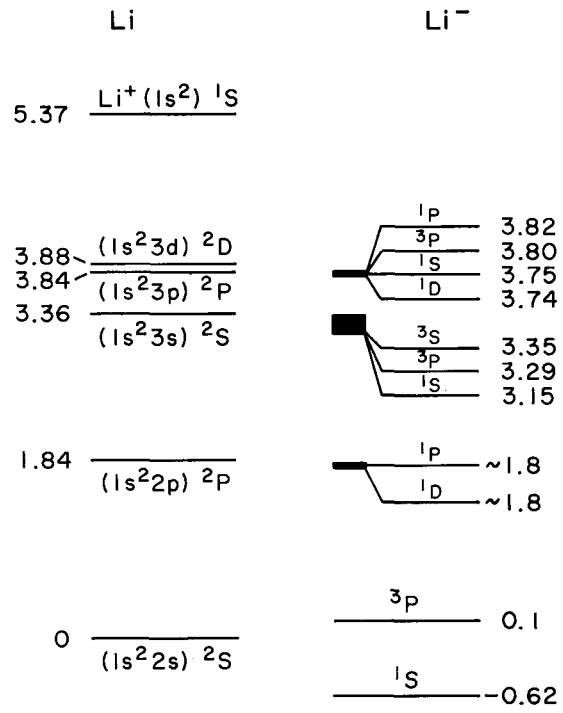

FIG. 41. Approximate energy level diagram for lithium and the compound states calculated theoretically. Values for the compound states are taken mainly from the work of Moores and Norcross (1972) and Fung and Matese (1972). The energy values, in eV, are only approximate. The electron affinity is taken from Weiss (1968).

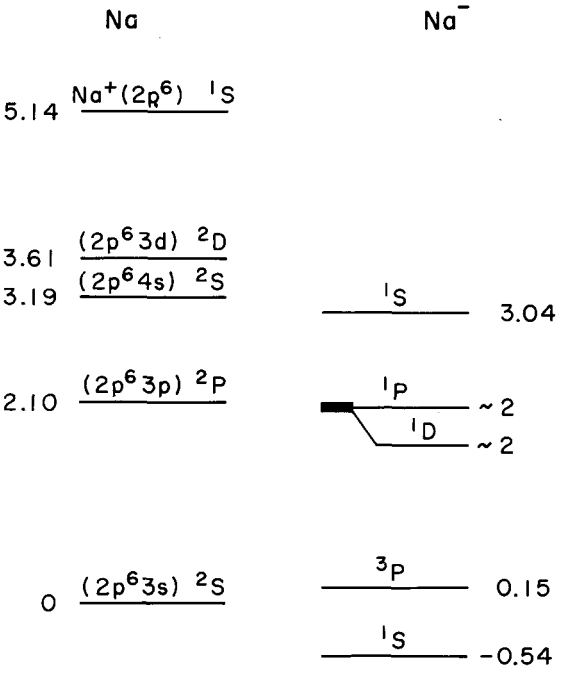

FIG. 42. Approximate energy level diagram for sodium and the compound states calculated theoretically. Values for the compound states are taken mainly from the work of Moores and Norcross (1972) and Fung and Matese (1972). The energy values, in eV, are only approximate. The electron affinity is taken from Weiss (1968), whose calculated value of 0.539 eV is in excellent agreement with recent photodetachment experiments of Hotop, Patterson, and Lineberger (0.542±0.01 eV).

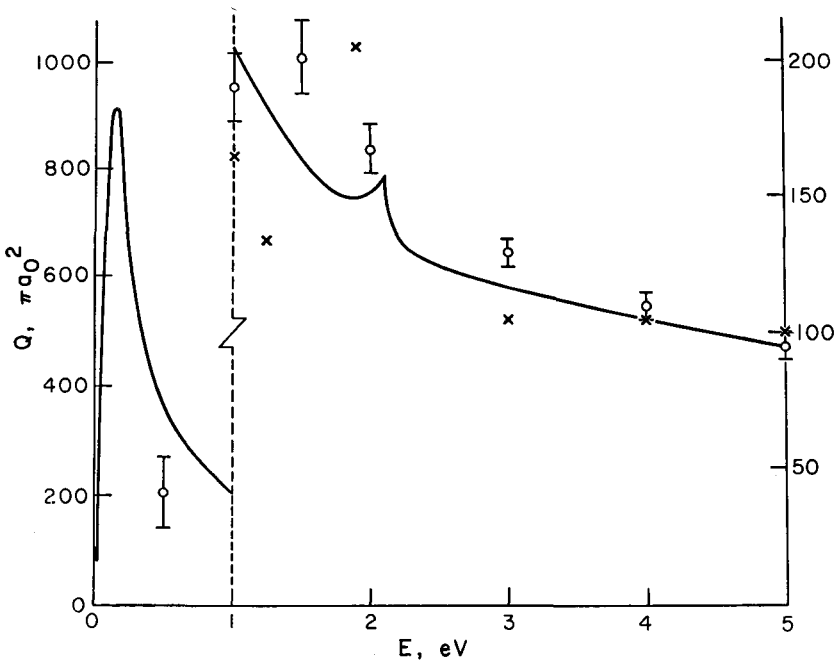

FIG. 43. Total cross section for scattering of electrons by sodium. Full curve—theory of Moores and Norcross (1972); ×—experiment of Brode (1929) divided by two; O—experiment of Perel, Englander, and Bederson (1962) normalized to theory at 5 eV. [From Moores and Norcross (1972).]

periments (Andrick and Ehrhardt, 1966). The information in these rare gases is more limited than in the case of He, since information on the excitation of electronically excited states of these gases is only now becoming available (Swanson *et al.*, 1971, 1973). Optical experiments with a good energy resolution in the electron beam are also very sparse [Sharpton *et al.* (1970) observe a sharp structure in photon emission at 18.6 eV in neon.]

Figures 34–36 show the experimental evidence for resonances in neon, and Fig. 37 shows an energy level diagram of Ne with the resonances included. Appendix V gives a comparison between the available experiments in tabulated form. A clearcut assignment of the higher-lying compound states is not yet available. The characteristics of Ar, Kr, and Xe are similar to those of neon. Energy level diagrams are shown in Figs. 38–40 and the energy values are listed in Appendixes VI–VIII.

B. Resonances above the Ionization Potential

Above the ionization potential of Ne, Ar, Kr, and Xe, a number of features have been detected, some of which are undoubtedly resonances associated with singly excited states of the neutral atom. The energy range of these features spans the regions 42–50 eV in Ne, 24–32 eV in Ar, 22–27 eV in Kr, and 18–20 eV in Xe. These features are discussed in connection with the transmission experiment by Sanche and Schulz (1972), in connection with the trapped-electron method by Grissom, Garrett, and Compton (1969), and in connection with positive ion detection by Bolduc, Quéméner, and Marmet (1972). The reader is referred to these papers for an up-to-date discussion and for a list of previous references. One of the difficulties inherent in these studies lies in distinguishing between resonances and the onset of highly excited autoionizing states of the neutral atom. Thus one has to rely heavily on measurements of the structure in the photoionization continuum, which provides the location of optically allowed transitions to highly excited states (see, e.g., Ederer, 1971). Some of the energies at which resonances are believed to occur in Ne and Ar are listed in Appendix IX.

V. LITHIUM AND SODIUM

Electron scattering in alkali atoms has been of considerable interest in the past years (Bederson and Kieffer, 1971), but high-resolution experiments with monochromatic electron beams have only recently become available. Thus much of our knowledge regarding resonances in these atoms comes from theory. There is general agreement that at low energies ($\sim$0.15 eV) the spin exchange cross section in both Li and Na has a sharp rise (Karule, 1965; Burke and Taylor, 1969; Norcross, 1971; Moores and Norcross, 1972). This sharp rise is attributed to the existence of a ^3P compound state at about 0.15 eV. The width of this resonance is believed to be relatively large ($>$0.1 eV). The ^3P resonance also affects the phase shift of the elastic cross section (Moores and Norcross, 1972). The elastic cross section calculated from these phase shifts agrees with the cross section measured by Rubin *et al.* (unpublished).

In the vicinity of the $(1s^22p)^2P$ state of lithium, two resonances, ^1D and ^1P, are postulated (Burke and Taylor, 1969). For reasons which are not entirely clear, Fung and Matese (1972) do not find these states using their multiconfiguration Hartree–Fock method; possibly the width of these states is too large. However Fung and

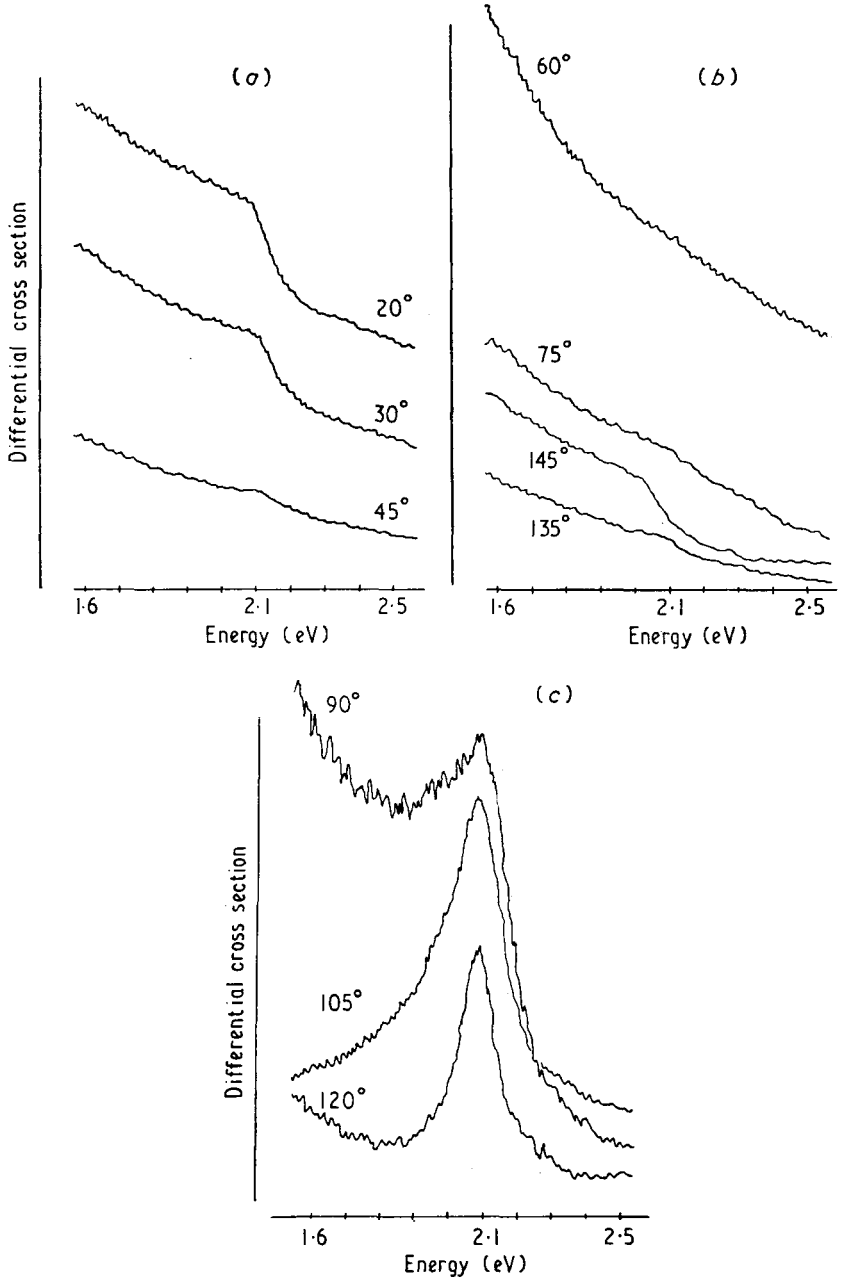

FIG. 44. Differential experimental cross section for elastic scattering of electrons on sodium. The angle of observation is indicated. Scales (b) and (c) are expanded with respect to scale (a) by factors of 3.7 and 25, respectively. [From Andrick, Eyb, and Hofmann (1972).]

Matese find three compound states lying below the $(1s^23s)^2S$ state and four states below the $(1s^23p)^2P$ state of Li. A schematic diagram, constructed from the results discussed above is shown in Fig. 41.

In sodium, an analogous situation prevails (Moores and Norcross, 1972) and the appropriate energy level diagram is shown in Fig. 42. Fung and Matese find only a single compound state in the 3-eV region of Na.

The existence of the ^1P and ^1D resonances just below the threshold of the first electronic state should dominate the excitation function to that state, and it appears that this is the case in Na (Enemark and Gallagher, 1972; Moores and Norcross, 1972).

The energy dependence of the total elastic and the differential elastic cross section in sodium exhibit a dramatic cusp at the energy of the ^2P state at 2.1 eV. This cusp is shown in Fig. 43 for the total cross section, as derived from the close-coupling theory of Moores and Norcross. The experimental results of Andrick, Eyb, and Hofmann (1972) for the differential elastic cross section are shown in Fig. 44. The close-coupling theory of Moores and Norcross is in very good agreement with the experiment. The structure shown in Figs. 43 and 44 is strongly influenced by the presence of the ^1P and ^1D states near 2 eV (Norcross and Moores, 1972).

It is noteworthy that the calculated cross sections for photodetachment of electrons from Li^- and Na^- in

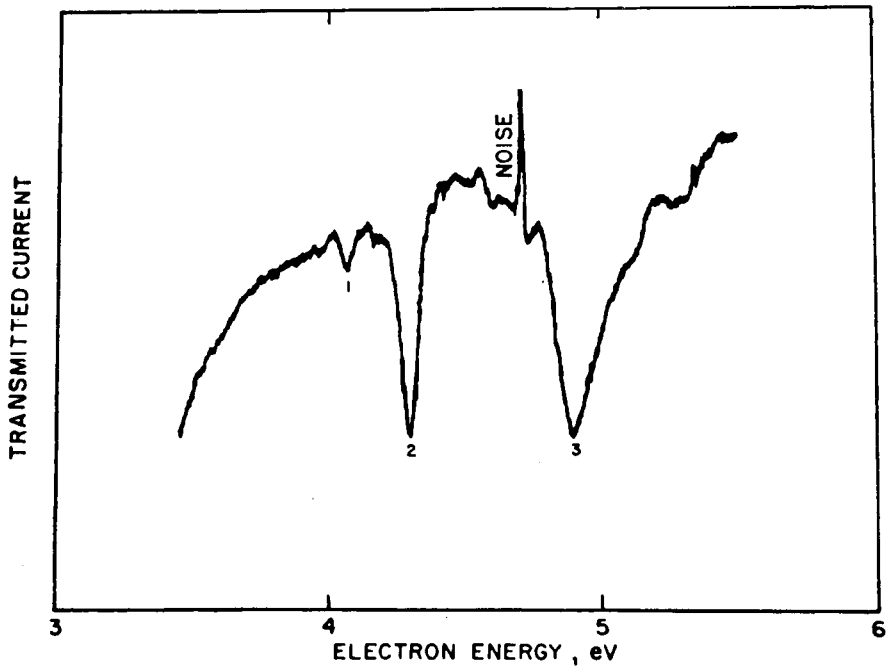

FIG. 45. Transmission experiment in Hg. The three low-lying resonances are clearly visible as dips in the transmitted current. [From Fano and Cooper (1965).]

their ground states show a sharp peak near 2 eV (Norcross and Moores, 1972). This effect is attributed to the presence of the ^1P resonance near the threshold of the first excited state of the neutral atom.

VI. MERCURY

Kuyatt, Simpson, and Mielczarek (1965) observe many resonances in their study of transmission of electrons through mercury. All resonances appear as dips in the transmitted current. An example of their data is shown in Fig. 45 and the positions of these resonances are shown on the energy level diagram of Fig. 46 in conjunction with the known electronically excited states of Hg. The lowest three resonances (marked 1, 2, 3) have been given the assignment $(6s6p^2)\,^4P_{1/2}$, $^4P_{3/2}$, $^4P_{5/2}$ (Fano and Cooper, 1965). The ground state of Hg is $(5d^{10}6s^2)\,^1S_0$.

Kuyatt *et al.* point out that the resonances at higher energies (near 8 eV) lie too high in energy to be attributed to higher levels (^2D, ^2S, ^2P) of the $6s6p^2$ configuration. Rather, Kuyatt *et al.* suggest that the parents of some of the resonances in the 8-eV region are

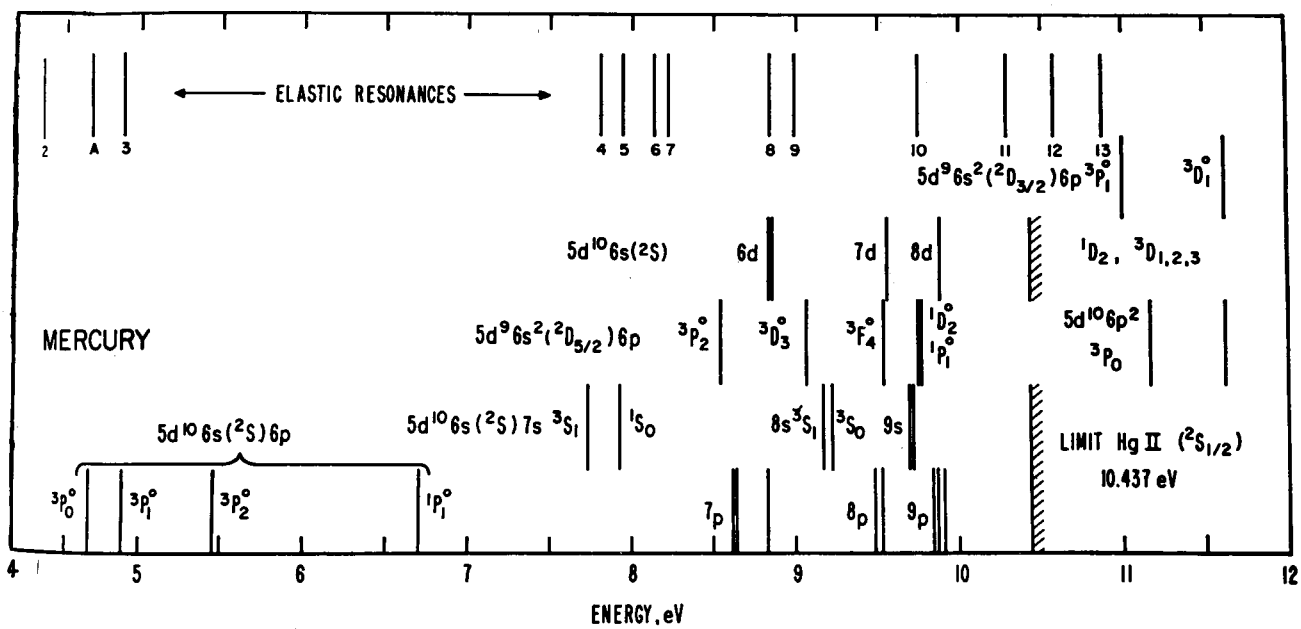

FIG. 46. Energy level diagram for Hg and the associated resonances. The resonances are numbered and their energies are listed in Appendix IX. [From Kuyatt, Simpson, and Mielczarek (1965).]

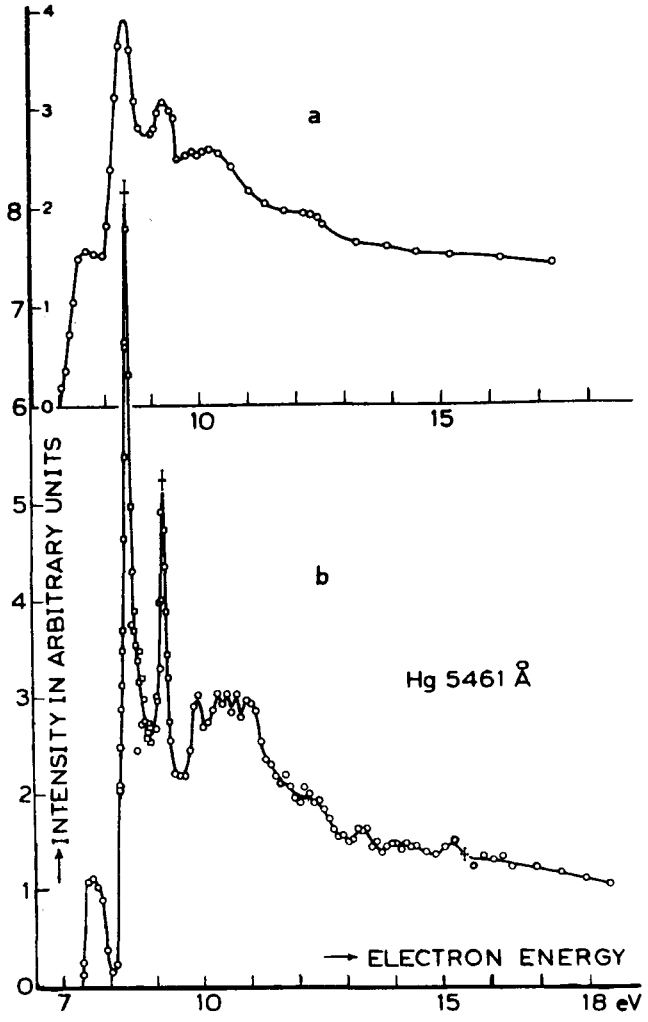

FIG. 47. Excitation function of the 5461-Å line of Hg. (a) Low-resolution results of Jongerius; (b) result obtained by Smit and Fijnaut (1965) using the retarding-potential difference method with a resolution of 0.1 eV. [From Smit and Fijnaut (1965).]

states of the configuration $5d^96s^26p$. The resonances would then have configurations such as $5d^96s^26p^2$.

The structures observed in transmission experiments can be compared with structures observed in optical excitation functions; care must be exercised in excluding structures resulting from sharp thresholds of higher energy levels which may contribute structure in low levels due to cascading.

Figure 47 shows the structure obtained by Smit and Fijnaut (1965) using a relatively narrow electron energy distribution (~0.1 eV) and observing the 5461-Å line in Hg. These results are in very good agreement with the work of Zapesochnyi and Shpenik (1966) who also used monoenergetic electrons for their observations and in addition to Hg (λ=2537 Å, 5461 Å, 3650 Å, 4916 Å) examined a wide variety of optical excitation functions in He, Zn, Cd, Na, and K. Zapesochnyi and Shpenik list the positions of the structure they observe. Appendix X compares their observed structures with the structures listed by Kuyatt *et al.* (1965). On the whole, there seems to be good agreement. It should be noted that Zapesochnyi and Shpenik interpret the observed structures in terms of cascading. However, it appears that the interpretation in terms of resonances could be equally valid.

VII. OXYGEN (O)

The determination of the location of compound states in atomic species which occur naturally as molecules is very difficult, as pointed out in connection with the discussion of atomic hydrogen. Normally, one attempts to form a beam of the atomic species and crosses this beam with monochromatic electrons. A novel method for measuring compound states has been recently presented by Edwards, Risley, and Geballe (1971) and applied to atomic oxygen. In this method, a beam of stable O^- ions with about 2 keV of kinetic energy is incident on a rare gas target (He) and the electrons resulting from this interaction are energy-analyzed and recorded. Structure in the energy spectrum of the electrons is observed and is associated with the existence of resonances. Figure 48 shows an example. The peaks in Fig. 48 seem to arise from the reaction

$$O^-+He\rightarrow O^{-*}+He\rightarrow O+He+e,$$

where O^{-*} denotes the compound state.

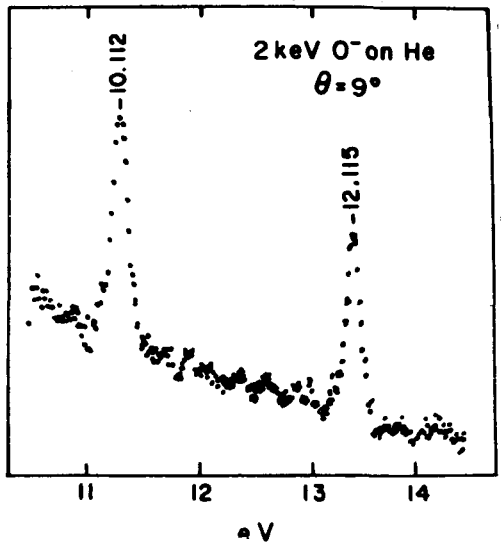

FIG. 48. Electron energy spectrum obtained after colliding a 2-keV beam of O^- with He. The electron energies given above the peaks are corrected for the velocity of O^- and are the proper energies for compound states. The peaks are interpreted as resulting from the formation of compound states up atomic oxygen. [From Edwards, Risley, and Geballe (1971).]

Since the electrons are ejected from a moving O^- particle, the measured electron energy must be corrected, and the "unshifted" energy must be determined. The energies indicated above the peaks of Fig. 48 refer to these corrected, "unshifted" values. Edwards *et al.* calibrate their energy scale by observing the reactions O^-+H_2 and O^-+Ar. In the former reaction, electrons resulting from compound states $H^-(^1D)$ at 10.13 eV and from $H^-(^1S)$ and $H^-(^3P)$ were observed, although the latter two states could not be clearly resolved. In the reaction O^-+Ar, the two low-lying resonances of Ar could be observed, and in fact the observed splitting (173 meV) is in agreement with other experiments (see Table II). These calibration experiments establish the reliability of the observations in oxygen. The energy level diagram of Fig. 49 shows schematically the configuration suggested by Edwards *et al.* to interpret their observations.

In order to test the results of the above experiment, Ormonde, Smith, Torres, and Davies (1973) performed a multi-configuration close-coupling calculation. They calculate elastic and inelastic cross sections and search for resonances. The ^3P and ^3D terms, which are possible parents for resonances are retained in the theory. A single resonance is found at 10.38 eV (0.25 eV above the experimental value quoted above), with a width of 20 meV. The discrepancy between theory and experiment in the energy of the resonance is attributed by Ormonde *et al.* (1973) to limitations of the theory. The assignment of the resonance given by Edwards *et al.* (1971) does not appear to be altered by the results of the theory.

A search for the higher-lying resonance (12.115 eV) found experimentally by Edwards *et al.* was also undertaken by Ormonde *et al.* (1973) using the close-coupling theory. No sharp resonances were found, but a shape resonance in the $^2P^\circ$ partial wave was found near 11.5 eV, with a width about 1 eV. This shape resonance is probably in addition to the sharp structure at 12.115 eV found by Edwards *et al.*

Very recently, Matese, Rountree, and Henry (1973) undertook a configuration-interaction study of doublet resonances in atomic oxygen. They calculate the following levels of O^-:

$2p^3(^4S^0)3s3p(^2P)$ at 9.50 eV,

$2p^3(^2D^0)3s^2(^2D^0)$ at 12.05 eV,

$2p^3(^2P^0)3s^2(^2P^0)$ at 13.65 eV,

$2p^3(^4S^0)3p^2(^2P^0)$ at 10.87 eV.

A reasonable estimate of possible errors in the above-quoted energies is ± 0.1 eV. Matese *et al.* suggest that the 12.115-eV peak observed experimentally by Edwards, Risley, and Geballe corresponds to the $2p^3(^2D^0)3s^2(^2D^0)$ state, thus confirming the original assignment for the upper state of Edwards *et al.*, as plotted on Fig. 49.

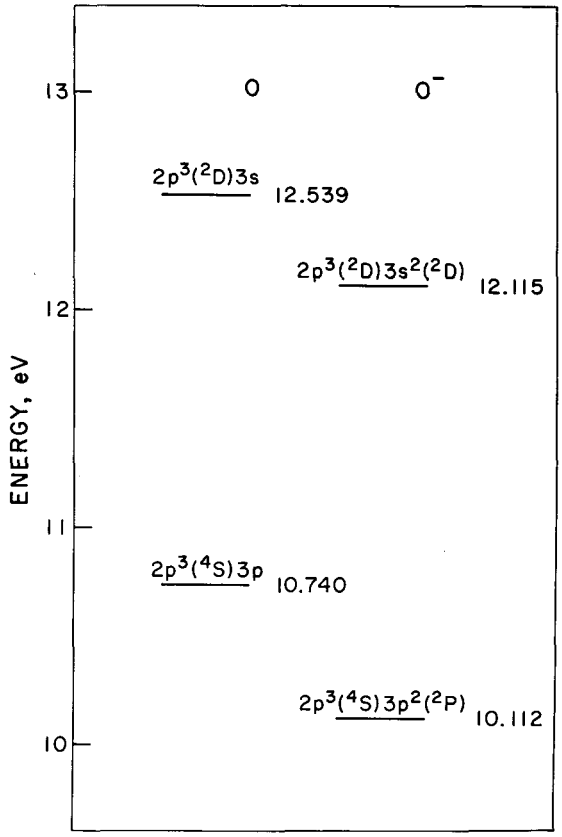

FIG. 49. Energy level diagram for O and O^-, invoked by Edwards *et al.* (1971) to interpret the data of Fig. 48. The two states of O are considered to be parents of the compound states (O^-) indicated. Energies are given in eV. The interpretation must be considered preliminary.

ACKNOWLEDGMENTS

The author is very grateful to U. Fano, F. Linder, L. J. Kieffer, C. E. Kuyatt, A. V. Phelps, and H. S. Taylor, all of whom read portions of the manuscript and generously supplied many comments and corrections. A portion of this review was written at JILA, University of Colorado, Boulder and the author is grateful for the hospitality of the JILA staff, and for the excellent editorial services rendered by Mrs. Lorraine Volsky and her staff. The author also wishes to acknowledge the support he received, at various stages, from the Westinghouse Research Laboratories, the National Science Foundation, the Army Research Office, and the Office of Naval Research. To his colleagues at Yale, particularly to A. Herzenberg, P. D. Burrow, M. J. W. Boness, and L. Sanche go thanks for many stimulating discussions and for help in unravelling the many effects described in this paper. To his wife, Rose, go thanks for her acquiescence that resonances should take precedence over a lot of other things.

APPENDIX I

Resonances in H (below $n=2$).

State	Energy (eV)	Width (eV)	Method	Author
^1S	9.61	0.109	cc	Burke and Schey (1962), Smith *et al.* (1962)
	9.559		var	O'Malley and Geltman (1965)
	9.557		var	Bhatia *et al.* (1967)
	9.56			Gailitis (1965)
	9.55			Holøien and Midtdal (1966)
	9.56	0.048		Burke and Taylor (1966)
	9.575	0.0543	cc	Burke (1968)
	9.560	0.0475	ccc	Burke (1968)
	9.587	0.0501	ps. st.	Burke, Gallaher, and Geltman (1969)
	9.56±0.01	0.043±0.006	Exp	McGowan (1967)
	9.558±0.01		Exp	Sanche and Burrow (1972)
^1S	10.178		var	O'Malley and Geltman (1965)
	10.177		var	Bhatia *et al.* (1967)
	10.178	0.00241	cc	Burke (1968)
	10.178	0.00219	ccc	Burke (1968)
^3S	10.149		var	O'Malley and Geltman (1965)
	10.146		var	Bhatia *et al.* (1967)
	10.151	1.89×10^{-5}	cc	Burke (1968)
	10.150	2.06×10^{-4}	ccc	Burke (1968)
^1P	10.178		var	O'Malley and Geltman (1965)
	10.179	2.26×10^{-5}	cc	Burke (1968)
	10.177	4.50×10^{-5}	ccc	Burke (1968)
^3P	9.727		var	O'Malley and Geltman (1965)
	9.731		var	Bhatia *et al.* (1967)
	9.768	0.00797	cc	Burke (1968)
	9.740	0.00594	ccc	Burke (1968)
	9.759	0.00571	ps. st.	Burke, Gallaher, and Geltman (1969)
	9.71±0.03	>0.009	Exp	McGowan (1967)
	9.73±0.12		Exp	Kleinpoppen and Raible (1965)
	9.70±0.15		Exp	Schulz (1964)
	9.738±0.01	0.0056±0.0005	Exp	Sanche and Burrow (1972)
^1D	10.160	0.0078	cc	Burke (1968)
	10.125	0.0088	ccc	Burke (1968)
	10.128±0.01	0.0073±0.002	Exp	Sanche and Burrow (1972)
	10.13±0.015		Exp	Ormonde *et al.* (1969)
^3P	10.194	0.0008	cc	Ormonde *et al.* (1969)
	10.190	0.0002	6-state	Ormonde *et al.* (1969)
	10.198		var	O'Malley and Geltman (1965)
^3S	10.202		var	O'Malley and Geltman (1965)
^1P	10.203		var	O'Malley and Geltman (1965)

Abbreviations: cc: close-coupling calculations. ccc: close-coupling plus correlation. ps.st: pseudo-state calculations. var: variational calculations. Exp: experiment.

APPENDIX II

Values for the $1s(2s)^2\,{}^2S$ resonance in helium.

Energy	Width	Method	Author
		Experiment	
19.30±0.05	...	72° elastic	Schulz (1963)
19.31±0.03	...	Transmission	Kuyatt *et al.* (1965)
19.285±0.025	...	Total (elastic)	Golden and Bandel (1965)
19.3±0.1	...	90° elastic	McGowan (1965)
19.30±0.01	0.008	Transmission	Golden and Zecca (1970, 1971)
19.34±0.02	...	Transmission	Sanche and Schulz (1972)
19.35±0.02	...	90° elastic	Mazeau *et al.* (1972)
	0.008	Differential	Gibson and Dolder (1969)
	0.015–0.020	Differential	Andrick and Ehrhardt (1966)
19.355±0.008	...	Differential	Cvejanovic *et al.* (1973)
		Theory	
19.5(+0.1, −0.2)	0.008 0.03	Variational	Kwok and Mandel (1965)
19.33	0.039	Close-coupling	Burke *et al.* (1966)
19.67	...	Variational	Young (1968)
19.3	...	Stabilization	Eliezer (1970)
19.34	...	Bound-state	Weiss and Krauss (1970)
19.69	...		Perkins (1971)
19.363	0.014	Quasi-projection	Temkin *et al.* (1972)
19.4	0.015	Variational	Sinfailam and Nesbet (1972)

APPENDIX III

Position of resonances below ionization in helium (eV).

	Transmission experiments		Metastable production	Differential	
Feature number (Fig. 13)	Sanche and Schulz (1972)	Kuyatt *et al.* (1965)	Pichanick and Simpson (1968)	Ehrhardt and co-workers	Designation
1–1′	19.30–19.37	19.31–19.37 19.43–19.47			2^2S
2–2′	19.80–19.90	19.818			Wigner cusp+2^3S
			20.34	20.45	2^2P
3–3′	20.58–20.62	20.59			Wigner cusp+2^1S
			20.99	21.00	2^2D
4	21.19				
		21.50–21.55			
5–5′–5″	22.34–22.42–22.50	22.34–22.39	22.44	22.42	3^2S
6–6′–6″	22.60–22.65–22.73	22.54–22.60	22.55/22.67	22.55/22.60	3^2P
7–7′–7″	22.88–22.92–22.97	22.81–22.85	22.75/22.86	22.75/22.85	
8	23.05		23.05		
9–9′	23.35–23.43	23.30–23.44	23.39		$n=4$
10–10′	23.48–23.55	23.49			
11–11′–11″	23.82–23.88–23.93	23.75–23.82			$n=5$
12	24.03				

APPENDIX IIIa

Larger structures in the optical excitation functions of He.

Preliminary data.

Energy eV	Wavelength of observation (Å)	Ref.	Possible designation
22.96	7065	(a)	4^2S
23.12	7065	(a)	
23.25	7065	(a)	
23.31	7065	(a)	
23.47–23.62	3889	(b)	$^2P(?)$
23.41	5876	(a)	
23.50	5876		
23.86	5876	(a)	
	4472	(a)	
	4922	(a)	
23.94	5876	(a)	
	4472	(a)	5^2S
	5047	(c)	
	4713	(c)	
24.0	4472	(a)	
	4922	(a)	
	3188	(b)	
24.08	5047	(a)	
	4713	(a)	

Transition	3^3S–2^3P	3^3D–2^3P	4^3D–2^3P	4^1D–2^1P
Wavelength (Å)	7065	5876	4472	4922
Transition	4^1S–2^1P	4^3S–2^3P	3^3P–2^3S	4^3P–2^3S
Wavelength (Å)	5047	4713	3889	3188

[a] Kurepa and Heddle (1972).
[b] Kisker (1972b).
[c] Heddle, Keesing, and Kurepa (1973).

The data have been arbitrarily selected by the author to indicate the main peaks observed in optical spectra. Many more, smaller structures have been reported. This table must therefore be considered preliminary, subject to change. This does not apply to the structures for which the wavelength is *underlined*. These are large and well-defined. The structure for which the wavelength is doubly underlined is "enormous".

APPENDIX IV

Position of resonances above the ionization potential in He.

Authors	$(2s^22p)^2P$	$(2s2p^2)^2D$
Experiments		
Kuyatt *et al.* (1965)	57.1±0.1	58.2±0.1
Golden and Zecca (1970)	56.7/56.93	57.87/58.08
Burrow and Schulz (1969)	56.93±0.1	58.04±0.1
Sanche and Schulz (1972)	57.16±0.05	58.25±0.05
Quéméner *et al.* (1971)	57.15±0.04	58.23±0.04
Grissom *et al.* (1969)	57.21	58.31
Theories		
Eliezer and Pan (1970) (stabilization)	57.3	58.3
Nicolaides (1972) (projection and correlation)	57.3	58.4

APPENDIX V

Position of resonances in neon (eV).

Feature designations[a]	Transmission experiments: Sanche and Schulz (1972)	Transmission experiments: Kuyatt *et al.* (1965)	Metastable production: Pichanick and Simpson (1968)	Designation
1–1′	16.10–16.12[c]	16.04		$(2p)^5(3s)^2\,{}^2P_{3/2}$
2–2′	16.19–16.22[c]	16.135		$(2p)^5(3s)^2\,{}^2P_{1/2}$
3–3′(*A*)	16.85–16.91		16.92	
...	...	18.18		
...	...	18.29		
4(*B*, *C*)	18.55	18.46	18.35–18.43	Optical excitation[b] 5852 Å
5–5′(*D*, *E*)	18.65–18.70	18.56	18.58–18.66	Kisker (1972b)
6(*F*, *G*)	18.95		18.86–18.97	
7	19.47			19.50–19.54
8	19.57			19.60–
9	19.65			
10(*H*)	19.71		19.69	–19.70
				19.77–19.82
11–11′(*I*)	19.97–20.03		19.83	19.91–19.99
12–12′(*J*)	20.07–20.13		20.1	20.03–20.07
				–20.19
				20.60–20.64
				20.70–20.74

[a] The "feature designations" refer to Fig. 25 (numbers) and Fig. 26 (letters), respectively.

[b] The first energy refers to a maximum, the second to a minimum.

[c] The widths of the $^2P_{3/2}$, $^2P_{1/2}$ resonances have been deduced from experiment by Haselton (1973). He finds $\Gamma = 8.95 \pm 0.34$ meV.

APPENDIX VI

Position of resonances in argon (eV).

Transmission experiments: Sanche and Schulz (1972)	Transmission experiments: Kuyatt *et al.* (1965)	Metastable production: Pichanick and Simpson (1968)	Designation
11.10–11.13	11.064–11.094		$3p^54s^2\,{}^2P_{3/2}$
11.27–11.30	11.235–11.267		$^2P_{1/2}$
11.71		11.72	$3p^54s4p(?)$
11.91		11.88–11.98	$3p^54s4p(?)$
12.89–12.92		12.80–12.93	
12.95–13.06–13.11		13.08	
13.22–13.28		13.17–13.24	
13.33		13.37	
13.45–13.50		13.55	
14.03–14.07–14.10			

APPENDIX VII

Position of resonances in krypton (eV).

Transmission exp.	Differential elastic and inelastic	Metastable production	
Sanche and Schulz (1972)	Swanson *et al.* (1973)	Pichanick and Simpson (1968)	Designation
9.50–9.53	9.52		$4p^5 5s^2\ ^2P_{3/2}$
10.16–10.19	10.14	10.05	$^2P_{1/2}$
10.66–10.69	10.67	10.63	
11.29	11.29	11.10–11.20	
11.40	11.42		
11.54		11.42	
11.67	11.67	11.70	
11.97–12.04–12.10	11.97	11.94–12.04	
	12.04	12.28	
	12.10	13.08	

Optical excitation experiments in krypton[a] (Kisker, 1972b).

4502 Å	4464 Å	4274 Å	4376 Å
12.90–12.95			
	12.93–13.00		12.97–13.04
	13.19–13.25	13.13–13.18	13.11–13.18
		13.23–	13.24–13.30
			13.36–

[a] Given are values for max–min.

Swanson, Cooper, and Kuyatt (1973) compare the resonances in krypton with optical absorption data of Rb I. Such a comparison leads them to interpret the resonances in the energy range 10.5 eV–12 eV (i.e., all but the two lowest states) as $4p^5 5s4d$ states. The $4p^5$ ion core can have $J=\frac{1}{2}$ or $\frac{3}{2}$.

APPENDIX VIII

Position of resonances in xenon (eV).

Transmission experiments		Metastable production	
Sanche and Schulz (1972)	Kuyatt *et al.* (1965)	Pichanick and Simpson (1968)	Designation
7.80–7.90–7.92	7.74–7.77		$5p^6 6s^2\ ^2P_{3/2}$
8.48			
9.11–9.26	9.02	9.0	$^2P_{1/2}$
9.52			
9.56		9.5	
9.65			
10.92	10.81–10.86	10.3	
11.00			

Appendix VIII—*Continued*

Optical excitation experiments[a] (Kisker, 1972c)

4624 Å	4671 Å	4079 Å	4583 Å	4734 Å
11.02–11.05				
11.12–11.15	11.11–		11.16–11.20	
11.22–11.31	–11.27			
11.40–11.46	11.39–11.45			
	11.53–11.58	11.51–11.55		
		11.61–11.65		
		11.83–11.90	11.75–11.87	11.81–11.95
			12.03–12.09	12.03–12.10
	12.13–12.23	12.19–12.28	12.20–12.27	–12.20

[a] In this table, the first energy corresponds to an observed maximum, the second energy value on the same line corresponds to an observed minimum.

APPENDIX IX

Suggested resonances in Ne and Ar.

Energy eV	Method	Observer	Designation
		Neon	
41.98	Transmission	Sanche and Schulz (1972)	
42.1	Trapped electrons	Grissom *et al.* (1969)	
43.05	Transmission	Sanche and Schulz (1972)	
44.35	Transmission	Sanche and Schulz (1972)	
44.25	Trapped electrons	Grissom *et al.* (1969)	
47.6	Transmission	Sanche and Schulz (1972)	
47.57	Trapped electrons	Grissom *et al.* (1969)	
		Argon	
24.44	Ar^+	Bolduc *et al.* (1972)	$3s3p^64s^2\ ^2S$
24.53	Transmission	Sanche and Schulz (1972)	
26.87	Transmission	Sanche and Schulz (1972)	
27.91	Transmission	Sanche and Schulz (1972)	
28.9	Transmission	Sanche and Schulz (1972)	

APPENDIX X

Position of resonances in mercury (eV).

Feature No. (Fig. 38)	Kuyatt *et al.* (1965) Transmission	Zapesochnyi and Shpenik (1966) 6^3P_1 $\lambda = 2537$ Å $E_x = 4.89$ eV	7^3S_1 5461 Å 7.73 eV	6^3D 3650 Å 8.9 eV	8^1S_0 4916 Å 9.2 eV	Fano and Cooper (1965) Designation
1	4.07	...	...	...	...	$(6s6p^2)^4P_{1/2}$
2	4.30	...	...	...	...	$(6s6p^2)^4P_{3/2}$
3	4.89	...	...	...	...	$(6s6p^2)^4P_{5/2}$
	...	5.0				
	...	5.3				
	...	5.6				
4	7.81					
5	7.94					
6	8.14					
7	8.22	8.5	8.2	...		
8	8.83	...	8.8	...		
9	8.99	9.0	9.0	9.1		
10	9.75	9.7	9.6	9.8	9.5	
11	10.29	10.0	10.2	10.2	10.2	
12	10.58	10.4	...	...	...	
13	10.88	...	...	...	...	
	...	11.2	11.1	11.1	11.4	
	...	...	11.9	11.7	11.9	
	...	...	...	~12.2	12.4	
	...	12.5	~12.5	12.6		

*The writing of this review was supported in part by the National Bureau of Standards, Office of Standard Reference Data, as part of the National Standard Reference Data Program.

Adams, A., and F. H. Read, 1972, J. Phys. E **5**, 156.
Andrick, D., and H. Ehrhardt, 1966, Z. Phys. **192**, 99.
Andrick, D., H. Ehrhardt, and M. Eyb, 1968, Z. Phys. **214**, 388.
Andrick, D., M. Eyb, and M. Hofmann, 1972, J. Phys. B **5**, L15.
Baranger, E., and E. Gerjuoy, 1957, Phys. Rev. **106**, 1182.
Barker, R. B. and H. W. Berry, 1966, Phys. Rev. **151**, 14.
Bauer, E., and N. H. Browne, 1964, in *Atomic Collision Processes*, edited by M. R. C. McDowell (North-Holland, Amsterdam), p. 16 (1964).
Baumann, H., E. Heinicke, H. J. Kaiser, and K. Bethge, 1971, Nucl. Instrum. Methods **95**, 389
Baz, A. I., 1957, Zh. Eksp. Teor. Fiz. **33**, 923. [Sov. Phys.-JETP **6**, 709.]
Bederson, B., 1968. Methods Exp. Phys. **7A**, 67.
Bederson, B., and L. J. Kieffer, 1971, Rev. Mod. Phys. **43**, 601
Bhatia, A. K., A. Temkin, and J. F. Perkins, 1967, Phys. Rev. **153**, 177.
Blatt, J. M., and V. F. Weisskopf, 1952, *Theoretical Nuclear Physics* (Wiley, New York, 1952).
Bolduc, E., J.J. Quéméner, and P. Marmet, 1971, Can. J. Phys. **49**, 3095.
Bolduc, E., J. J. Quéméner, and P. Marmet, 1972, J. Chem. Phys. **57**, 1957.
Brode, R. B., 1929, Phys. Rev. **34**, 673.
Burke, P. G., 1965, Advances in Physics, (Phil. Mag. Suppl.) **14**, 521.
Burke, P. G., 1968, Adv. At. Mol. Phys. **4**, 173.
Burke, P. G., J. W. Cooper, and S. Ormonde, 1966, Phys. Rev. Lett. **17**, 345.
Burke, P. G., 1969, Phys. Rev. **183**, 245.
Burke, P. G., D. F. Gallaher, and S. Geltman, 1969, J. Phys. B **2**, 1142.
Burke, P. G., S. Ormonde, and W. Whitaker, 1967, Proc. Phys. Soc. Lond. **92**, 319.
Burke, P. G., and H. M. Schey, 1962, Phys. Rev. **126**, 147.
Burke, P. G., and A. J. Taylor, 1966, Proc. Phys. Soc. Lond. **88**, 549.
Burke, P. G., 1969, J. Phys. B **2**, 869.
Burrow, P. D., 1970, Phys. Rev. A **2**, 1774.
Burrow, P. D., and G. J. Schulz, 1969, Phys. Rev. Lett. **22**, 1271.
Chamberlain, G. E., 1967, Phys. Rev. **155**, 46.
Chamberlain, G. E., and H. G. M. Heideman, 1965, Phys. Rev. Lett. **15**, 337.
Chamberlain, G. E., S. J. Smith, and D. W. O. Heddle, 1964, Phys. Rev. Lett. **12**, 647.
Comer, J., and F. H. Read, 1972, J. Phys. E **5**, 211.
Cooper, J. W., and J. B. Martin, 1962, Phys. Rev. **126**, 1482.
Crooks, G. B., R. D. DuBois, D. E. Golden, and M. E. Rudd, 1972, Phys. Rev. Lett. **29**, 327.

Kuyatt, C. E., and J. A. Simpson, 1967, Rev. Sci. Instrum. **38,** 103.
Kuyatt, C. E., 1968, Methods Exp. Phys. **7A,** 1.
Kwok, K. L., and F. Mandl, 1965, Proc. Phys. Soc. Lond. **86,** 501.
LaBahn, R. W., and J. Callaway, 1964, Phys. Rev. **135,** A1539.
Long, R. L., D. M. Cox, and S. J. Smith, 1968, J. Res. Natl. Bur. Stand. (U.S.) A **72A,** 521.
Macek, J., 1967, Proc. Phys. Soc. Lond. **92,** 365.
Macek, J., and P. G. Burke, 1967, Proc. Phys. Soc. Lond. **92,** 351.
Marriott, R., and M. Rotenberg, 1968, Phys. Rev. Lett. **21,** 722.
Massey, A. S. W., and E. H. S. Burhop, 1969, *Electronic and Ionic Impact Phenomena* (Oxford University Press, London), Vols. I and II.
Matese, J. J., S. P. Rountree, and R. J. W. Henry, 1973, Phys. Rev. A 7. 846.
Mazeau, J., F. Gresteau, G. Joyez, J..Reinhardt, and R. I. Hall 1972, J. Phys. B **5,** 1890.
McDaniel, E..W., 1964, *Collision Phenomena in Ionized Gases* (Wiley, New York).
McGowan, J. W., 1966, Phys. Rev. Lett. **17,** 1207.
McGowan, J. W., 1967, Phys. Rev. **156,** 165.
McGowan, J. W., 1970, Science **167,** 1083.
McGowan, J. W., E. M. Clarke, and E. K. Curley, 1965, Phys. Rev. Lett. **15,** 917.
McGowan, J. W., J. F. Williams, and E. K. Curley, 1969, Phys. Rev. **180,** 132.
Moores, D. L., and D. W. Norcross, 1972, J. Phys. B **5,** 1482.
Myerscough, V. P., 1965, Phys. Lett. **19,** 120.
Neynaber, R. H., E. W. Rothe, L. L. Marino, and S. M. Trujillo, 1961, Phys. Rev. **123,** 148.
Nicolaides, C. A., 1972, Phys. Rev. A **6,** 2078.
Norcross, D. W., 1971, J. Phys. B **4,** 1458.
Norcross, D. W., and D. L. Moores, 1972, *Atomic Physics III, Proceedings IIIrd International Conference on Atomic Physics,* Boulder (Plenum, New York).
Olmsted, J. III, A. S. Newton, and K. Street, Jr., 1965, J. Chem. Phys. **42,** 2321.
O'Malley, T. F., and S. Geltman, 1965, Phys. Rev. **137,** A1344.
Ormonde, S., J. McEwen, and J. W. McGowan, 1969, Phys. Rev. Lett. **22,** 1165.
Ormonde, S., K. Smith, B. W. Torres, and A. R. Davies, 1973 (to be published).
Ott, W. R., W. Kauppila, and W. L. Fite, 1970, Phys. Rev. A **1.** 1089.
Pavlovic, Z., M. J. W. Boness, A. Herzenberg, and G. J. Schulz, 1972, Phys. Rev. A **6,** 676.
Peart, B., D. S. Walton, and K. Dolder, 1970, J. Phys. B **3,** 1346.
Perel, J., P. Englander, and B. Bederson, 1962, Phys. Rev. **128,** 1148.
Perkins, J. F., 1971, Phys. Rev. A **4,** 489.
Phelps, A. V., 1955, Phys. Rev. **99,** 1307.
Pichanick, F. M. J., and J. A. Simpson, 1968, Phys. Rev. **168,** 64.
Quéméner, J. J., C. Paquet, and P. Marmet, 1971, Phys. Rev. A **4,** 494.
Read, F. H., 1970, J. Phys. E **3,** 127.
Read, F. H., 1971, J. Phys. E **4,** 562.
Rudd, M. E., 1964, Phys. Rev. Lett. **13,** 503.
Rudd, M. E., 1965, Phys. Rev. Lett. **15,** 580.
Sanche, L., and G. J. Schulz, 1972, Phys. Rev. A **5,** 1672.
Sanche, L., and P. D. Burrow, 1972, Phys. Rev. Lett. **29.** 1639.
Sawada, T., J. E. Purcell, and A. E. S. Green, 1971, Phys. Rev. A **4,** 193.
Schowengerdt, F. D., S. R. Smart, and M. E. Rudd, 1973,
Cvejanovic, S., J. Comer, and F. H. Read, 1973, in *Eighth International Conference on the Physics of Electronic and Atomic Atomic Collisions: Abstracts of Papers* (Belgrade, Yugoslavia).
Drake, G. W. F., 1970, Phys. Rev. Lett. **24,** 126.
Ederer, D. L., 1971, Phys. Rev. A **4,** 2263.
Edwards, A. K., J. S. Risley, and R. Geballe, 1971, Phys. Rev. A **3,** 583.
Ehrhardt, H., 1969, in *Physics of the One- and Two-Electron Atoms,* edited by F. Bopp and H. Kleinpoppen (North-Holland, Amsterdam, 1969).
Ehrhardt, H., L. Langhans, and F. Linder, 1968, Z. Phys. **214,** 179.
Ehrhardt, H., and K. Willmann, 1967, Z. Phys. **203,** 1.
Eliezer, I., and Y. K. Pan, 1970, Theor. Chim. Acta **16,** 63.
Enemark, E. A., and A. Gallagher, 1972, Phys. Rev. A **6,** 192.
Fano, U., 1961, Phys. Rev. **124,** 1866.
Fano, U. and J. W. Cooper, 1965a, Phys. Rev. **137,** A1364.
Fano, U., and J. W. Cooper, 1965b, Phys. Rev. **138,** A400.
Fleming, R. J., and G. S. Higginson, 1963, Proc. Phys. Soc. Lond. **81,** 974.
Fung, A. C., and J. J. Matese, 1972, Phys. Rev. A **5,** 22.
Gailitis, M., 1965, in *IVth International Conference in the Physics of Electronic and Atomic Collisions: Abstracts of Papers,* edited by L. Kerwin and W. Fite (Science Bookcrafters, Hastings-on-Hudson, N. Y.), p. 10.
Gailitis, M., and R. Damburg, 1963, Proc. Phys. Soc. Lond. **82,** 192.
Geltman, S., and P. G. Burke, 1970, J. Math. Phys. **3,** 1062.
Gibson, J.R., and K. T. Dolder. 1969, J. Phys. B **2,** 741.
Golden, D. E., and H. W. Bandel, 1965, Phys. Rev. **38,** A14.
Golden, D. E., and A. Zecca, 1970, Phys. Rev. A **1,** 241.
Golden, D. E., and A. Zecca, 1971, Rev. Sci. Instrum. **42,** 210.
Grissom, J. T., R. N. Compton, and W. R. Garrett, 1969, Phys. Lett. **30A,** 117.
Grissom, J. T., W. R. Garrett, and R. N. Compton, 1969, Phys. Rev. Lett. **23,** 1011.
Hall, R. I., J. Reinhardt, G. Joyez, and J. Mazeau, 1972, J. Phys. B **5.** 66.
Haselton, H. H., 1973, Bull. Am. Phys. Soc. **18,** 710.
Hasted, J. B., 1964, *Physics of Atomic Collisions* (Butterworths, London).
Hazi, A. U., and H. S. Taylor, 1970, Phys. Rev. A **1,** 1109.
Heddle, D. W. O., 1970, JILA Rept. 104 (University of Colorado, Boulder, Colo.).
Heddle, D. W. O., R. G. W. Keesing, and J. M. Kurepa, 1973, (to be published).
Herzenberg, A., 1971, Phys. Bull. Inst. Phys. Phys. Soc. Lond. **22,** 521.
Herzenberg, A., 1972 (private communication).
Herzenberg, A., and D. Ton-That, 1973 (to be published).
Herzenberg, A., K. L. Kwok, and F. Mandl, 1964, Proc. Phys. Soc. Lond. **84,** 345.
Holøien, E., 1960, J. Chem. Phys. **33,** 301.
Holøien, E., and J. Midtdal, 1966, J. Chem. Phys. **45,** 2209.
Karule, E. M., 1965, in *Atomic Collisions III,* edited by V. Ia. Veldre (Akad. Nauk Latv. SSSR, Inst. Fiz. English translation, JILA Information Center Report #3, University of Colorado 1966. Available through SLA translation center, John Crerar Library, Chicago, Ill. Translation # TT-66-12939.
Karule, E. M., 1970, J. Phys. B **3,** 860.
Kisker, E., 1972a. Phys. Lett. **38A,** 79
Kisker, E., 1972b, Z. Phys. **256,** 121.
Kisker, E., 1972c, Z. Phys. **257,** 51.
Kleinpoppen, H., and V. Raible, 1965, Phys. Lett. **18,** 24.
Klemperer, O., 1965, Rep. Prog. Phys. **28,** 77.
Kurepa, J. M., and D. W. O. Heddle, 1972, Proceedings of the VI Yugoslav Symposium on Physics of Ionized Gases.
Kuyatt, C. E., J. A. Simpson, and J. A. Mielczarek, 1965, Phys. Rev. **138,** A385.

Phvs. Rev. A 7, 560.
Schulz, G. J., 1959, Phys. Rev. **116,** 1141.
Schulz, G. J., 1963, Phys. Rev. Lett. **10,** 104.
Schulz, G. J., 1964a, Phys. Rev. Lett. **13,** 583.
Schulz, G. J., 1964b, Phys. Rev. **136,** A650.
Schulz, G. J., and R. E. Fox, 1957, Phys. Rev. **106,** 1179.
Schulz, G. J., and J. W. Philbrick, 1964, Phys. Rev. Lett. **13,** 477.
Sharpton, F. A., R. M. St. John, C. C. Lin, and F. E. Fajen, 1970, Phys. Rev. A **2,** 1305.
Shore, B. W., 1967, Rev. Mod. Phys. **39,** 439.
Simpson, J. A., 1964, Rev. Sci. Instrum. **35,** 1698.
Simpson, J. A., 1967, Rev. Sci. Instrum. **38,** 103.
Simpson, J. A., and U. Fano, 1963, Phys. Rev. Lett. **11,** 158.
Simpson, J. A., M. G. Menendez, and S. R. Mielczarek, 1966, Phys. Rev. **150,** 76.
Sinfailam, A. L., and R. K. Nesbet, 1972, Phys. Rev. A **6,** 2118.
Smit, C., and H. M. Fijnaut, 1965, Phys. Lett. **19,** 121.
Smith, K., 1966, Rep. Prog. Phys. **29,** 373.
Smith, K., R. P. Eachran, and P. A. Fraser, 1962, Phys. Rev. **125,** 553.
Stamatovic, A., and G. J. Schulz, 1970, Rev. Sci. Instrum. **41,** 423.
Sunshine, G., B. B. Aubrey, and B. Bederson, 1967, Phys. Rev. **154,** 1.
Swanson, N., J. W. Cooper, and C. E. Kuyatt, 1971, in *Electronic and Atomic Collisions*, Abstracts of Papers of the VIIth International Conference on the Physics of Electronic and Atomic Collisions (North-Holland, Amsterdam,), p. 323. See also, 1973, Phys. Rev. (to be published).
Taylor, A. J., and P. G. Burke, 1967, Proc. Phys. Soc. Lond. **92,** 336.
Taylor, H. S., 1970, Adv. Chem. Phys. **18,** 91.
Taylor, H. S., G. V. Nazaroff, and A. Golebiewski, 1966, J. Chem. Phys. **45,** 2872.
Taylor, H. S., and L. D. Thomas, 1972, Phys. Rev. Lett. **28,** 1091.
Temkin, A., 1957, Phys. Rev. **107,** 1004.
Temkin, A., A. K. Bhatia, and J. N. Bardsley, 1972, Phys. Rev. A **5,** 1663.
Walton, D. S., B. Peart, and K. Dolder, 1970, J. Phys. B **3,** L148.
Weiss, A. W., 1968, Phys. Rev. **166,** 70.
Weiss, A. W., and M. Krauss, 1970, J. Chem. Phys. **52,** 4363.
Wigner, E. P., 1948, Phys. Rev. **73,** 1002.
Young, A. D., 1968, J. Phys. B **1,** 1073.
Zapesochnyi, I. P., and O. B. Shpenik, 1966, Sov. Phys.-JETP **23,** 592.

Resonances in Electron Impact on Diatomic Molecules*

George J. Schulz

Department of Engineering and Applied Science, Mason Laboratory, Yale University, New Haven, Connecticut 06520

In this review we present the energies, configuration, and other properties of resonances (also called "compound states" and "temporary negative ions") in diatomic molecules. Much of the information is presented in the form of tables and energy level diagrams. Vibrational, rotational, and electronic excitation are discussed whenever these processes have given information on resonances; often these excitation processes proceed via resonances. The paper is divided according to molecular species (H_2, N_2, CO, NO, O_2), but the main conclusions are discussed by the nature of the processes involved.

Key words: Compound states; cross-sections; diatomic molecules, H_2, N_2, CO, NO, O_2; electron impact; electronic excitation; energy levels; resonances; rotational excitation; temporary negative ions; vibrational excitation.

CONTENTS

This paper is a continuation of the one immediately preceding, which deals with resonances occurring when electrons are incident on atoms. In the present paper we present a review of the energy levels, the designations, and the general properties of compound states in *diatomic molecules*. An attempt is made to present much of the information in the form of tables and energy level diagrams.

I. INTRODUCTION

Compound states are formed by the interaction of an incident electron with a target molecule in which the incident electron is temporarily captured in the neighborhood of the molecule. The complex thus formed can also be called a *temporary negative ion* or a *resonance*.

TABLE I. Semantics of resonances.

First name	Last name	Parent	Energy *vis a vis* parent	Some characteristics	Examples
Single-particle Shape (1 particle, 0 holes)	...	Ground electronic state	above (0–4 eV)	Vibrational excitation; dissociative attachment at low energy	N_2 (2.3 eV) H_2 (2–4 eV)
Core-excited Particle–hole (2 particles, 1 hole)	Feshbach; Type I; closed-channel	Mostly Rydberg excited state	below (~0.5 eV)	Bands correlated to grandparent; sharp structure; many decay channels	N_2 (11.48 eV) H_2 (Bands "a"–"g")
	Shape; Type II; open-channel	Rydberg or valence excited state	above (0–2 eV)	Dissociative attachment	N_2 (9–11 eV) H_2 (8–12 eV)
Doubly core-excited (3 particles, 2 holes)	Feshbach	Doubly excited Rydberg and valence states	below	Above ionization; 2-electron decay	He (57.16 eV)
	Shape		above		N_2 (22 eV)

The latter term indicates that the attachment of the electron often occurs at a definite energy, leading to sharp structures in the cross section. However, sometimes the lifetime of the compound state is so short that the *width* of the state, as given by the uncertainty principle, is large. The terms *compound state, temporary negative ion,* or *resonance* are used interchangeably and authors have even used superfluous nomenclatures such as "temporary negative ion resonance."

The first reference to the possibility that compound states might exist can be traced to a paper by Franck and Grotrian (1921). Experimental evidence for structure in the total cross section (e.g., N_2) became available shortly thereafter, but a resonance model was not

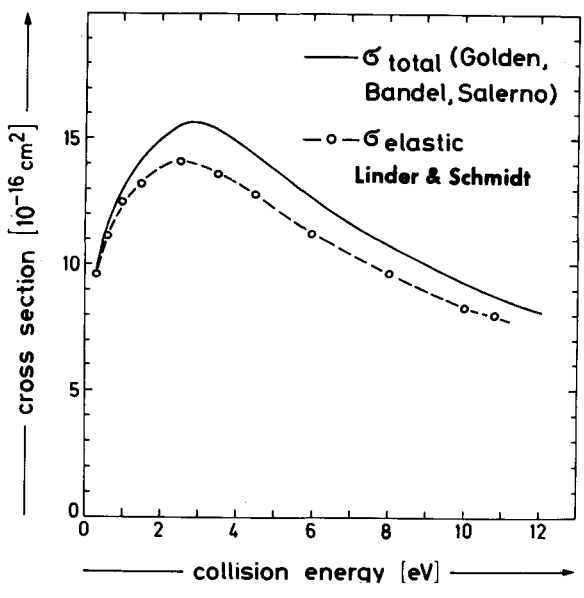

FIG. 1. Total cross section in H_2 (Golden *et al.*, 1966) and elastic portion alone (Linder and Schmidt, 1971a). The absolute magnitude of Linder's curve is normalized to Golden's value at the lowest energy. The difference between the two curves represents the sum of all inelastic cross sections. [From Linder and Schmidt (1971a).]

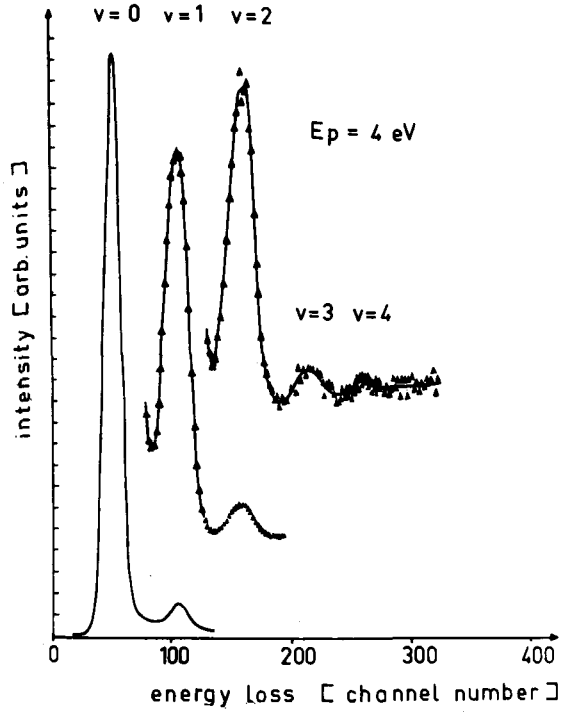

FIG. 2. Energy loss spectrum of 4-eV electrons after collision with H_2 molecules. The peak marked $v=0$ represents elastic scattering. The peaks marked $v=1$, 2, 3, and 4 represent the excitation of vibrational quanta of the neutral molecule via the short-lived negative ion state $^2\Sigma_u^+$. [From Ehrhardt, Langhans, Linder, and Taylor (1968).]

applied to these observations at that time. Although there was a need to understand such structures in the cross section and also the large vibrational cross sections observed experimentally (e.g., H_2), the resonance model remained confined for a long time to nuclear physics alone. The application of the resonance model to molecules in the early 1960's led to a rapid progress in our understanding of electron impact on molecules and solved many long-standing puzzles in atomic physics.

Compound states in molecules which have been observed to date have a lifetime in the range 10^{-10}–10^{-15} sec ($\tau=\hbar/\Gamma$, where τ is the lifetime and Γ is the width of the state). They decay by the emission of an electron into various final states which are accessible energetically. The beauty of molecules is the variety of decay

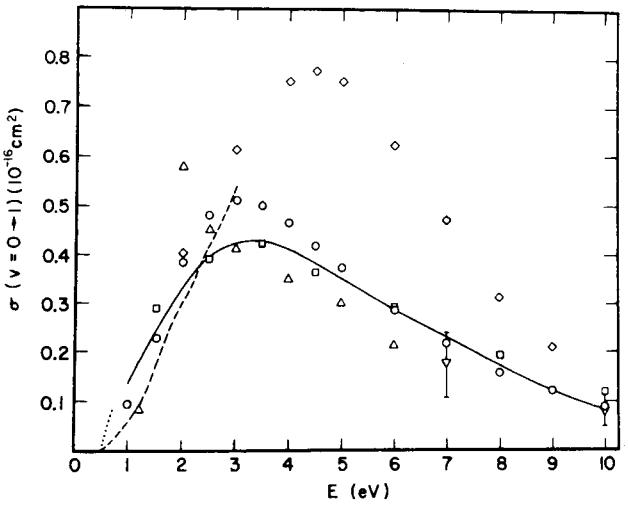

FIG. 3. Total vibrational cross section to $v=1$ in H_2. *Experimental results using double electrostatic analyzers*: □ Linder and Schmidt (1971a); ○ Ehrhardt *et al.* (1968); ▽ Trajmar *et al.* (1970); △ Schulz (1964). *Experimental results using swarms*: ◇ Engelhardt and Phelps (1963); - - - Crompton *et al.* (1970). *Experimental results using the trapped-electron method*: ··· Burrow and Schulz (1969). *Theory*: — Henry and Chang (1972). [From Henry and Chang (1972).]

channels that are possible for compound states: vibrational and rotational excitation, electronic excitation, elastic scattering, dissociative attachment, three-body attachment, and others. Often, a major portion of the cross section for these processes proceeds via a compound state. This is especially true in the case of vibrational excitation and in several instances of electronic excitation near threshold. Dissociative attachment can be completely understood in terms of the formation of a compound state which subsequently autoionizes and also separates into a neutral atom and a negative ion. The lifetime of the compound state, together with the separation time, determine the magnitude of the dissociative attachment cross section.

The preferential decay of some compound states into inelastic channels offers certain advantages for the

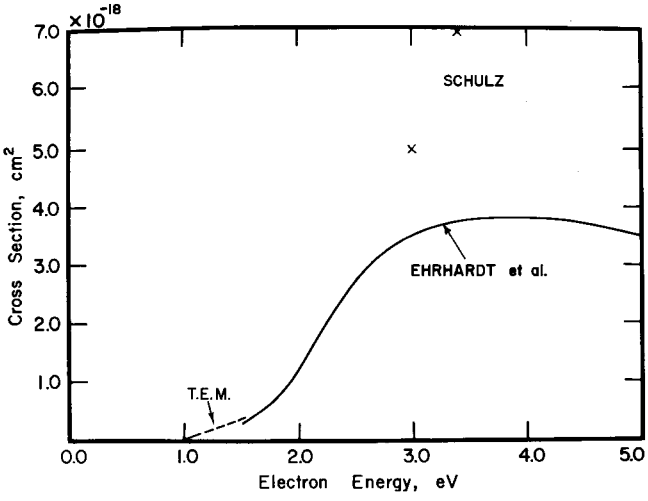

FIG. 4. Vibrational cross section to $v=2$ in hydrogen. The slope of the cross section near threshold is determined using the trapped electron method and is indicated by the dashed lines, marked TEM (Burrow and Schulz, 1969). Also shown are the double electrostatic analyzer data of Ehrhardt *et al.* (1968) and Schulz (1964a). [From Burrow and Schulz (1969).]

study of compound states. When the bulk of the inelastic cross section consists of the decay of the compound state, then the direct-scattering contribution is nearly absent and one can observe the resonant contribution alone, without interference with the nonresonant contribution. When one considers the Breit–Wigner formula, which governs the shape of single

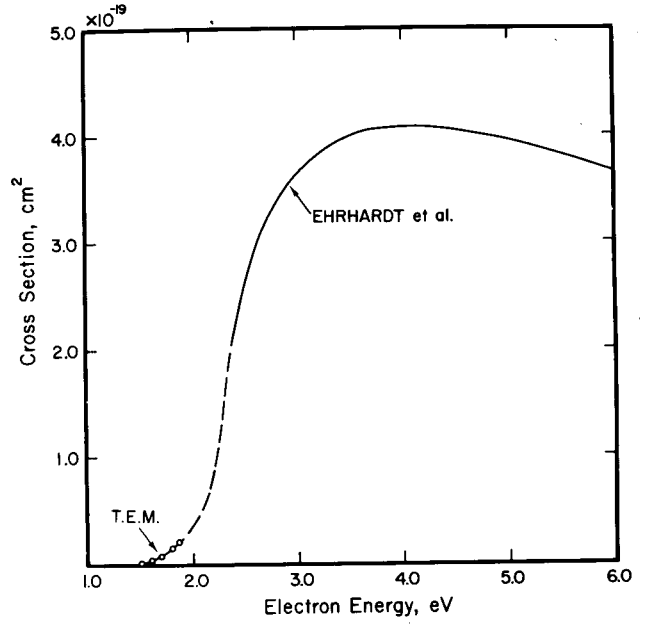

FIG. 5. Vibrational cross section to $v=3$ in hydrogen. The cross section near threshold is determined by Burrow and Schulz (1969) using the trapped electron method, shown by the open circles. The double electrostatic analyzer data of Ehrhardt *et al.* (1968) are shown by the solid line. The dashed line is an interpolation. [From Burrow and Schulz (1969).]

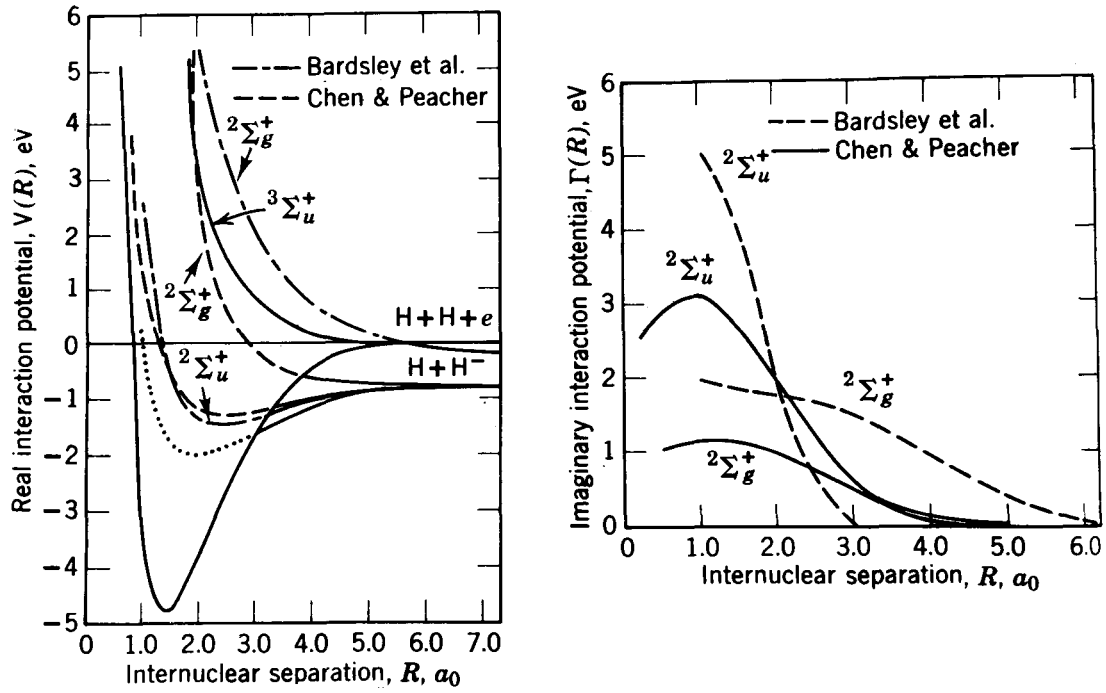

FIG. 6. The real and imaginary parts of the potential energy curves for the $^2\Sigma_u^+$ and $^2\Sigma_g^+$ states of H_2^-. On the left-hand side are shown the potential energy curves for H_2 (—), and the potential energy curves for H_2^- derived by Bardsley *et al.* (1966a) and by Chen and Peacher (1968a). The dotted curve indicates the real part of the potential curve for the $^2\Sigma_u^+$ state which is needed to obtain agreement with the vibrational cross section of Ehrhardt, *et al.* (1968). The repulsive curve for $H_2^-(^2\Sigma_g^+)$ of Chen and Peacher (1968a) is in very good agreement with the curve derived by Eliezer, Taylor, and Williams (1967), which is shown in Fig. 25(a). The potential energy curves for the lowest states of $H_2(^1\Sigma_g^+$ and $^3\Sigma_u^+)$ are taken from Kolos and Wolnicwicz (1965). The right-hand side of the figure shows the calculated widths of the $^2\Sigma_u^+$ and $^2\Sigma_g^+$ states. [From Chen 1969.]

compound states, namely,

$$\sigma(E) \propto |A+(\Gamma_{in}\Gamma_{out})^{1/2}/(E-E_0+\tfrac{1}{2}i\Gamma)|^2,$$

then the term A, representing the direct contribution to scattering, is small compared to the resonance term in inelastic processes. Above, Γ_{in} is the partial width for decay into the ground state, Γ_{out} is the partial width for decay into the excited state, and Γ is the total width, related to the partial widths by $\Gamma=\Gamma_{in}+\Gamma_{out}$. E_0 is the resonant energy.

Other review papers have recently appeared: Taylor *et al.* (1966), Bardsley and Mandl (1968), Burke (1968), Massey and Burhop (1969), Chen (1969), Herzenberg (1970, 1971), Taylor (1970). The nomenclature and general approach used in this review have been strongly influenced by these papers. Phelps (1968) has recently reviewed vibrational and rotational cross sections; Takayanagi and Itikawa (1970) have reviewed rotational cross sections. Golden, Lane, Temkin, and Gerjuoy (1971) have reviewed low-energy scattering experiments and rotational excitation and have given a review of experimental techniques. The aim of the present review is the tabulation and discussion of experimental values for compound states: their positions, widths, and classifications. Theoretical considerations are brought in only in those cases where they are needed for the discussions, but no attempt is made to include the bulk of theoretical considerations. Experimental methods are briefly discussed in the paper immediately preceding, which deals with compound states in atoms.

A. Classification of Compound States

We can classify compound states in molecules, in an analogous manner to that in atoms (see preceding

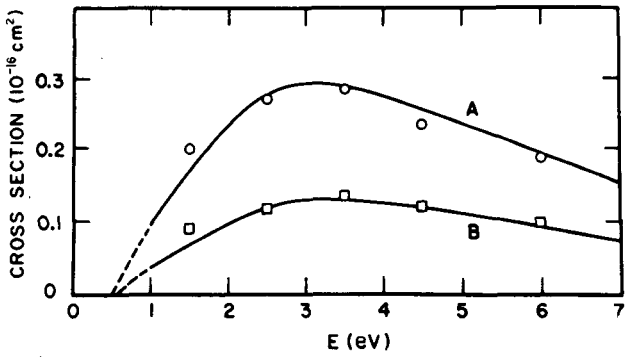

FIG. 7. Curve A: Energy dependence of pure vibrational cross section, $\sigma(v=0\to1,\ \Delta j=0)$. Curve B: Energy dependence of rotational-vibrational cross section, $\sigma(v=0\to1,\ j=1\to3)$. Points are experimental (Linder and Schmidt, 1971a), lines are theoretical (Henry and Chang, 1972). [From Henry and Chang (1972).]

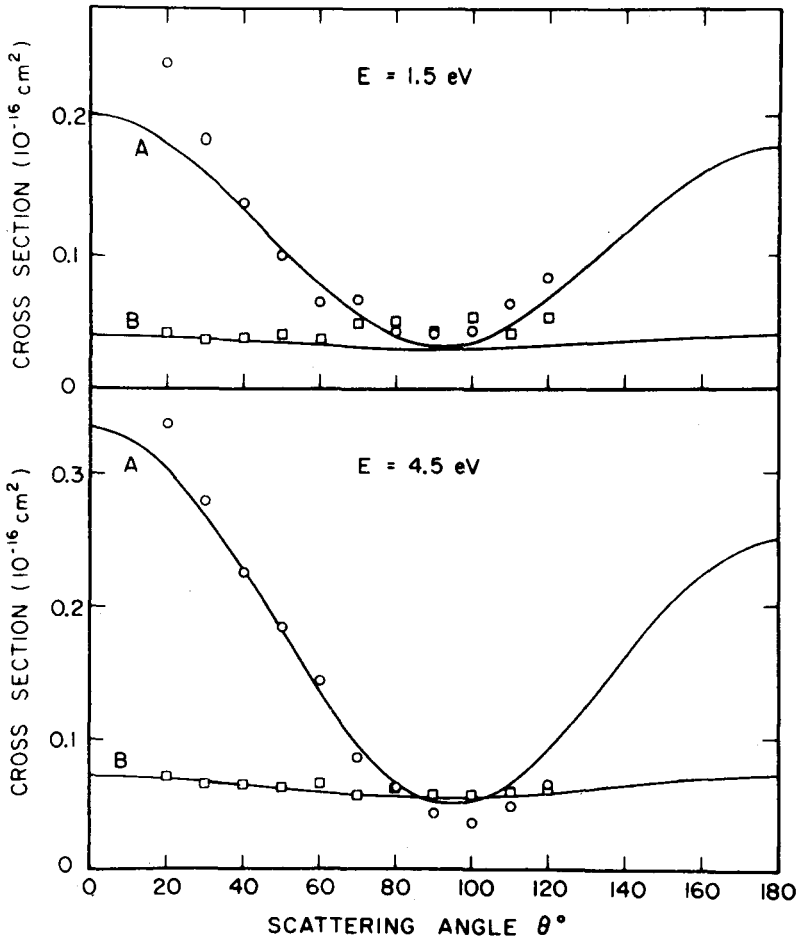

FIG. 8. Curve A: Angular distributions for pure vibrational excitation $\sigma(v=0\rightarrow1; \Delta j=0)$. Curve B: Angular distribution for rotational–vibrational excitation, $\sigma(v=0\rightarrow1; j=1\rightarrow3)$. Points are experimental (Linder and Schmidt, 1971a) and lines are theoretical. [From Henry and Chang (1972).]

paper), into two major categories depending on the state of the target molecule to which the incident electron attaches. Table I may serve as a helpful guide to the semantics of compound states.

When the incident electron is trapped in the potential connected with the ground electronic state, we speak of *shape* resonances or *single particle* resonances. The two terms are synonymous. In this case, the centrifugal, polarization, and exchange forces combine to create a potential with a penetrable barrier. Thus, it is the *shape* of the potential which is responsible for the trapping of the particle and for the resonance. Shape resonances associated with the ground electronic state have been substantiated in all diatomic molecules studied to date (H_2, D_2, HD, O_2, N_2, NO, CO). They occur at low energies (0–4 eV), exhibit a lifetime in the range 10^{-15} sec to 10^{-10} sec or even longer, and decay into vibrational and rotational levels of molecules and sometimes into negative ions by dissociative attachment. In all cases described in this review, vibrational excitation proceeds predominantly via shape resonances; resonances also play an important role in rotational excitation. Thus shape resonances are very important in our understanding of low-energy impact on molecules.

Since typical vibrational times are $\sim10^{-14}$ sec, shape resonances may be short-lived, long-lived, or comparable to vibration times. When the lifetime is short (e.g., H_2), the energy dependence of the vibrational cross section exhibits a broad peak; when the lifetime is long (e.g., O_2), the compound state itself can vibrate and the energy dependence of the cross section to a given final vibrational state exhibits a series of spikes at the location of the vibrational levels of the compound state. When the lifetime of the compound state is comparable to typical vibration times (e.g., N_2, CO) an intermediate situation prevails. In such a case, the compound state may perform about one vibration before decaying and the cross section to the final vibrational state will exhibit several broadened spikes.

The location on the energy scale and the particular properties of shape resonances are described under a separate heading for each molecule.

Core-excited resonances are associated with an electronically excited state of the molecule, which is called the "parent." Core-excited resonances thus consist of a "hole" in one of the orbitals normally occupied by an electron, and of two "particles", i.e., electrons in normally unoccupied orbitals. We can also visualize reso-

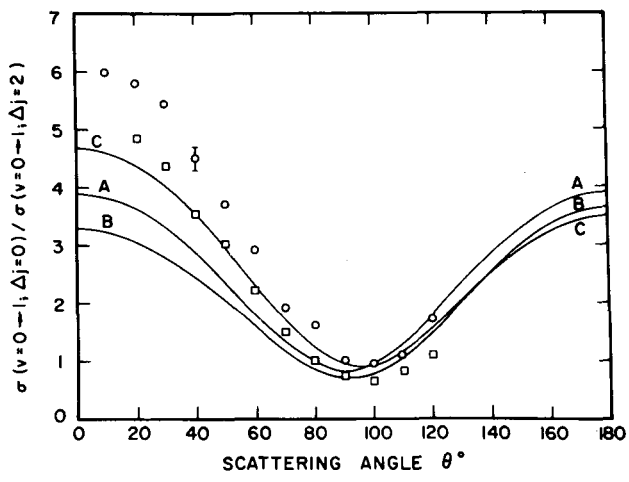

FIG. 9. Ratio $\sigma(v=0\rightarrow1,\ \Delta j=0)/\sigma(v=0\rightarrow1,\ j=1\rightarrow3)$ vs scattering angle at an electron energy of 4.5 eV. Experiment: ○ Ehrhardt and Linder (1968); □ Linder and Schmidt (1971); Theory: A—Abram and Herzenberg (1969); B—Henry (1970); C—Henry and Chang (1972). [From Henry and Chang (1972).]

nances consisting of two "holes" and three "particles"; such resonances have been recently postulated (Pavlovic *et al.*, 1972) and are well known in atoms (e.g., the $2s^22p$ state in He^- near 57 eV). Higher hole–particle states appear to be plausible.

Core-excited resonances can lie either below or above their parent. When they lie *below* their parent, one may say that they exhibit a positive electron affinity. Such states are called Feshbach-type (after Feshbach, 1958, 1962) or Type I, or closed-channel resonances (decay into the parent state is forbidden). When core-excited resonances lie *above* their parent, they are called Type II or core-excited shape resonances. These resonances are similar to single-particle shape resonances, except that they are associated with an electronically excited state.

B. Parentage of Core-Excited Feshbach Resonances

The parents for core-excited resonances may be, in principle, either valence or Rydberg excited states. Singly excited states of molecules may be classified into valence and Rydberg states. Both these types of excited states of the neutral molecule are formed by the promotion of a single electron from the ground state configuration into an orbital which is not filled in the ground state. When the promotion takes place into a low-lying vacant orbital, the principal quantum number of the electron does not change, and we designate the excited state as a valence state. When the principal quantum number does change by unity or more, we designate such an excited state as a Rydberg state. Rydberg states lie at higher energies and the orbitals being filled look like atomic orbitals. This gives rise to a Rydberg series of electronic states whose limit corresponds to an ionization limit of the molecules.

Calculations (Weiss and Krauss, 1970) on the binding of the additional electron show that preferentially *Rydberg excited* states have a positive electron affinity for a fixed internuclear separation in the Franck–Condon region. We therefore expect to find Feshbach-type resonances, which lie below their parent, mostly associated with Rydberg excited states. In this case, the temporary negative-ion complex consists of two electrons in Rydberg orbitals trapped in the field of a positive ion core, which is called the "grandparent" state. The parent (or parents) consists of a single Rydberg electron bound by the field of the same ionic core.

Core-excited Feshbach resonances have lifetimes (10^{-12}–10^{-13} sec) which are long compared to the vibrational period of a molecule and therefore can give rise to *bands*, each of which consists of a progression of vibrational levels. Since the two Rydberg electrons trapped by the ion core are located far outside the ion core we expect the negative ion and its grandparent positive ion core to have similar vibrational spacings and Franck–Condon probabilities. One can therefore compare the vibrational spacings and Franck–Condon probabilities for a given band of negative ion vibronic states with the corresponding values for the many possible positive ion states of a molecule in order to identify the parentage and electron affinity of the band under investigation. This type of correlation has been made

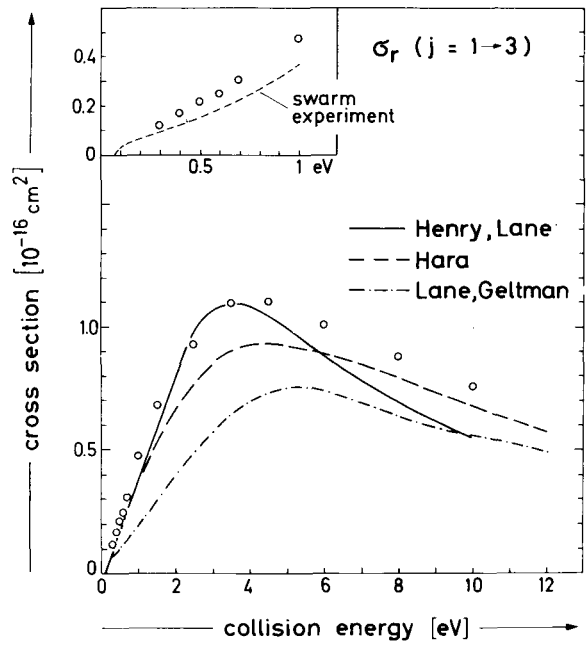

FIG. 10. Pure rotational excitation in H_2. Shown is the cross section $\sigma(j=1\rightarrow3)$. The circles are the experimental results of Linder and Schmidt (1971a). The lines are the theories of Henry and Lane (1969), of Hara (1969), and of Lane and Geltman (1967). The swarm data shown in the inset are recalculated for $\sigma(j=1\rightarrow3)$ by Linder and Schmidt (1971a) from the original experiment of Crompton *et al.* (1969) which gives $\sigma(j=0\rightarrow2)$. [From Linder and Schmidt (1971a).]

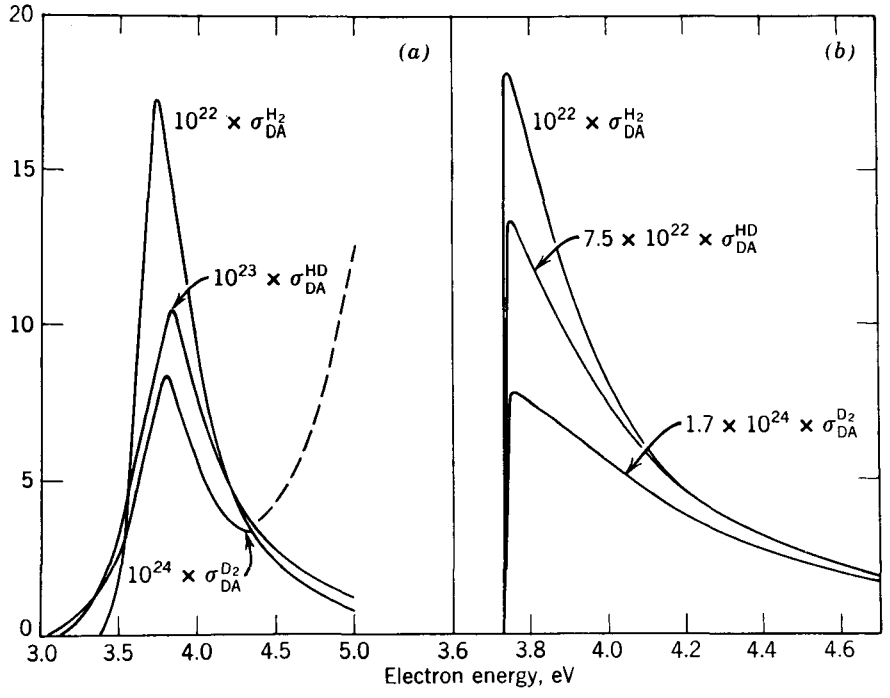

FIG. 11. The energy dependence of the total cross section for dissociative attachment in H_2, HD, and D_2 near 3.7 eV. The process shows a very large isotope effect and proceeds via the $^2\Sigma_u^+$ states of H_2^-. Part (a) shows the experimental results of Schulz and Asundi (1967) and part (b) shows the unfolded cross sections as reported by Chen and Peacher (1968a). It should be noted that the experimental curves of Schulz and Asundi, shown on the left side of the diagram, have peak cross sections differing by orders of magnitude (1.6×10^{-21} cm^2 for H_2, 1×10^{-22} cm^2 for HD, and 8×10^{-24} cm^2 for D_2). Whereas the H^-/H_2 cross section was obtained with an electron energy distribution of 0.1 eV the curves for HD and D_2 had to be taken with an energy distribution of 0.45 eV in order to gain sensitivity. This accounts for the difference in the threshold behavior. The rising portion of the D^-/D_2 cross section, indicated by dashes, is real having been reproduced by Ziesel and Schulz (unpublished). It could result partially from the wings of the $^2\Sigma_g^+$ resonance near 10 eV.

by Sanche and Schulz (1971, 1972), who find that many experimentally observed negative ion bands can be simply correlated with grandparent positive ion states. They find that the compound states usually lie about 4 eV below the grandparent from which they are derived, i.e., the binding energy of the two Rydberg electrons is 4 eV.

Resonances associated with *valence* excited states are also known, but as pointed out above, they do not seem to lead to sharp structures in cross sections. Their effect has been studied in dissociative attachment and in vibrational excitation; they may also play a role in excitation of electronic states of molecules. It is pointed out by Pavlovic *et al.* (1972) that at higher energies the density of doubly excited valence states becomes large and that resonances associated with each valence states may make a dominant contribution to excitation functions at energies in the 20-eV range.

II. HYDROGEN

The ground state of H_2 consists of two electrons in the $1s\sigma_g$ ($=\sigma_g 1s$) orbital (Herzberg, 1950). The lowest unfilled orbital, in the notation of the united molecule, is $2p\sigma_u$, which is equivalent to $\sigma_u 1s$. It is this orbital which the incident electron occupies when forming a resonance at low energy. In escaping from this orbital the electron must tunnel through a p-wave barrier. Bardsley *et al.* (1966b) and Eliezer *et al.* (1967) have shown that the ground state of H_2^- is indeed a shape resonance and that its designation is $^2\Sigma_u^+$. The angular distribution measurements of Ehrhardt *et al.* (1968) on electrons having excited the $v=1$ vibrational state of H_2 show a p-wave character (minimum at 90°) and thus confirm the designation given above.

A. Resonance at Low Energy: 0–4 eV ($^2\Sigma_u^+$)

1. Elastic Cross Section

The lifetime of the $^2\Sigma_u^+$ state is very short and the width very large; therefore there is little or no evidence for the $^2\Sigma_u^+$ state in the elastic cross section (Golden and Nakano, 1966). Figure 1 shows the energy dependence of the total cross section as measured in a Ramsauer-type apparatus by Golden and Nakano and the elastic cross section only, as measured by Linder and Schmidt (1971a). No clear-cut evidence of the action of a resonance can be seen in these curves. Rather, one has to study other decay channels to establish the existence of this state. Vibrational excitation, rotational excitation (including angular distribution), as well as dissociative attachment, are the possible decay channels that can be usefully studied by electron impact in order to establish the existence of such resonances. Also, angular distribution measurements are very useful in establishing the existence of resonances. These are discussed separately for each molecule and a summary is given in Sec. VII. The experimental and theoretical considerations regarding elastic and rotational cross sections in H_2 have been recently reviewed by Golden *et al.* (1971) and the reader is referred to this reference.

2. Vibrational Excitation in H_2 via $^2\Sigma_u^+$

It is only in the past 10 years that experiments on vibrational excitation have led to the present-day under-

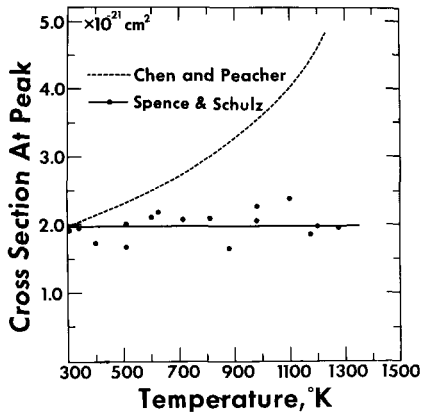

FIG. 12. Temperature dependence of the cross section for H^- formation from H_2 at 3.75 eV. The experimental results (Spence and Schulz, 1971) show that the negative ion formation is independent of rotational excitation of the target, whereas the theory of Chen and Peacher (1967) shows a strong dependence. [From Spence and Schulz (1971).]

standing of the process. The first observation of a large vibrational cross section was due to Ramien (1931) whose results at 3.5 and 7 eV were essentially correct but were widely disbelieved because no simple interpretation could be found (Massey and Burhop, 1952). The use of a rather complex experimental method (Hertz diffusion) and the limited nature of the observation (only two energies given) contributed to the skepticism.

Subsequent experiments by Schulz (1964) and by Engelhardt and Phelps (1963) confirmed the large cross section for vibrational excitation, as did the experiments of Ehrhardt *et al.* (1968). This large vibrational cross section was successfully interpreted in terms of

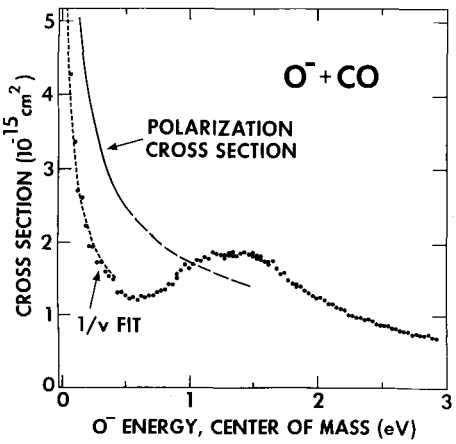

FIG. 13. The cross section for total electron detachment for the reaction of O^- with CO. The lower dashed line is the $1/v$ fit while the upper line is the polarization cross section. The closed circles are data points. The magnitude is calibrated by assuming that the detachment rate at thermal energies is 5.6×10^{-10} cm³ sec^{-1} (Ferguson, 1968), but this value is known to an accuracy of only ±30%. The polarization cross section was calculated using 19.5×10^{-25} cm³ as the polarizability of CO. [From Mauer and Schulz (1972).]

the resonance model by Bardsley, Herzenberg, and Mandl (1966b) and the energy dependence of the measured vibrational cross section could be well reproduced.

The energy-loss spectrum for 4-eV electrons in H_2 is shown in Fig. 2, which clearly shows peaks due to the excitation of four vibrational states. The energy dependence of the vibrational cross section for $v=1$ is shown in Fig. 3 in comparison with the newest theory due to Henry and Chang (1972). The theory of Faisal

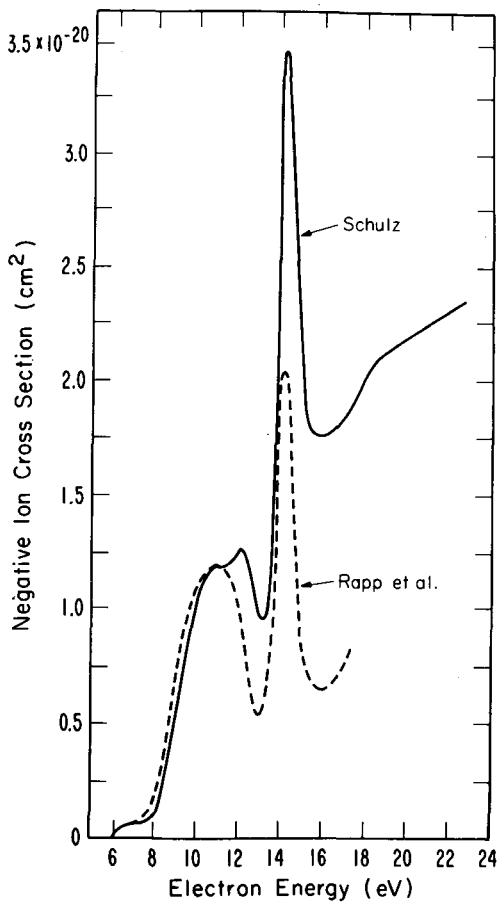

FIG. 14. Formation of stable negative ions, H^-, by dissociative attachment in hydrogen via a repulsive curve. Shown are the results of Rapp *et al.* (1965) and Schulz (1959a). The broad peak around 10 eV is interpreted as the reaction $e+H_2\rightarrow H_2^-(^2\Sigma_g^+)\rightarrow H^-+H$. The peak near 14.2 eV is interpreted in terms of the formation of excited H, $e+H_2\rightarrow H^-+H(2^2S,\ 2^2P)$. The small structure near 12 eV shown on Schulz's curve has been studied in detail by Dowell and Sharp (1968) and is shown in Fig. 16.

and Temkin (1972) is also in agreement with the experiments.

Although Fig. 3 presents fairly good agreement between experiments, it is pointed out by Crompton *et al.* (1970) and also discussed by Golden *et al.* (1971) that the slope near threshold, as determined from electron beam experiments by Burrow and Schulz (1969) or by Ehrhardt *et al.* (1968) is too large to fit the measured transport coefficients. In order to perform such an

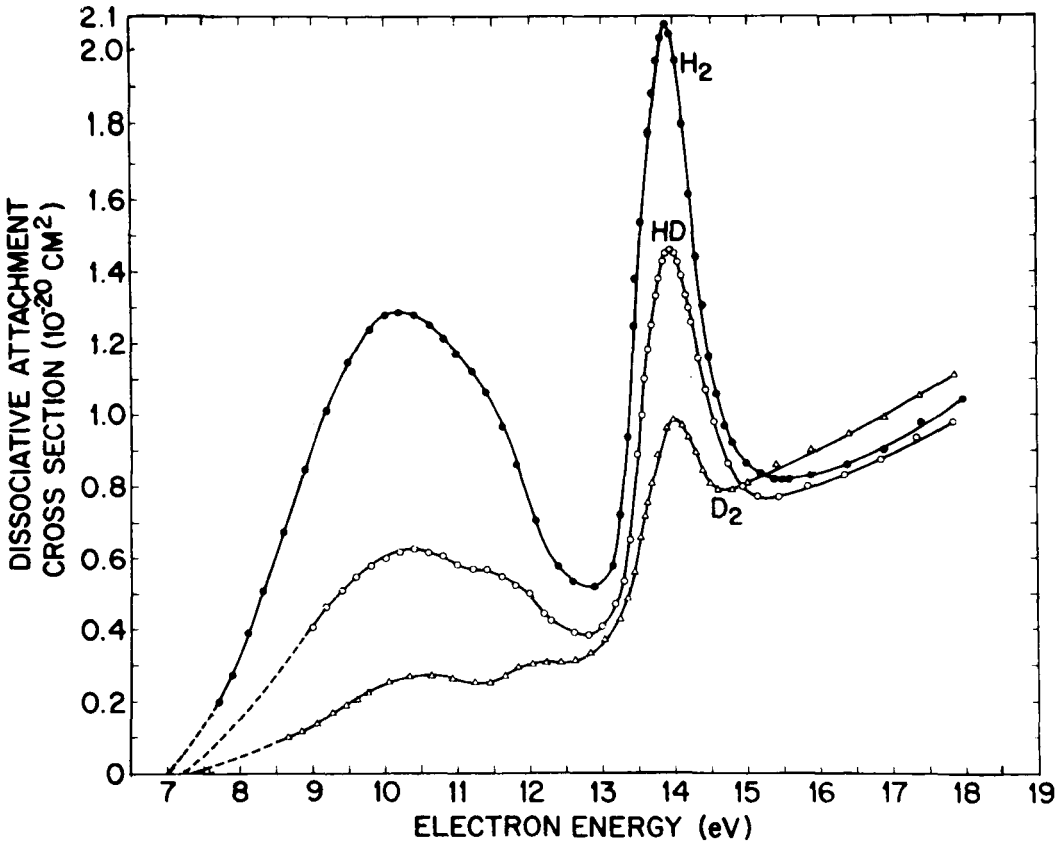

FIG. 15. Isotope effect in dissociative attachment in the neighborhood of 10 eV in H_2, HD, and D_2. [Taken from Rapp, Sharp, and Briglia (1965).]

analysis, Crompton *et al.* have to assume a reasonable energy dependence for the rotational cross section and that their approximation to the solution of the Boltzmann transport equation is applicable. To that extent, a discrepancy exists in the threshold behavior, as deduced from beam and from swarm experiments. Crompton's results based on an analysis of transport coefficients are also shown in Fig. 3.

The cross sections for excitation of the second and third vibrational states of H_2 come from electron beam experiments and are shown in Figs. 4 and 5, respectively.

The experimental results presented lead to the conclusion (Bardsley *et al.*, 1966b; Eliezer *et al.* 1966) that the $^2\Sigma_u^+$ state of H_2^- is involved in the excitation process. The width of this state is several eV, as can be seen in Fig. 6, which shows the dependence of the width on internuclear separation. Also, shown in Fig. 6 is the dependence on internuclear separation of the real part of the potential energy curves.

Breig and Lin (1965) and Takayanagi (1965) calculate the vibrational cross section to $v=1$ without invoking a compound state, but they include the dependence of the polarization on the internuclear separation. Breig and Lin obtain fairly good agreement with the experimental observations. (See, e.g., Chen, 1969.) The argument is sometimes made that the resonance model is not needed for an interpretation of vibrational excitation. However, it is often easier to understand the physical processes involved and the processes become more explicit and readily understandable when one uses the resonance model. There seems to be no compelling reason to "hide" the compound state. The resonance model becomes even more useful for an understanding of the isotope effect in dissociative attachment, as will be discussed below.

3. *Rotational Excitation via the $^2\Sigma_u^+$ State and Angular Distributions*

The general problem of rotational excitation of molecules has been very recently reviewed by Golden, Lane, Temkin, and Gerjuoy (1971) and by Takayanagi and Itikawa (1970). The reader is referred to these reviews for reference. Of interest for the present purposes is pure rotational excitation and rotational excitation which accompanies vibrational excitation, both processes proceeding via the $^2\Sigma_u^+$ compound state in H_2. Figure 7 shows that the energy dependence of the cross section for simultaneous rotational and vibrational ex-

TABLE II. Summary of experimental data on H_2^-. This table gives the band designation which we use in the present review (Bands "a"–"g"). For each author, listed in the first column, we give the nomenclature he used for a given band (e.g., "Series I," "strong") and also the final state in which the band was observed (e.g., $X\,^1\Sigma_g^+$, $b\,^3\Sigma_u^+$), and the energy of the first resonance, in eV.

Possible equivalence[a]							
Band designation	"a"	"b"	"c"	"d"	"e"	"f"	"g"
Kuyatt *et al.* (1966) (transmission)	"strong" 11.28	×[e]	"weak" 11.46				
Comer and Read (1971a)	$X\,^1\Sigma_g^+(v)$ 11.30	$X\,^1\Sigma_g^+$ ($v>8$) 10.93[f]	$X\,^1\Sigma_g^+(v)$ 11.19[g]				
Weingartshofer *et al.* (1970)	"Series I" $X\,^1\Sigma_g^+$, $b\,^3\Sigma_u^+$ 11.30			"Series I" $B\,^1\Sigma_u^+$ 11.30	"Series II" $B\,^1\Sigma_u^+$ 11.50	$C\,^1\Pi_u$ 13.63	
Sanche and Schulz (transmission) (1972)	11.32	×	11.43			13.66	15.09
Width, Γ (eV)	≤0.016 (H_2)[g] 0.03 (D_2)	0.03[c]	<0.016[g]			0.08[b]	
Symmetry	$^2\Sigma_g^+$	$^2\Sigma_g^+$	$^2\Sigma_g^+$; $^2\Pi_u$	$^2\Pi_g$ (?)		$^2\Sigma_g^+$	
Observed in	H_2, HD, D_2	H_2	H_2, HD, D_2	H_2	H_2	H_2, D_2	H_2, D_2
R_e (Å)[c]	0.97±0.01	1.175±0.01		0.97			
a (eV)[c,d]	0.345±0.015	0.19±0.015		0.345			
b (eV)[c,d]	0.0135±0.003	0.005±0.003		0.0135			
E_0 (eV)[c,d]	11.40	11.11		11.40			

[a] The arrows indicate that band "a" could be identical to band "d" and that band "c" may be identical to band "e." See text.
[b] From Weingartshofer *et al.* (1970).
[c] From Comer and Read (1971a).
[d] Defined by the equation $E=E_0+a(v+\frac{1}{2})-b(v+\frac{1}{2})^2$.
[e] The symbol × indicates that band "b" is observable only in the high vibrational states ($v>8$) of the $^1\Sigma_g^+$ state and thus cannot be observed in transmission experiments.
[f] Extrapolated to $v=0$; see Appendix I.
[g] From Joyez, Comer, and Read (1973).

citation ($v=0\rightarrow1$; $j=1\rightarrow3$) is similar to the cross section for vibrational excitation alone ($v=0\rightarrow1$; $\Delta j=0$) and thus both processes seem to be dominated by the $^2\Sigma_u^+$ resonance. Angular distribution measurements by Ehrhardt and Linder (1968) and by Linder (1969) (Fig. 8), shows that pure vibrational excitation exhibits a $p\sigma$-wave dependence, i.e., the scattered electrons exhibit a minimum at 90 degrees. These observations are in agreement with the theory which predicts an approximate angular distribution of the form $(1+2\cos^2\theta)$. [See Bardsley and Read (1968), Ehrhardt, Langhans, Linder, and Taylor (1968), and O'Malley and Taylor (1968).]

When rotational levels are excited in addition to vibrational levels, a flat (isotropic) angular distribution is observed. Figure 8 shows the results for the transition $\Delta j=2$, $\Delta v=1$. The ratio of the vibrational cross section without rotational excitation to that with rotational excitation, $\sigma(\Delta j=0;\ \Delta v=1)/\sigma(3\leftarrow1;\ \Delta v=1)$ is shown in Fig. 9 in comparison with the theories of Abram and Herzenberg (1969), of Henry (1970), and of Henry and Chang (1972). The theory of Abram and Herzenberg is based on the quantum mechanical impulse approximation and neglects the kinetic energy of rotation of the molecule during the collision. The work of Henry and Chang uses the theory of frame transformation as developed by Chang and Fano (1972). The p-wave nature of the ratio is obvious from the figure.

As far as pure rotational excitation, in which the vibrational quantum number does not change, is concerned, there are available the experimental data of Ehrhardt and Linder (1968) and the improved data of Linder and Schmidt (1971a). It is the latter data that are shown in comparison with theory in Fig. 10.

As pointed out most recently by Linder and Schmidt

(1971a), all the rotational effects can be interpreted by considering both the direct-excitation component and the resonance component to the phase shifts. The theory of Abram and Herzenberg (1969) which is based on a pure resonance model accounts well for the angular distributions observed by Linder and Schmidt (1971a) for pure rotational excitation, $\sigma(j=1\rightarrow 3)$.

The suggestion has been advanced by Frommhold (1968) that electrons of thermal energy (10–100 meV) exhibit resonant behavior in exciting rotational states of H_2 and D_2. Evidence for this hypothesis comes from the pressure dependence of the drift velocity, which is observed by Frommhold and by Crompton and Robertson (1971) in swarm experiments.

Recently, Raith and Land (1972) used a time-of-flight electron spectrometer to perform a transmission experiment in H_2 and D_2 in order to confirm the existence of resonances at very low electron energies in H_2 and D_2. In H_2, they observe structures in the transmitted current at about 24 meV and in the range 60–90 meV. In D_2 the results are qualitatively different, with structure appearing between 26 and 60 meV. The width of the 24-meV structure in H_2 is approximately 3 meV, of which about 1.5 meV can be attributed to Doppler broadening. Rotational excitation is expected to be governed by the selection rule $\Delta l=0, \pm 2$, where l is the orbital quantum number of the scattered electron. Thus we expect inelastic processes to have thresholds at 44 meV (for $J=0\rightarrow 2$) and at 75 meV (for $J=1\rightarrow 3$) in H_2 and at half these values in D_2. The observed structure thus lies below the first inelastic process in H_2 and above it in D_2. If the structures observed in the experiment of Raith and Land are resonances, which is by no means certain, one must await

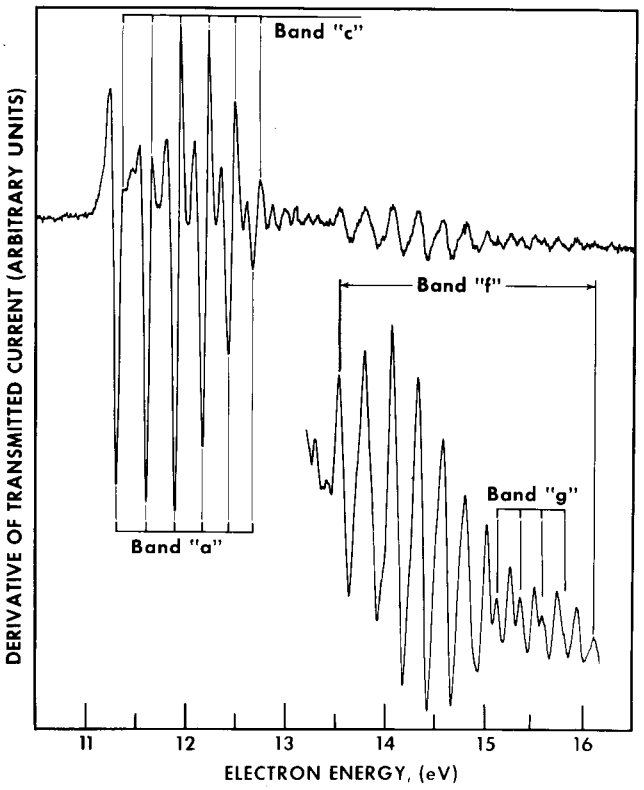

FIG. 17. Derivative of transmitted current vs electron energy in H_2. Four progressions of negative ion states are labelled "a," "c," "f," and "g." See Table II. Band "b" seems to be observable only in high vibrational states, and thus does not seem to appear in transmission experiments. Band "d," if it exists as a separate entity, is energetically coincident with band "a." For the lower portion of the figure, which shows bands "f" and "g," the gain has been increased by a factor of seven. [From Sanche and Schulz (1972).]

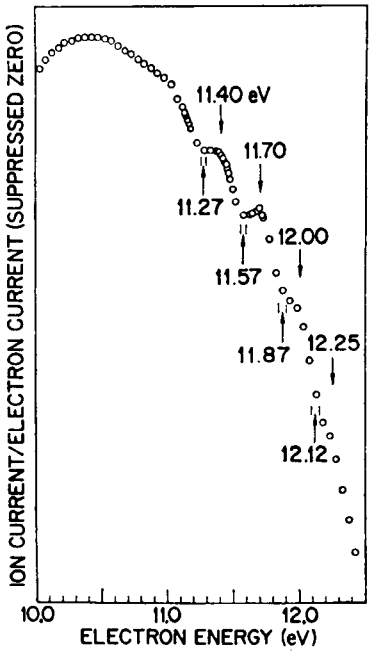

FIG. 16. Fine structure in dissociative attachment in H_2. [Taken from Dowell and Sharp (1968).]

a theoretical interpretation for an understanding of this phenomenon.

The preliminary theoretical work by Kouri (1968) has not confirmed the reality of this process, and further developments must be awaited. At this writing, the existence of resonances in the energy range 10–100 meV is puzzling, since no molecular orbitals are available at such low energies, and since close-coupling calculations (Henry and Lane, 1969) do not give an indication for rotational resonances.

4. Dissociative Attachment at 3.75 eV

The $^2\Sigma_u^+$ state of H_2^- also plays a role in dissociative attachment. It is characteristic of many compound states that they decay into all channels that are energetically accessible and allowed by selection rules. The dissociative attachment channel opens up at an electron energy $(D-A)$, where D is the dissociation energy of H_2 (4.48 eV) and A is the electron affinity of H (0.75 eV). Thus one would expect a threshold for H^- formation from H_2 at 3.73 eV. Figure 11 shows the experimental result of Schulz and Asundi (1967), who ob-

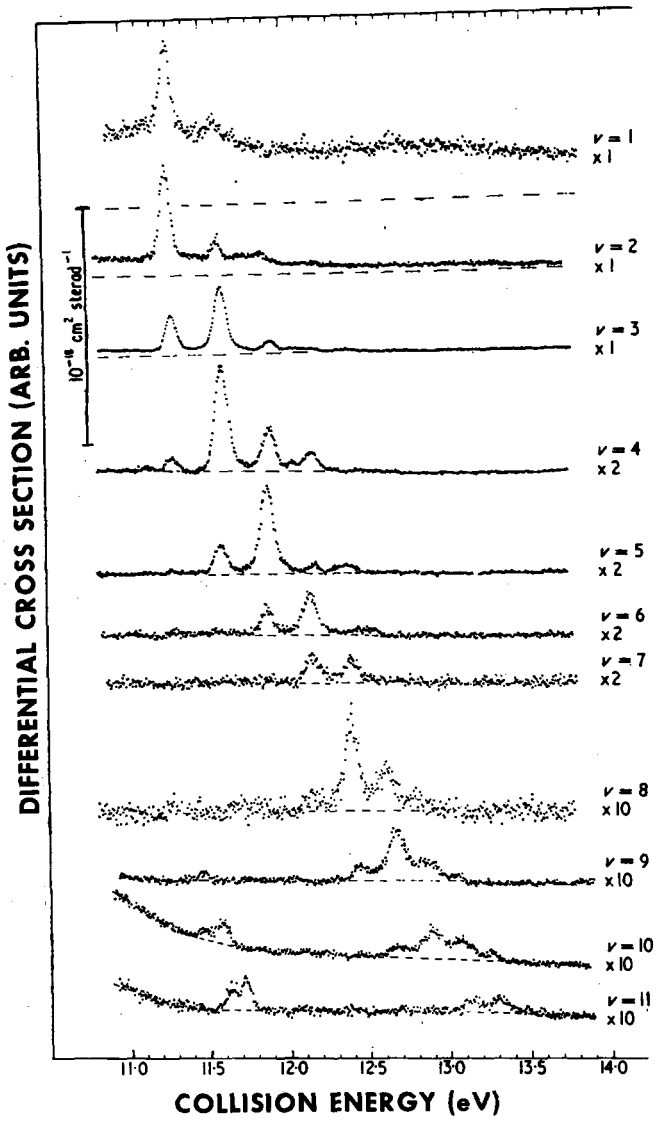

FIG. 18. Energy dependence of the absolute differential cross sections for excitation of vibrational states in H_2 above 11 eV. The scattering angle is 85°. For each curve the cross section scale should be multiplied by the factor indicated. The zero lines are shown broken. The structure observed in the vibrational states $v=1$ to $v=8$ is associated with series "a." For $v=9$ to $v=11$, series "a" is visible in the energy range 12.48–13.33 eV, and series "b" appears at the low-energy end, i.e., in the energy range 11.49–11.74 eV. [From Comer and Read (1971a).]

served the onset for H^- production at the predicted value. Also shown in Fig. 11 are the unfolded cross sections for the three isotopes of H_2 (Chen and Peacher, 1968). The isotope effect was first interpreted by Demkov (1964) as a consequence of the smaller survival probability factor for heavier atoms. Thus, D_2 requires a longer time to separate and remains in the region of autodetachment for a longer time than does H_2. The formation of D^-/D_2 is therefore smaller than H^-/H_2. Bardsley, Herzenberg, and Mandl (1966b) give a simple expression for the cross section leading to dissociative attachment:

$$Q_-=Q_0 \exp-\left(\int_{R_0}^{R'} \frac{\Gamma(R)dR}{\hbar v(R)}\right).$$

Here, Q_0 is the cross section for formation of the compound state and the exponential term represents the probability that the system in fact survives to a stabilization point R'. The term Γ is the width (and

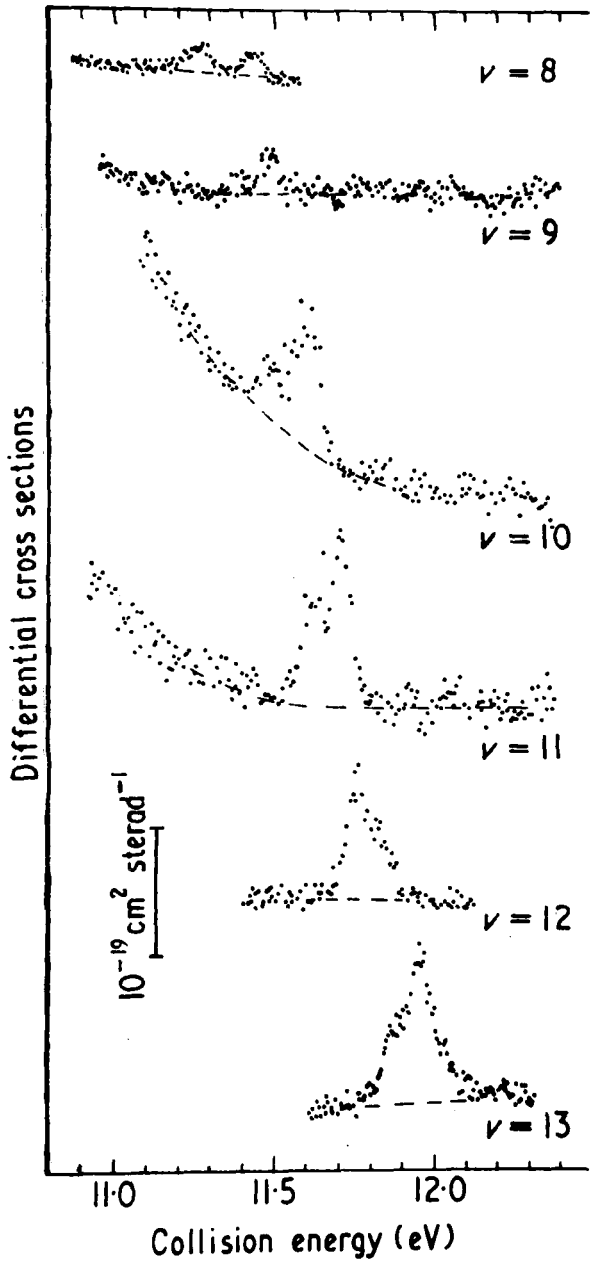

FIG. 19. Energy dependence of the absolute differential cross section for excitation of high vibrational states in H_2 above 11 eV. The scattering angle is 85°. The zero lines are shown broken. Only series "b" is shown. [From Comer and Read (1971a).]

$\hbar/\Gamma$ is the lifetime) of the compound state with respect to autodetachment. This width is a function of the internuclear separation R. The integration extends from the formation point R_0 to the stabilization distance R' and $v(R)$ is the relative velocity of separation of the nuclei. We can replace the exponent by the appropriate average width $\bar{\Gamma}$ and by the time τ, which is needed for the products to reach the stabilization point. We then write

$$Q_-=Q_0 \exp(-\bar{\Gamma}\tau/\hbar).$$

It should be noted that the total width is the sum of the partial widths for decaying into the various vibrational states of the (H_2+e) system. Separation into three particles $(H+H+e)$ is energetically possible at energies above 4.46 eV. In this model the isotope effect arises from the variation of the survival probability $(\exp-\Gamma\tau/\hbar)$ with mass. It is pointed out by Chen and Peacher (1968a) that the above expressions are only approximate and that the capture cross section, resulting from the nuclear overlap integral, becomes as sensitive to the mass as the survival probability itself. Nevertheless, the simplicity of separating the dissociative attachment cross section into two physically meaningful simple terms has accounted for the extensive use of the above expressions. Also, Chen and Peacher's considerations have not as yet been tested against experiment.

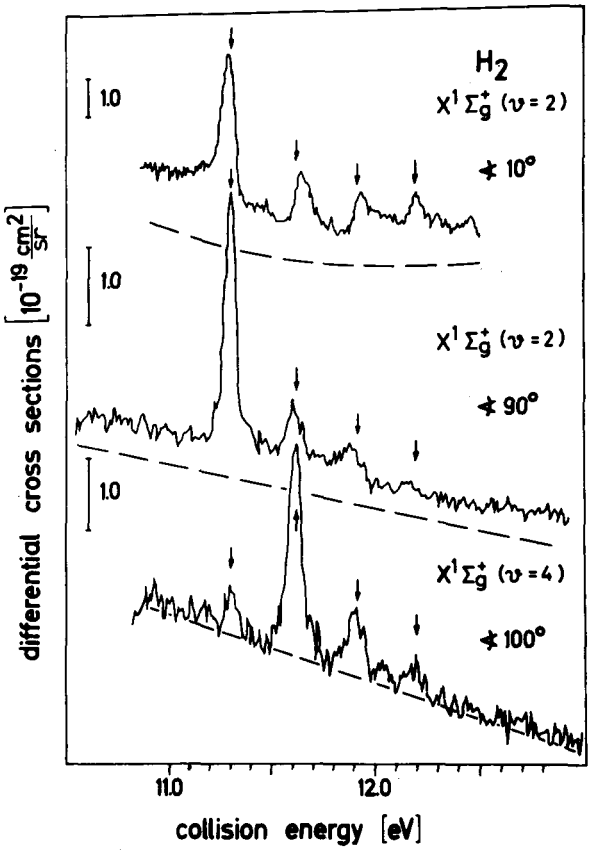

FIG. 20. Energy dependence of the absolute differential cross sections for different scattering angles and into two different exit channels, $v=2$ and 4 of the electronic ground state. The zero lines are dashed. The length of the bars to the left represent the scaling factors in units of 1.0×10^{-19} cm²/sr. The resonances are members of band "a." [From Weingartshofer *et al.* (1970).]

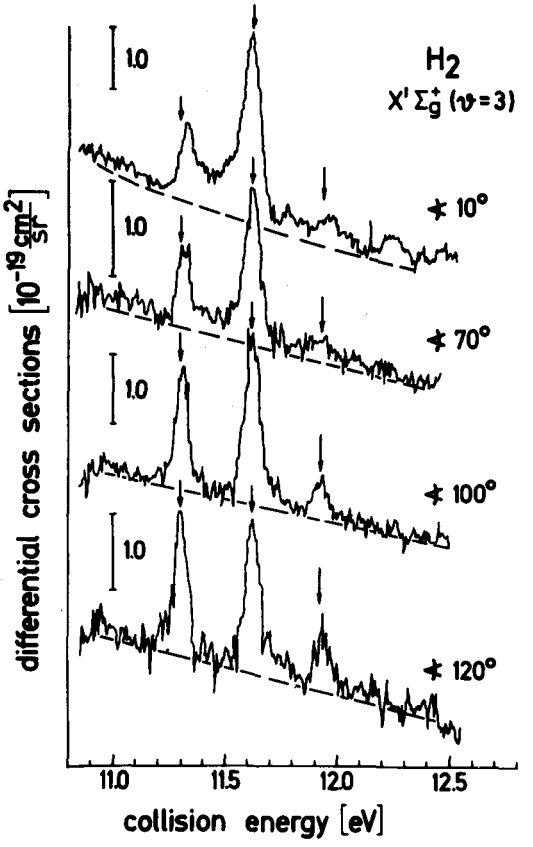

FIG. 21. Energy dependence of the absolute differential cross sections to the $v=3$ vibrational level of the electronic ground state of H_2 for four different scattering angles. The zero lines are dashed. The length of the bars to the left of each curve represents the absolute scaling factors in units of 1.0×10^{-19} cm²/sr. The resonances are members of band "a." [From Weingartshofer, Ehrhardt, Hermann, and Linder (1970).]

5. *Effect of Rotational Levels of the H_2 Target Molecule on H^- Formation near 3.75 eV*

Chen and Peacher (1967) predict theoretically a profound effect of rotationally excited levels of H_2 for the reaction $e+H_2\rightarrow H_2^-\rightarrow H^-+H$ at 3.75 eV. In this reaction the products depart with zero kinetic energy, and Chen and Peacher predict a large increase in the survival factor leading to an increased cross section for this process as the population of higher rotational states is increased. Chen and Peacher's suggestion seems to stem from the effect of the centrifugal repulsion on the time the nuclei take to separate. To test this theory, and to determine the effect of rotational levels, Spence and Schulz (1971a) have studied the temperature dependence of the dissociative attachment cross section in H_2 at 3.75 eV.

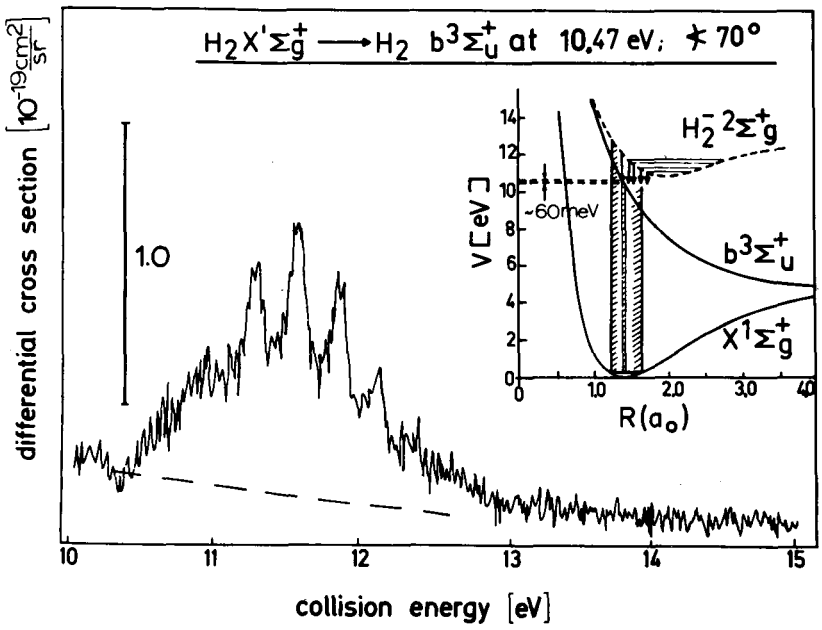

FIG. 22. Energy dependence of the absolute differential cross section for excitation into a narrow band (~60 meV) at 10.47 eV in H_2. The final state is the dissociative continuum, $b\,^3\Sigma_u^+$. The zero line is dashed. The length of the bar to the left of the curve represents the absolute scaling factor in units of 1.0×10^{-19} cm²/sr. The insert illustrates the autoionization of the H_2^- ion into the energy band. [From Weingartshofer, Ehrhardt, Hermann, and Linder (1970).]

The experimental cross section at the peak of the 3.75 eV process is plotted as a function of gas temperature in Fig. 12. Spence and Schulz (1971a) find that the cross section is independent of temperature in the range 300–1300°K and conclude that rotational excitation of H_2 plays no role in the dissociative attachment process at 3.75 eV in the above temperature range. Also shown are the theoretical points calculated using the theory of Chen and Peacher (1967) normalized to the experimental data at 300°K. In this calculation it is assumed that the electron capture cross section is independent of the initial rotational state, which should be a reasonable assumption in the present case.

It is, actually, not surprising to find that the dissociative attachment cross section is independent of the rotational states of the target. The vibrational time, and thus the dissociation time, are shorter than rotational times and one would therefore suppose that the molecule is essentially nonrotating during the capture and the breakup process. In fact, Bardsley, Mandl, and Herzenberg (1966b) calculate with good success the dissociative attachment in H_2 by regarding the axis of the diatomic molecule as fixed, thus ignoring rotational motion. The experimental results of Fig. 12 seem to confirm such a model.

6. *Associative Detachment:* $H^-+H\rightarrow H_2^-\rightarrow H_2+e$

There is a close relationship between dissociative attachment reactions at low energy, which are discussed in the preceding paragraphs, and low-energy associative detachment reactions of the type $H^-+H\rightarrow H_2^-\rightarrow H_2+e$. Associative detachment is the inverse of dissociative attachment and at low energies of the colliding partners, the two processes proceed via the same compound state, in this case H_2^-. For a review of associative detachment cross sections at thermal energy, see Ferguson (1970). In the case of H^-+H, the reaction partners approach each other along the potential energy curves $^2\Sigma_u^+$ and $^2\Sigma_g^+$. The former exhibits a short lifetime for autodetachment; thus all or almost all collisions which proceed along this potential energy curve lead to associative detachment. The $^2\Sigma_g^+$ curve is repulsive and reactions proceeding along this curve at low energy lead only to reflection or elastic scattering. One can therefore expect that the low-energy associative detachment cross section should be about one-half of that given by the Langevin polarization cross section. This prediction has been approximately checked for *thermal* ions (Schmeltekopf *et al.*, 1967).

Since associative detachment proceeds via the same intermediate state as dissociative attachment, there is a strong connection between the two processes. However, in associative detachment there is the probability that the resulting molecule is left in a highly excited vibrational state, provided that the compound state is short lived. Thus detailed balancing cannot be used for predicting the bulk of the associative detachment cross section from its inverse, since dissociative attachment is generally studied only for molecules in their lowest vibrational states.

For the case of $H^-+H\rightarrow H_2+e$, theoretical treatments are also available. Bates and Massey (1954) and also Dalgarno (1961) have suggested that associative detachment cross sections could be large and that they could play an important role in upper atmosphere reactions. Recently, more complete theoretical treatments have become available. [Herzenberg (1967), Chen and Peacher (1968) and Browne and Dalgarno (1969), and also the review by Chen (1969)]. The main conclusions from these considerations are: At low

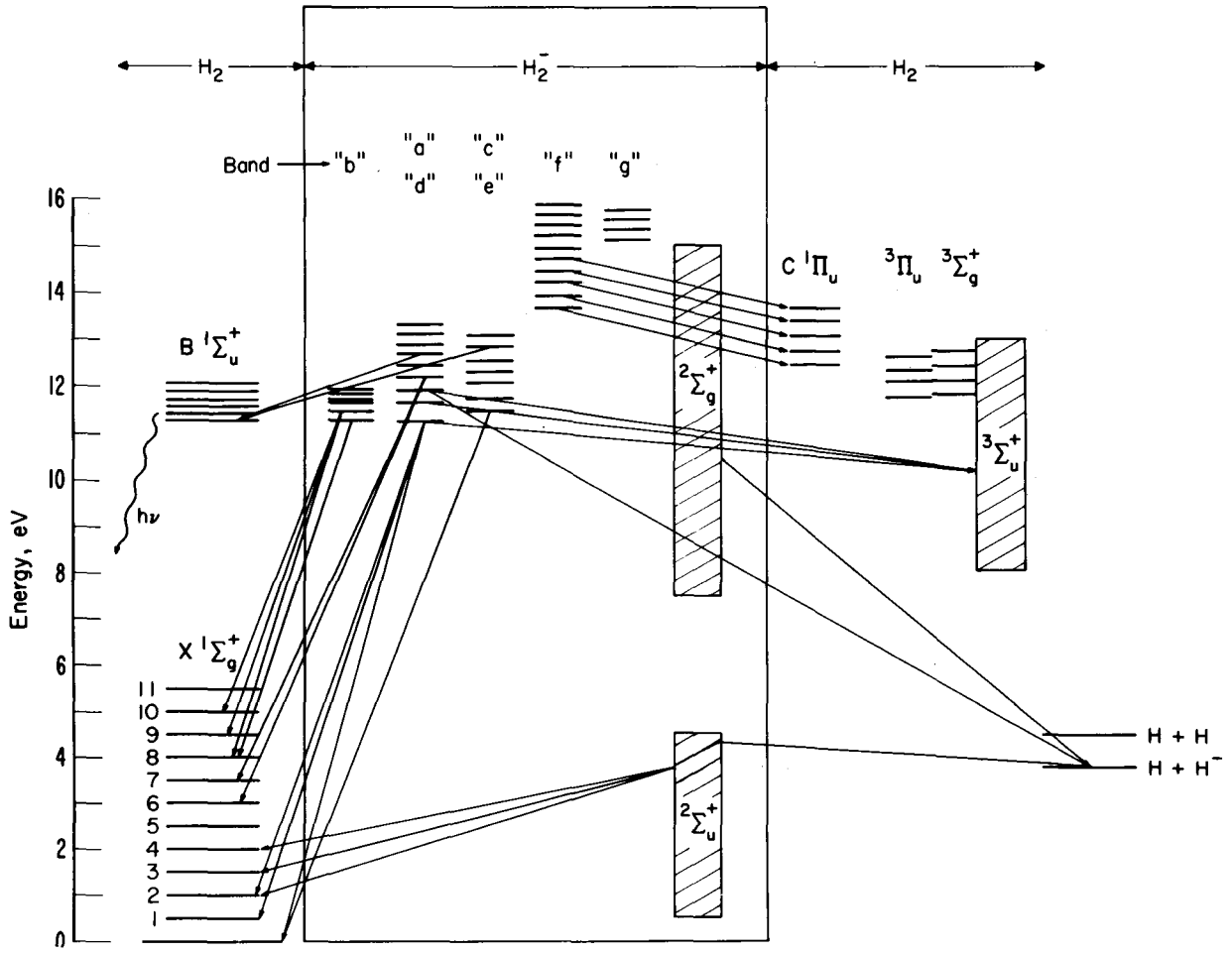

FIG. 23. A schematic summary of the decay of five energetically distinct compound states into various decay channels. In the middle of the figure we show the positions of bands "a" through "g," and on the left and right we show states of H_2. The arrows point to those decays that have been experimentally determined, but not all decay channels could be given on the figure. Band "f" seems to decay into the $C\,^1\Pi_u$ state without change of vibrational quantum number, and this is properly recorded on the figure. Band "b" seems to decay only into high vibrational states of the $X\,^1\Sigma_g^+$ ground state. Decay into $H+H^-$ (dissociative attachment) is also indicated.

energy the cross section becomes very large due to Langevin spiralling arising from long-range polarization (Herzenberg, 1967); the compound state is essential for an understanding of the process; the H_2 produced in the reaction is highly excited (Herzenberg, 1967; Chen and Peacher, 1968b) and an inverted population may result.

Experimentally, the reaction $H^-+H\rightarrow H_2+e$ has not yet been studied using ion beams because of the difficulties associated with this type of experiment. However, similar reactions

(e.g., $O^-+CO\rightarrow CO_2^-\rightarrow CO_2+e$;

$O^-+H_2\rightarrow H_2O^-\rightarrow H_2O+e$)

have been studied both in swarm experiments (see, e.g., Ferguson, 1968, Moruzzi *et al.*, 1968) and in beam experiments (Mauer and Schulz, 1973). In both these reactions, a compound state is involved. In the case of CO_2^- the state is $^2\Pi_u$ (Claydon, Segal, and Taylor, 1970; Krauss and Neumann, 1972), and in the case of H_2^-, the state is $^2\Sigma_u^+$ and has been previously discussed. The $CO_2^-(^2\Pi_u)$ state has a lifetime which is somewhat longer (Burrow and Sanche, 1972, give a width, $\Gamma=0.13$–0.26 eV) than the compound state in H_2 ($\Gamma\sim 1$ eV).

The experiments of Mauer and Schulz (1972) show that at very low energies, the cross section is given by a $1/v$ functional form, where v is the relative velocity. Thus polarization dominates, consistent with previous swarm experiments (Moruzzi *et al.*, 1968; Ferguson, 1970). Because Mauer and Schulz used a beam experiment, they could extend the range of incident ion energies; they find that at higher energies (e.g., 1.5 eV in the center of mass for the reaction O^-+CO) the cross section rises and exhibits a maximum, as shown

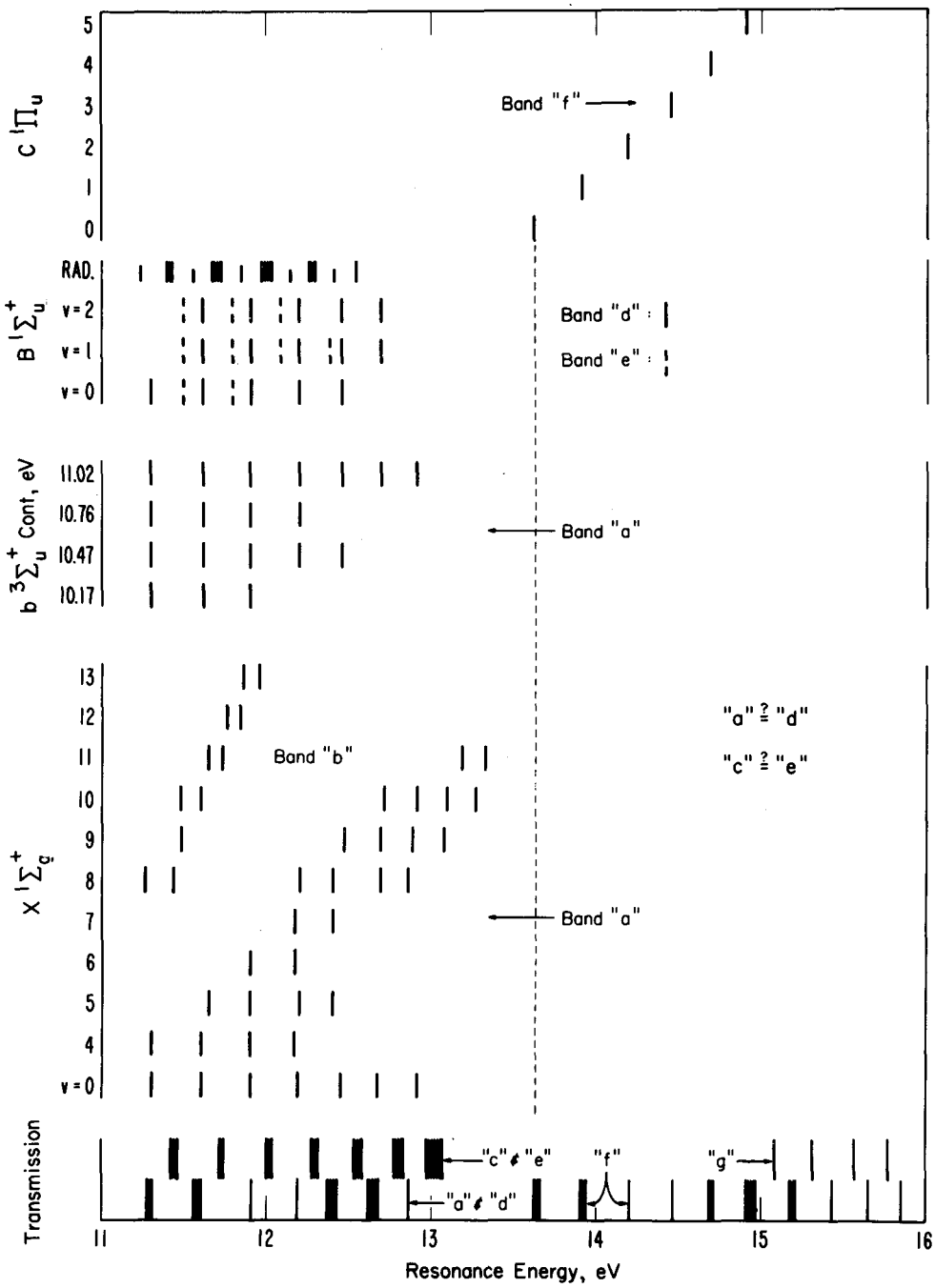

FIG. 24. Position of compound states, as observed in various decay channels. On the bottom, the position of various bands is shown, as observed in transmission experiments. The shaded region shows the extent of the discrepancy between experiments. Higher on the figure, we show the positions of the compound states as observed in various excited states and in the emission of radiation (marked RAD). The assignment to various bands is noted.

in Fig. 13. This rise is due mainly to the following effect: At very low ion energies, ions can reach the region of large associative detachment, which occurs at relatively small internuclear separations, only via an attractive curve. Ions entering the process along repulsive curves cannot get close enough for associative detachment to take place. However, at higher kinetic energies, even ions entering the reaction along repulsive curves can get close enough to the neutral species to detach. Thus, the cross section exhibits a subsidiary rise at 1.5 eV in the case of O^-+CO and at 0.25 eV in the case of O^-+H_2.

Mauer and Schulz (1972) also performed an energy analysis of the detached electrons and found that the reaction leads predominantly to very low-energy electrons, near zero eV. Thus very high vibrational states of CO_2 are excited.

The experimental evidence from the reaction O^-+

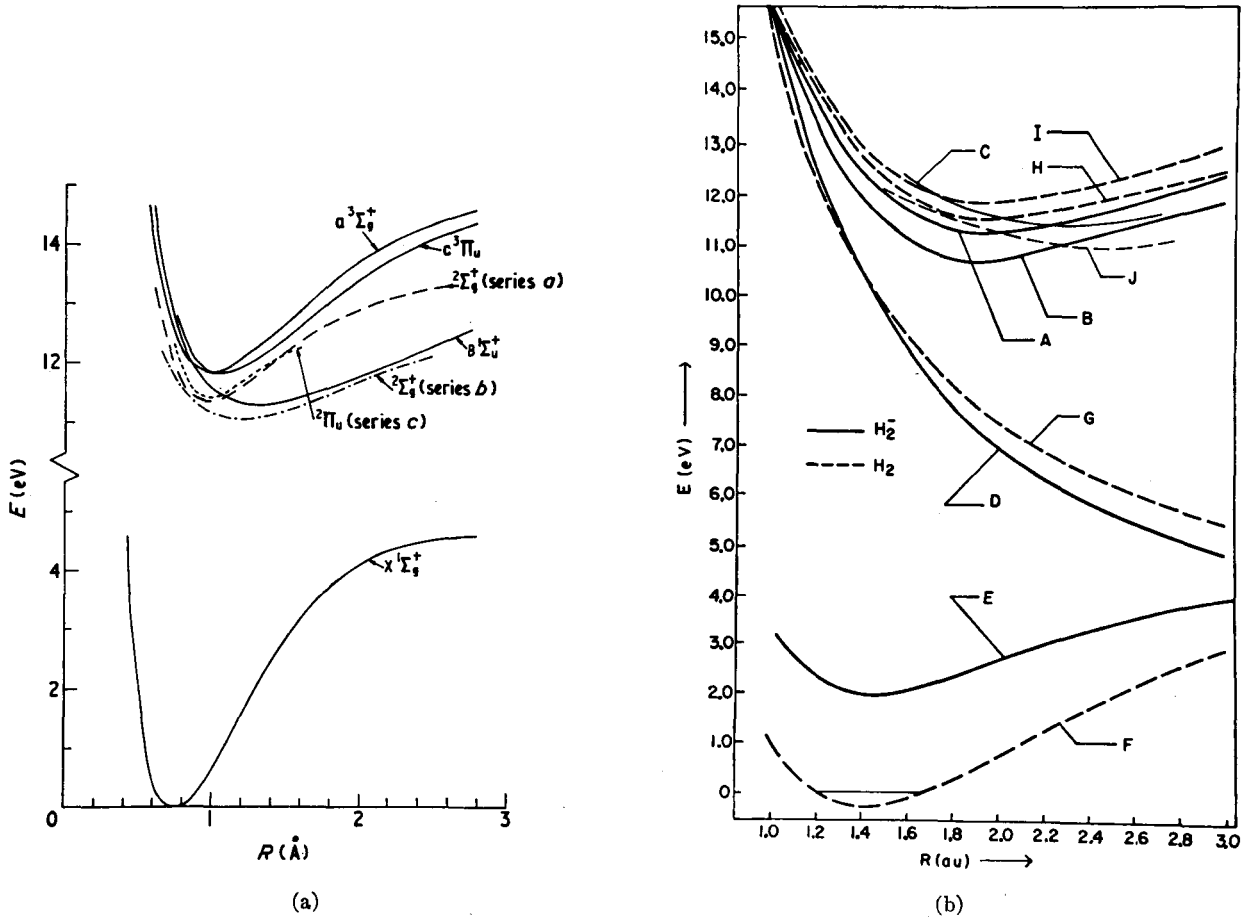

FIG. 25. (a) Potential energy curves for H_2^- state (broken curves) which give the best fits to experimental data. Corresponding curves for some H_2 states (full curves) are also shown (Sharp, 1971). It should be noted that the energy scale is taken with respect to the bottom of the ground-state potential curve. [From Comer and Read (1971a).] (b) Potential energy curves for H_2^- derived from calculations. The full curves represent the calculated compound states and the dashed curves are some of the parent H_2 states. (A) H_2^- $^2\Sigma_g^+$ consisting of $C\,^1\Pi_u \cdot \pi_u 2p'$; (B) H_2^- $^2\Sigma_g^+$ consisting of $C\,^3\Pi_u \cdot \pi_u 2p'$; (C) H_2^- $^2\Sigma_g^+$ consisting of $B\,^1\Sigma_u^+ \cdot \sigma_u 1s'$; (D) H_2^- $^2\Sigma_g^+$ consisting of $^3\Sigma_u^+ \cdot \sigma_u 1s'$; (E) H_2^- $^2\Sigma_u^+$ consisting of $X\,^1\Sigma_g^+ \cdot \sigma_u$; (F) H_2 $X\,^1\Sigma_u^+$; (G) One configuration result for H_2 $^3\Sigma_u^+$ $1\sigma_g 1\sigma_u$. This curve lies about 0.32 eV above the "exact" $^3\Sigma_u^+$ curve, but is used as a comparison with the H_2^- calculation consisting of this configuration plus an extra electron; (H) Two configuration result for H_2 $^3\Pi_u(1\sigma_g 1\pi_u + 1\sigma_u 1\pi_g)$. The minimum of this curve lies about 0.14 eV above the experimental minimum. The H_2 $a\,^3\Sigma_g^+$ curve lies so close to this one that they are indistinguishable on this scale; (I) Same as H for $C\,^1\Pi_u$ and $E\,^1\Sigma_g^+$; (J) H_2 $B\,^1\Sigma_u^+$. [From Eliezer, Taylor, and Williams (1967).]

$CO \rightarrow CO_2 + e$ indicates that the theoretical predictions for $H^- + H$, $\rightarrow H_2 + e$, as outlined above, are probably correct.

B. Resonance in the 10-eV Region ($^2\Sigma_g^+$)

The first excited state of H_2 is the $(1s\sigma_g)(2p\sigma_u)^3\Sigma_u^+$ state. In the notation for separated atoms this becomes $(\sigma_g 1s)(\sigma_u 1s)^3\Sigma_u^+$. The dominant configurations of the compound state associated with this excited state is $(1s\sigma_g)(2p\sigma_u)^2\,^2\Sigma_g^+$ or, in the notation of separated atoms, $(\sigma_g 1s)(\sigma_u 1s)^2\,^2\Sigma_g^+$. Agreement exists on this assignment (Bardsley, Herzenberg, and Mandl, 1966a; Eliezer, Taylor, and Williams, 1967; Bardsley and Mandl, 1968).

When the real part of the potential energy curve for the $^2\Sigma_g^+$ is calculated as a function of internuclear separation, it is found (Bardsley and Mandl, 1968; Eliezer *et al.*, 1967) that the potential energy curve crosses the potential energy curve of the parent, i.e., the $^3\Sigma_u^+$ state. As long as the potential energy curve for H_2^- lies below the parent we are dealing with a core-excited resonance of the Feshbach type. When the potential energy curve lies above the parent we are dealing with a core-excited shape resonance. In this case the assignment varies as a function of internuclear separation.

Information regarding the $^2\Sigma_g^+$ state of H_2^- comes from experiments on dissociative attachment. In other channels, this state has not yet been observed. A comparison of two recent experiments on negative ion formation with H_2 in the range 7–17 eV is shown in Fig. 14. An interesting isotope effect, not as dramatic as the one for the $^2\Sigma_u^+$ state, has been discovered by Rapp

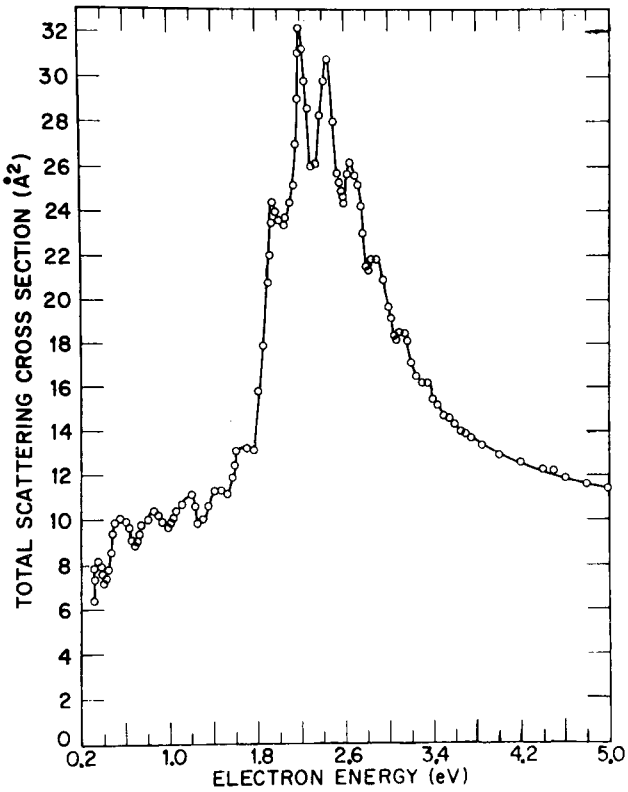

FIG. 26. The absolute total cross section for scattering of electrons on N_2, as obtained using a modified Ramsauer technique. The total cross section includes elastic and inelastic components. The structure above 1.8 eV is indicative of the pseudovibrations of the $^2\Pi_g$ compound state. The structure below 1.8 eV has not been substantiated by other experiments, although attempts at confirming it have been made. The structure below 1.8 eV must be considered in doubt at the present time. [From Golden (1966).]

et al. (1965). These results are shown in Fig. 15. Similar considerations as those discussed in Sec. IIA4 also apply here. In fact, Bardsley, Herzenberg, and Mandl (1966b) have obtained a good theoretical fit to the curves of Fig. 15, and they point out that decay of the $^2\Sigma_g^+$ state of H_2^- to the $^3\Sigma_u^+$ excited state is more probable than decay to the ground state. The overlap is more favorable when the compound state can decay into its parent ($^3\Sigma_u^+$) state. This may explain why it has not been possible to detect the decay of the $H_2^-(^2\Sigma_g^+)$ state to the ground electronic state. The total width of the $^2\Sigma_g^+$ state is estimated to be $\Gamma=0.8$ eV and the entry width from the ground electronic state is 0.004 eV.

The potential energy curves for the $^2\Sigma_u^+$ and the $^2\Sigma_g^+$ states, derived by Bardsley *et al.* (1966a) and by Chen and Peacher (1968a), have already been discussed in connection with Fig. 6. Also shown are the imaginary parts of the potential curves, i.e., the width Γ, as a function of internuclear separation. The potential energy curves of Eliezer *et al.* (1967) are shown in Fig. 25(b).

The H^- formation via the $^2\Sigma_g^+$ state extends well into the 11–12 eV region, in which a multitude of resonances are observed in elastic and inelastic scattering (see Sec. IIC). It is therefore not surprising that high-resolution experiments on negative ion formation would show structure in the 11–12 eV region. The decay of bound compound states into the dissociative attachment channel was observed by Dowell and Sharp (1968) and is shown in Fig. 16. The mechanisms for this coupling have been discussed by Eliezer *et al.* (1967) in terms of a radiationless intramolecular transition.

The structure shown in Fig. 16 is further discussed in Sec. IIC.

C. Core-Excited Resonances in the 11–15 eV Region

Resonances of the core-excited (Feshbach) type in H_2 were discovered by Kuyatt, Mielczarek, and Simpson (1964) in the energy range 11.62 to 13.31 eV by

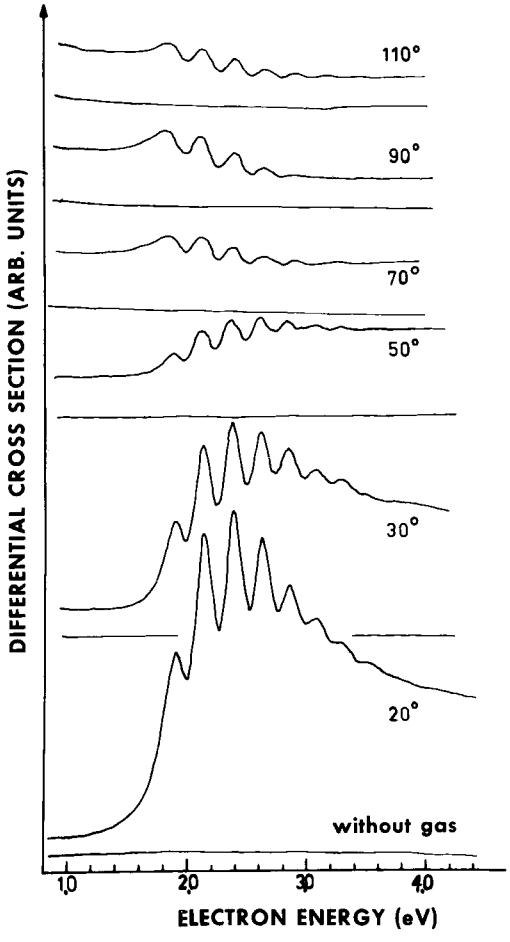

FIG. 27. Energy dependence of the "elastic" cross section in N_2 at various angles of observations. The experiment uses an electrostatic monochromator and an electrostatic analyzer, which accepts only "elastically" scattered electrons. Since the resolution is not sufficiently good to resolve rotational states, all rotational transitions are included in the measurement. [From Ehrhardt and Willmann (1967).]

observing elastically scattered electrons. These structures were confirmed by Golden and Bandel (1965) in a Ramsauer-type experiment for both H_2 and D_2. Menendez and Holt (1966) found the structure in the excitation of the $v=1$ and $v=2$ vibrational states of the ground electronic state, $H_2(X\,^1\Sigma_g^+)$, thus indicating a decay of the resonances into vibrational states. Heideman, Kuyatt, and Chamberlain (1966) were the first to observe the decay of these compound states into electronically excited states of H_2 by studying the energy dependence of the $v=0$ and $v=1$ vibrational states of the $B\,^1\Sigma_u^+$ state of H_2. Also, it was understood both theoretically (Eliezer *et al.*, 1967) and experimentally (Kuyatt *et al.*, 1966) that more than one compound state contributes to the observed structure, and that the isotopes HD and D_2 exhibit a set of similar structures but that they show differences in the relative strength of the series.

Experimentally, five series of resonances have been definitely identified, and as many as seven can be invoked to explain the experimental data. Comer and Read (1971a) have suggested a classification scheme,

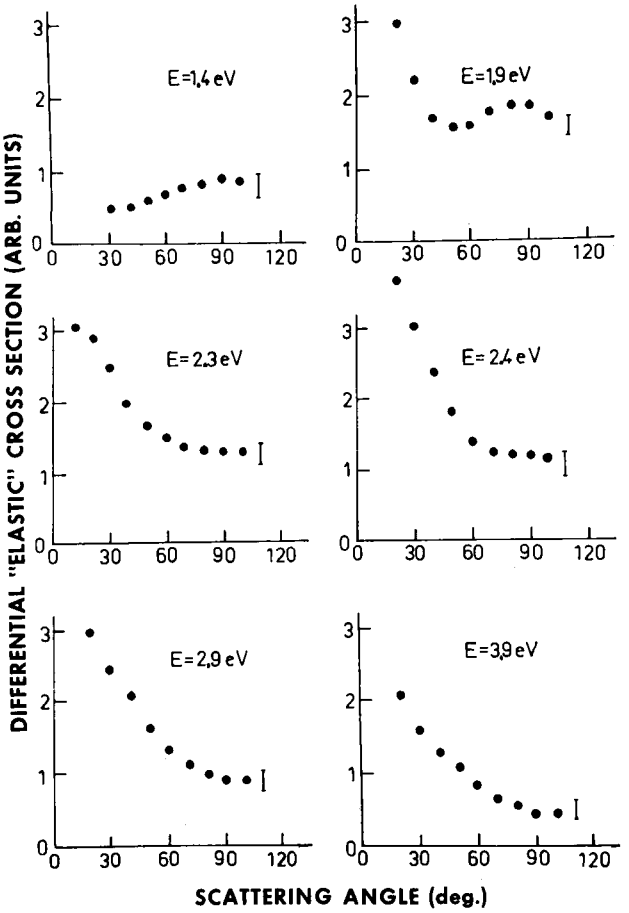

FIG. 28. Angular dependence of "elastically" scattered electrons at various fixed electron energies E. A common scale is used for all curves. [From Ehrhardt and Willmann (1967).]

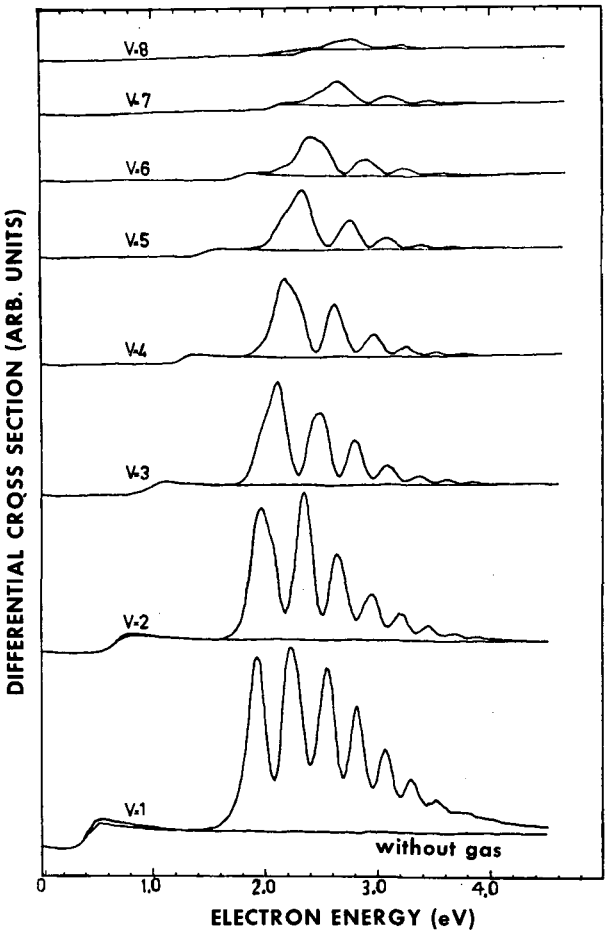

FIG. 29. Energy dependence of the vibrational excitation in N_2 at a scattering angle of 20°. Excitation to eight vibrational states ($v=1-8$) is observed in the region of the $^2\Pi_g$ compound state. [From Ehrhardt and Willmann (1967).]

which was later adopted by Sanche and Schulz (1972), and which is followed in the present review. We designate the different bands with the letters "a" to "g." Table II provides a listing of the bands and indicates the names given to the bands by different authors, the decay channel in which the bands were observed, and the energy of the first feature. The table is presented to provide a "dictionary" which is helpful in reading the original literature.

It should be noted that series "a" and "d" have the same starting energy and the same spacing. The need for postulating two separate series with similar molecular parameters is brought about by angular distribution measurements (Comer and Read, 1970). Series "a" is of the Σ-type and thus is expected to exhibit an isotropic behavior. Weingartshofer *et al.* (1970) observe structure in the $B\,^1\Sigma_u$ state at the positions of the resonances in series "a." However, the angular distribution in this channel of decay is *not* isotropic. Therefore, Comer and Read find it necessary to postulate a state of Π symmetry around 11.40 eV. They have considered the possibility that the observed anisotropy

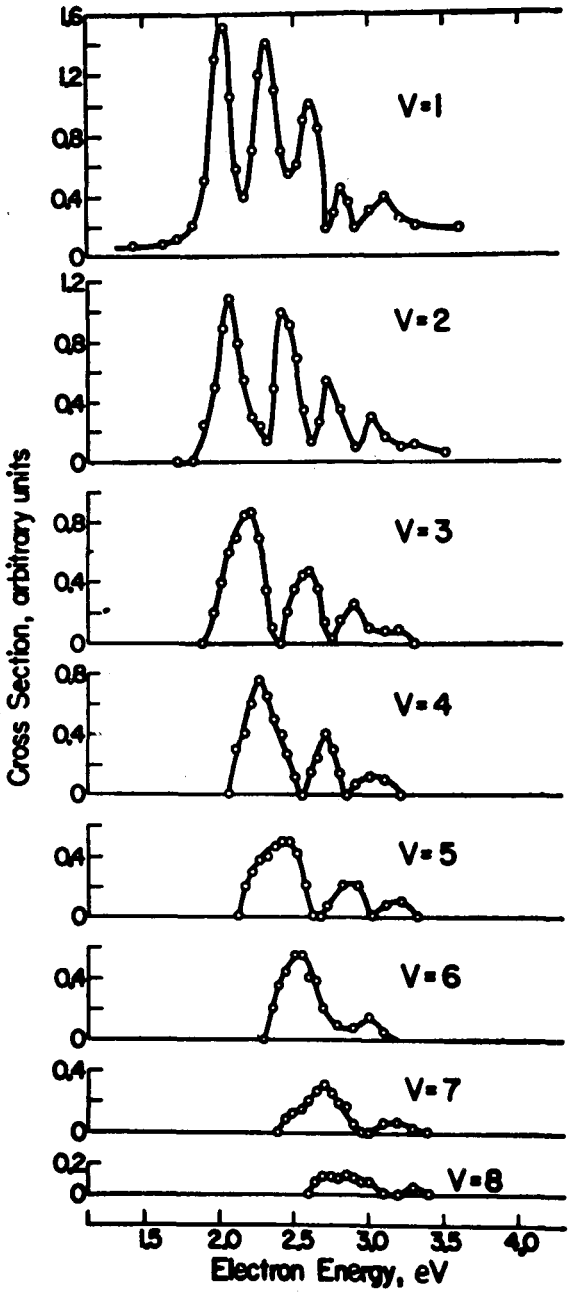

FIG. 30. Energy dependence of the vibrational excitation in N_2. The angle of observation was 72 degrees. As in Fig. 29, eight vibrational states are visible in the region of the $^2\Pi_g$ compound state. The similarity of the curves with those shown in Fig. 29 indicates that the structures in the vibrational cross sections are independent of angle of observation. [From Schulz (1964).]

of the resonances in the $B\,^1\Sigma_u^+$ states results from a d-wave component in the entrance channel, but have discarded this interpretation because it leads to an unreasonably large d-wave amplitude in the entrance channel.

The above considerations relay heavily on angular distribution measurements which, in molecules, may not be as well understood as one would wish. For example, Black and Lane (1971) point out that in certain decay channels transitions may show preference for a change in rotational quantum number, e.g., $j=0\rightarrow j=1$. Such an effect would upset the simple interpretation of angular distribution measurements and may render unnecessary the assignment of a separate series for bands "d" and "e." More detailed analysis must be awaited.

These uncertainties are taken into account in Table II. Arrows point to series "a" and "d" and to series "c" and "e," indicating that future consideration may show that "a"="d" and "c"="e." In energy, these two sets of series ("a" and "d"; "c" and "e") are almost coincident.

Samples of recent experimental results, as observed in different decay channels, are shown in Figs. 17–22. Figure 17 shows the results of a transmission experiment by Sanche and Schulz (1972) in which the derivative of the transmitted current is measured directly. This experiment, following closely in concept the experiments of Kuyatt *et al.* (1964) and Schulz (1964), exhibits higher sensitivity to sharp structures than previous transmission experiments. In the experiment of Sanche and Schulz (1972), optical focussing effects are largely eliminated by the use of an axial magnetic field and the detection sensitivity is enhanced by modulating the electron energy in the collision chamber. The advantage of the transmission experiment is the overview that it provides for a large region of energy. However, many details of resonances, such as the decay channel and the angular distribution of scattered electrons, cannot be easily extricated from transmission experiments.

Figures 18 and 19 show the results of Comer and Read (1971a) for which a double electrostatic analyzer was used. By studying resonances in high vibrational states of the electronic ground state, Comer and Read are able to eliminate all interference effects between resonant and nonresonant scattering; in fact they discovered series "b" by observing resonant structure in vibrational levels above $v=8$, as is shown in Fig. 19. It

TABLE III. Position of maxima in the elastic and inelastic cross sections of N_2 (Ehrhardt and Willmann, 1967).

	Energy, eV	
v'	$v=0$	$v=1$
0	1.89	1.93
1	2.15	2.24
2	2.40	2.55
3	2.65	2.82
4	2.89	3.07
5	3.13	3.31
6	3.36	3.53
7	3.58	3.76

should be noted that most of the structure visible in the lower vibrational states of Fig. 18 consists of series "a". The values of the resonant energies obtained by Comer and Read are tabulated for H_2^- in Appendix I, and for D_2^- in Appendix II. The results for D_2^- are very similar to those for H_2^-.

Studies similar to those of Comer and Read, using a similar technique had been previously undertaken by Weingartshofer *et al.* (1970). Their results (in absolute units) at different angles of observation are shown in Figs. 20 and 21. In addition to the $X\ ^1\Sigma_g^+$ decay channel, Weingartshofer *et al.* examined other decay channels: the dissociation continuum, $b\ ^3\Sigma_u^+$ (see Fig. 22); $c\ ^3\Pi_u$; $a\ ^3\Sigma_g^+$; and several vibrational levels of the states $C\ ^1\Pi_u$, $B'\ ^1\Sigma_u^+$, and $D\ ^1\Pi_u$. The branching ratios for the decay into some of these channels are listed, in absolute units, in Appendix III. Molecular radiation emanating from the $B\ ^1\Sigma_u^+$ state of H_2 and D_2 also shows the appropriate resonances, as has been shown by McGowan and Williams (1969) and by Pichanick *et al.* (1971).

Figure 23 shows a schematic diagram of the five energetically distinct compound states of H_2^- and some of the decay channels. Figure 24 shows the energies at which various resonances have been observed in different channels of decay. On the bottom of the

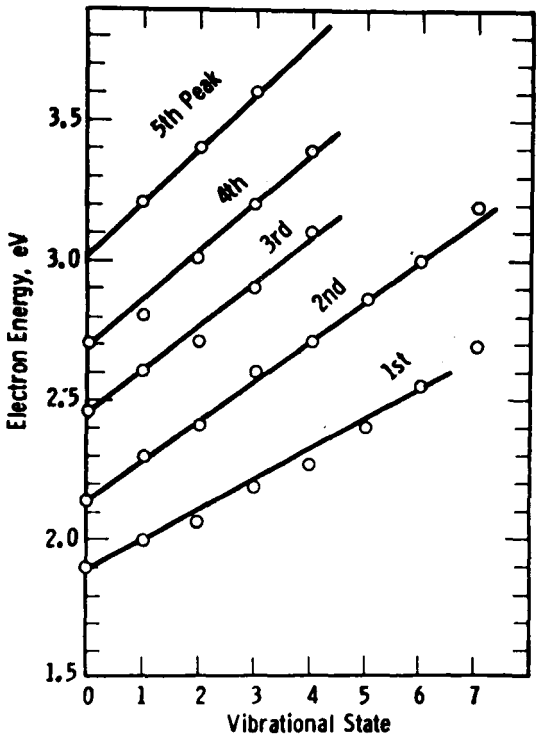

FIG. 31. Position of the peaks in the cross section vs quantum number of the final state. If the $^2\Pi_g$ compound state were long-lived compared to vibrational times, the solid lines would be horizontal, i.e., the peaks would occur at the same energy regardless of the final vibrational state. The effect shown on this figure indicates that the lifetime of the $^2\Pi_g$ compound state is comparable to a vibrational period. [From Schulz (1964).]

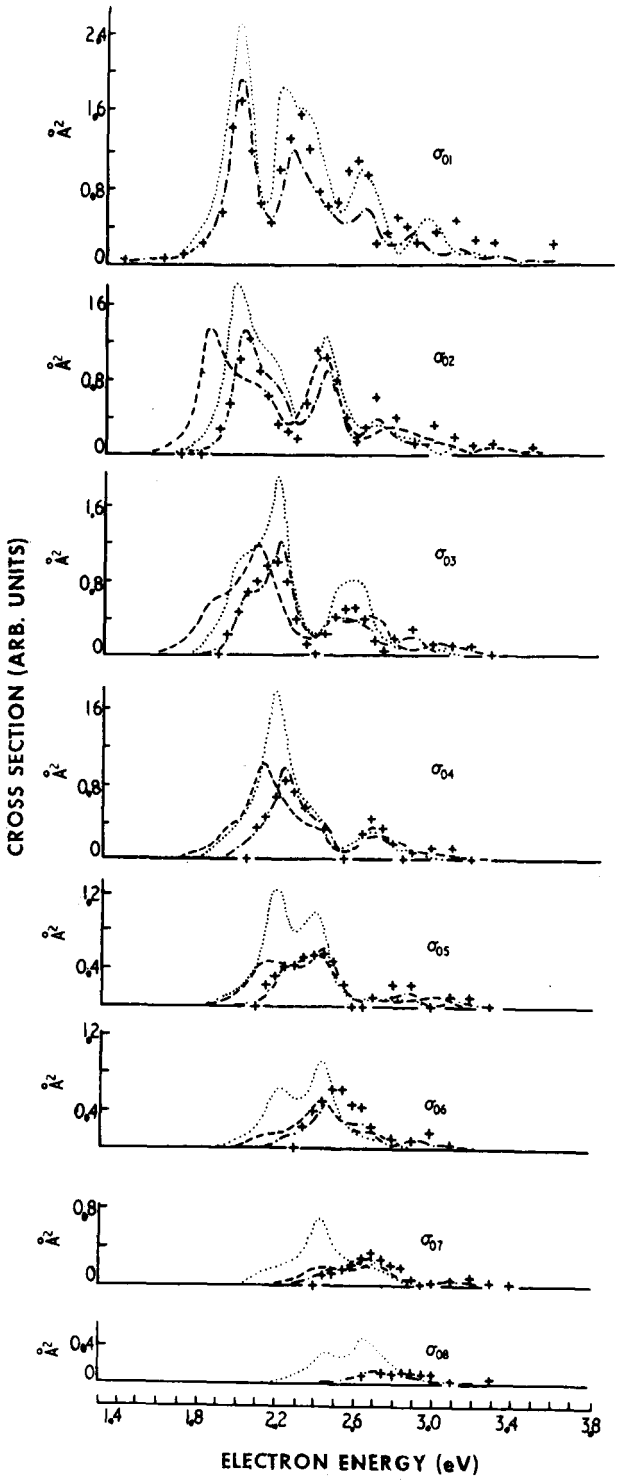

FIG. 32. Comparison of experimental and theoretical vibrational cross sections for resonant e-N_2 scattering. Crosses are the experimental results of Schulz (1964). The curves show various theoretical attempts to fit the experimental cross sections without allowing for the variation of Γ with internuclear separation. None of these theoretical curves reproduce the regularity of the experimental structure. The broken curve: Herzenberg and Mandl (1962); chain curve: Chen (1964); dotted curve: Hasted and Awan (1969). [From Birtwistle and Herzenberg (1971).]

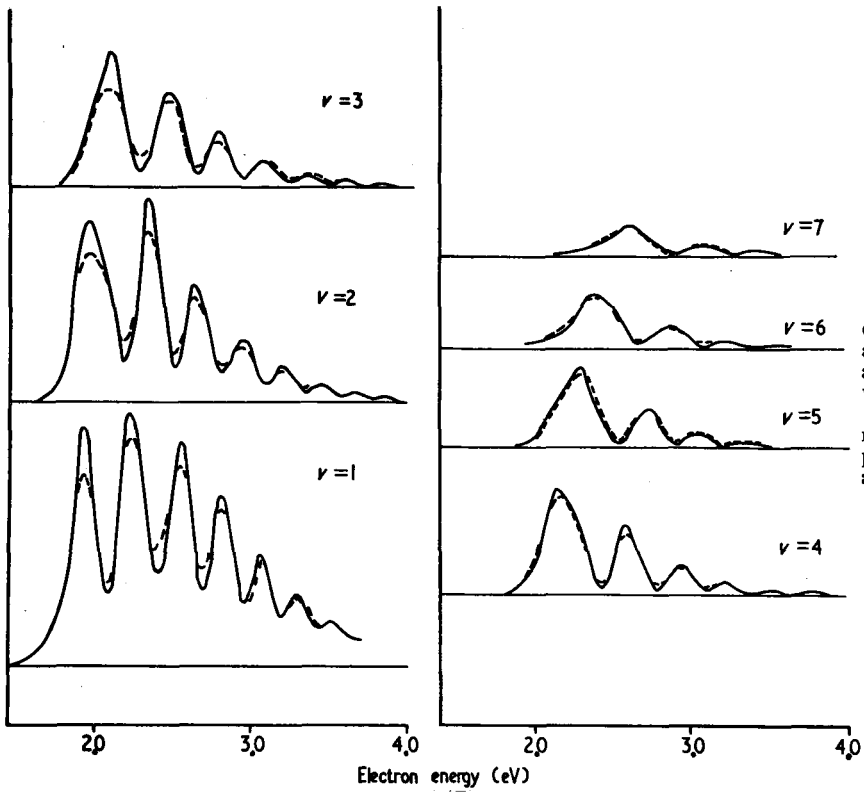

FIG. 33. Comparison of the theoretical cross section for vibrational excitation using a variable Γ. The dashed curve (Birtwistle and Herzenberg, 1971) is theoretical, using a variable Γ, and the full curve is experimental (Ehrhardt and Willmann, 1967). The theoretical cross section is calculated using the parameters of Table IV. [From Birtwistle and Herzenberg (1971).]

figure, the position of resonances is indicated as they appear in transmission experiments. The energy positions of the transmission experiments of Kuyatt *et al.* (1966) and of Sanche and Schulz (1972) are shown. The shaded region indicates the spread of values, which rarely exceeds 50 meV. Thus the agreement is considered excellent.

Higher on Fig. 24, we show decay into high vibrational states of the ground electronic state, into the $b\,^3\Sigma_u^+$ continuum, and the $B\,^1\Sigma_u^+$ state as well as the $C\,^1\Pi_u$ states in the low vibrational levels.

Decay into the $B\,^1\Sigma_u^+$ state followed by the emission of a photon is also indicated. Whereas McGowan and Williams (1969) observe a "strong" and a weak series, Pichanick *et al.* (1971) observe only the "strong" series. The shaded area indicates the degree of uncertainty between the two above-mentioned experiments. The short lines indicate the positions of the "weak series" in the radiation. The "strong" lines agree best with series "c" (or "e") and the weak ones with series "a" (or "d"). Why this is so, i.e., why one band seems to dominate in radiative decay when it is not observed in inelastic channels, is not understood.

Below we discuss some of the more prominent features of the different bands. Appendixes I and II list the energies in tabular form for H_2 and D_2.

A set of potential energy curves has been derived from purely experimental information by Comer and Read (1971a) and is shown in Fig. 25(a). A quasi-variational calculation of Eliezer *et al.* (1967) gives very good agreement with some of the experimental observations and points to the proper designation of the states. Eliezer *et al.* find that the lowest two compound states have $^2\Sigma_g^+$ symmetry and that they consist of the $C\,^3\Pi_u$ and $C\,^1\Pi_u$ states, respectively, with an electron attached which has $(\pi_u 2p')$ symmetry. See Fig. 25(b).

1. Band "a"

Band "a" seems to decay into all possible decay channels. The agreement between various groups as to

TABLE IV. Characteristics of N_2^- ($^2\Pi_g$) resonance at 2.3 eV.

	Birtwistle and Herzenberg (1971)	Krauss and Mies (1970)
$R_0^- - R_0$ (cm)[a]	$0.095(\pm 0.003)\times 10^{-8}$	0.12×10^{-8}
$\hbar\omega$ (eV)[b]	0.244 ± 0.003	0.24
x_e[c]	0.0051 ± 0.0017	0.0046
$\Gamma(R_0)$ (eV)[d]	0.57 ± 0.02	0.8

[a] R_0^-, R_0 are the equilibrium internuclear separations for N_2^- and N_2, respectively.

[b] $\hbar\omega$ is the vibrational spacing of N_2^-.

[c] x_e is the anharmonic constant.

[d] $\Gamma(R_0)$ is the width at R_0.

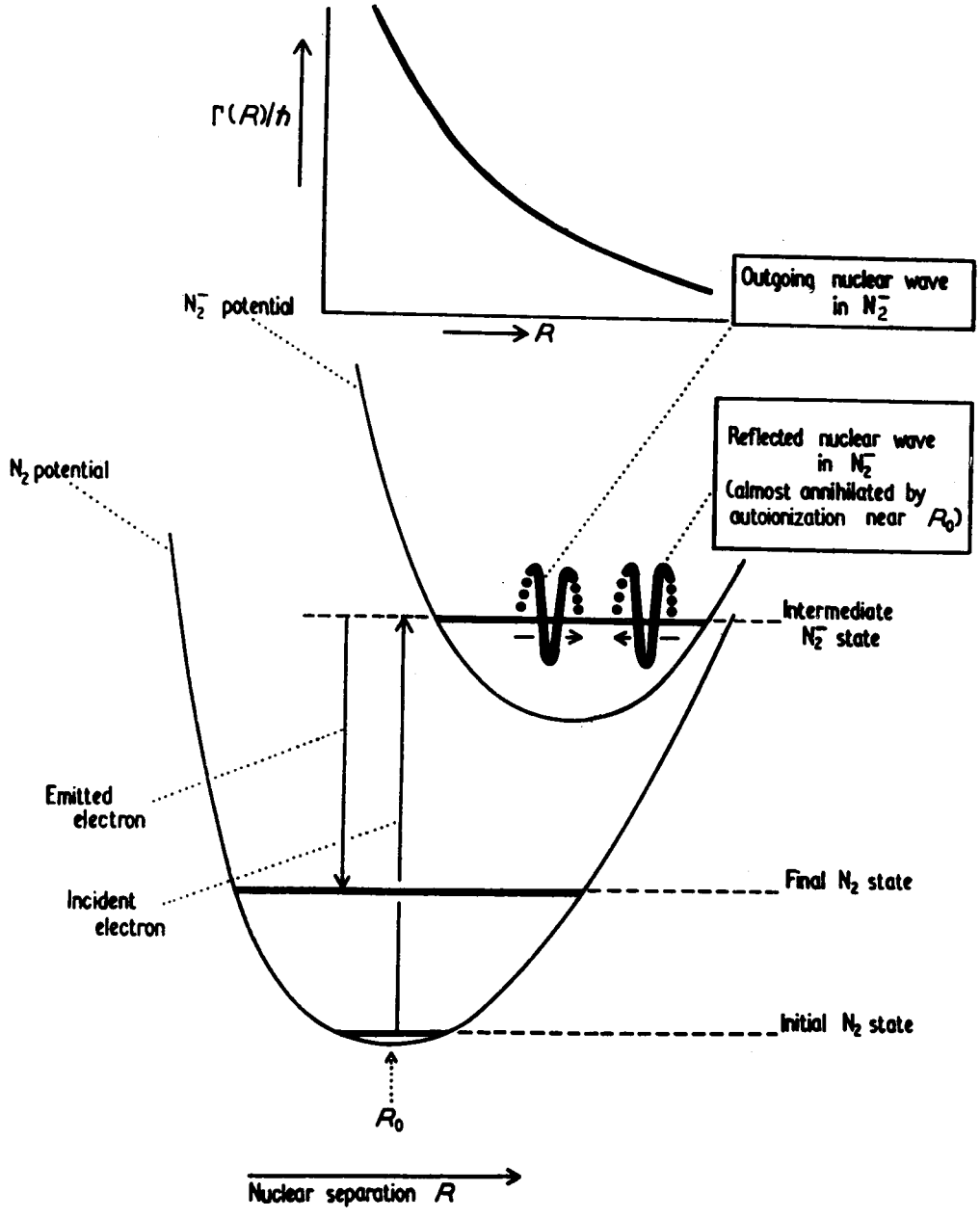

FIG. 34. The "boomerang" model of the nuclear wave function applied to the N_2^- ion. This schematic model is discussed by Herzenberg (1968). It is based on the assumption that the magnitude and R dependence of $\Gamma(R)$ are such that only a single outgoing and a single reflected wave matter. [From Birtwistle and Herzenberg (1971).]

the location on the energy scale is very satisfactory. Small discrepancies in energy probably result from the method of evaluating the position of the resonances. Also, interference effects can shift the position of the peaks, which are not necessarily the true positions of the resonances. The results of Weingartshofer *et al.* (1970) and of Comer and Read (1970a), who observe resonances in those channels in which very little interference takes place (e.g., high vibrational states), are free from such errors.

Eliezer *et al.* (1967) assign to this band the configuration $(\sigma_g 1s)(\pi_u 2p)(\pi_u 2p')\,^2\Sigma_g^+$, consisting predominantly of $(C\,^3\Pi_u + e)$. When one arbitrarily adds 0.25 eV to Eliezer's calculated values, excellent agreement exists between theory and experiment. (see Appendix I). In any case, the spacing calculated by Eliezer *et al.* for band "a" agrees with experiment and thus the assignment appears convincing. Comer and Read obtain values of 0.975 Å and 11.40 eV for the equilibrium internuclear separation and the energy minimum, respectively, whereas the values deduced by Eliezer *et al.* are 1.03 Å and 11.18 eV. Band "a" seems to be firmly established.

2. *Band "b"*

Band "b" has been observed only by Comer and Read (1971a) in high vibrational levels of the ground state of H_2. They obtained a natural width of 30 meV

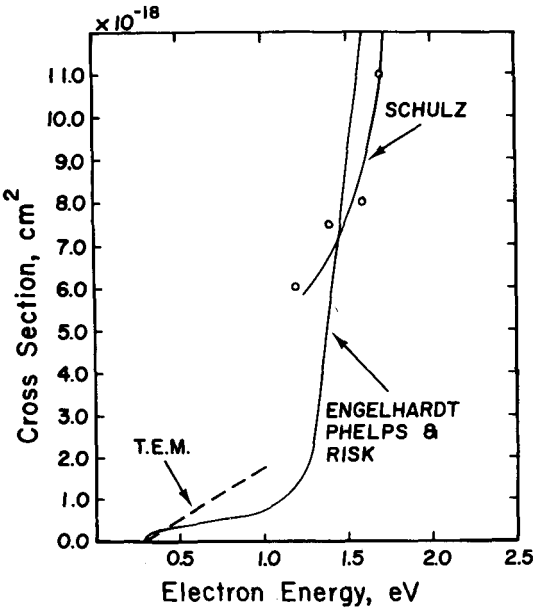

FIG. 35. Excitation function for $v=1$ in N_2 near threshold. Shown are the results of Engelhardt, Phelps, and Risk (1964) obtained from an analysis of swarm experiments, the double electrostatic analyzer measurements of Schulz (1964), and the slope near threshold obtained using the trapped-electron method (TEM) by Burrow and Schulz (1969). The low-energy portion of the theoretical cross section (Chen, 1964a) is identical to that of Engelhardt, Phelps, and Risk below 1.2 eV. [From Burrow and Schulz (1969).]

for band "b" and suggested that the new resonance has the configuration $(\sigma_g 1s)(\sigma_u 1s)^2\,{}^2\Sigma_g^+$, representing an electron bound to the $B\,{}^1\Sigma_u^+$ excited state of H_2. This band has not been observed in any transmission experiment. The assignment is still in doubt, especially since the potential energy curve for the $(\sigma_g 1s)(\sigma_u 1s)^2$ compound state should have a larger equilibrium internuclear separation than the parent $B\,{}^1\Sigma_u^+$ state (H. S. Taylor, private communication). In order to interpret their experiment, Comer and Read (1971a) must assign a smaller equilibrium internuclear separation to the $(\sigma_g 1s)(\sigma_u 1s)^2$ state compared to the parent $B\,{}^1\Sigma_u^+$ state, as shown in Fig. 25(a).

3. Band "c"

Band "c" has been observed in the transmission experiments of Kuyatt *et al.* (1966) and of Sanche and Schulz (1972) in both H_2 and D_2. In their early work, Comer and Read (1971a) observed band "c" only in D_2 and not in H_2. They assign to band "c" the configuration $(\sigma_g 1s)(\pi_u 2p)(\sigma_g 2s)\,{}^2\Pi_u$. Recently, however, Joyez, Comer, and Read (1973) were able to observe band "c" in a high resolution experiment in H_2. Their value for the width is $\Gamma \leq 16$ meV and the starting energy is about 11.19 eV, with subsequent values at 11.50, 11.80, and 12.07 eV. If the starting value of 11.19 for band "c" is substantiated, then the quantum numbers for band "c" as assigned by the other investigators listed in Appendix I will have to be incremented by unity.

As pointed out previously, band "c" appears strongly in vacuum uv emission.

The calculated progression of Eliezer *et al.* (1967) for the configuration $^2\Sigma_g^+(\sigma_g 1s)(\pi_u 2p)(\pi_u 2p')$ agrees well with most of the experimental energy positions, as shown in Appendix I. However, there is a problem in understanding the angular dependences found by Comer *et al.*

The detailed understanding of bands "c" and "e" is still missing and the above considerations must be considered as preliminary.

4. Band "d"

This band was postulated by Comer and Read (1971a) from an analysis of the results of Weingartshofer *et al.* (1970). On the basis of the angular distribution of electrons observed by Weingartshofer *et al.* in the $B\,{}^1\Sigma_u$ exit channel, Comer and Read suggest that the compound state involved must have $^2\Pi_g$ symmetry. Although the results of Weingartshofer are coincident in

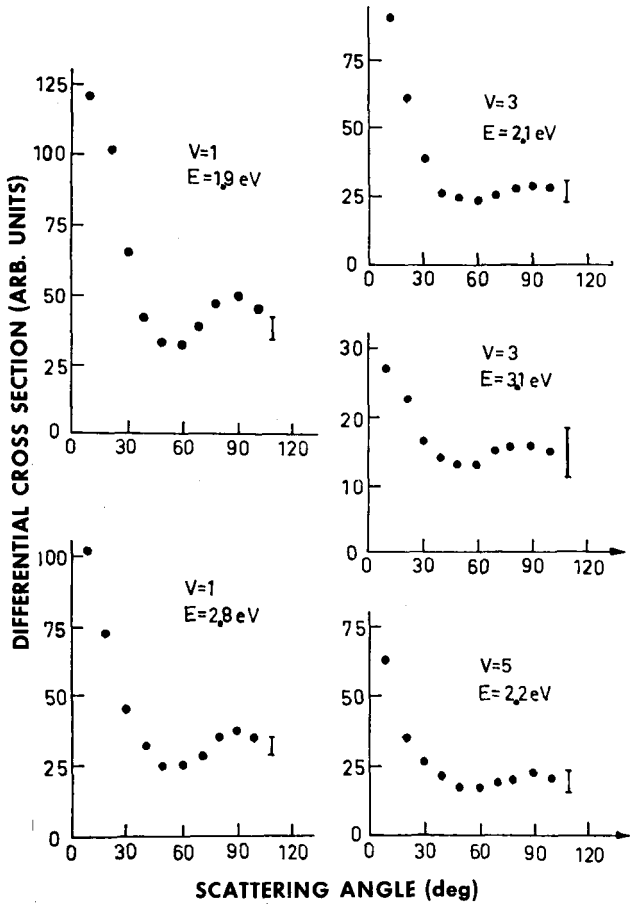

FIG. 36. Angular dependence of the cross section for vibrational excitation to $v=1$, 3, and 5 in N_2. The electron energy is indicated. The subsidiary peaks near 90° result from d-wave scattering. [From Ehrhardt and Willmann (1967).]

energy with series "a," Comer and Read suggest that the compound state is not the same since series "a" involves a $^2\Sigma_g^+$ state. However, Black and Lane (1971) have recently pointed out that angular distributions are not a simple guide to the assignment of symmetries because different rotational transitions may be dominant in various decay channels. Thus Black and Lane show that the rotational transition $j=0\rightarrow j=1$ dominates in the process $e+H_2(X\,^1\Sigma_g^+)\rightarrow H_2^-(e+C\,^1\Pi_u)\rightarrow H_2(B\,^1\Sigma_u^+)+e$. If such mechanisms are present, angular distributions will have to be analyzed in more detail.

5. Band "e"

Under the heading of band "e" we list the measurement of Weingartshofer *et al.* (1970) who observed inelastically scattered electrons having excited the $B\,^1\Sigma_u^+$ state.

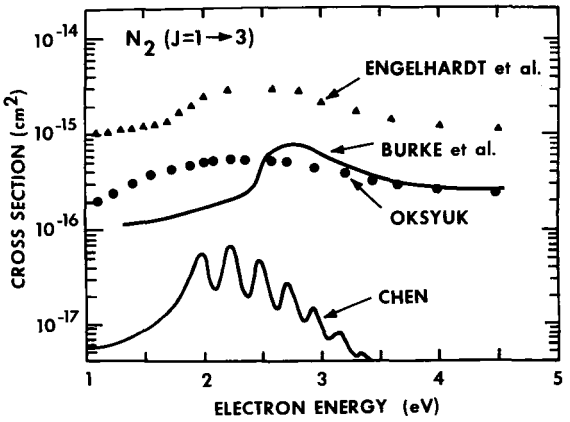

FIG. 37. Pure rotational excitation ($J=1\rightarrow3$) in the region of the $^2\Pi_g$ compound state in N_2. Shown are the theoretical results of Oksyuk (1966), Burke and Sinfailam (1970), and Chen (1966b), and the momentum transfer cross section of Engelhardt, Phelps, and Risk (1964).

Comer and Read advocate such a separation because of a discrepancy in the energy scale, but there is a good possibility that band "e" may be the same progression as band "c".

6. Band "f"

Band "f" extends from approximately 13.5 to 16 eV in H_2 and from 13.5 to 14.5 eV in D_2. This band corresponds to the 13.63-eV progression found by Ehrhardt and Weingartshofer (1969) in the $C\,^1\Pi_u$ decay channel of H_2. It has also been observed by Golden (1971) in a transmission experiment using a derivative technique similar to that of Sanche and Schulz (1972). In transmission experiments, band "f" exhibits a width of about 90 meV in both H_2 and D_2, in good agreement with the natural width of 80 meV estimated by Ehrdhardt *et al.* (1969). The $^2\Sigma_g^+$ symmetry for band "f" was assigned by these authors.

Band "f" shows peculiar characteristics: it decays

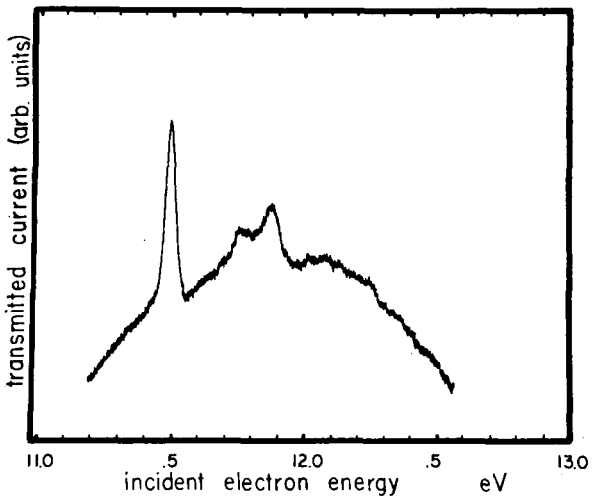

FIG. 38. Transmission of electrons by N_2, showing a sharp "window"-type resonance at 11.48±0.05 eV. The zero of current has been displaced. Additional structure occurs at 11.75 and 11.87 eV. The latter is partly due to an inelastic threshold ($E\,^3\Sigma_g^+$). The nitrogen pressure was ~0.04 Torr. [From Heideman, Kuyatt, and Chamberlain (1966a).]

preferentially to identical vibrational levels of the $C\,^1\Pi_u$ state, i.e., in the decay process the vibrational quantum number does not change (Weingartshofer *et al.*, 1970). This is clearly evident from Figs. 23 and 24. It is therefore likely that the potential energy curve responsible for band "f" has the same shape and the same equilibrium internuclear separation as the $C\,^1\Pi_u$ or $D\,^1\Pi_u$ states.

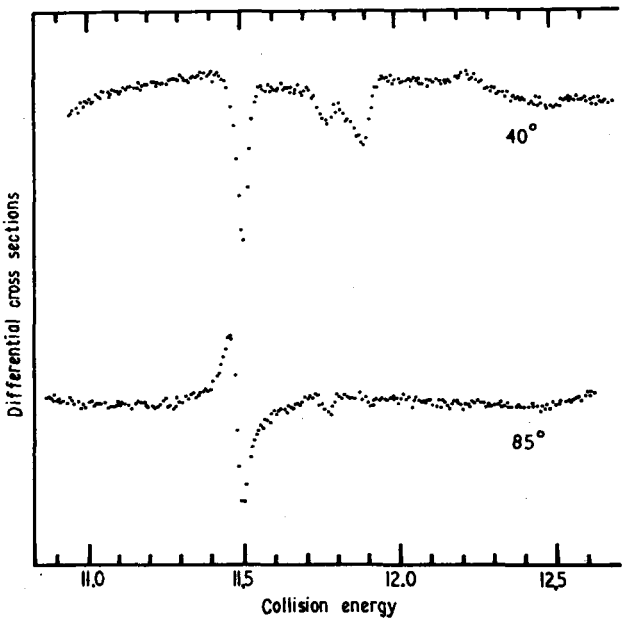

FIG. 39. Energy dependence of the differential elastic cross section for N_2 at 40° and 85°. The largest structure shown occurs at 11.48 eV and is coincident in energy with the transmission peak shown in Fig. 38. The designation is $^2\Sigma_g^+$. The energies of the other structures are listed in Appendix V. [From Comer and Read (1971b).]

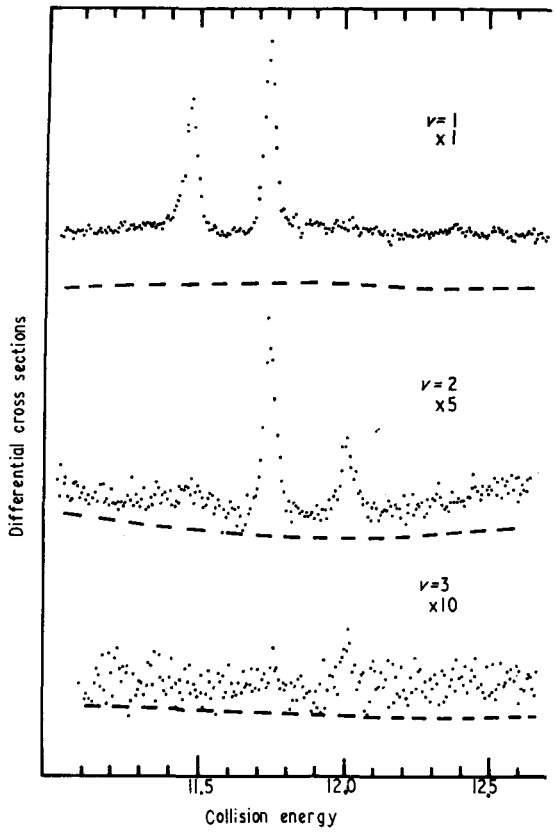

FIG. 40. Energy dependence of the differential vibrational cross sections for scattering of electrons from N_2. The exit channels are vibrational levels of the electronic ground state and the scattering angle is 70°. The curves do not have the same cross section scale but the peak intensities can be obtained from Table II. The zero lines are shown broken. [From Comer and Read (1971).]

7. *Band "g"*

Figure 17 shows that band "f" appears perturbed by the presence of other structures. This new band is labelled "g" and tabulated in Appendix I. It appears much more clearly in D_2 where bands "f" and "g" do not overlap. Three features around 16 eV in the data of Golden (1971) in H_2 which he attributed to autoionization could be members of band "g."

III. NITROGEN

A. Resonance at Low Energy (1.7–4 eV) $^2\Pi_g$

The earliest experiments on the total cross section in N_2 showed a broad peak in the region around 2.3 eV in N_2 (Ramsauer and Kollath, 1931), but it was not until the early 1960's that an understanding of this effect became available, largely as a result of improved experimental techniques and the pioneering theoretical contribution of Herzenberg and Mandl (1962). From an experimental viewpoint one obtains the most detailed information on the nature of the compound state involved by studying structure in the elastic and vibrational cross sections vs energy and by studying angular distributions of the scattered electrons. It should be recalled that, in the case of H_2, the dissociative attachment decay channel provided valuable understanding. However, since no stable N^- ion exists, such a study is not feasible in N_2.

The history of this discovery has been well reviewed by Massey and Burhop (1969), by Chen (1969), by Birtwistle and Herzenberg (1971), and by Bardsley and Mandl (1968). Following the total cross section measurements by Ramsauer and Kollath (1931), Haas (1957) established that the vibrational cross section exhibits a peak in the 2.3-eV energy range and that a temporary negative ion is involved. Schulz (1959) confirmed these observations using the trapped-electron method, but not until he used double electrostatic analyzers (Schulz 1962a, 1964a, 1966) could he establish the details of the resonance process.

The nitrogen molecule has the configuration $(\sigma_g 1s)^2 (\sigma_u 1s)^2 (\sigma_g 2s)^2 (\sigma_u 2s)^2 (\pi_u 2p)^4 (\sigma_g 2p)^2$. The first unfilled orbital is $\pi_g 2p$ ($= 3d\pi_g$ in the united-molecule notation) and the incident low-energy electron temporarily occupies this orbital. As the electron escapes, it encounters a *d*-wave barrier through which it must tunnel. This shape resonance has a symmetry $^2\Pi_g$ and it is centered around 2.3 eV. It dominates the low-energy electron impact cross sections in N_2, as shall be discussed in the following sections. A summary of shape resonances in other molecules is given in Sec. VII.

1. *Elastic Cross Section via* $^2\Pi_g$

The energy dependence of the total scattering cross section, obtained by Golden (1966) using a modified Ramsauer apparatus, is shown in Fig. 26. The structure in the cross section above 1.8 eV is clearly visible. This structure can be observed in a Ramsauer-type apparatus when the energy distribution of the electrons

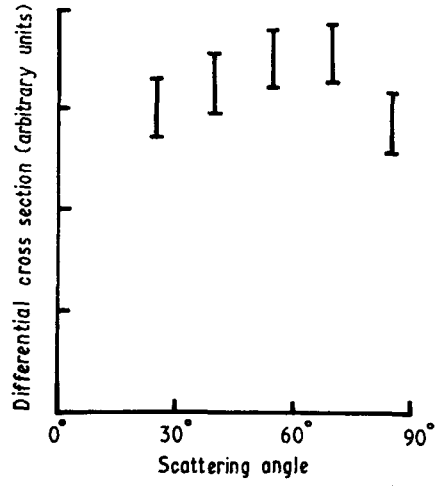

FIG. 41. Angular distribution for the two resonant peaks observed in the $v=1$ exit channel (see Fig. 40). [From Comer and Read (1971b).]

is narrow. The structure above 1.8 eV had been previously observed in the vibrational cross section by Schulz (1964) and interpreted as evidence for the $^2\Pi_g$ compound state, which in N_2 is sufficiently long-lived to show vibrational structure. Below 1.8 eV, Schulz did not observe any structure or other evidence for a compound state, whereas the total cross section of Golden, shown in Fig. 26, exhibits such structure below 1.8 eV.

In order to resolve this discrepancy, Ehrhardt and Willmann (1967) re-examined the elastic and inelastic differential cross sections as well as the total cross section, but were unable to reproduce the structures below 1.8 eV. In order to insure the proper working order of their apparatus, Ehrhardt and Willmann studied the low-energy structure in NO, which had previously been measured by Boness and Hasted (1966), and confirmed this structure both in the total cross section as well as in the elastic cross section. Thus it is highly probable that the structure below 1.8 eV, shown in Fig. 26, is spurious.

The differential elastic cross section at different scattering angles is shown in Fig. 27 and the angular distribution is shown in Fig. 28.

The structure in the elastic cross section above 1.8 eV, as well as in the vibrational excitation indicates the existence of a compound state whose lifetime is comparable to or longer than a vibrational period. The compound state is formed by the addition of an electron in a π_g orbital to the ground electronic state of N_2 (Gilmore, 1965; Krauss and Mies, 1970), and this assignment is proven by angular distribution studies (Ehrhardt *et al.*, 1967, 1968) of inelastically scattered electrons.

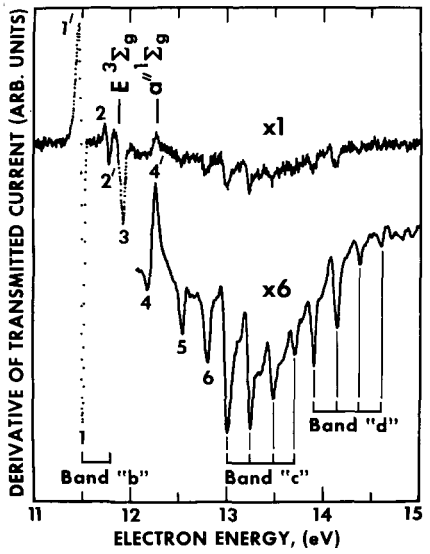

FIG. 42. Derivative of the transmitted current vs electron energy in N_2 (11–15 eV). The giant resonance marked 1–1′ is the $^2\Sigma_g^+$ state and forms the starting member of band "b," whose parents are the $E\,^3\Sigma_g^+$ and $a\,^1\Sigma_g^+$ Rydberg states of N_2. The grandparent is the ground state of N_2^+. Structures 3 and 4 are shape resonances. The other resonances, including bands "c" and "d" which appear on the higher sensitivity run on the bottom of the figure, have the $A\,^2\Pi_u$ state of N_2^+ as a grandparent. [From Sanche and Schulz (1972).]

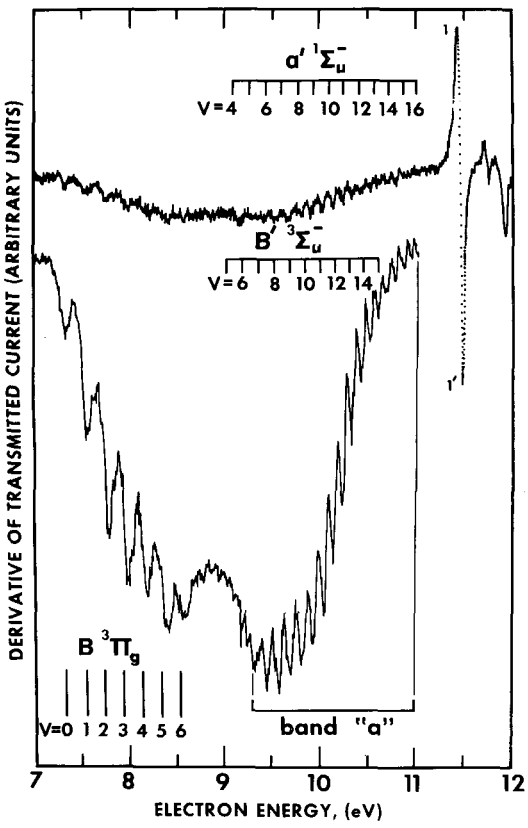

FIG. 43. Derivative of the transmitted current vs electron energy in N_2 (7–12 eV). Structure in the region 7–9 eV is due to inelastic processes involving the $B\,^3\Pi_g$ state of N_2. The locations of the $B\,^3\Pi_g$ state, the $B^1\,^3\Sigma_u^-$ state, and the $a\,^1\Sigma_u^-$ state of N_2 are indicated. Band "a" is a progression of core-excited shape resonances associated with the $B\,^3\Pi_g$ state, and the large structure (1–1′) is the first Feshbach resonance, $^2\Sigma_g^+$. The bottom trace is taken with a higher sensitivity. [From Sanche and Schulz (1972).]

2. *Vibrational Excitation via* $^2\Pi_g$

The vibrational excitation cross sections for the excitation of the first eight levels of the ground electronic state of N_2 clearly show structure which is characteristic of the compound state. Figures 29 and 30 show the vibrational cross sections at 20° and 72°, respectively, as obtained by two different groups. The shape and general behavior of the cross sections are in good agreement. Table III lists the positions of the maxima of the features, as observed in the $v=0$ and $v=1$ decay channels. Actually, the positions of the peaks occur at different positions, depending on the channel of observation, i.e., the peaks shift to higher energies for higher vibrational states. This effect, first discussed by Schulz (1964), is shown in Fig. 31. This feature, as well as the regularity of the structure in the vibrational cross section, stimulated theoretical interest in the

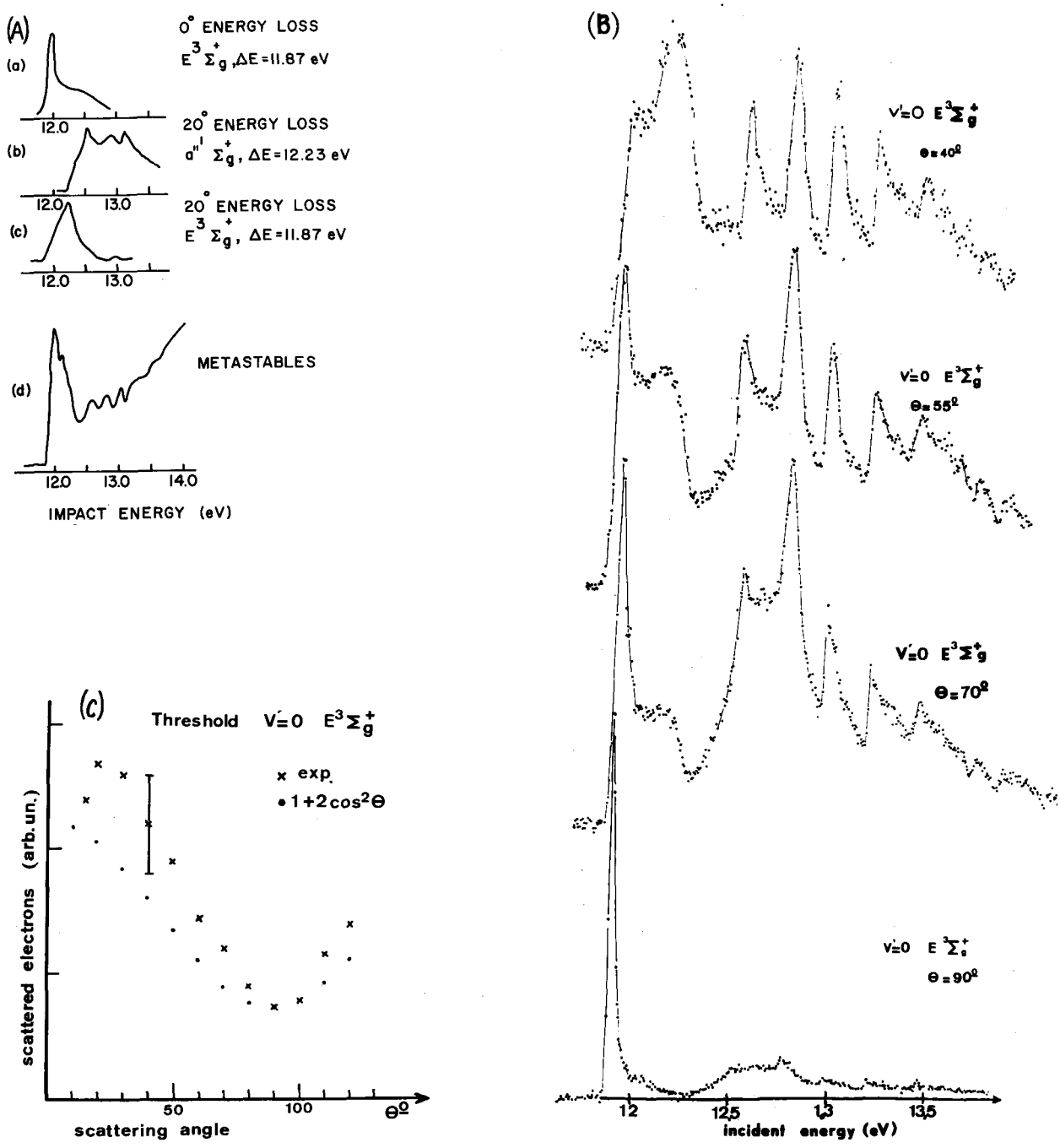

FIG. 44. (A) Threshold region for excitation of the $E\,^3\Sigma_g^+$ and $a''\,^1\Sigma_g^+$ states of N_2. Shown are the differential cross sections of Heidemann *et al.* (1966a) at 0°, and Ehrhardt and Willmann (1967) at 20°. Also shown is the excitation function for metastables (Lawton and Pichanick, 1973). [From Lawton and Pichanick (1973).] (B) Energy dependence of the differential excitation cross section for the $E\,^3\Sigma_g^+(v=0)$ state of N_2, at different angles of observation. The sharp peak near 11.90 eV has a half-width of 35±5 meV at 90° and exhibits the angular behavior shown in Fig. 44(C). [From Mazeau, Hall, Joyez, Landau, and Reinhardt (1972b).] (C) Angular distribution of electrons having excited the $E\,^3\Sigma_g^+(v=0)$ state in N_2 at 11.90 eV. Also shown is an angular distribution of the form $(1+2\cos^2\theta)$, normalized to the experimental data at 90°. The good agreement between the angular distributions points to a $p\sigma$ partial wave, indicating that the threshold behavior is dominated by a shape resonance. [From Mazeau, Hall, Joyez, Landau, and Reinhardt (1972b).]

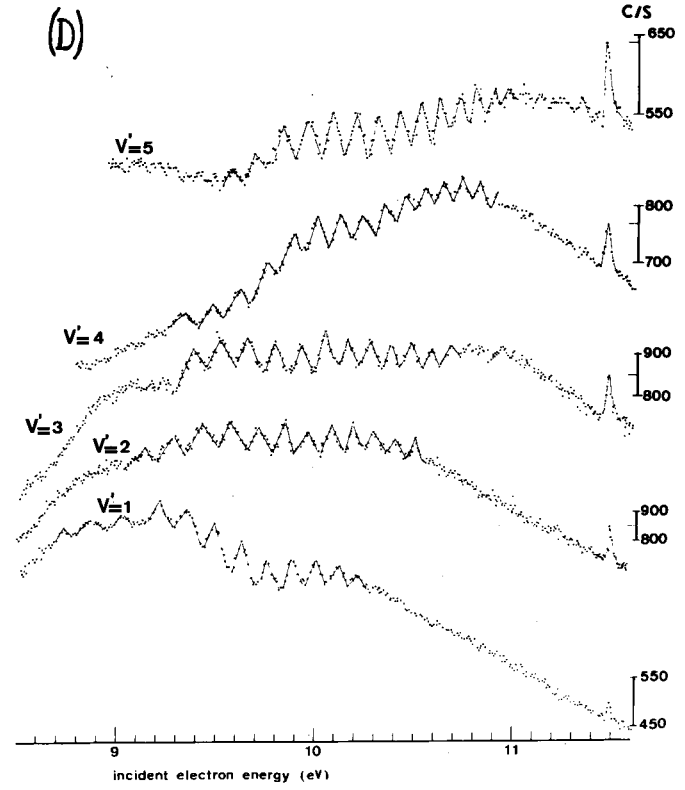

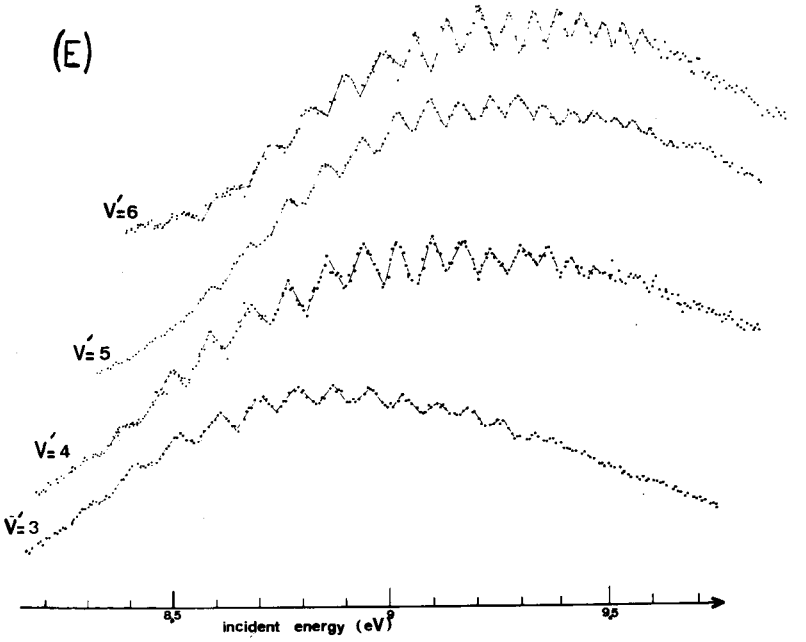

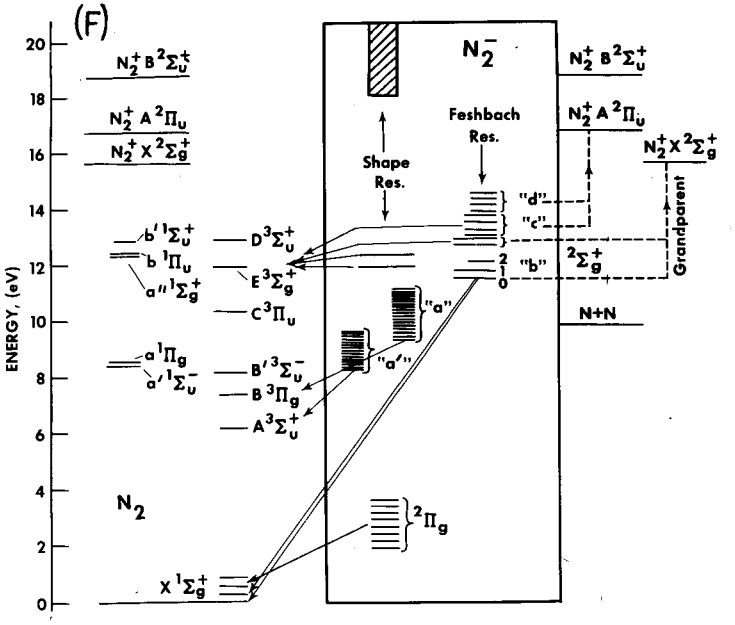

FIG. 44. (D) Energy dependence in N_2 of the differential cross section at 90° for the $B\,^3\Pi_g$ state in the vibrational states $v=1$–5. The scale for each curve is shown in the right side of the figure. The structures are due to core-excited shape resonances associated with the $B\,^3\Pi_g$ state and are designated as band "a". The energies are listed in Appendix V. Note that the location of the peaks shift. See text. [From Mazeau, Gresteau, Hall, Joyez, and Reinhardt (1972c).] (E) Energy dependence of the differential cross section at 90° for the $A\,^3\Sigma_u^+$ state in the vibrational states $v=3$–6. The structures are due to core-excited shape resonances associated with the $A\,^3\Sigma_u^+$ state of N_2. The band is designated "a'" and the energies are listed in Table V. [From Mazeau, Gresteau, Hall, Joyez, and Reinhardt (1972c).] (F) Energy level diagram of N_2 and N_2^- in schematic form. The energy levels in the boxed portion marked N_2^- are the compound states and are divided into shape resonances and Feshbach resonances. Some, but not all, decay channels are indicated by lines with arrows. The dashed lines leading to the positive ion states indicate the grandparents of the Feshbach resonances.

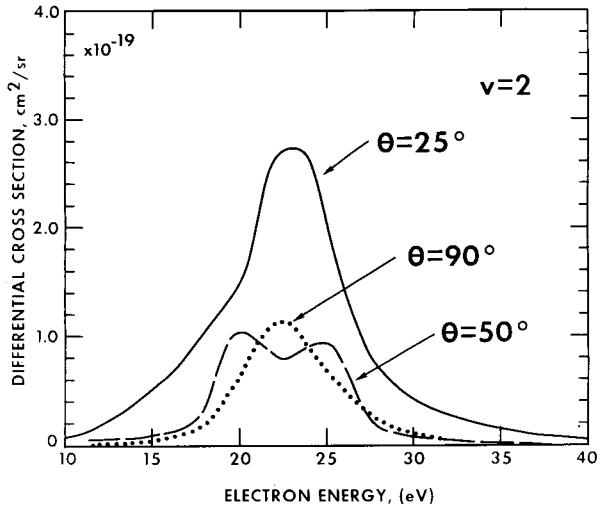

FIG. 45. Energy dependence of the differential cross section for vibrational excitation to $v=2$ in N_2 for three angles of observation. The energy range is 15 to 30 eV. The peak in the vibrational cross section possibly indicates the existence of a high density of overlapping compound states around 20 eV. The curves for $v=1$ and $v=3$ are similar to that shown. [From Pavlovic, Boness, Herzenberg, and Schulz (1972).]

problem. However, the early theoretical approaches, although correct in principle, could not reproduce unambiguously these properties (Herzenberg and Mandl, 1962; Chen, 1964; Hasted and Awan, 1969).

It was pointed out by Herzenberg (1968) that it is essential to consider the variation of the width Γ with internuclear separation. Such a variation is expected from the dependence of the penetrability of the centrifugal barrier with the energy of the emitted electron, which varies with R. Without allowing for such a variation, theory cannot reproduce the simplicity and regularity of the experimental results (see Fig. 32), and it certainly cannot reproduce the simple shift in peaks shown in Fig. 31.

Birtwistle and Herzenberg (1971) used a variable Γ in their theory and obtained excellent agreement with experiment, as shown in Fig. 33.

TABLE V. Derived properties of the 11.48-eV core-excited Feshbach resonance in N_2^-.[a]

Symmetry	$^2\Sigma_g^+$
Parent	$E\,^3\Sigma_g^+$
R_e (Å)	1.115±0.01
a (eV)	0.270±0.02
b (eV)	0.002±0.002
Γ (eV)	6×10^{-4}
E_0 (eV)	11.345

[a] The quantities a and b are the Morse parameters of the potential curve defined so that the energy E of the vibrational level v, with respect to the $v=0$ level of the ground state, is given by $E=E_0+a(v+\frac{1}{2})-b(v+\frac{1}{2})^2$. R_e is the equilibrium internuclear separation. [From Comer and Read (1971).]

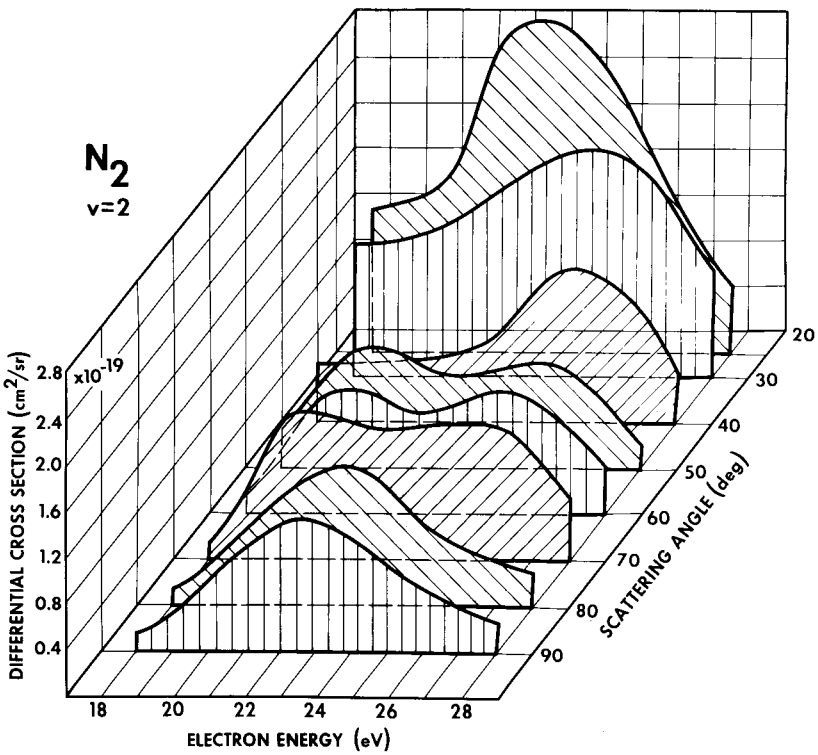

FIG. 46. Combined angular and energy dependence of the differential cross section for vibrational excitation to $v=2$ in N_2. The energy dependence of the process observed depends on the angle of observation. The complexity of the curves makes it probable that a superposition of many compound states is involved. [From Pavlovic, Boness, Herzenberg, and Schulz (1972).]

TABLE VI. Geneology of Feshbach resonances in N_2.

Resonance N_2^-			Grandparent N_2^+			Binding
Designation	Energy, eV	Spacing	Designation	Energy, eV	Spacing	eV
"b" ($^2\Sigma_g^+$)	11.48	0.27	$X\,^2\Sigma_g^+$	15.6	0.27	4.1
	11.75					
	12.02					
"5"	12.64	0.23	$A\,^2\Pi_u$	16.7	0.23	4.1
"6"	12.87					
"c"	13.00	0.23				
"d"	13.88	0.22				

The best fit to the experiment was obtained when Birtwistle and Herzenberg (1971) used the parameters for N_2^- shown in Table IV. For comparison, Table IV also shows the parameters for the N_2^- state from ab initio calculation of Krauss and Mies (1970). The excellent agreement obtained from these completely independent approaches is most gratifying.

The model of Birtwistle and Herzenberg (1971) leads to the conclusion that the N_2^- compound state has only

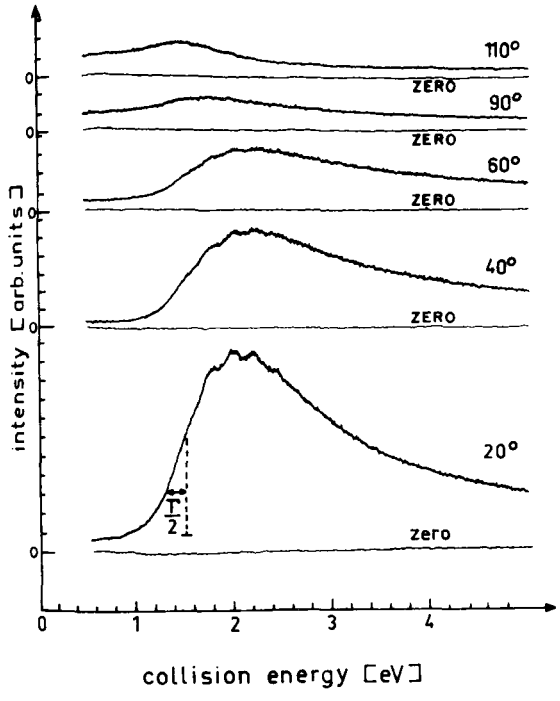

FIG. 47. Energy dependence of the elastic differential cross section for CO at different scattering angles. The first peak is only weakly indicated as a shoulder at 1.5 eV. $\Gamma/2$ is an approximate measure of the half-width of the compound state. The structures are better developed in the vibrational cross section (see Fig. 48). The intensity scales for all curves are the same. [From Ehrhardt, Langhans, Linder, and Taylor (1968).]

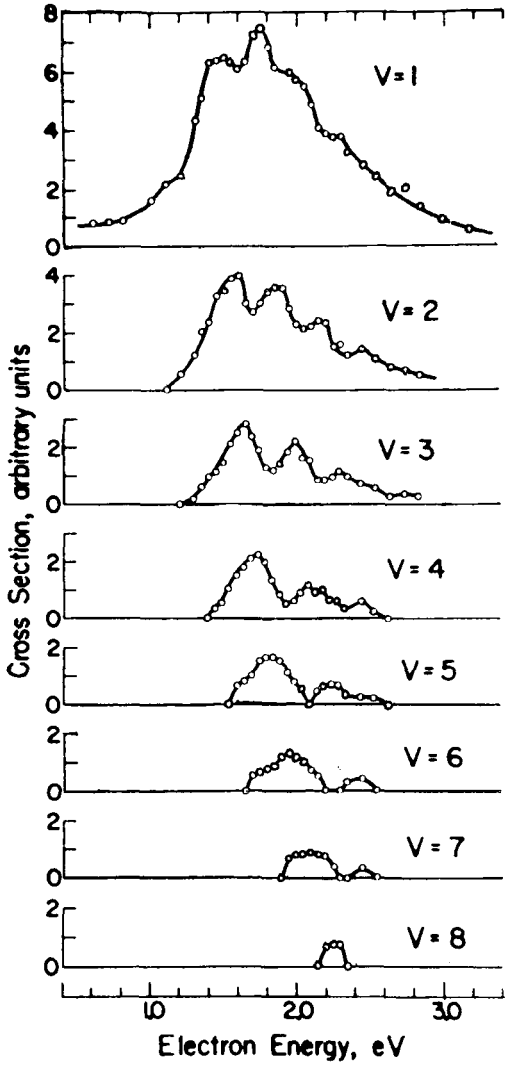

FIG. 48. Energy dependence of differential vibrational excitation in CO at an angle of observation of 72°. The structure resulting from the $^2\Pi$ compound state is more pronounced than in elastic scattering but broader than the equivalent structure in N_2 [From Schulz (1964).]

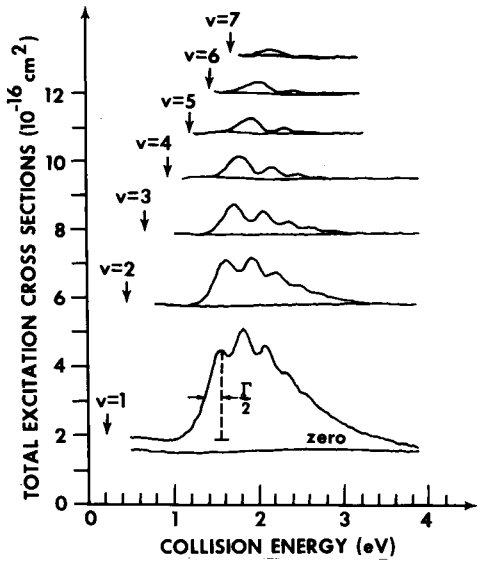

FIG. 49. Absolute cross sections for vibrational excitation of the CO molecule. The arrows point to the threshold energies of the individual vibrational states. [From Ehrhardt, Langhans, Linder, and Taylor (1968).]

time enough to vibrate once before autoionization takes place. Thus the $N_2^-(^2\Pi_g)$ state lies intermediate in lifetime between long-lived compound states [e.g., $O_2^-(X\,^2\Pi_g)$] and short-lived compound states [e.g., $H_2^-(^2\Sigma_u^+)$]. This "boomerang" model is shown schematically in Fig. 34.

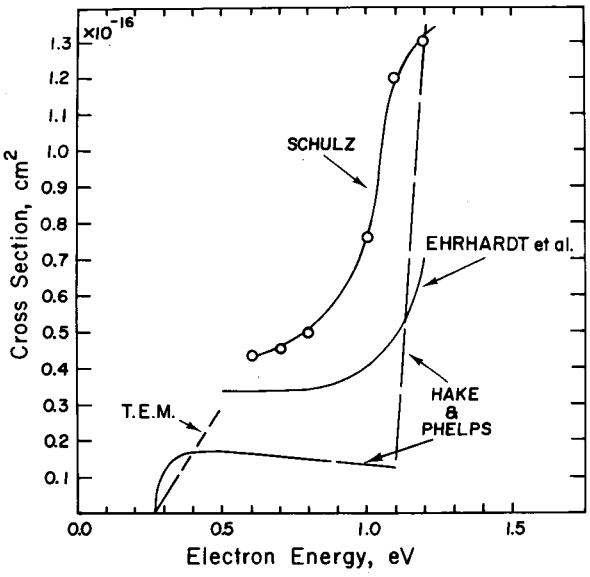

FIG. 50. Threshold behavior of the cross section for exciting the $v=1$ state in CO. Shown are the results of Hake and Phelps (1967). The portion of the data by Hake and Phelps indicated by the dashed line are only approximate. Also shown are the results of Ehrhard *et al.* (1968), Schulz (1964), and the trapped-electron data (marked TEM) giving the slope near threshold (Burrow and Schulz, 1969). [From Burrow and Schulz (1969).]

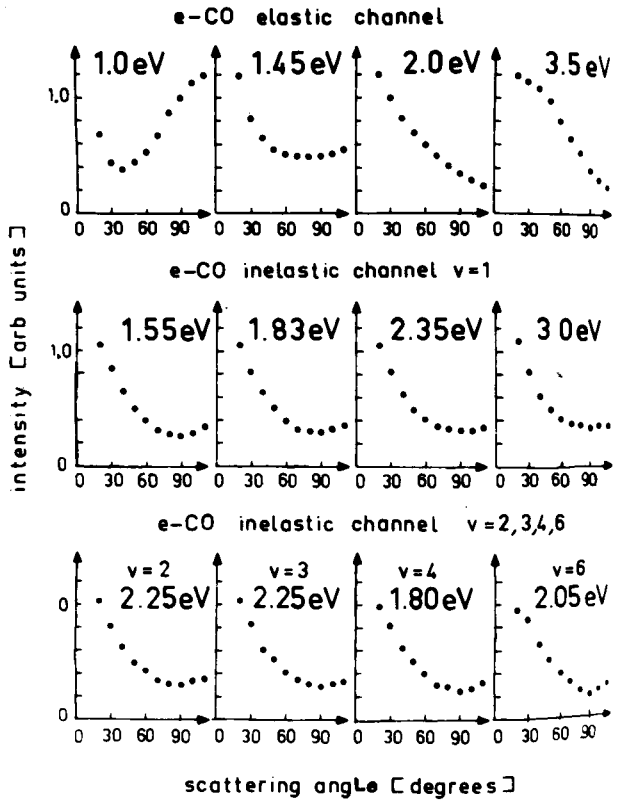

FIG. 51. Angular dependences of elastic and inelastic scattering of electrons by CO molecules at different collision energies. In the elastic channel (upper row) the angular dependence changes rapidly with energy since the scattering contains several partial waves with varying phase shifts (energy close to threshold). The constancy of the curve shapes for all inelastic channels at energies within the resonance region demonstrates that a compound state with a well-defined set of quantum numbers exists. [From Ehrhardt, Langhans, Linder, and Taylor (1968).]

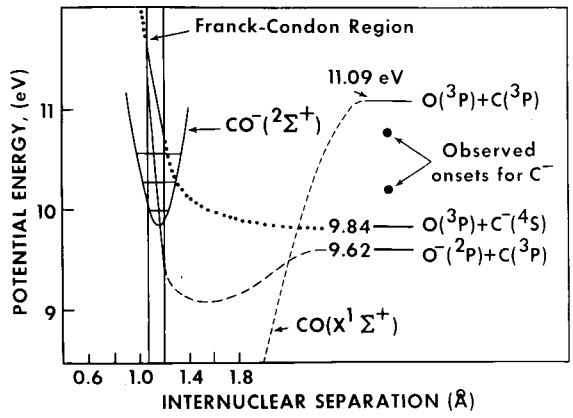

FIG. 52. Hypothetical potential energy curves for CO^- systems showing the possible decay of the $^2\Sigma^+$ resonance at 10 eV into the $O^-(^2P)+C(^3P)$ and $O(^3P)+C^-(^4S)$ dissociative attachment channels. The onsets for the negative ions are taken from the work of Stamatovic and Schulz (1970). [From Sanche and Schulz (1972).]

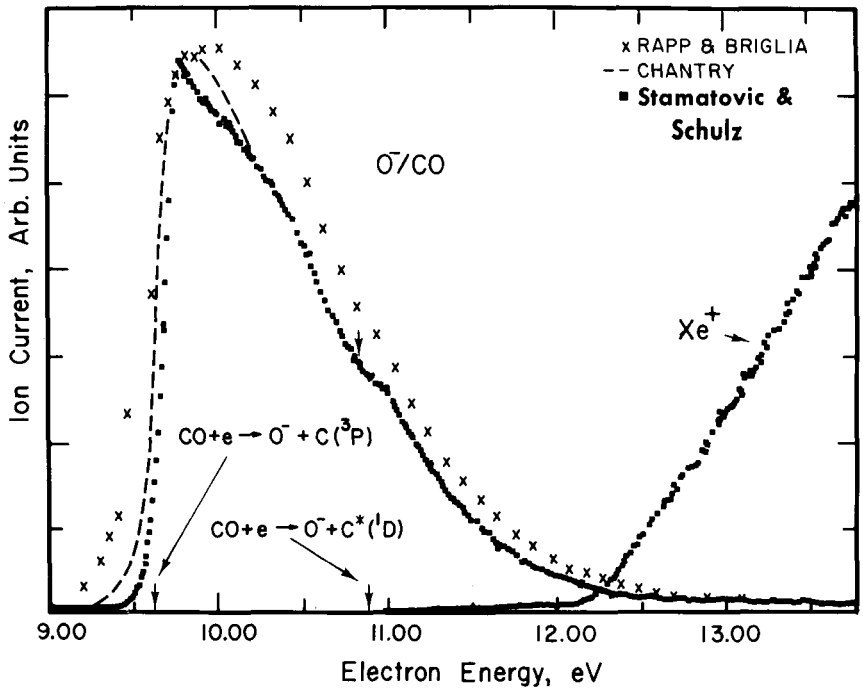

FIG. 53. Formation of O^- from CO by dissociative attachment. Shown are the curves of Stamatovic and Schulz 1970 (points) and their calibration against the onset of Xe^+. Also shown are the results of Chantry (1968) by the dashed line and of Rapp and Briglia (1965) by the crosses. The structure near 10 eV on the curve by Stamatovic and Schulz is caused by the $^2\Sigma^+$ resonance existing at 10.04 eV. [From Stamatovic and Schulz (1970).]

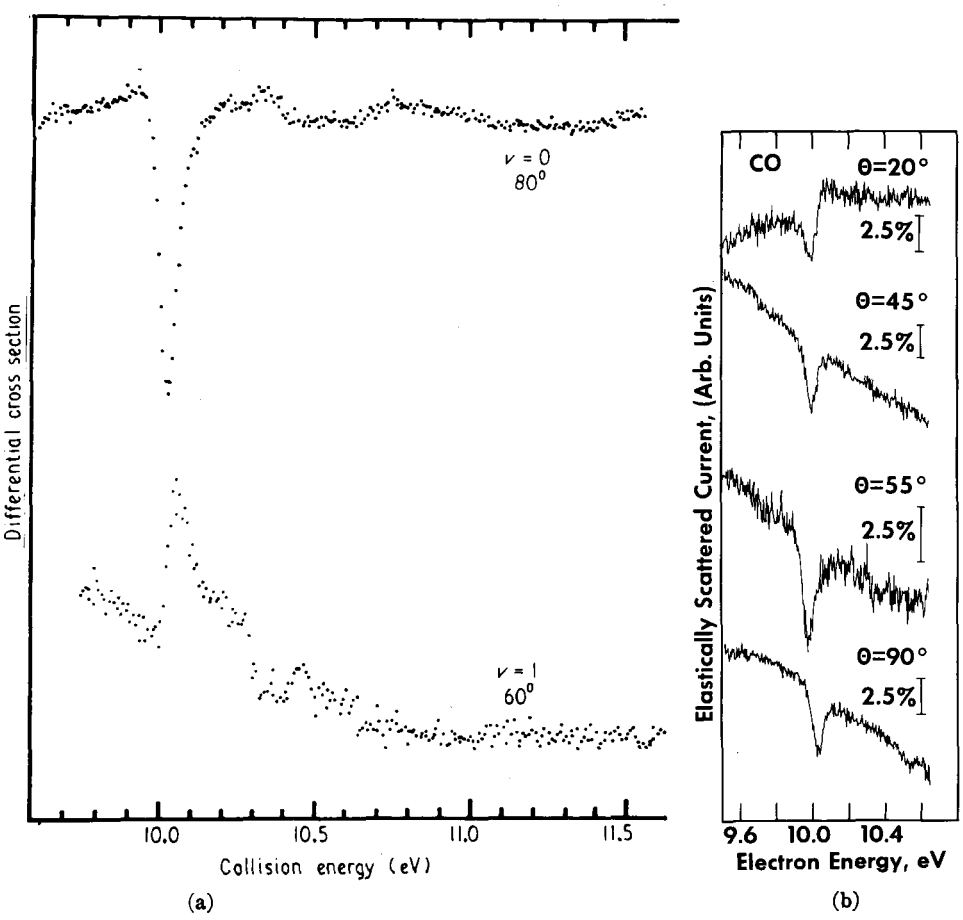

FIG. 54. (a) Energy dependence of the differential cross section in CO. The exit channels are the $v=0$ and $v=1$ vibrational states of the ground electronic state. The positions of the resonances are listed in Appendix VI. [From Comer and Read (1971c).] (b) Energy dependence of the elastic cross section in the vicinity of the $^2\Sigma^+$ resonance at 10.04 eV at different angles of observation. The shape is characteristic of an s-wave resonance. [From Pavlovic (to be published).]

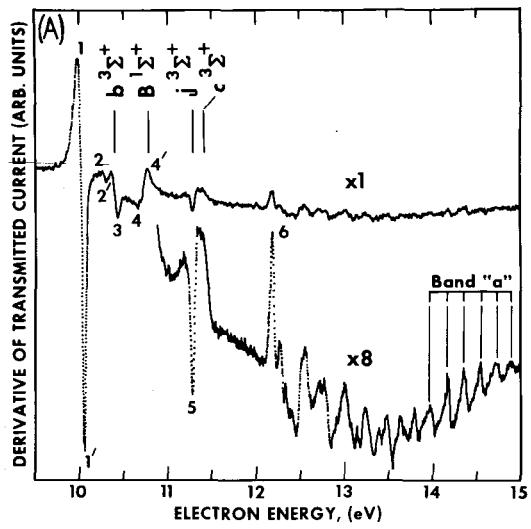

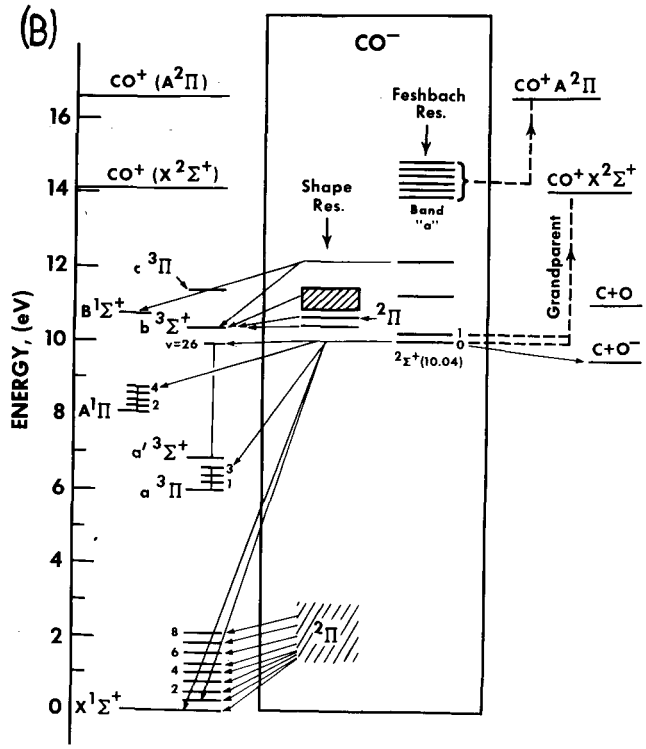

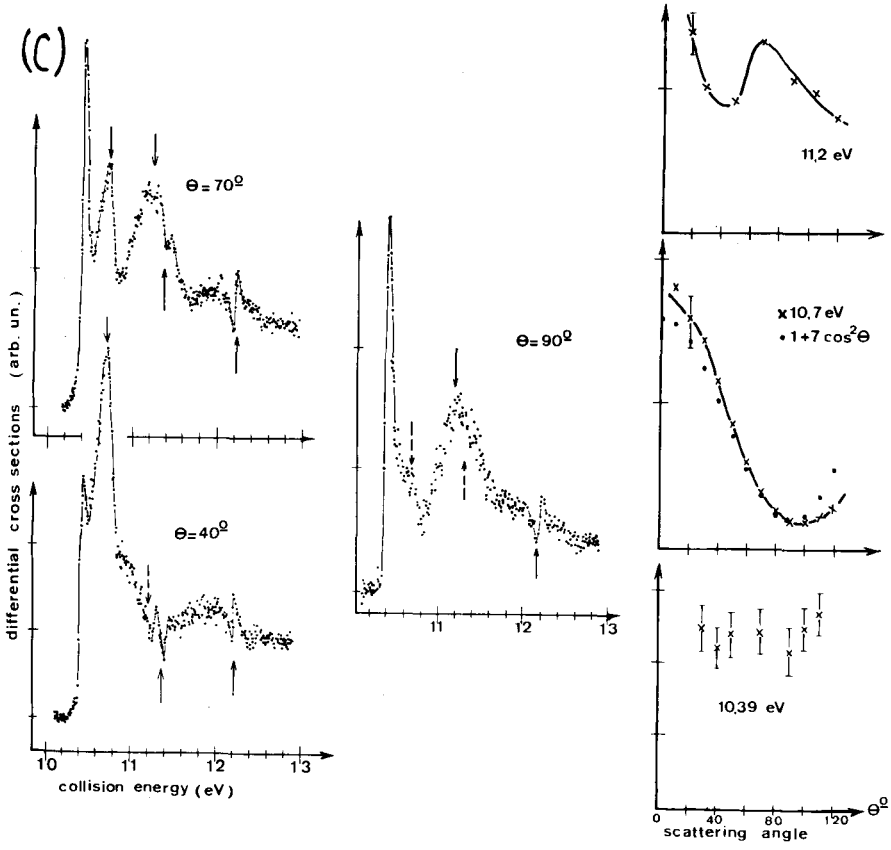

FIG. 55. (A) Derivative of transmitted current vs electron energy in CO. Resonances 1–4 are associated with the $b\,^3\Sigma^+$ and $B\,^1\Sigma^+$ parent states of CO. The locations of these states and the j and c states are indicated. Band "a" whose grandparent is the $A\,^2\Pi$ state of CO^+, appears near the end of the spectrum. The gain on the lower curve has been increased by a factor of 8. The smaller structures on that curve represent variations in the transmitted current of about 0.01% which is the detection limit of the present experiment. [From Sanche and Schulz (1972).] (B) Schematic energy level diagram of CO and the compound states. The lines with the arrows show the preferred decay channels for the compound states. On the left side of the diagram are shown the low states of CO, i.e., $a\,^3\Pi$ (6.01 eV); $a'\,^3\Sigma^+$ (6.86 eV); $A\,^1\Pi$ (8.03 eV); $b\,^3\Sigma^+$ (10.39 eV); and $B\,^1\Sigma^+$ (10.78 eV). The preferential decay is based on the work of Comer and Read and of Mazeau *et al.* The decay into $C+O^-$ (dissociative attachment) is shown on the right side. (C) Differential excitation functions for the $b\,^3\Sigma^+$ $v'=0$ level in CO. The curves on the left show the energy dependence at 40°, 70°, and 90°. The downward pointing arrows point to shape resonances at 10.7 and 11.2 eV. The upward pointing arrows indicate Feshbach resonances (11.3 and 12.2 eV). The diagrams on the right side show angular distributions at specified electron energies. The points on the diagram in the center (10.7 eV) represent the function $(1+7\cos^2\theta)$, normalized at 90°. [From Mazeau, Gresteau, Joyez, Reinhardt, and Hall (1972a).]

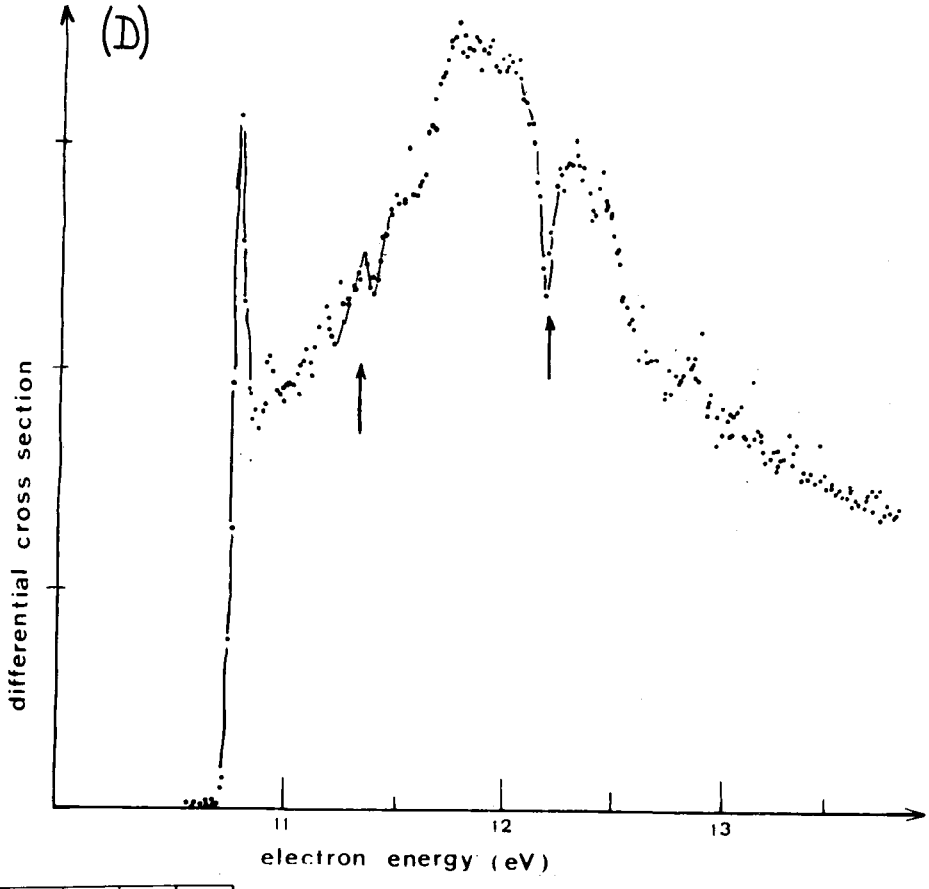

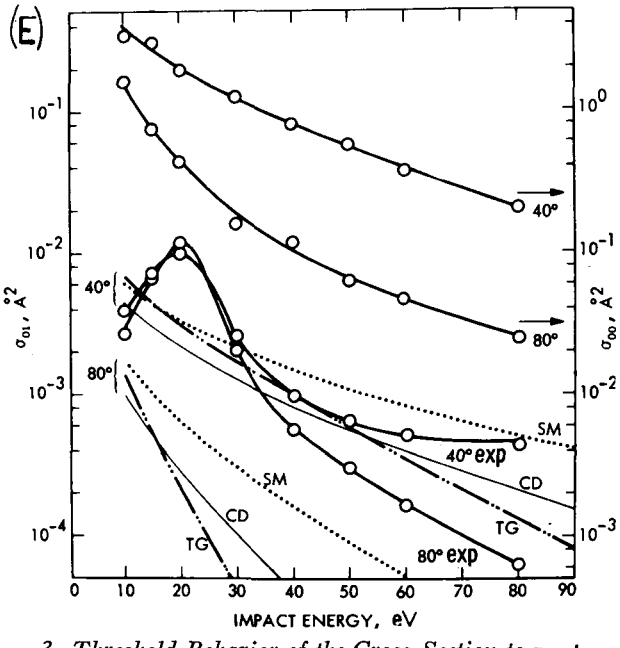

FIG. 55. (D) Differential excitation function of the $B\,^1\Sigma^+$ $v'=0$ level at 40°. Arrows indicate Feshbach resonances at 11.3 and 12.2 eV. [From Mazeau *et al.* (1972a).] (E) Differential cross sections at 40° and 80° scattering angles for elastic scattering and for vibrational excitation to the $v=1$ state in CO. The top two curves are experimental elastic cross sections at 40° and 80°. The appropriate cross section scale for these two curves is read on the right; all other curves are read on the left. The two curves marked "40° exp" and "80° exp" are experimental vibrational cross sections at 40° and 80°, respectively, for $v=0\rightarrow1$. (Note peak near 20 eV.) Also shown are theoretical results for 40° and 80° using the polarized Born approximation based on the potentials of Takayanagi and Geltman, 1965 (TG); Sampson and Mjolsness, 1965 (SM); Crawford and Dalgarno, 1971 (CD). [From Chutjian *et al.* (1972).]

3: Threshold Behavior of the Cross Section to $v=1$

The "direct" component of the vibrational cross section in N_2 is small and therefore the onset of an appreciable cross section for vibrational excitation is delayed. This can be seen in Fig. 35, which compares three measurements in the threshold region. The small cross section near threshold may be due to direct excitation or to the residual effect of the compound state.

4. Angular Distributions

It has already been pointed out that angular distribution measurements are a powerful tool for the deter-

mination of the symmetry of compound states. Under favorable circumstances the angular distribution of inelastically scattered electrons is determined uniquely by comparing the symmetries of the resonant state, the initial state, and the final state. The conditions under which a unique angular distribution can be obtained from symmetry considerations are listed by Bardsley and Read (1968) and by O'Malley and Taylor (1968):

(a) The scattering must be dominated by a single resonant state, so that nonresonant scattering and the contributions from other resonances are both negligible. This situation is often found in the study of inelastic collisions, but for elastic scattering there are always considerable nonresonant contributions.

(b) The molecule does not rotate appreciably during the lifetime of the resonant state.

(c) It must be assumed that when the resonant state is expanded in spherical harmonics the contribution from the lowest allowed value of l are dominant. For resonances at low energies this is nearly always true.

(d) It must also be assumed that the Born–Oppenheimer separation of electronic and vibrational motion is valid.

In the case of the $N_2^-(^2\Pi_g)$ resonance near 2.3 eV, the extra electron must go into the π_g orbital. It must have even orbital angular momentum ($l \geq 2$) and the projection of the angular momentum on the molecular axis must be unity. We may speak of a $d\pi$-wave. The expected d-wave behavior of the cross section to various vibrational states of N_2 should show a subsidiary peak near 90°. The experimental results of Ehrhardt *et al.* (1968), shown in Fig. 36, exhibit such behavior, and thus the angular distribution measurements confirm the designation of $^2\Pi_g$ for the first shape resonance in N_2.

5. *Pure Rotational Excitation via* $^2\Pi_g$

Pure rotational transitions can also be excited by compound states. It has already been pointed out that experiments on the "elastic cross section" exhibit structure in the energy dependence which can be attributed to the $^2\Pi_g$ resonance. However, beam experiments do not have the resolution necessary for a study of rotational excitation, or for distinguishing rotational levels in vibrational transitions. Thus, in the case of N_2 and in fact all molecules except H_2, one has to rely on theory. The results of the theory, for rotational excitation $J=1\rightarrow3$, are shown in Fig. 37. Wide discrepancies exist in the region of the $^2\Pi_g$ compound state. The results of Chen (1966b) using projection operators seem to be much below the close-coupling results of Burke and Sinfailam (1970) and those of Oksyuk (1966). It should be noted that in the resonance region quantum jumps $J=0\rightarrow4$ or $J=1\rightarrow5$, i.e., $\Delta J=4$, are possible in addition to the usual quantum jumps, $\Delta J=2$. Chen (1966b) has calculated the cross sections for these transitions, with and without vibrational excitation.

B. Core-Excited Resonances in the 11–15 eV Region

As pointed out previously, Feshbach-type resonances are more likely to occur below Rydberg excited states of molecules. In N_2, the lowest Rydberg state is the $E\,^3\Sigma_g^+$ state (Mulliken, 1957) at 11.87 eV and one would expect that a sharp resonance would occur about 0.5 eV below this state. Such is actually the case. Heidermann, Kuyatt, and Chamberlain (1966a) discovered a very sharp resonance at 11.48 eV, using a transmission experiment (Fig. 38). Comer and Read (1971b) performed a different scattering experiment in which the decay of the resonance could be observed for $v=0$, 1, 2, and 3 of the ground electronic state. Their results are shown in Figs. 39 and 40 and the angular distributions for electrons having excited the $v=1$ state are shown in Fig. 41. From these observations, Comer and Read deduce that the symmetry of the 11.48-eV resonance is $^2\Sigma_g^+$ and that the most likely parent is the $E\,^3\Sigma_g^+$ state. Actually, Fig. 40 shows that a progression is involved here, of which the 11.48-eV state is the first member. The other members of this band, which we choose to call band "b" are listed in Appendix IV in comparison with other experiments. Table V lists the parameters of the $^2\Sigma_g^+$ state. It should be noted that the 11.48-eV $^2\Sigma_g^+$ resonance has also been observed as a sharp peak in the optical excitation function ($\lambda=3371$ Å) of the $C\,^3\Pi_u$ state (Kisker, 1972).

The results of the recent transmission experiment of Sanche and Schulz (1972) are shown in Figs. 42 and 43. The features are numbered and the more obvious progressions are given letter names. The energy values are tabulated in Appendix IV, in comparison with other experiments.

The total production of metastable states has been measured by Lawton and Pichanick (1972) and their results are shown in Fig. 44(A). The differential inelastic cross sections to the $E\,^3\Sigma_g^+$ ($v=0$ and $v=1$), $a''\,^1\Sigma_g^+$ ($v=0$), and other electronically excited states, have been studied by Mazeau *et al.* (1972b). Samples of their results on the energy dependence and the angular distribution of scattered electrons are shown in Figs. 44(B)–(E). Figure 44(F) is a schematic energy level diagram of the N_2 and N_2^- systems and the decay scheme for various resonances. We have indicated in separate columns shape resonances and Feshbach resonances.

Below we discuss the properties of individual bands, as deduced from the various experiments. In Appendixes IV and V we list the energies of the resonances.

1. *Band "b"-*$^2\Sigma_g^+$

Three members of band "b" are listed in Appendix IV. The $^2\Sigma_g^+$ resonance at 11.48 eV consists of two

electrons of the Rydberg orbital symmetry $3s\sigma_g$ temporarily bound in the field of the grandparent $X\,^2\Sigma_g^+$ core of N_2^+. This is evidenced by the fact that both the spacing between the vibrational levels of band "b" and the amplitudes of the structures are close in magnitude to the corresponding values for excitation of the ground state $X\,^2\Sigma_g^+$ of N_2^+. The spacing between the structures of band "b" is 270 meV and the ratio of magnitudes of the two peaks is 10 ± 0.5. These experimental results agree well with the values for the $X\,^2\Sigma_g^+$ state of N_2^+, which has a spacing of 271 meV between the $v=0$ and $v=1$ states and which has a ratio of 9.96 for the Franck–Condon probabilities for exciting these vibronic states.

Table VI shows these comparisons: The binding between the lowest member of band "b" and the grandparent $X\,^2\Sigma_g^+$ state of N_2^+ is 4.1 eV. This value represents the binding of the two $3s\sigma_g$ electrons to the positive ion core. It is noteworthy that the value of about 4.1 eV does not change as different grandparents are considered, and in fact the value remains constant even for other molecules (see Table X). But the value is applicable only to the *lowest* band. The same grandparent can give rise to other bands, lying higher in energy.

Only the zeroth level of the $X\,^2\Sigma_g^+$ grandparent state is strongly excited in molecular transitions from the ground state of N_2 and we would expect that a similar situation prevails for the resonances associated with the $X\,^2\Sigma_g^+$ grandparent state. Thus we would not expect to observe a long progression of vibronic states of the $^2\Sigma_g^+$ resonance.

2. *Shape Resonances and Inelastic Thresholds*

Structures 3 and (4–4′) of Fig. 42 (at 11.92 and 12.2 eV) have been identified as p-wave shape resonances associated with the $E\,^3\Sigma_g^+$ Rydberg state of N_2 (Sanche and Schulz, 1972). The first of these lies near the threshold for the $E\,^3\Sigma_g^+$ state (11.87 eV), so that one would expect a dramatic influence of the 11.92-eV p-wave shape resonance on the threshold behavior of the $E\,^3\Sigma_g^+$ state. That the $E\,^3\Sigma_g^+$ state and also the $a''\,^1\Sigma_g^+$ state at 12.26 eV show a very sharp rise near threshold has been observed by many investigators (Heideman *et al.*, 1966a; Ehrhardt and Willmann, 1967; Swanson *et al.*, 1971; Mazeau *et al.*, 1972b; Lawton and Pichanick, 1973).

Figures 44(A) and 44(B) clearly show that the cross section as well as the differential cross section to the $E\,^3\Sigma_g^+$ state rise very steeply near threshold. *A priori*, a sharp rise near threshold can arise from three causes:

(i) The existence of a shape resonance just above the threshold. The angular distribution in this case would exhibit a p-type (e.g., $p\sigma$) behavior.

(ii) The existence of a Feshbach-type resonance below the threshold can influence the inelastic cross section above threshold (Ehrhardt and Weingartshofer, 1969; Taylor, 1970). In the case of N_2, we would be dealing with the "wings" of the $^2\Sigma_g^+$ resonance which lies 390 meV below the E state. Herzenberg and D. Ton-That point out that the opening of a new channel of decay (as is the case when the electron energy passes through the energy of an excited state) leads to an abrupt increase in the total width Γ. This effect is especially pronounced when the electronic state is the "parent" of the resonance, since the decay width into the parent is generally large. Herzenberg and D. Ton-That have worked out these considerations for the case of the ^2S resonance in helium decaying into the 2^3S state, showing that a sharp peak in the excitation cross section of the 2^3S state near threshold results. It is expected that the model will be valid in other cases as well. It leads to an s-wave behavior in the angular distribution of inelastically scattered electrons.

(iii) The existence of a "virtual" state, similar to one existing near the 2^1S threshold in helium (see preceding paper).

In order to distinguish between the three possibilities outlined above, Mazeau *et al.* (1972b) studied the angular distribution of the electrons having excited the $E\,^3\Sigma_g^+$ $(v=0)$ state. Figure 44C shows that the angular distribution near the threshold of the E state approximates the shape expected for a $p\sigma$-wave. This experiment demonstrates that the threshold behavior of the $E\,^3\Sigma_g^+$ state is dominated by the p-wave resonance near 11.9 eV, and also confirms the assignment given to this resonance by Sanche and Schulz (1972).

The resonance (4–4′) of Fig. 42, which lies between 12.1–12.2 eV, is also believed to be a shape resonance (Mazeau *et al.*, 1972b; Sanche and Schulz, 1972), probably of $^2\Pi$ symmetry. The angular distribution of the scattered electrons having excited the $E\,^3\Sigma_g^+$ $(v=0)$ state near 12.1 eV exhibits, approximately, the shape characteristic of a $p\pi$-wave (Mazeau *et al.*, 1972b).

The sharp onset of the excitation function is characteristic of the $E\,^3\Sigma_g^+$ and the $a''\,^1\Sigma_g^+$ states at 11.87 and 12.26 eV, respectively. Other inelastic cross sections, examined by Swanson *et al.* (1971), ($A\,^3\Sigma_u^+$, $B\,^3\Pi_g$, $B'\,^3\Sigma_u^-$, $a'\,^1\Sigma_u^-$, $a\,^1\Pi_g$, $C\,^3\Pi_u$, $E\,^3\Pi_g$, $a''\,^1\Sigma_g^+$) do not exhibit a sharp rise near threshold.

3. *Structures 5 and 6*

The energy of the lowest Feshbach resonance composed of two Rydberg electrons trapped in the field of the $A\,^2\Pi_u$ core of N_2^+ can be estimated by adding to the energy of the $^2\Sigma_g^+$ resonance (11.48 eV) the difference between the ionization potential for the $X\,^2\Sigma_g^+$ and the $A\,^2\Pi_u$ states of N_2^+. Such an estimate gives 12.62 eV for the energy of that $^2\Pi_u$ resonant state which would consist of two $3s\sigma_g$ electrons bound to the $A\,^2\Pi_u$ core. Resonances 5 and 6 of Fig. 42 (at 12.64 and 12.87 eV) probably belong to that state. In fact,

resonance 5 lies at 12.64 eV, only 20 meV above the estimated position (Sanche and Schulz, 1972). The parent of these structures can be the $F\,^3\Pi_u$ state lying at 12.75 eV. This state has a $^2\Pi_u$ core with an extra $3s\sigma_g$ electron attached. Mazeau *et al.* (1972b) suggest that the $G(^3\Pi_u)$ state at 12.8 eV could be admixed.

Structures 5 and 6 are also replicated in the differential cross section of the $E\,^3\Sigma_g^+$ ($v=0$) state and these structures appear at 12.54 and 12.78 eV, respectively, as shown in Fig. 44(B) and in Appendix IV. Structures 5 and 6 are not visible in the $E\,^3\Sigma_g^+$ ($v=1$) decay channel.

4. Bands "c" and "d"

Two short bands ("c" and "d") in the 13–15 eV energy range are shown in Fig. 42. They start at 13.00 and 13.88±0.05, respectively. Here the overlap between the different resonances makes an accurate reading of the spacing between the vibrational members of each band difficult. Nevertheless, the average spacing of 230±5 meV for band "c" and 225±5 meV for band "d" lies close to the value of 228 meV for the corresponding average spacings of the vibrational levels of the $A\,^2\Pi_u$ state of N_2^+ which is the suggested grandparent for the two bands. Mazeau *et al.* (1972b) suggest that the parent of band "c" is the state H which they have recently discovered. The state H is a triplet, and its $v=0$ level lies at 13.15±0.01 eV. The spacing of the two lowest vibrational levels is 240 meV.

The band "c" has been observed in the decay channels $E\,^3\Sigma_g^+$ ($v=0$, $v=1$), $a''\,^1\Sigma_g^+$ ($v=0$), and also $C\,^3\Pi_u$ by Mazeau *et al.* (1972b). The energies of bands "c" and "d" are listed in Appendix IV.

C. Bands "a" and "a′": Core-Excited Shape Resonances

At lower energies (7–11 eV) other structures are visible in the total scattering cross section of N_2. These structures are clearly seen in derivative transmission spectra for N_2 shown in Fig. 43. The progression of dips between 7 and 9 eV in the transmission spectrum is interpreted predominantly as the excitation of vibrational levels of the $B\,^3\Pi_g$ valence state of N_2 and indicates that the cross section for excitation of the B state rises sharply at threshold. This finding confirms similar conclusions derived from studies using the trapped-electron method (Brongersma and Oosterhoff, 1969, 1967; Hall *et al.*, 1970).

The next structures (band "a" in Fig. 43) form a very well-developed progression of 18 vibrational levels which extends from 9 to 11 eV. The energy of each structure and the corresponding spacings are given in Appendix V. When one attempts to correlate the energies of this progression with vibrational energy levels of the known states in this energy region, namely the $B'\,^3\Sigma_u^-$, $a'\,^1\Sigma_u^-$, $a\,^1\Pi_g$, and $W\,^1\Delta_u$ valence excited states, it is found that none of these states nor any combination of them could reproduce the spacing of band "a" (Sanche and Schulz, 1972).

Structures at the same energies as band "a" have also been observed, superimposed on a continuum, in the excitation function to various vibrational states ($v=1-5$) of the $B\,^3\Pi_g$ valence state of nitrogen. This is shown in Fig. 44D.

We are dealing here with a vibrational progression of core-excited shape resonances, similar to those existing near 2.3 eV in N_2, i.e., the $^2\Pi_g$ state of N_2^-. Many of the features of band "a", when observed in the decay into the $B\,^3\Pi_g$ parent state are reminiscent of the features already discussed in connection with the 2.3-eV shape resonance in N_2. The position on the energy scale of the peaks observed in different vibrational decay channels of the $B\,^3\Pi_g$ state shift. This can be clearly seen in Fig 44D and in Appendix V, where the energy values are tabulated. The shifting of the peaks is reminiscent of a similar effect already discussed in connection with the 2.3-eV shape resonance in nitrogen (see Figs. 31 and 33), and the Boomerang model (Fig. 34) developed by Herzenberg (1968) and by Birtwistle and Herzenberg (1971). A band similar to band "a" is also associated with the $A\,^3\Sigma_u^+$ state, as evidenced by the structure in the cross section to various vibrational states of the $A\,^3\Sigma_u^+$ final state, in the energy range 8.22–9.57 eV (Fig. 44E). As in the case of band "a", the locations of the peaks shift on the energy scale. The parent of this band is the $A\,^3\Sigma_u^+$ state. Appendix V gives the energies of the structures, as observed in the $v=2$–6 states of the $A\,^3\Sigma_u^+$ electronic state.

The energy level diagram, Fig. 44F, indicates schematically some of the decay channels. The core-excited shape resonance associated with the $A\,^3\Sigma_u^+$ state is marked "a′".

D. Resonances above the Ionization Potential in N_2

Pavlovic *et al.* (1972) have observed vibrational excitation for the levels $v=1$, 2, 3 in N_2 in the energy range 20–24 eV. They also observed the angular distribution of electrons having excited these states and found that the angular distribution depends strongly on the incident energy, and in fact the shape of the energy dependence depends on the angle of observation. These anomalies in the angular distribution, coupled with the large size of the observed cross section, led Pavlovic *et al.* to prefer an interpretation in terms of resonances associated with doubly excited states of the nitrogen molecule rather than singly excited Rydberg states. Further experimental work will, however, be needed before this model is reliably proved.

Resonances associated with doubly excited states of atoms (e.g., $2s^22p$ in the case of He) are well known. In the case of small systems such as helium, one expects these resonances to be spaced well apart compared to their width, whereas in systems with more electrons (e.g., N_2) there is the possibility of many doubly ex-

cited states which are closely spaced (~0.25 eV), each of which may have an associated compound state. Thus it may not be possible to resolve individual states, especially since the states themselves may be relatively broad.

The resonances discussed above would have two holes in the normally filled shells of N_2, $(KK)(\sigma_g 2s)^2(\sigma_u 2s)^2(\sigma_g 2p)^2(\pi_u 2p)^4$ and would have three electrons in the vacant orbitals, $(\pi_g 2p)$ and $(\sigma_u 2p)$. Pavlovic *et al.* (1972) calculate that, in the 22-eV region, the spacing of such resonances is less than 0.25 eV.

We note that the resonances discussed in the previous section (core-excited shape resonances, a and a', connected with the $A\,^3\Sigma_u^+$ and $B\,^3\Pi_g$ states, respectively) have one hole in the normally filled shell and two electrons in the vacant orbitals, whereas the resonances near 2.3 eV (connected with the ground $X\,^1\Sigma_g^+$ state of N_2) have zero holes and one electron in the vacant orbitals. Thus the shape resonances invoked by Pavlovic *et al.* follow logically from the two types already discussed.

Figures 45 and 46 show the energy dependence and the angular dependences observed by Pavlovic *et al.* (1972) for the excitation of $v=2$. The energy dependence of the cross section for exciting $v=1$ and $v=3$ is very similar to that shown.

A measurement and an analysis of the angular distribution of electrons having excited the $v=1$ vibrational state of N_2 (and also CO) has been performed by Truhlar *et al.* (1972) with the aim of testing whether a simple nonresonant mechanism can explain the vibrational excitation near 20 eV. Such a model appears to be applicable in the 20-eV energy range in the case of H_2 (Trajmar *et al.*, 1970). Truhlar *et al.* find that a resonance model must be involved in the case of N_2 and CO in order to interpret the experimental results on vibrational excitation near 20 eV. It should be noted that the *experimental* results of Truhlar *et al.* (1972) are in good agreement with those of Pavlovic *et al.* (1972).

IV. CARBON MONOXIDE

The electron configurations and the resulting levels of compound states of diatomic molecules are determined essentially by the number of electrons. Therefore N_2 and CO, being isoelectronic molecules, should exhibit very similar properties. In fact this is the case. However, the positions of the compound states and their widths differ somewhat.

The CO molecule is not symmetric with respect to inversion so that the $g-u$ symmetry is not preserved. Also, the permanent dipole of CO often cannot be ignored. The following review of the carbon monoxide molecule follows closely the discussion of N_2.

A. Resonance at Low Energy (1–3 eV) $^2\Pi$

The configuration of CO is identical to that already listed for N_2, except that the subscripts g and u now lose their meanings (see Table IX). As a consequence, the $3d\pi$ orbital contains a p-wave component (Bardsley and Mandl, 1968; O'Malley and Taylor 1968; Read, 1968). Thus the trapped electron tunnels through a p-wave barrier which is not as high as a d-wave barrier and, as a result, the width of the state is expected to be larger (the lifetime is shorter) than in N_2. These expectations agree with the experimental results.

1. Elastic Cross Section via $^2\Pi$

The energy dependence of the differential elastic cross section for CO is shown in Fig. 47. Compared to N_2, the structure in the cross section is less pronounced, although the peak in the neighborhood of 2 eV is especially clear at 20 and 40 degrees. The individual resonances become more obvious when the vibrational cross sections are studied. Ehrhardt *et al.* (1968) estimate the width at 0.4 eV.

2. Vibrational Excitation via $^2\Pi$

The energy dependence of the vibrational cross section, as observed at an angle of 72 degrees, is shown in Fig. 48. This curve, obtained by Schulz (1964) is in all respects similar to the curve obtained at 20 degrees (Ehrhardt *et al.*, 1968), indicating that the shape of the cross section does not depend on angle. The sum of all vibrational cross sections has a relatively smooth behavior, with a single peak at 1.7 eV and a magnitude

$$\sum_{v=1}^{8} \sigma_v = 3.5\times 10^{-16}\ \text{cm}^2.$$

In obtaining this value, Ehrhardt *et al.* (1968) took into account the variation of the cross sections with angle. The vibrational cross sections in absolute units is shown in Fig. 49.

A notable difference exists between N_2 and CO if one observes that the cross section for $v=1$ has a long tail which extrapolates to the onset for $v=1$ (see Phelps, 1968) whereas N_2 shows a tail which is smaller by an order of magnitude. A direct dipole-type process is probably responsible for the difference. Figure 50 shows the details of the threshold region for excitation of $v=1$ in CO, as determined by different methods of measurement.

The other notable difference between N_2 and CO is the larger width of the observed structure. As already noted, this larger width is a result of the barrier being predominantly of a p-wave character in CO, with d wave mixed in. In N_2, the barrier is predominantly d wave.

3. Angular Distributions

Figure 51 shows the angular distributions obtained by Ehrhardt *et al.* (1968) for electrons which are scattered elastically and inelastically. Qualitatively, the curves for the inelastically scattered electrons show a p-type behavior of the curves, with a minimum at 90 degrees.

A fairly good, but not perfect, fit to the experimental curves was obtained by O'Malley and Taylor (1968) whose theory gives the angular distribution in the form $(1+7\cos^2\theta)$. The deviation between this expression and the experiment is of the order of 10%. Read (1968) was able to improve the fit to the angular distribution of inelastically scattered electrons in CO, using a mixture of $p\pi$ and $d\pi$ waves. The mixing of the $p\pi$ and $d\pi$ waves is left as a parameter and the mixing parameters are adjusted until a good fit to the experimental angular distribution is obtained.

B. Dissociative Attachment (9.65–12 eV)

Dissociative attachment in CO leads to the formation of O^- via the reactions (Chantry, 1968)

$$e+CO\rightarrow O^-+C(^3P)\ [9.62\ eV]$$

and

$$e+CO\rightarrow O^-+C(^1D)\ [10.88\ eV].$$

A much smaller cross section ($\sim 6\times 10^{-23}$ cm^2) exists for the reaction (Stamatovic and Schulz, 1970)

$$e+CO\rightarrow O+C^-(^4S)\ [10.20\ eV].$$

Whereas the experimentally observed appearance potentials for the reaction leading to O^-+C, given in brackets above, occur at the expected position for these reactions, the formation of $O+C^-$ is "delayed" by about 360 meV from the energetically lowest value that can give the reaction (9.84 eV). A hypothetical potential energy diagram showing some of the observed features is shown in Fig. 52.

Figure 53 shows the dissociative attachment cross section for O^- formation as measured by Stamatovic and Schulz (1970), by Chantry (1968), and by Rapp and Briglia (1965). Stamatovic and Schulz detect structure in the dissociative attachment curve near 10 eV, which can be interpreted by the presence of the $^2\Sigma^+$ core-excited resonance (to be discussed in the following section) interacting with the potential energy curve responsible for O^- formation.

C. Core-Excited Resonances in the 10–15 eV Region

Core-excited resonances in CO strongly resemble those of N_2. Just as in N_2, the lowest Rydberg state of CO, $b\,^3\Sigma^+$, can support a strong core-excited resonance of the Feshbach type. This resonance, discovered in a transmission experiment by Sanche and Schulz (1971a), was further studied by Comer and Read (1971c), by Swanson *et al.* (1971, 1972) and by Mazeau *et al.* (1972a). Uniform agreement exists on the location of this resonance as measured by Sanche and Schulz, i.e., 10.04±0.03 eV, with a width about 45 meV. Angular distribution measurements (Mazeau *et al.*, 1972a; Pavlovic *et al.*, 1973) show that the resonance exhibits itself in the s wave and thus the symmetry is $^2\Sigma^+$.

Figure 54(a) shows the energy dependence of the differential cross section for the $v=0$ and $v=1$ exit channels of the ground electronic state at angles of 80 and 60 degrees, respectively, and Fig. 54(b) shows the elastic differential cross section at other angles of observation. The transmission experiment of Sanche and Schulz is shown in Fig. 55(A). The features are numbered and the positions of the features are listed in Appendix VI in comparison with the features observed by Comer and Read (1971c) and Mazeau *et al.* (1972a).

The principal decay channels are indicated on the energy level diagram [Fig. 55(B)], mostly based on the work of Mazeau *et al.* (1972a), Swanson *et al.* (1972), and Comer and Read (1971c). The excitation function of electronically excited states at different angles of observation is shown in Figs. 55(C) and 55(D).

The features observed in CO are discussed in greater detail below.

1. $^2\Sigma^+$ Resonances (10.04 eV, 10.28 eV)

Structures (1–1′) to (4–4′) in the derivative transmission spectrum of CO, shown in Fig. 55(A), exhibit a remarkable resemblance to the structures (1–1′) to (4–4′) in N_2 and can be interpreted similarly. Structures 1–1′ (10.04 eV) and 2–2′ (10.28 eV) can be identified as two members of a vibrational sequence of Feshbach resonances whose parents are the $b\,^3\Sigma^+$ and $B\,^1\Sigma^+$ states of CO at 10.39 and 10.77 eV, respectively. The grandparent is the $X\,^2\Sigma^+$ ground state of CO^+ and the resonance itself has a symmetry $^2\Sigma^+$. The binding of the two $3s\sigma_g$ electrons with respect to the grandparent state is 4.1 eV, similar to other cases studied (see summary, Table X).

The $^2\Sigma^+$ resonance at 10.04 eV also influences dissociative attachment as has been discussed by Sanche and Schulz (1972), who reinterpreted the dissociative attachment experiments of Stamatovic and Schulz (1970) and pointed out that the structure near 10 eV in the O^- production from CO may be due to the $^2\Sigma^+$ resonance. Also, the formation of C^- from CO can be interpreted in terms of this resonance.

Although compound state formation is expected to be similar in the isoelectronic molecules N_2 and CO, the $^2\Sigma^+$ resonance in CO has a natural width ($\Gamma\simeq 40$ meV) which is almost two orders of magnitude greater than that found for the $^2\Sigma_g^+$ resonance at 11.48 eV in N_2 ($\Gamma\simeq 0.6$ meV). The larger width in CO probably results from the partial decay of the $^2\Sigma^+$ resonance into the $O^-(^2P)+C(^3P)$ channel. In N_2 dissociative processes are not observed and the potential energy curve corresponding to the one leading to O^-+C in CO could occur at a different energy where it would not interact with the $^2\Sigma_g^+$ state of N_2^-. Thus the natural width of the $^2\Sigma_g^+$ state in N_2 would be small since this state decays predominantly to the ground state of the molecule.

The decay of the $^2\Sigma^+$ resonance has been studied by

Mazeau *et al.* (1972a) and by Swanson *et al.* (1972). They find that the $^2\Sigma^+$, $v=0$ resonance at 10.04 shows a preference for decay into high vibrational levels of valence-excited electronic states: the $v=3$ state of $a\,^3\Pi$, the $v=4$ state of $A\,^1\Pi$, and the $v=25$ or 26 state of $a'\,^3\Sigma^+$. Schematically, these observations are shown on the energy level diagram, Fig. 55(B). One can understand the experimentally determined decay scheme by considering the equilibrium internuclear separation of the various states (Mazeau *et al.*, 1972; Swanson *et al.*, 1972). The $^2\Sigma^+$ compound state, being a Rydberg state, should have an equilibrium internuclear separation close to that of the positive ion $X\,^2\Sigma^+$ ($r_e=1.11$ Å) or the two parents $b\,^3\Sigma^+$ ($r_e=1.11$ Å) or $B\,^1\Sigma^+$ ($r_e=1.12$ Å); this places r_e for the compound state near 1.11 Å. The decay takes place to electronic states with a larger equilibrium internuclear separation ($X\,^1\Sigma^+$: $r=1.13$ Å; $a\,^3\Pi$: 1.20 Å; $A\,^1\Pi$: 1.23 Å; $a'\,^3\Sigma^+$: 1.35 Å). Thus, high vibrational quantum numbers will be preferred in the decay, especially when the final state has an r_e very large, as is the case for the $a'\,^3\Sigma^+$ state.

2. *Shape Resonances and Inelastic Thresholds*

Structures 3 and (4–4′) of Fig. 55(A) at 10.42 and 10.7 eV, respectively, are probably shape resonances, by analogy with similar structures observed in nitrogen. Angular distribution measurements in the $b\,^3\Sigma^+$ decay channel indicate that the 10.7-eV resonance has $a\,^2\Pi$ symmetry. Figure 55(C) shows this measurement of the angular distribution, and also the differential excitation cross section to the $b\,^3\Sigma^+$ state at 10.39 eV.

The excitation cross section to the $b\,^3\Sigma^+$ state shown in Fig. 55(C) exhibits a sharp rise near threshold and a number of structures above threshold. At first sight, this excitation function appears similar to the excitation cross section to the $E\,^3\Sigma_g^+$ state in N_2 [Fig. 44(B)]. However, there is a notable difference: Whereas the angular distribution near the threshold of the $E\,^3\Sigma_g^+$ state in N_2 exhibited a p-wave dependence [see Fig. 44(C)] characteristic of the decay of a p-type shape resonance, in the case of the $b\,^3\Sigma^+$ state in CO, we see from Fig. 55(C) that the angular distribution is isotropic. Thus, an s wave is indicated.

We have already pointed out in Sec. IIIB2 that the decay of the wings of the $^2\Sigma^+$ resonance, lying 350 meV below the threshold of the $b\,^3\Sigma^+$ state, can cause a sharp structure in the threshold behavior. This appears to be the case. The large width of $^2\Sigma^+$ resonance in CO, about 45 meV (vs only 0.6 meV for the $^2\Sigma_g^+$ resonance in N_2 at 11.48 eV) would provide a favorable circumstance for the observation of the decay of the $^2\Sigma^+$ resonance into an inelastic channel.

3. *Band "a"*

At higher energies in CO, the transmission experiment (Fig. 55) shows many overlapping resonances and

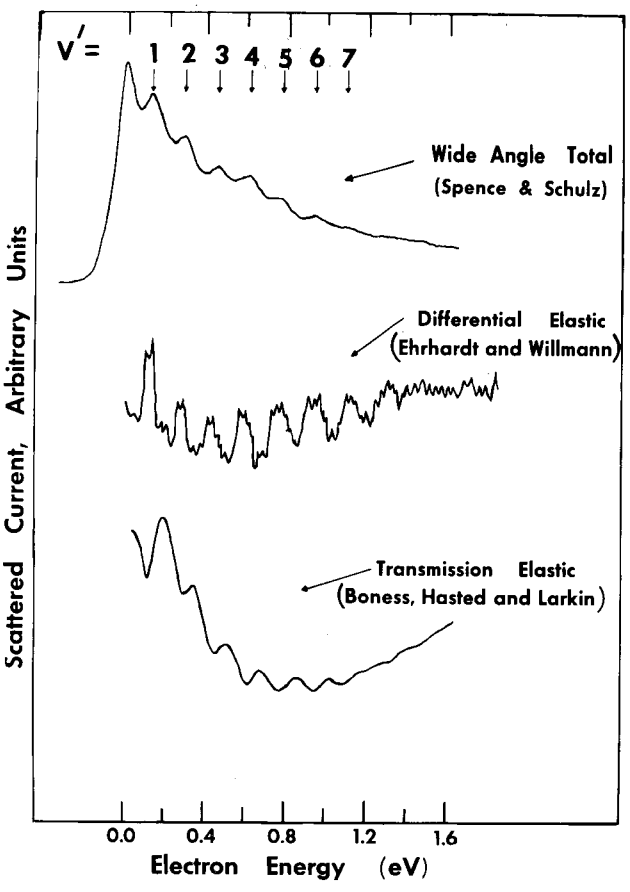

FIG. 56. Comparison of experiments on the structure in the low-energy cross section of NO. The top curve represents a recorder tracing of electrons scattered over a wide acceptance angle (mostly elastic) (Spence and Schulz, 1971b). The middle curve is the differential elastic cross section (Ehrhardt and Willmann, 1967). The bottom curve, which has been shifted by about 0.4 eV to overlap the present results, represents the transmission experiment of Boness, Hasted, and Larkin (1968). The structure is interpreted as the resonant contribution to the elastic cross section and the spacing of the structure is interpreted as the spacing of the $NO^-\,^3\Sigma^-$ system. [From Spence and Schulz (1971b).]

identification of particular bands is not possible. However, one can identify six vibrational levels belonging to a common progression (band "a") near the end of the spectrum shown in Fig. 55. This progression starts at 13.95±0.05 eV with a spacing of 205, 190, 185, 175, and 165±5 meV, respectively. The probable grandparent is the $A\,^2\Pi$ state of CO^+.

D. Resonances above the Ionization Potential in CO

It was pointed out in Sec. IIID that there exist resonances above the ionization potential of nitrogen, in the range 20–24 eV. A similar process exists in carbon monoxide. Chutjian *et al.* (1972) and Truhlar *et al.* (1972) have measured the cross section for excitation of the $v=1$ vibrational state in CO [see Fig. 55(E)] and find a broad peak around 20-eV energy. They find that theories relying on potential scattering alone are

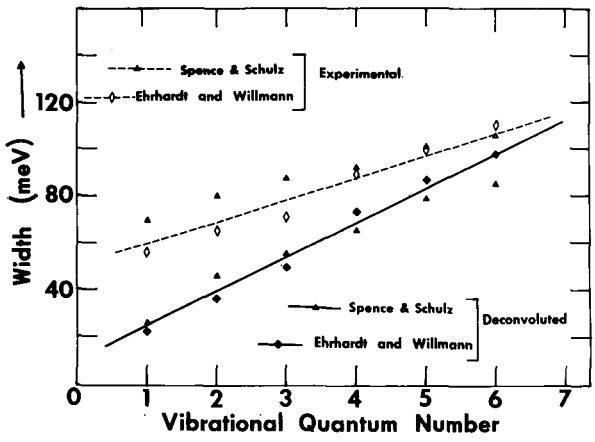

FIG. 57. Width of resonances in the elastic cross section of NO. Open symbols represent the experimental observations and the dashed line is drawn through these points. Filled-in symbols with the solid line drawn through them represent the "real" width of the resonances, obtained by deconvolution. In the deconvolution both the electron-energy distribution and the resonances are assumed to be Gaussian. The data shown are those of Spence and Schulz (1971) and of Ehrhardt and Willmann (1967). The width is defined as the full width at half-maximum. [From Spence and Schulz (1971b).]

not adequate to explain this peak and conclude that a resonance or a series of resonances must be involved to explain the cross sections near 20 eV.

V. NITRIC OXIDE, NO

A. Compound State at Low Energy (0–1.5 eV) $X\,^3\Sigma^-$

Nitric oxide, like O_2, forms a stable parent negative ion and thus NO has a positive electron affinity. The lowest negative ion state is the $X\,^3\Sigma^-$ state whose zeroth vibrational level is stable with respect to autodetachment; however, the higher vibrational states autodetach since they lie energetically above the $v=0$ state of NO ($X\,^2\Pi_r$). For an understanding of electron scattering, one wishes to know the electron affinity, the vibrational spacings of NO^-, the anharmonicity, and the equilibrium internuclear separation. Information regarding these parameters comes from various types of experiments, discussed below, which shed light on the nature of the shape resonance in NO.

1. Elastic Scattering

The values of the vibrational spacings of the low-lying shape resonance are deduced (for both O_2 and NO) primarily from electron scattering experiments: The energy dependence of the elastic cross section exhibits structure at the positions of the vibrational levels. The *vibrational* cross section to various states of NO also exhibits relatively sharp peaks at the positions of the vibrational states of NO^-.

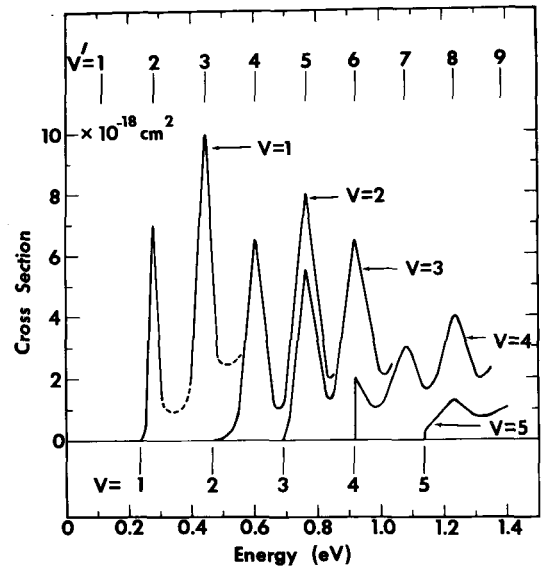

FIG. 58. Approximate cross sections for vibrational excitation of NO by electron impact. The vibrational spacing of the neutral molecule is indicated below the curves, and the vibrational spacing of NO^- above the curve. [From Spence and Schulz (1971b).]

TABLE VII. Parameters of $NO^-(X\,^3\Sigma^-)$.

	Electron scattering: (Spence and Schulz)	Photodetachment: (Siegel *et al.*)
Equilibrium separation, r_e	1.286 Å[a]	1.258±0.010 Å[b]
Electron affinity, EA(NO)	50 meV	24(+10, −5) meV[b]
ω_e	170±20 meV	182±25 meV
$\omega_e x_e$	1.0±0.25 meV	...

[a] Values obtained using Badger's rule.
[b] Preferred values.

Figure 56 shows the structure in the elastic cross section as observed by Spence and Schulz (1971b), by Ehrhardt and Willman (1967), and by Boness, Hasted, and Larkin (1968). The spacing of the peaks is about 160 meV and the agreement between various experiments appears good. Interestingly, the *width* of the observed peaks increases as the quantum number increases, from 70 meV for the first peak to 100 meV for the fifth. This effect can be clearly seen from Fig. 57. A similar broadening may also occur in O_2, but has not been observed experimentally because the width of the peaks in O_2 is much narrower than in NO, and thus the experimentally observed width of the peaks in O_2 are almost entirely caused by the instrumental resolution. Any changes in the natural width are hidden, in the case of O_2, by the instrumental resolution.

2. *Vibrational Excitation (0–1.4 eV)*

The vibrational cross section, as measured by Spence and Schulz (1971) using the trapped-electron method, exhibits (similar to the case of O_2) a series of spikes superimposed on a slowly rising background ("direct") cross section. The results are shown in Fig. 58. Here, the vibrational levels of the compound state (as determined by the elastic scattering experiments of Fig. 56) are shown by the vertical lines. The agreement between the location of the "spikes" in the vibrational cross section and the location of the compound states from elastic scattering is very good and justifies the model used.

One important result obtained by Spence and Schulz involves the observation that the $v=4$ state of NO is accidentally coincident in energy (within ± 10 meV) with the $v'=6$ state of NO^-. The trapped-electron method has a high sensitivity for detection of such coincidences. This comes about by plotting the positions of the peaks in the trapped-electron current as a function of well depth. If an excitation function contains a dominant spike (resulting from a resonance), then the peak of the trapped-electron current occurs at the energy of the spike and a plot of the position vs well depth is a horizontal straight line. Otherwise, such a plot is a straight line with slope of unity.

Spence and Schulz (1971b) observe that the branching ratio, i.e., the ratio of cross sections for various final states of NO via a given state of NO^-, is close to unity, in sharp contrast to the case of O_2. They deduce that the barrier height involved in the case of NO is lower than that in O_2 and that probably a p wave dominates the electron escape. The resulting lower barrier leads to a short lifetime of NO^- ($\sim 10^{-14}$ sec) compared to the lifetime of O_2^- ($\sim 10^{-10}$ sec). The assumption of a p-wave barrier is consistent with the theoretical considerations of Bardsley and Read (1968) who point out that the partial waves which are being mixed are the $p\pi$ and $d\pi$ waves (see Sec. VII). Bardsley and Read also point out that in resonance formation and decay at low energies, a p-wave component is much more efficient than a d-wave component. The centrifugal barrier through which the incoming or outgoing electron must tunnel is much higher for d waves than for p waves. Although d waves may be more important than p waves in the interior of the molecule, this is not necessarily true near the surface.

Spence and Schulz (1971b) deduce the values of ω_e from the spacing of the peaks in the elastic and the vibrational cross sections, and they calculate the equilibrium internuclear separation for NO^- using Badger's rule (Badger, 1935). Table VII shows a comparison of the values thus calculated with the values from photodetachment experiments. The schematic potential energy curve deduced by Spence and Schulz is shown in Fig. 59. In order to bring the NO^- curve into agreement with the results of photodetachment experiments, one should decrease r_e to 1.258 Å and should decrease the spacing of the NO^- levels somewhat so that the coincidence of the level $v'=6$ of NO^- with $v=4$ of NO can be maintained and so that the $v'=0$ level comes to -0.024 eV.

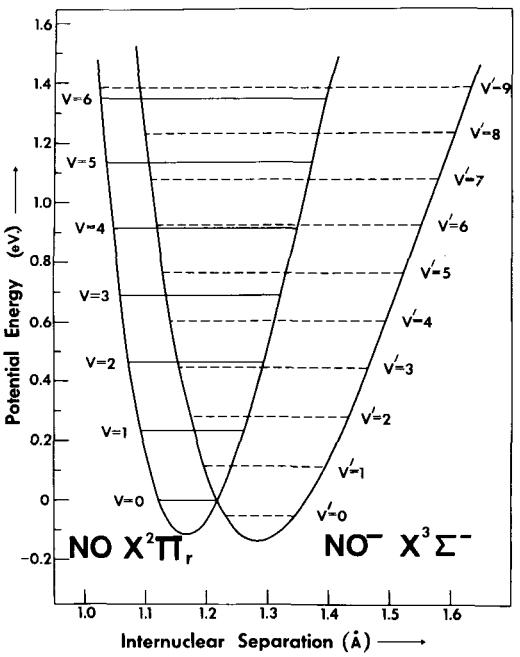

FIG. 59. Potential-energy curves for $NO(X\,^2\Pi_r)$ and $NO^-(X\,^3\Sigma^-)$. The width of the levels of NO^- have been omitted. In order to bring the NO^- curve into agreement with the results of photodetachment experiments, one should shift the minimum of the NO^- curve to 1.258 Å and the spacings of the vibrational levels should be decreased. [From Spence and Schulz (1971b).]

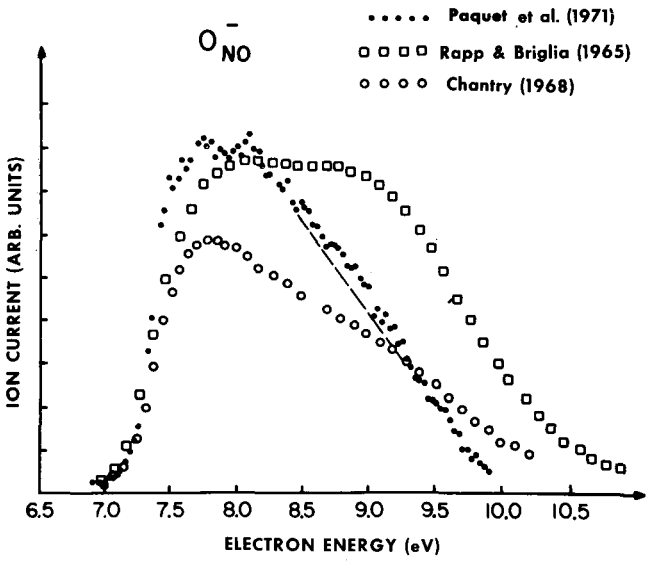

FIG. 60. Negative ion formation by dissociative attachment in NO. Shown are the results of Paquet, Marchant, and Marmet (1971), of Chantry (1968), and of Rapp and Briglia (1968). Dissociative attachment in NO leads exclusively to electronically excited N. [From Paquet, Marchand, and Marmet (1971).]

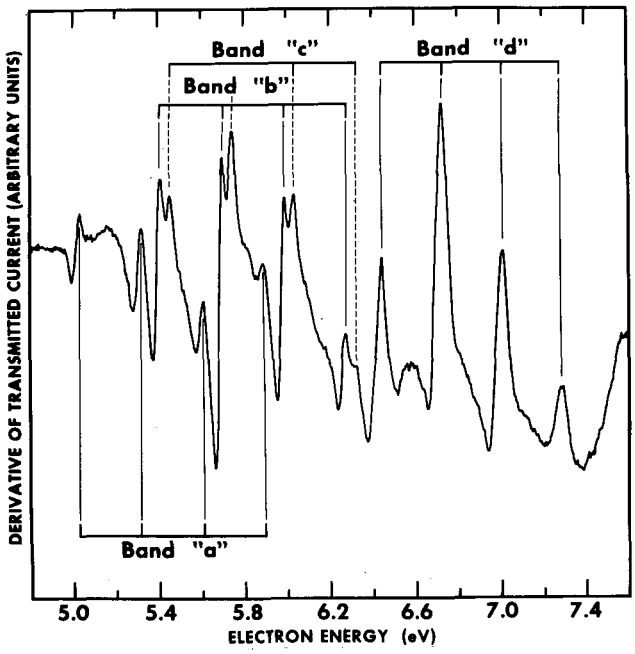

FIG. 61. Derivative of transmitted current vs electron energy in the 5–7.5 eV region in NO. Four bands belonging to a Rydberg series of NO^- states are shown; each band consists of a vibrational progression. The spacing of each vibrational progression agrees with the vibrational spacing of the $X\,^1\Sigma^+$ ground state of NO^+, which is the grandparent. [From Sanche and Schulz (1972).]

3. *Equilibrium Internuclear Separation and Electron Affinity: Photodetachment Spectroscopy*

Values of the electron affinity of NO (and also of O_2) have been in a state of violent fluctuation until very recently. But as a result of the recent photodetachment experiments of Siegel *et al.* (1972), a reliable value is now available:

$$EA(\mathrm{NO}) = 24(+10, -5)\ \mathrm{meV}.$$

In the experiments of Siegel *et al.*, an argon-ion laser photodetaches electrons which are energy-analyzed. A Franck–Condon factor analysis of the observed cross sections determines the molecular constants for NO^-: $\omega_e = 1470 \pm 200$ cm^{-1}; $r_e = 1.258 \pm 0.010$ Å; and $B_e = 1.427 \pm 0.02$ cm^{-1}, and also the electron affinity quoted above (24 meV). The very recent value of McFarland *et al.* (1972) is 28 ± 14 meV, in good agreement with Siegel. Older values of the electron affinity of NO are listed by Siegel *et al.* (1972) but they all seem less reliable: The other values are 900 ± 100 meV (Farragher *et al.*, 1964), 650 meV (Stockdale *et al.*, 1969), 90 ± 100 meV (Berkowitz *et al.*, 1971), 0 (Lacman and Herschbach, 1970), and 50 meV (Spence and Schulz, 1971b).

B. Dissociative Attachment (7–10 eV)

Dissociative attachment in NO, leading to the formation of O^-, indicates the existence of a repulsive potential energy curve in the region 7–10 eV, as shown by the negative ion production of Fig. 60. The structure observed by Paquet *et al.* (1971) may well be due to the traversal of the repulsive curve responsible for O^- production through the potential energy curves responsible for the core-excited resonances. Noteworthy is the conclusion of Chantry (1968), who determined from kinetic energy measurements of the O^- ion, that the dissociative attachment process leads exclusively to the formation of electronically excited N, i.e., $e + \mathrm{NO} \rightarrow \mathrm{O}^- + \mathrm{N}(^2D)$.

C. Core-Excited Resonances in NO

Fewer experiments on core-excited resonances are available in NO than in the molecules previously discussed. Differential measurements have not yet become available. Nevertheless it was the NO molecule which revealed the interpretation of core-excited resonances in terms of Rydberg compound states (Sanche and Schulz, 1971). Figures 61 and 62 show a plot of the derivative of the transmitted current vs electron energy in the energy range 5–18 eV. The features on Fig. 61 are given letter designations and are discussed below.

1. *Bands "a" to "d"*

The location of four bands of resonances, "a", "b", "c", and "d", is indicated in Fig. 61 by vertical lines

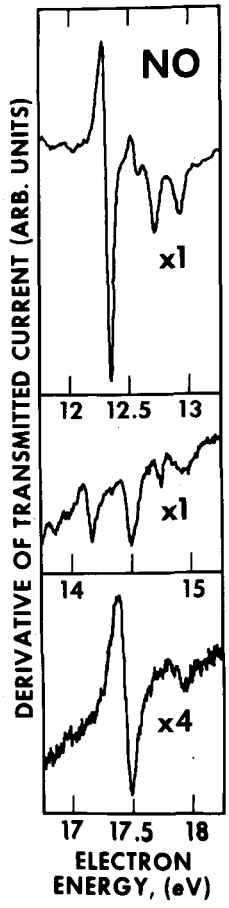

FIG. 62. Electron transmission spectra for NO in the 12–13 eV, 14–15 eV, and 17–18 eV regions. Each segment shows resonances associated with the $b\,^3\Pi$, $A\,^1\Pi$, and $B\,^1\Pi$ excited states of NO^+ which are the respective grandparents. The binding of the first compound state in each segment relative to the corresponding grandparent state is nearly constant. [From Sanche and Schulz (1972).]

pointing to each vibrational member of a given band. The first 3 bands have four vibrational members and the bands start at 5.04, 5.41, and 5.46 eV, respectively. Band "d" starts at 6.45 eV and six vibronic states belonging to that band have been observed; four of these are shown in Fig. 61. The vibrational spacings of each band and the Franck–Condon probabilities for bands "a", "b", and "d" are compared with the corresponding values for the $X\,^1\Sigma^+$ ground state of NO^+ in Appendix VII. Bands "a", "b", and "c" have about the same spacing, which agrees well with the spacing of the grandparent NO^+ core. Band "d" deviates slightly from the grandparent spacing. Franck–Condon probabilities for bands "a", "b", and "d" agree qualitatively with those of the NO^+ ion core, even though bands "a", "b", and "c" overlap. All Franck–Condon probabilities listed are normalized to $v=1$ for comparison purposes.

The comparisons suggest that all four bands in NO are composed of two Rydberg electrons temporarily bound to the same $X\,^1\Sigma^+$ core of NO^+. The parent of band "a" is probably the $A\,^2\Sigma^+$ Rydberg state of NO which lies at 5.48 eV. The A state, whose electron affinity from the above argument is 0.45 eV, corresponds to an electron in a Rydberg orbital of the symmetry $3s\sigma$ bound to the $X\,^1\Sigma^+$ core of NO^+. The addition of another $3s\sigma$ electron to the core gives the $^1\Sigma^+$ symmetry for band "a".

Bands "b" and "c" which lie 0.07 and 0.02 eV below the $A\,^2\Sigma^+$ state of NO, respectively, could result from the addition of a $3p\sigma$ or $3p\pi$ electron to the A state. Alternatively, the parents of bands "b" and "c" could be the $C\,^2\Pi$ and $D\,^2\Sigma^+$ states of NO, which lie at 6.49 and 6.60 eV, respectively. As far as band "d" is concerned the only likely parents are the C and D states of NO.

Paquet, Marchand, and Marmet (1971) have recently postulated the presence of two long-lived bound negative ion states at 7.8 and 8.2 eV, in order to explain two peaks they observe in the cross section for O^- formation from NO at these energies. The postulated states should appear in the total scattering cross section. The 5th vibrational member of band "d," which lies at 7.83 eV, could possibly account for the 7.8-eV peak in the O^- data at Paquet *et al.*

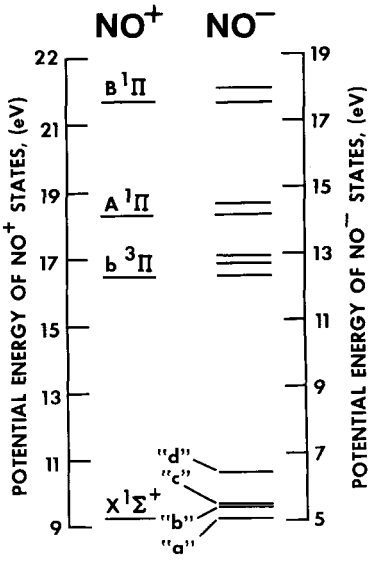

FIG. 63. The energy level diagram of relevant NO^+ grandparent states (left side of diagram) compared with the energy level diagram of the NO^- states observed in the present experiment (right side of diagram). The two energy scales have been displaced by the binding energy of the lowest member of band "a" with respect to its grandparent $X\,^1\Sigma^+$ state of NO^+. Each state of NO^+, shown on the left of the diagram, gives rise to a Rydberg series of NO^- states. [From Sanche and Schulz (1972).]

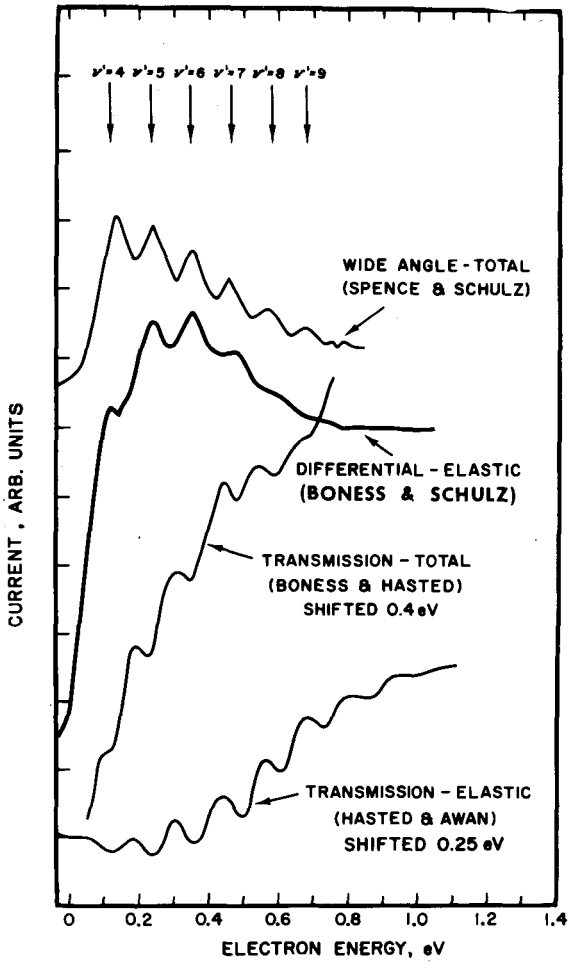

FIG. 64. Comparison of four experiments on the structure in the electron impact cross section in O_2. The top curve shows the wide-angle total cross section (Spence and Schulz, 1970), the next curve shows the differential elastic cross section (Boness and Schulz, 1970). The bottom two curves represent transmission experiments. The curve by Boness and Hasted (1966) is shifted by 0.4 eV and the curve by Hasted and Awan (1969) is shifted by 0.25 eV, both to lower energies. The agreement in the spacing of the structures is considered good. The indicated quantum numbers refer to the $O_2^-(X\,^2\Pi_g)$ state. [From Boness and Schulz (1970).]

2. Region 12 eV–18 eV

The resonances shown in Fig. 62 for the energy range 12–18 eV seem to have as their grandparents *excited* states of NO^+. At least ten bound excited states of NO^+ are known at the present time and four of these, namely the $b\,^3\Pi$, $A\,^1\Pi$, $c\,^3\Pi$, and $B\,^1\Pi$ ion states, can be con-

TABLE VIII. Molecular orbital configuration of the ground states and of shape resonances in diatomic molecules. The extra electron, which is responsible for the shape resonance, occupies the lowest vacant orbital shown in the fourth column.[a]

Molecule	Molecular orbitals of ground state	Ground state	Lowest vacant orbital	Compound state	Dominant partial wave
H_2	$(1s\sigma_g)^2$	$^1\Sigma_g^+$	$2p\sigma_u$	$^2\Sigma_u^+$	$p\sigma$
N_2	$(1s\sigma_g)^2(2p\sigma_u)^2(2s\sigma_g)^2(3p\sigma_u)^2(3s\sigma_g)^2(2p\pi_u)^4$	$^1\Sigma_g^+$	$3d\pi_g$	$^2\Pi_g$	$d\pi$
O_2	----------$(3d\pi_g)^2$	$^3\Sigma_g^-$	$3d\pi_g$	$^2\Pi_g$	$d\pi$
CO	$(1s\sigma)^2(2s\sigma)^2(2p\sigma)^2(2p\pi)^4(3s\sigma)^2(3p\sigma)^2$	$^1\Sigma^+$	$3p\pi$	$^2\Pi$	$d\pi+p\pi$
NO	----------$(3p\pi)$	$^2\Pi_r$	$3p\pi$	$^3\Sigma^-$	$d\pi+p\pi$

[a] The notation used is the "united atom" notation of Herzberg (1950). See also Bardsley and Mandl (1968). The notation used in the column entitled "dominant partial wave" is $d\pi$, $p\pi$, and $p\sigma$. The first, Latin letter, refers to the angular momentum of the electron partial wave at infinity, i.e., $l=2$, and 1, respectively. The Greek letter refers to the component of this angular momentum along the internuclear axis of the molecule as the electron comes close to the molecule.

sidered as possible candidates for compound state formation from the ground state since their internuclear distances lie close to the internuclear distance of the NO ground state. These states are listed in Appendix VIII where their energies are given. Also shown in Appendix VIII are the position of the resonances in the energy range 12–18 eV. In the last column of Appendix VIII we calculate the "binding" energy by taking the difference between the energies of the assumed grandparent and the lowest value of the resonance. The constancy of the binding energy indicates that the proper grandparents have been assigned and that the potential well which binds the two $3s\sigma$ electrons does not change. The binding energy of band "a" (previously discussed) with respect to the $X\,^1\Sigma^+$ ground state is 4.23 eV, in very good agreement with the other values for the binding energy shown in Appendix VIII.

The various structures listed in Appendix VIII have been interpreted by Sanche and Schulz (1972) as core-excited Feshbach resonances or as core-excited shape resonances, and their parents have been suggested. For example, the 12.57-eV feature listed in Appendix VIII is interpreted as the $v=1$ state belonging to the progression starting at 12.36 eV, since the spacing and the Franck–Condon factors agree with those of the $b\,^3\Pi$ grandparent state.

An energy level diagram of the zeroth vibronic level of each NO^- state is shown on the right side of Fig. 63. On the left side of this figure the energy levels of the NO^+ grandparent states are shown. The two scales have been displaced by the difference in energies between the lowest member of band "a" with respect to its grandparent, the $X\,^1\Sigma^+$ core of NO^+ (4.23 eV), in order to show the relationship between the NO^+ state and its grandchildren NO^- states. This comparison demonstrates that the binding energy of two $3s\sigma$ Rydberg electrons does not depend on the configuration of the positive ion core. It also illustrates that in NO only Rydberg excited states give rise to core-excited resonances in the total scattering cross section.

VI. OXYGEN

A. Compound State at Low Energy: $X\,^2\Pi_g$ (0–1 eV)

The lowest compound state of O_2 is the $X\,^2\Pi_g$ state. The vibrational states $v'=0$ to $v'=3$ of $O_2^-(X\,^2\Pi_g)$ lie below the $v=0$ state of $O_2(X\,^3\Sigma_g^-)$ and cannot autodetach. These vibrational states of O_2^- are therefore stable. For higher quantum numbers, autodetachment can take place and these higher vibrational states form the lowest compound state of O_2. As in the case of NO, a variety of experiments must be brought to bear on the problem in order to gain a full picture which has recently emerged. The important experiments are elastic scattering, inelastic scattering (i.e., vibrational excitation), photodetachment, various measurements of the electron affinity, and three-body attachment.

The molecular orbital notation for the lowest states of O_2 and O_2^- is given in Table VIII, Sec. VII.

1. Elastic Scattering

The structure, consisting of peaks, in the elastic differential and total cross sections of electrons on O_2 gives us the information on the position of the vibrational levels of the O_2^- system. Figure 64 shows a compilation of several experiments, suitably presented. The spacings are also listed in Appendix IX. The assignment of the proper vibrational quantum number does not come from the elastic experiment alone. Rather, the electron affinity of O_2 must be known in order to achieve such an assignment and a backward extrapolation, using the measured spacings and the anharmonicity, must be performed. Until recently the value for the electron affinity was being questioned (see Sec. VI A3) but we can now be confident that the values of Pack and Phelps (1966) (0.43±0.02 eV) and of Celotta *et al.* (1972) (0.440±0.008 eV) are correct.

When the backward extrapolation is performed and terminated at the electron affinity of 0.44 eV, one obtains a value of 132 meV (Spence and Schulz, 1972) or 135 meV (Linder and Schmidt, 1971b) or 140 meV (Gray *et al.*, 1971) for the spacing of the lowest vibrational states, i.e., $v'=0 \rightarrow v'=1$ of O_2^-. These values compare to a value of 135 meV deduced by Holzer *et al.* (1968) from Raman spectroscopy of alkali halide crystals in which O_2^- is trapped. The agreement between all these values appears to be good.

A high-resolution (10 meV) transmission experiment by Land and Raith (1973) shows that the $v'=4$ peak is split by spin-orbit coupling into $^2\Pi_{3/2}$ and $^2\Pi_{1/2}$ components, separated by 20±2 meV. The center of the $v'=4$ state is determined to be at 91±5 meV.

2. *Vibrational Excitation of O_2 at Low Energy (0–1.0 eV)*

The vibrational cross section in O_2 should consist of a "direct" component and a "compound-state" component at the position of the compound state, O_2^-.

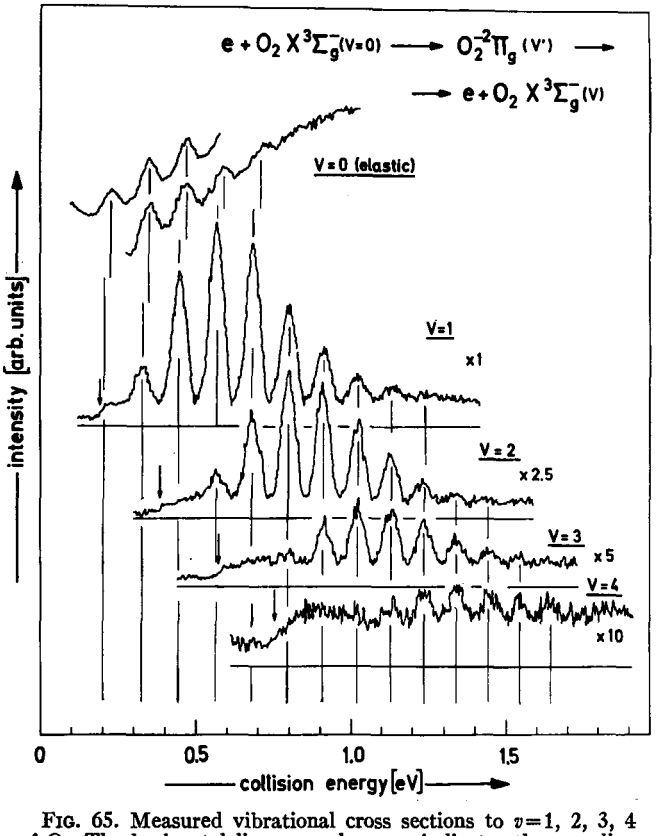

FIG. 65. Measured vibrational cross sections to $v=1$, 2, 3, 4 of O_2. The horizontal line at each curve indicates the zero line of the stored signal. Two runs of the energy dependence of elastic scattering are also shown in the upper part of the figure. The scattering angle is 60° for all curves. The vertical lines indicate the energy position of the resonance peaks. The threshold onsets of the excitation functions are marked by small arrows. Energy-integrated cross sections in absolute units are listed in Appendix X. [From Linder and Schmidt (1971b).]

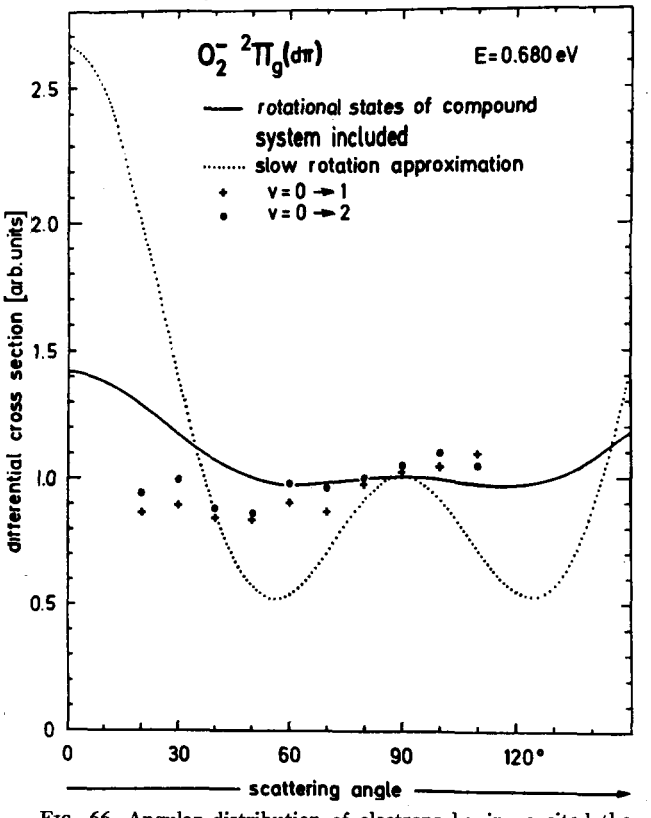

FIG. 66. Angular distribution of electrons having excited the $v=1$ and $v=2$ vibrational states in O_2. The points are experimental (error ~10%). The lines represent theoretical models with and without rotational states of the compound state. The curves have been normalized at or near 90°. [From Linder and Schmidt (1971b).]

This model was invoked by Hake and Phelps (1967) and by Schulz and Dowell (1962) to explain swarm and trapped-electron experiments, respectively.

Recent trapped-electron experiments by Spence and Schulz (1970) led to the conclusion that the vibrational cross sections in O_2 consist of series of spikes at the position of the compound state which had been previously established from elastic scatterings. This finding is corroborated by the differential cross section measurements of Linder and Schmidt (1971), whose data are shown in Fig. 65.

The trapped-electron method possesses a high sensitivity for detecting when a level of O_2 and a level of O_2^- occur accidentally at the same energy. Spence and Schulz find that the $v'=8$ level of O_2^- is coincident in energy with the $v=3$ level of O_2, thus fixing the relative positions of the vibrational levels of the two systems. This coincidence has been confirmed by Linder and Schmidt, who find that the coincidence between these two levels is within 1 meV, as well as by Land and Raith (1973).

In order to obtain an absolute magnitude from their differential cross section, Linder and Schmidt have to know the angular distribution of the scattered electrons. Figure 66 shows that the experimentally ob-

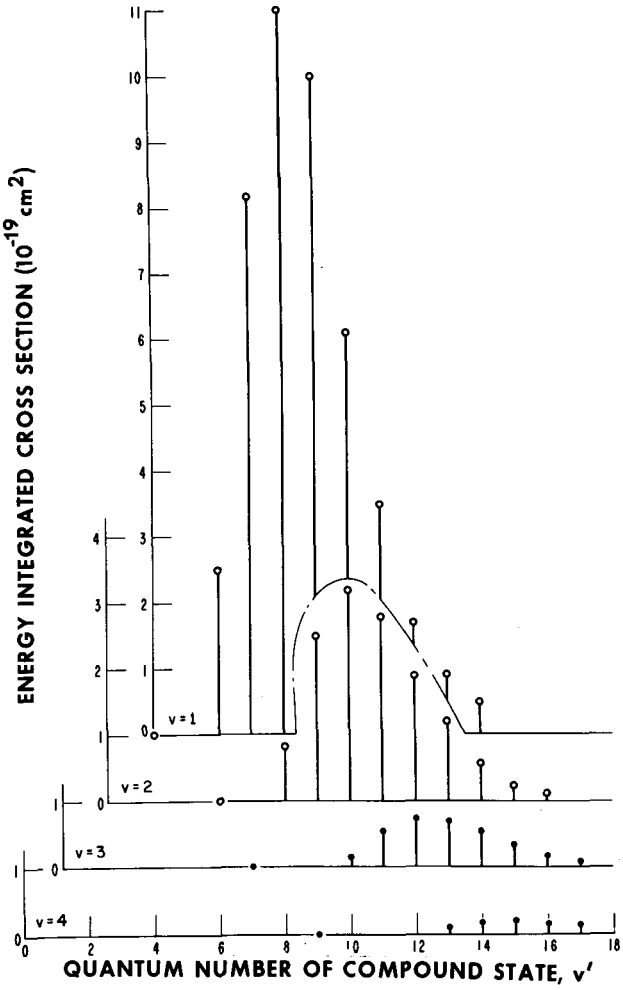

FIG 67. Plot of energy-integrated cross section for vibrational excitation to $v=1, 2, 3, 4$ vs quantum number of compound state, as measured by Linder and Schmidt (1971b). The cross sections consist of a series of narrow spikes at the positions of the vibrational levels, v', of the compound state.

served angular distribution is isotropic. The lifetime of the $X\,^2\Pi_g$ compound state, O_2^-, is long (i.e., $\sim 10^{-10}$ sec for the lowest vibrational member, $v'=4$), as will be discussed below. For such a long-lived object, one has to include rotation in the theory and the result of such a theory yields a near-isotropic angular distribution, as shown in Fig. 66. It is pointed out in Sec. VII that the partial wave in which the resonance occurs is $d\pi$.

The absolute magnitude of the energy-integrated vibrational cross sections for the $v=1, 2, 3, 4$ state of O_2 are shown in Fig. 67 and are listed in Appendix X. Spence and Schulz also measured the energy-integrated cross sections, but their set of measurements is less complete than that of Linder and Schmidt.

Disturbingly, Spence and Schulz' values are by a factor of 10 lower than the values of Linder and Schmidt for those states which are measured in both experiments. No clear-cut criticism can be found in either experiment. However, the values of Linder and Schmidt must be preferred at this time since they agree better in order of magnitude with the analysis of swarm experiments (Hake and Phelps, 1967) although a detailed comparison is not yet possible because the analysis of swarm experiments has not been performed with the proper set of relative cross sections.

An interesting feature of the data can be brought out by plotting the branching ratio of the cross sections for $v=2$ to $v=3$ and $v=1$ to $v=2$ vs quantum number of the compound state as is done in Fig. 68. Both curves show an enormous rise as the quantum number v' is lowered, indicating that a given compound state (especially for low quantum numbers, v') prefers to decay to the lowest possible state of the neutral molecule. The lowest possible state of the neutral molecule is reached by the emission of an electron with the highest possible energy, in the reaction $O_2^- \rightarrow O_2(v)+e$. A high-energy electron penetrates the potential barrier with a higher probability than a low-energy electron. Thus the emission of a high-energy electron is favored. For d-wave scattering which is involved in the present reaction, the barrier penetration is proportional to $E^{5/2}$ (Blatt and Weisskopf, 1952), where E is the energy of the electrons.

When the ratio of electron energies of the ejected electrons leading to various decay channels is large (as is the case at low quantum numbers v') a large branching ratio results. It should be noted that the branching ratio for low-lying vibrational states in N_2 and CO is close to unity. This results from the fact that

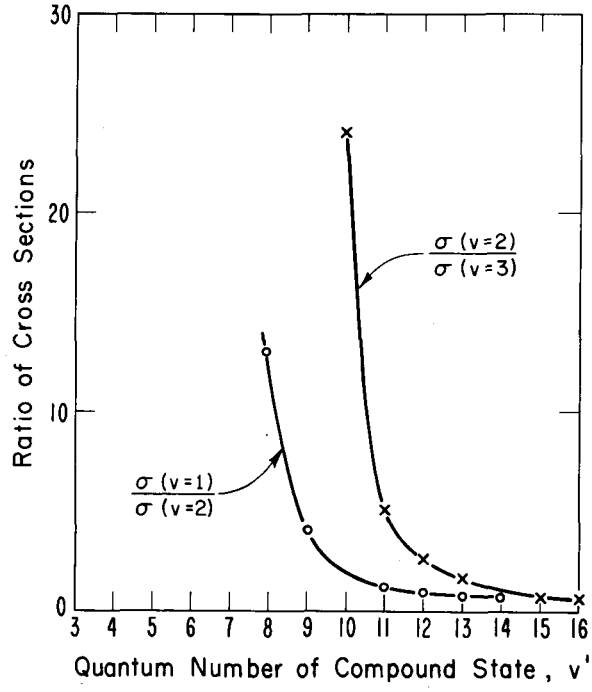

FIG. 68. Ratio of vibrational cross sections vs quantum number, v', of compound state. From data of Linder and Schmidt (1971b).

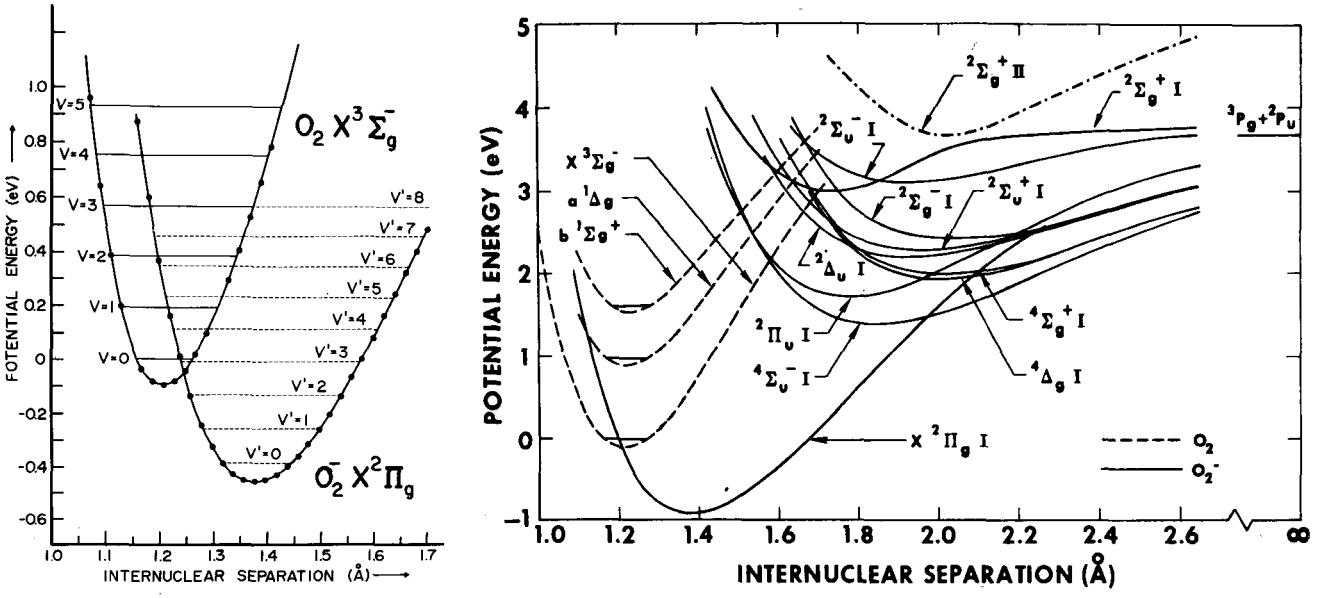

FIG. 69. (a) Approximate potential energy curves for O_2 and O_2^-. The O_2^- curve should have its minimum at 1.341 Å (Celotta *et al.*, 1972). The center of the $v'=4$ state is located at 0.091 ± 0.005 eV and it has a fine structure splitting ($\Pi_{3/2}-\Pi_{1/2}$) of 20 ± 2 meV (Land and Raith, 1973). The $v=3$ level of $O_2(X\ ^3\Sigma_g^-)$ is coincident in energy with the $v'=8$ level of $O_2^-(X\ ^2\Pi_g)$ (Spence and Schulz, 1970). [From Boness and Schulz (1970).] (b) *Ab initio* calculations of adiabatic potential energy curves for O_2^-. [From Michels and Harris (1971).]

the ratio of energies of the ejected electrons is also close to unity since the compound state in N_2 is located near 2.3 eV and the spacing of vibrational levels is about 0.3 eV. Thus the barrier penetration in N_2 does not differ much for the decay channels leading to the low vibrational states.

The widths of the $v'=4-10$ vibrational states of $O_2^-(X\ ^2\Pi_g)$ have been calculated by Koike and Watanabe (1973) who find a value of 0.004 meV for the $v'=4$ state. This value has a confidence limit of a factor of about two (Watanabe, private communication) and thus it is in good agreement with the estimate of 0.002 meV made by Herzenberg (1969) from the absolute magnitude of the vibrational cross section in O_2. The calculated values of Koike and Watanabe are listed in Appendix X.

3. *Potential Energy Curve for $O_2^-(X\ ^2\Pi_g)$*

Using a Morse-function representation together with parameters derived from electron spectroscopy, Boness and Schulz (1970) derived the potential energy curve for the $O_2^-(X\ ^2\Pi_g)$ state. This curve, together with the curve for the ground state of $O_2(X\ ^3\Sigma_g^-)$, is shown in Fig. 69(a). The curve is drawn so that the $v=3$ level of $O_2(X\ ^3\Sigma_g^-)$ coincides in energy with the $v'=8$ level of $O_2^-(X\ ^2\Pi_g)$. This coincidence has been established by Spence and Schulz (1970) and by Linder and Schmidt (1971). In order to bring the O_2^- curve into agreement with the results of Celotta *et al.* (1972), it should be shifted to smaller internuclear separations by 0.036 Å, so that the minimum of the potential energy curve would be at 1.341 Å.

Ab initio calculations for the low-lying potential energy curves have been performed by Michels and Harris (1971) and by Krauss, Neumann, Wahl, Das, and Zemke (1973). The agreement between the two sets of theoretical calculations appears to be good. The set by Michels and Harris is shown in Fig. 69(b).

4. *Equilibrium Internuclear Separation and Electron Affinity: Photodetachment Spectroscopy*

As in the case of NO, the electron affinity of O_2 was a matter of dispute for a long period of time. The various values have been summarized, as of 1970 by Boness and Schulz (1970). At that time it appeared that only the value of Pack and Phelps (1966), obtained from drift-tube studies of attachment and detachment coefficients in thermal equilibrium, was free of serious objections. The value of Pack and Phelps (0.43 eV) has recently been confirmed in a conclusive experiment involving photodetachment. The value of Celotta *et al.* (1972) is 0.440 ± 0.008 eV.

Other recent values for the electron affinity converge on the above value. Among these are the experiments of Nalley and Compton (1971), and those of Berkowitz *et al.* (1971) as interpreted by Chantry (1971).

The photodetachment experiment of Celotta *et al.* (1972) also gives a value of the equilibrium internuclear separation, $r_e=1.341\pm0.010$ Å, making obsolete

TABLE IX. Parameters of $O_2^-(X\,^2\Pi_g)$.[a]

	Celotta *et al.* (1972)	Boness and Schulz (1970)	Linder and Schmidt (1971b)	Gray *et al.* (1971)
Equilibrium separation, r_e Å	1.341±0.010	•••	•••	•••
Electron affinity, eV	0.440±0.008	•••	•••	•••
B_e (cm^{-1})	1.17±0.02	•••	•••	•••
$\hbar\omega_e$ (meV)	•••	135	135	140
$\hbar\omega_e x_e$ (meV)	•••	1.5	1.0	3.0

[a] Additional features: The fine-structure splitting is 22±2 meV (Land and Raith, 1972).

the previous determination of Boness and Schulz (1970), obtained by use of Badger's rule from the vibrational spacings of O_2^-.

Table IX lists the parameters for $O_2^-(X\,^2\Pi_g)$ deduced from photodetachment spectroscopy and from electron impact spectroscopy. It is seen that the values deduced from these two types of experiments complement each other. The value deduced by Boness and Schulz (1970) from the vibrational spacing of O_2^- using Badger's rule (i.e., $r_e=1.377$ Å) is not listed since the value deduced from photodetachment spectroscopy is considered more reliable.

From the foregoing discussion it should be fairly obvious that photodetachment spectroscopy is a powerful tool for determining electron affinities and the structure of negative ions. In both of the cases in which a stable negative ion exists, namely O_2 and NO, no evidence exists for excited negative ions lying below the neutral species, i.e., only one electronic state exhibits a positive electron affinity. Photodetachment experiments do not, however, rule out the possibility of the existence of excited states of O_2^- which have a large equilibrium internuclear separation. The calculations of Michels and Harris (1971) show that only the $X\,^2\Pi_g$ state of O_2^- lies below the ground state of O_2. Thus one must conclude that the only stable state of O_2^- which lies energetically below the ground state of O_2 is the $X\,^2\Pi_g$ state.

Figure 69(b) shows the potential energy curves for O_2^- as calculated by Michels and Harris (1971). In addition to the $X\,^2\Pi_g$ state, Michels and Harris find 12 other attractive states arising from the limit $O+O^-$. All these states are qualitatively similar, exhibiting shallow potential wells at large internuclear separations (1.8–2.0 Å). The existence of a large number of autodetaching states, O_2^-, is consistent with the experiments, on associative detachment (Ferguson, 1968). The thermal rate constant for the associative detachment reaction, $O^-+O\rightarrow O_2^-\rightarrow O_2+e$, is large [Ferguson (1968) gives a value of 3×10^{-10} cm^3 sec^{-1} at 300°K], and it is reasonable to suppose that some of the O_2^- states shown in Fig. 69(b) serve as intermediates.

Recently, Lineberger and Patterson (1972), using two-photon photodetachment spectroscopy, discovered an excited state of a negative ion which lies below the ground state of the neutral molecule. The molecule is C_2. The ground state of the negative ion, $C_2^-(^2\Sigma_g^+)$ lies ~3.5 eV below the neutral ground state, $C_2\,^1\Sigma_g^+$. About 2 eV above $C_2^-(^2\Sigma_g^+)$ there is an excited state of the negative ion, $C_2^-(^2\Sigma_u^+)$. It may be of interest to study such systems using electron spectroscopy to obtain complementary data.

5. *Three-Body Attachment in O_2*

Three-body attachment, i.e., the reaction $e+2O_2\rightarrow O_2^-+O_2$, is now known to proceed via the $X\,^2\Pi_g$ compound state of O_2. The reaction can therefore be written as a two-step process: $e+O_2\rightarrow O_2^{-*}$, followed by

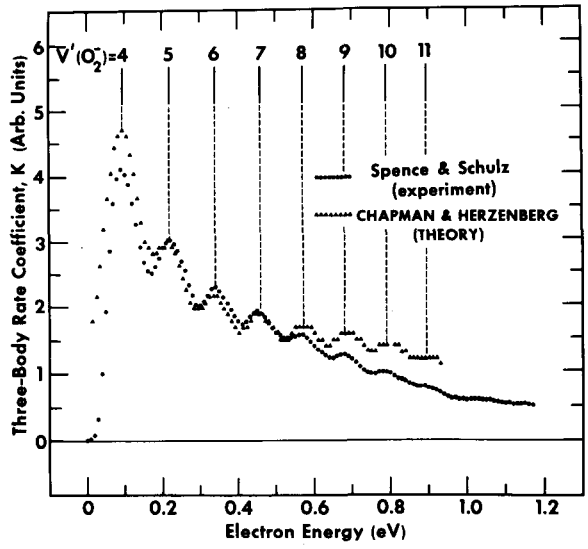

FIG. 70. The three-body attachment coefficient of production of O_2^- in O_2 in comparison with the theory. The theory is normalized to the experimental data at the second peak. The vibrational levels of the $O_2^-(X\,^2\Pi_g)$ state are indicated by the lines on top. The structure in the three-body attachment coincides with the positions of the vibrational states of O_2^-. This figure shows that three-body attachment on O_2 proceeds via the low-lying compound state of O_2. [From Spence and Schulz 1972).]

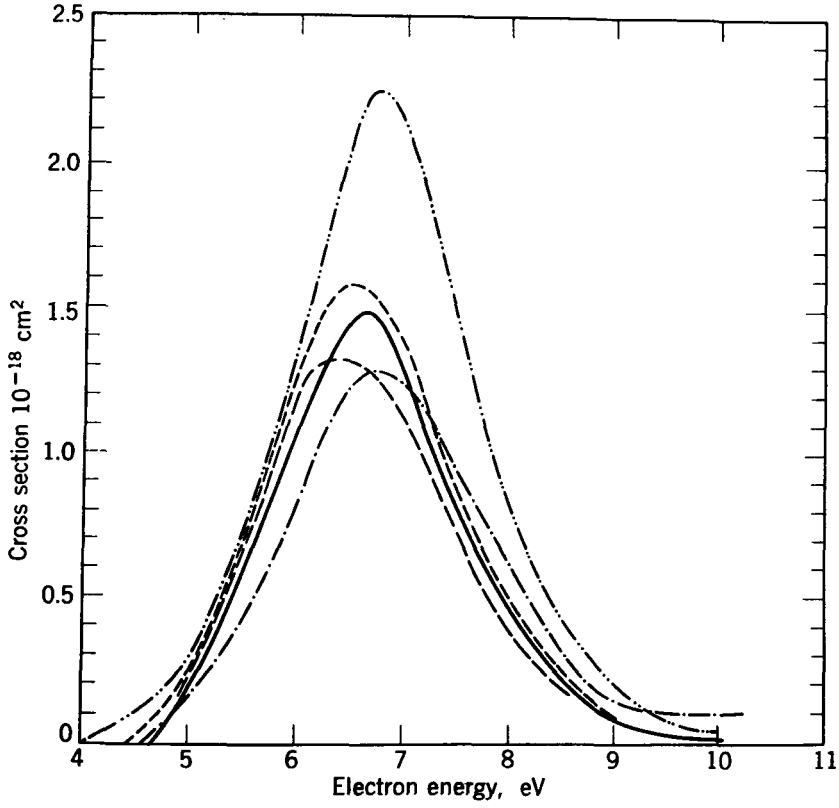

FIG. 71. The cross section for O^- formation by dissociative attachment in O_2. The value of Craggs *et al.* (1957) (–•••–) is undoubtedly too high. The values of Buchelnikova (1959) (- - -), of Schulz (1962b) (–•–), of Rapp *et al.* (1965) (– – –), and of Christophorou *et al.* (1965) (—) all agree very well. [From Chen (1969).]

$O_2^{-*}+O_2 \rightarrow O_2^- + O_2$. Here, O_2^{-*} denotes a particular vibrational level of the $O_2^-(X\,^2\Pi_g)$ state. The general features of this model have been deduced by Chanin, Phelps, and Biondi (1962) who clearly established the three-body nature of the process from their swarm data. The modern approach to the theoretical considerations is due to Herzenberg (1969). The swarm experiments of Chanin *et al.* show a smooth variation with energy of the three-body attachment coefficient as would be expected for swarm experiments.

If one performs an experiment with essentially monoenergetic electrons, the three-body attachment coeffi-

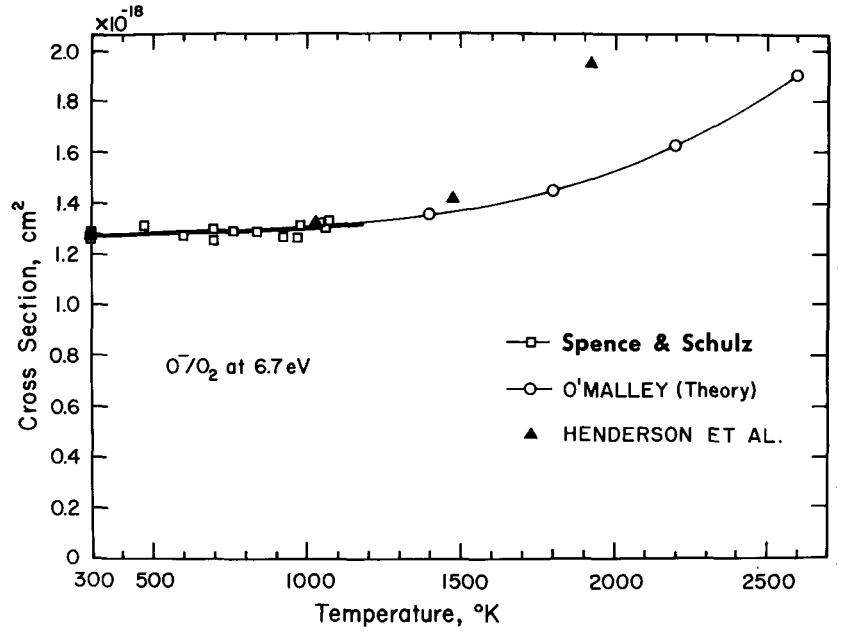

FIG. 72. The dependence on temperature of the peak dissociative attachment cross section in O_2. Shown are the results of Spence and Schulz (1969), of O'Malley (1967), and of Henderson, Fite, and Brackmann (1969). [From Spence and Schulz (1969).]

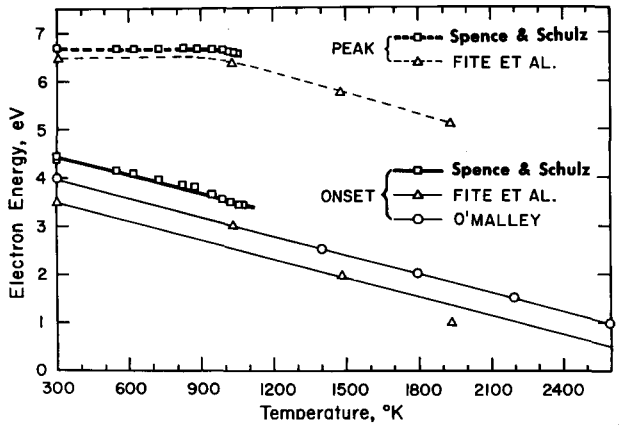

FIG. 73. Temperature dependence of energies of onset and energies at which peak of dissociative attachment occurs in O_2. Shown are the results of the same authors as Fig. 72. [From Spence and Schulz (1969).]

cient shows pronounced structure at the positions of the vibrational levels of the O_2^- system. The experimental results of Spence and Schulz (1972) are shown in Fig. 70, in comparison with the theory. The good agreement between the energy levels of the O_2^- system obtained from elastic scattering (shown on top of Fig. 70) and the positions of the peaks is convincing evidence that the process proceeds via the $O_2^-(X\,^2\Pi_g)$ state.

B. Dissociative Attachment (4.4–10 eV): $^2\Pi_u$ State

Dissociative attachment in O_2 has been studied in great detail and Fig. 71 shows that good agreement exists between the results of various experiments. The cross section for O^- production starts rising near 4.4 eV, reaches a maximum of about 1.3×10^{-18} cm^2 at 6.7 eV, and then drops. No structure of any kind has been detected in this cross section, nor is there a signal below 4.4 eV at room temperature (the theoretical onset for the reaction is about 3.6 eV), to a sensitivity 0.1% of the peak cross section. Spence and Schulz (1969) and Chen (1969) have reviewed the subject matter recently.

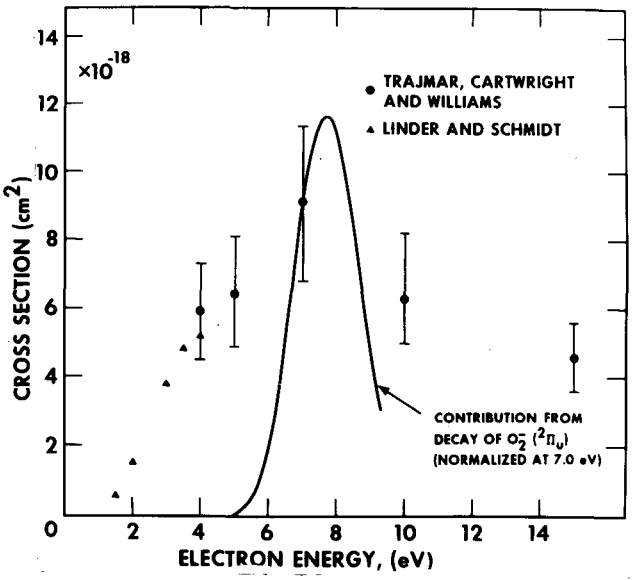

FIG. 74. Cross section for excitation of the $O_2(a\,^1\Delta_g)$ metastable state. Shown by the points are the data of Linder and Schmidt (1971) and of Trajmar, Cartwright, and Williams (1971). The solid curve, due to Burrow, shows that portion of the cross section to the $a\,^1\Delta_g$ state which proceeds via the $O_2^-(^2\Pi_u)$ state. The calculated curve represented by the solid line is normalized to the experimental value of Trajmar *et al.* at 7 eV. [From Burrow (1973).]

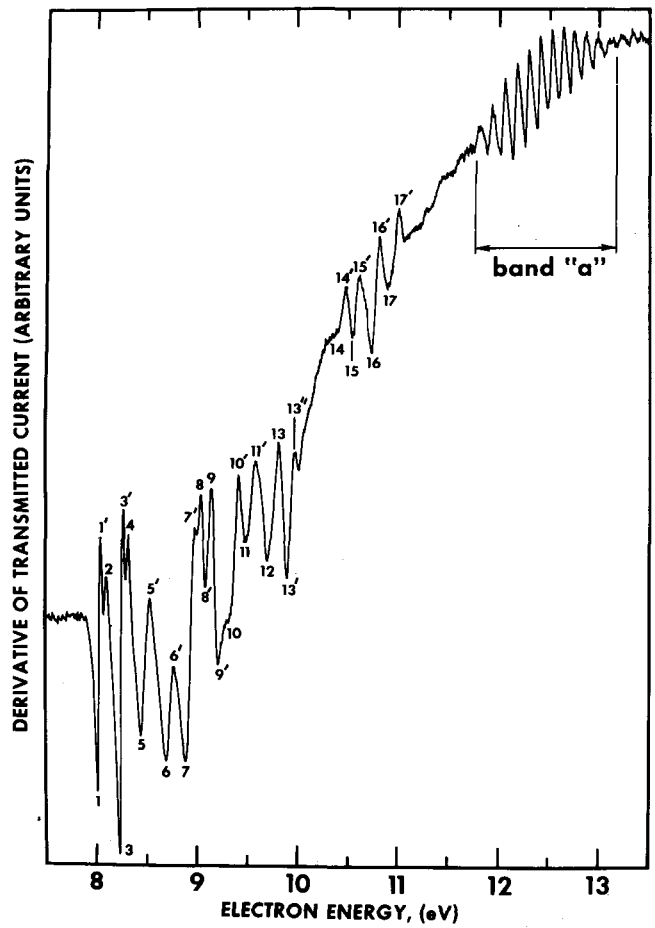

FIG. 75. Derivative of transmitted current vs electron energy in O_2. Structures 1–17 are interpreted as resonances whose grandparent is the ground state of O_2^+. A well-developed progression of ten resonances, marked band "a", appears near the end of the spectrum. The grandparent of band "a" is the $a\,^4\Pi_u$ state of O_2^+. [From Sanche and Schulz (1972).]

Noteworthy are the studies of the dependence on gas temperature of the onset and the absolute magnitude of the dissociative attachment cross section. These studies, performed by Henderson, Fite, and Brackmann (1969) and by Spence and Schulz (1969) show that the magnitude of the cross section increases as the gas temperature is raised and that the onset is lowered at higher temperatures. Figures 72 and 73 show the results of these studies.

The single peak at 6.7 eV suggests that a single compound state, $^2\Pi_u$, is responsible for dissociative attachment around 6.7 eV, although many more compound states exist in this energy range. This view is reinforced by the parametrization study of O'Malley (1967), who used the shape and the magnitude of the experimental cross section at room temperature and the temperature dependence to arrive at the shape of a single potential energy curve and the value for the width of the state. It is pointed out by O'Malley, and confirmed experimentally by Henderson *et al.* (1969) that the temperature effects in O^-/O_2 production can be explained solely on the basis of the vibrational excitation of the target molecule, and that rotational excitation does not play a significant role.

Vibrationally excited molecules have a large Franck–Condon region and if the electron is captured while the O_2 molecule is at a large internuclear separation, the survival probability for negative ion formation is enhanced. As a result, the dissociative attachment cross section increases for higher vibrational states.

The angular distribution of the O^- ions resulting from electron impact on O_2 in the energy range 5.75–8.40 eV has been studied by Van Brunt and Kieffer (1970). They find that the experimentally observed angular distributions can be explained most simply in terms of a transition to a single $^2\Pi_u$ repulsive state of O_2^-. They arrive at this conclusion by comparing the experimentally observed angular distributions with the theory of O'Malley and Taylor (1968) and the symmetry arguments of Dunn (1962). The interpretation in terms of a single compound state is consistent with the evidence coming from the temperature dependence of dissociative attachment and also with the measurements of the O^- kinetic energy (Schulz, 1962b; Chantry and Schulz, 1967). Van Brunt and Kieffer (1970) do not exclude the possibility that another closely spaced resonance also contributes, but they find this alternative less attractive.

Burrow (1973) has recently measured the dissociative attachment cross section from the $a\,^1\Delta_g$ state of O_2, i.e., the reaction $e+O_2(a\,^1\Delta_g)\rightarrow O_2^-(^2\Pi_u)\rightarrow O^-(^2P)+O(^3P)$ and finds that this cross section is larger by a factor of about 3.5 ± 1 compared to the ground-state dissociative attachment cross section. This measurement, coupled with an analysis based on O'Malley's theory, enables Burrow to calculate that portion of the excitation cross section to the $a\,^1\Delta_g$ state which proceeds via the $^2\Pi_u$ state, i.e., the reaction $e+O_2(X\,^3\Sigma_g^-)\rightarrow O_2^-(^2\Pi_u)\rightarrow O_2(a\,^1\Delta_g)+e$. The contribution from the decay of the compound state is found to be a large portion of the total excitation cross section at its maximum. The energy range over which this mechanism is important, together with experimental measurements of the $a\,^1\Delta_g$ excitation function, are shown in Fig. 74.

The most likely means of excitation to the $^1\Delta_g$ state from threshold to 5 eV and above 15 eV is provided by nonresonant exchange scattering. The cross section for this process has been calculated by Julienne and Krauss (1972) using the Ochkur–Rudge approximation to the exchange amplitude. The calculated cross section is somewhat smaller than the experimentally measured values.

Wong, Boness, and Schulz (1973) have recently observed vibrational excitation to the $v=1$, 2, 3, and 4 levels of the electronic ground state of O_2, in the energy range 4–15 eV, with a peak near 9 eV. For an interpretation of this process, Wong *et al.* invoke some of the O_2^- compound states which exist in this energy range, e.g., $^2\Sigma_u^-$, $^4\Sigma_u^-$, and $^2\Pi_u$ states and possibly others.

C. Core-Excited Resonances

The only information regarding core-excited resonances in O_2 comes from the transmission experiments of Sanche and Schulz (1972). Figure 75 shows the derivative of the transmitted current vs electron energy in the range 8–13 eV. The structures are labelled and are listed in Appendix XI. Because of the extreme complexity of the spectrum, especially in the energy range 8.5–12 eV, Sanche and Schulz were not able to identify the structures in detail.

The structures (1–1′) and (3–3′), spaced 220 meV apart probably have as a grandparent the $O_2^+(X\,^2\Pi_g)$ state, which has a spacing of 232 meV. These two resonances thus consist of two electrons in $(3s\sigma_g)$ Rydberg orbitals, attached to the $X(^2\Pi_g)$ core. The "binding" of the two electrons, i.e., the energy difference between the lowest resonance (8.04 eV) and the $O_2^+(X\,^2\Pi_g)$ state, is 4.02 eV, a number similar to that found in other molecules (see Table X).

Structures 2 and 4 lie 40 ± 5 meV above structures (1–1′) and (3–3′), respectively. They could reflect spin–orbit splitting of the $^2\Pi_g$ state of O_2^- into a $^2\Pi_{3/2}$ configuration for resonances (1–1′) and (3–3′) and a $^2\Pi_{1/2}$ configuration for resonances 2 and 4. The observed doublet spacing is larger than the value of 24 meV for the splitting of the ground state of O_2^+.

1. Band "a"

At higher energies a well-developed progression of ten resonances appears in the spectrum starting at 11.81 ± 0.05 eV. Sanche and Schulz (1972) compare the vibrational spacings and Franck–Condon probabilities of band "a" with those of the $a\,^4\Pi_u$ grandparent state of O_2^+. They find that there is remarkable agreement, whereas no such correspondence can be found when the experimental data are compared with other states of O_2^+, i.e., the $X\,^2\Pi_g$, $A\,^2\Pi_u$, $b\,^4\Sigma_g^-$, and $B\,^2\Sigma_g^-$ of O_2^+.

This suggests that band "a" results from vibrational structure of a $^4\Pi_u$ Rydberg negative ion, formed by the addition of two Rydberg electrons of the $3s\sigma_g$ orbital symmetry to a O_2^+ core in the $a\,^4\Pi_u$ valence excited state. The likely parents of the O_2^- state could be

formed by the addition of a single $3s\sigma_g$ electron to the $O_2^+(a\,^4\Pi_u)$ core, thus forming $^3\Pi$ and $^5\Pi$ Rydberg states. These states lie at 12.50 eV ($^3\Pi$) and 12.24 eV ($^5\Pi$), respectively, and the observed progression lies about 0.6 eV below the $^5\Pi$ state. Since a value of 0.6 eV is a reasonable value for the electron affinity, Sanche and Schulz (1972) consider this a further confirmation that the $^{3,5}\Pi$ states of O_2 are the parents of band "a". Again, the "binding" of the two $3s\sigma_g$ electrons to the grandparent is about 4.4 eV.

The quantum number of each vibrational level listed in Appendix XI is determined by fitting the Franck–Condon probabilities of the O_2 ion to those of the O_2^+ ion. The zeroth level of the O_2^- progression cannot be observed because its Franck–Condon probability is small.

2. Band "b"

Another band of O_2^- states (band "b") consisting of a progression of four vibrational members has been observed above ionization (Sanche and Schulz, 1972) and is listed in Appendix XI. In this case the vibrational spacings are close to those of the $b\,^2\Sigma^-$ state of O_2^+. The $^3\Sigma_u^-$ state which lies 0.210 eV above the zeroth level of band "b" and constitutes the lowest Rydberg excited state belonging to the $b\,^4\Sigma_g^-$ state of the positive ion system is the suggested parent for this progression.

VII. CONCLUSIONS

In this section we summarize some of the features discussed in the text, not by molecular species, but by the process involved.

A. Shape Resonances

All molecules discussed in this review exhibit shape resonances associated with the ground electronic state. These can be understood by referring to Table VIII. Listed are the molecular orbital configurations of the ground state of the respective molecule; the designation of the ground state; the lowest vacant orbital into which the electron attaches to form the shape resonance; the designation of the compound state; and the dominant electron partial wave responsible for forming the compound state.

The angular distribution measurements and the widths of compound states can be understood in terms of the partial wave which is dominant. In homonuclear diatomic molecules, having a center of symmetry, the allowed values of the angular momentum in the partial wave are either all even or all odd. Therefore it is unlikely that higher allowed partial waves, beyond those indicated, provide a significant contribution. In heteronuclear diatomic molecules, where there is no center of symmetry, one has to consider mixtures of partial waves. The dominant mixtures are indicated in Table VIII. For those molecules for which the lifetime of the compound state is short compared to the rotation time (all listed molecules except O_2), the angular distribution measurements show the behavior characteristic of the partial waves indicated. In heteronuclear molecules, the admixture of the two components must be adjusted properly in order to obtain agreement with the experiments, as has been done by Read (1968) for CO. Read (1968) has shown that "pure" partial waves, i.e., $p\sigma$, $p\pi$, $d\sigma$, $d\pi$, and $d\delta$ exhibit the characteristic shapes for p waves and d waves, in the sense that a minimum exists at 90° for the $p\sigma$ and $p\pi$ waves and a maximum exists at 90° for the $d\sigma$, $d\pi$, and $d\delta$ waves. However, the detailed shape is somewhat different from that of p and d waves: the $p\sigma$ and $p\pi$ waves do not lead to zero cross sections at 90°, and neither do the $d\sigma$, $d\pi$, and $d\delta$ waves show a zero near 60°.

When the lifetime of the compound state is comparable to or long compared to the rotational time, then the angular distribution becomes nearly isotropic, as is the case in O_2, and little information can be gained from angular distribution measurements, beyond the lifetime considerations.

The mixture of partial waves which one has to consider in the case of CO and NO contains p-wave components in the partial wave. Because the p-wave component leads to a much lower barrier than a d wave, the decay via the p-wave barrier is favored over escape via the d-wave barrier. Although d waves may be more important in the interior of the molecule, the p wave may dominate the decay and thus be responsible for the angular distribution and lifetime. These considerations explain the shorter lifetimes of the compound states in CO and NO, compared to N_2 and O_2.

B. Core-Excited Shape Resonances

Singly or doubly excited states of molecules also can bind an extra electron by the centrifugal barrier, thus forming shape resonances. The most extensive study has been made for the case of N_2, in which the singly excited valence states, $A\,^3\Sigma_u^+$ and $B\,^3\Pi_g$, have associated shape resonances. The progression of vibrational levels of these shape resonances are often long, exhibiting up to 18 vibrational states. These core-excited shape resonances have properties which are very similar to shape resonances associated with the ground state.

Core-excited resonances consisting of a doubly excited core plus an electron also have been postulated, for example in N_2 near 22-eV energy.

Although other molecules have not been studied in sufficient detail, it can be expected that core-excited shape resonances are the rule rather than the exception and that future energy level diagrams of negative molecular ions will show a fantastic number of compound states.

It should be noted that repulsive states of molecules also can have associated shape resonances, as is the case in H_2.

C. Binding of Rydberg Resonances

A recurrent theme throughout this review is the observation that most core-excited Feshbach resonances are associated with Rydberg excited states of the molecule. These states can be considered as being formed by the attachment of two electrons in Rydberg orbitals to the positive ion core, which we call the "grandparent." The *lowest configuration* that is possible contains the positive ion core plus two $3s\sigma_g$ electrons. Table X lists the "binding energy" of these two electrons to the various positive ion cores of H_2, NO, CO, N_2, and O_2. The "binding energy" is determined by taking the difference between the energy of a particular state of the positive ion and the experimentally observed energy of a particular resonance which we associate with this positive ion core. The association between the positive ion core and the resonance comes from a comparison of the vibrational spacings and Franck–Condon factors. The data used for constructing Table X are taken from Sanche and Schulz (1972) and are fully discussed in the body of this review.

It is obvious from Table X that all the molecules listed have binding energies for the two $3s\sigma_g$ electrons of about 4 eV.

TABLE X. "Binding" energy of two $3s\sigma_g$ electrons to grandparents.

Molecule	Positive ion State	Positive ion Energy eV	Associated resonance Energy eV	"Binding" energy eV
H_2	$X\,^2\Sigma_g^+$	15.42	11.32	4.1
N_2	$X\,^2\Sigma_g^+$	15.51	11.48	4.03
	$A\,^2\Pi_u$	16.62	12.64	3.98
CO	$X\,^2\Sigma^+$	14.1	10.04	4.1
	$A\,^2\Pi$	16.6	13.95	•••
NO	$X\,^1\Sigma^+$	9.27	5.04	4.23
	$b\,^3\Pi$	16.56	12.36	4.20
	$A\,^1\Pi$	18.32	14.19	4.23
	$B\,^1\Pi$	21.72	17.51	4.21
O_2	$X\,^2\Pi_g$	12.06	8.04	4.02
	$a\,^4\Pi_u$	16.10	~11.69[a]	4.4
	$b\,^4\Sigma_g^-$	18.16	14.27[b]	3.9

[a] The level $v=0$ is not observed. The value given is an extrapolation.

[b] The assignment as $v=0$ is uncertain.

D. Thresholds of Inelastic Cross Sections

It is pointed out in Sec. *IIIB2* that the threshold behavior of inelastic cross sections is often dominated by nearby resonances. Both core-excited shape resonances (which lie above the electronic state) and Feshbach resonances (which lie below their parent) are important. Sometimes, the influence of these two types of resonances can be distinguished and energy ranges can be specified which are dominated by the influence of one or the other resonance. This is the case for the 2^3S excitation function of helium. In other cases, the threshold is dominated only by a nearby shape resonance ($E\,^3\Sigma_g^+$ state in N_2). In still other cases the threshold behavior is dominated by a Feshbach resonance lying below the respective excited state ($b\,^3\Sigma^+$ state in CO). The width of the Feshbach resonance appears to be a dominant factor.

ACKNOWLEDGMENTS

The author is indebted to many people and to many agencies who made possible his participation, over the past eighteen years, in the exciting developments partially described in this report. Support for this work came at various stages from the Westinghouse Research Laboratories (1954–1966), from the National Science Foundation, the Defense Atomic Support Agency, the Advanced Research Projects Agency, and the Army Research Office, Durham. To these agencies go the thanks of the author for providing the funds which enabled him and his colleagues to participate in the progress of this field. Needless to say, many other advances, not reported in this survey, resulted from the above-mentioned support.

The scientists from whom the author learned about atomic collision processes along the way include U. Fano, E. Gerjuoy, A. Herzenberg, A. V. Phelps, H. S. Taylor, and many others.

The author received comments, suggestions, and corrections from J. Comer, U. Fano, E. Ferguson, F. Linder, C. Kuyatt, C. Lineberger, P. D. Burrow, A. Herzenberg, A. V. Phelps, H. S. Taylor, and M. J. W. Boness and wishes to express his thanks to them for reading portions of the manuscript.

A portion of this review was written while the author enjoyed the hospitality of JILA and special thanks go to L. J. Kieffer for his interest in this review, for carefully reading the whole manuscript, and for suggesting many changes and corrections. Mrs. L. H. Volsky of JILA and Mrs. M. R. Harrison of Yale provided editorial assistance. Lastly, the author is greatly indebted to his wive, Rose, whoselflessly tended to the problems of life, the family, and the home, and gave up a great many things for the cause of science.

APPENDIX I

Comparison of the values obtained by different authors for the H_2^- states (eV).

Vibrational quantum number (H_2^-)	Transmission		Inelastic		Theory
	Sanche and Schulz (1972)	Kuyatt *et al.* (1966)	Comer and Read (1971a)	Weingartshofer *et al.* (1970)	Eliezer *et al.* (1967)[a]
		Bands "a" and "d"			
0	11.32	11.28	11.30	11.30	11.32
1	11.62	11.56	11.62	11.62	11.62
2	11.91	11.84	11.91	11.92	11.91
3	12.19	12.11	12.19	12.20	12.18
4	12.44	12.37	12.45	12.46	12.44
5	12.68	12.62	12.68	12.70	12.68
6		12.86	12.89	12.93	
7			13.10		
8			13.28		
		Band "b"			
2			11.27		
3			11.47		
4			11.63		
5			11.75		
6			11.85		
7			11.96		
		Bands "c" and "e"			
0	11.43	11.46	11.19[b]	11.50	11.46
1	11.74	11.72	11.50[b]	11.79	11.75
2	12.03	11.99	11.80[b]	12.08	12.03
3	12.32	12.27	12.07[b]	12.38	12.31
4	12.58	12.53			12.58
5	12.83	12.77			12.84
6	13.06	12.97			
		Band "f"			
		Golden (1971)			
0	13.66	13.62		13.63	
1	13.94	13.91		13.93	
2	14.20	14.19		14.20	
3	14.45	14.46		14.47	
4	14.69	14.72		14.70	
5	14.93	14.97		14.92	
6	15.18	15.21			
7	15.43	15.44			
8	15.65	15.66			
9	15.85	15.87			
10		16.07			
11		16.26			
		Band "g"			
	15.09				
	15.32				
	15.57				
	15.77				

[a] The theoretical values of Eliezer, Taylor, and Williams (1967) for band "a" were incremented by 0.25 eV for purposes of direct comparison with the experimental values of Sanche and Schulz (1972).

[b] From Joyez, Comer, and Read (1973).

APPENDIX II

Comparison of the values obtained by different authors for D_2^- states (eV).

Vibrational quantum number (D_2^-)	Transmission: Sanche and Schulz (1972)	Transmission: Kuyatt *et al.* (1966)	Inelastic: Comer and Read (1971a)
	Band "a"		
0	11.34	11.28	11.32
1	11.56	11.48	11.54
2	11.76	11.69	11.75
3	11.97	11.89	11.96
4	12.17	12.09	12.15
5	12.36	12.28	12.32
6	12.55	12.47	12.48
7	12.71	12.64	12.61
8	12.88	12.85	12.75
9	13.05		
10	13.22		

Vibrational quantum number (D_2^-)	Transmission: Sanche and Schulz (1972)	Transmission: Kuyatt *et al.* (1966)	Inelastic: Comer and Read (1971a)
	Band "c"		
1	11.67		11.65
2	11.89		11.87
3	12.09		12.07
4	12.26		12.23
	Sanche and Schulz (1972)		
	Band "f"	Band "g"	
0	13.66	15.05	
1	13.86	15.22	
2	14.06	15.39	
3	14.25	15.55	
4	14.43	15.71	
5	14.57		

APPENDIX III

Relative branching ratios for the decay of resonance series "a" in H_2 in terms of absolute cross sections (10^{-17} cm^2). The estimated error for the cross sections is in the order of 20%.

Exit channel	$v'=0$	$v'=1$	$v'=2$	$v'=3$	$v'=4$	$v'=5$
$B\,^1\Sigma_u^+$						
$v=2$	...	0.27	0.39	0.09	0.14	0.14
$v=1$	...	0.41	0.29	0.39	0.18	0.10
$v=0$	0.67	1.4	0.76	0.21	...	...
$b\,^3\Sigma_u^+$ [a]						
11.02 eV	...	0.11	0.10	0.042	0.020	0.008
10.76 eV	0.031	0.087	0.063	0.039	0.015	...
10.47 eV	0.042	0.063	0.048	0.024	0.007	...
10.17 eV	0.033	0.045	0.022	0.011	0.004	...
$b\,^3\Sigma_u^+$—Integrated values	2.0	2.5	2.5	1.4	1.0	
$X\,^1\Sigma_g^+$						
$v=5$	...	0.09	...	...	...	...
$v=4$	0.04	0.2	0.06	0.02	...	...
$v=3$	0.14	0.23	0.02	...	...	...
$v=2$						
$v=1$						
$v=0$	Pronounced interference structure					

[a] Within an energy band of $\Delta E \approx 60$ meV. From Weingartshofer *et al.* (1970).

APPENDIX IV

Energies of resonances in N_2 (11–15 eV).

Feature number	Transmission		Differential elastic and inelastic	Trapped electron	Total metastable	$E\,^3\Sigma_g^+$, $a''\,^1\Sigma_g^+$
Fig. 42	Sanche and Schulz (1972)	Heideman *et al.* (1966a)	Comer and Read (1971b)	Hall *et al.* (1970)	Lawton and Pichanick (1973)	Mazeau *et al.* (1972b)
"b"	11.47–11.51	11.48	11.48 } band "b"			
	11.74–11.78	11.75	11.75 } band "b"			
			12.02 } band "b"			
3	11.92	11.87	11.87	11.87		11.90
4–4′	12.18–12.27		12.205	12.25	12.12/12.25	12.14
5	12.64				12.59	12.54
6	12.87		Ehrhardt and Willmann ($^1\Sigma_g^+$)			12.78
					12.80	
"c"	13.00		13.0		13.03	12.98
	13.23				13.24	13.21
	13.50				13.52	13.44
	13.70					13.66
"d"	13.88					
	14.12		14.2			13.73
	14.36					13.86
	14.57					

All structures are Feshbach-type resonances except structures 3 and 4–4′, which are identified as shape resonances. Additional shape resonances have been observed by Mazeau *et al.* (1972b) at 12.40 eV in the $E\,^3\Sigma_g^+$ ($v=1$) channel and at 12.70 eV in the $E\,^3\Sigma_g^+$ ($v=0$) channel.

APPENDIX V

Energies and spacings of shape resonances connected with the $B\,^3\Pi_g$ state in N_2.

Transmission (Sanche and Schulz, 1972)		$B\,^3\Pi_g$ decay channel (Mazeau *et al.*, 1972c) Energy,[c] eV				
Energy,[a] eV	Spacing,[b] meV	$v=1$	$v=2$	$v=3$	$v=4$	$v=5$
		9.070				
9.23		9.220	9.155			
9.35	130	9.360	9.300			
9.49	125	9.500	9.445	9.400	9.365	
9.61	120	9.635	9.590	9.540	9.505	
9.73	120	9.760	9.730	9.675	9.645	9.600
9.85	115	9.885	9.860	9.810	9.780	9.730
9.96	115	10.005	9.980	9.940	9.910	9.860
10.07	110	10.120	10.095	9.065	10.035	9.990
10.18	105		10.200	9.175	10.155	10.115
10.29	105		10.305	9.285	10.265	10.230
10.39	100		10.405	9.395	10.375	10.345
10.49	100		10.505	9.495	10.480	10.450
10.58	90			9.595	10.575	10.555
10.67	90			9.695	10.670	10.655
10.76	90				10.765	10.745
10.85	85				10.850	10.835
10.93	85				10.930	10.920
11.02	85					11.000
						11.075
						11.150

APPENDIX V—*Continued*

Energies of shape resonances connected with the $A\ ^3\Sigma_u^+$ state.
$A\ ^3\Sigma_u^+$ decay channel (Mazeau *et al.*, 1972c)[d]

$v=2$	3	4	5	6
8.225 (15)				
8.315 (15)	8.307 (10)			
8.415 (10)	8.415 (10)	8.395 (10)		
8.515 (10)	8.522 (10)	8.503 (5)		
8.610 (10)	8.620 (10)	8.595 (5)	8.603 (5)	8.553 (5)
8.705 (10)	8.715 (5)	8.690 (15)	8.698 (5)	8.653 (10)
8.800 (10)	8.800 (10)	8.778 (15)	8.785 (5)	8.745 (10)
	8.880 (5)	8.878 (15)	8.870 (5)	8.837 (10)
	8.960 (10)	8.950 (15)	8.958 (5)	8.925 (5)
	9.040 (5)	9.030 (15)	9.040 (5)	9.008 (5)
	9.120 (10)	9.110 (15)	9.115 (5)	9.088 (5)
	9.195 (10)	9.178 (15)	9.183 (10)	9.168 (5)
	9.263 (10)	9.245 (15)	9.250 (5)	9.238 (5)
		9.312 (15)	9.315 (5)	9.300 (5)
		9.375 (15)	9.373 (5)	9.358 (5)
		9.428 (15)	9.430 (10)	9.418 (5)
		9.480 (10)	9.482 (10)	9.468 (5)
			9.538 (10)	9.515 (5)
			9.575 (10)	9.562 (10)

[a] Absolute error of the energy is ±0.05 eV. Relative error ±0.003 eV.
[b] The spacings are given to the nearest 5 meV.
[c] Error approximately ±10 meV (see Mazeau *et al.*, 1972c).
[d] In parentheses are given the probable errors, in meV.

APPENDIX VI

Energies of features in CO (10–15 eV).

Feature number	Transmission Sanche and Schulz (1972)	Differential Comer and Read (1971c)		Mazeau *et al.* (1972a)	Designation
		$v=1$	$v=2$	$b\ ^3\Sigma^+$, $v=0$[a]	
1–1′	9.98–10.04	10.02	10.02	10.04[b]	$^2\Sigma^+$ $v=0$
2–2′	10.24–10.29		10.28		$v=1$
3	10.42	10.38	10.46		
4–4′	10.65–10.72	10.80		10.7	$^2\Pi$
5	11.27			11.3	
6	12.17			12.2	
Band "a"	13.95				
	14.155				
	14.345				
	14.530				
	14.705				
	14.870				

[a] The threshold for the $b\ ^3\Sigma^+$ state is 10.39 eV.
[b] Determined from elastic scattering at 90°. The calibration is performed against the $(1s2s^2)^2S$ resonance in helium which the authors locate at 19.35±0.02 eV. [Sanche and Schulz find 19.34±0.02 eV.]

APPENDIX VII

Comparison of vibrational spacings and Franck–Condon probabilities observed for four bands of NO^- with appropriate values for $NO^+(X\,^1\Sigma^+)$ Sanche and Schulz (1972).

Vibrational spacings (meV)

	NO^- band[a]				$NO^+(X\,^1\Sigma^+)$	
Δv	"a"	"b"	"c"	"d"	Experimental	Theoretical
0–1	286	290	292	282	290	
1–2	286	290	288	284	287	
2–3	282	284	286	275	283	
3–4				275	278	
4–5				275	273	

Franck–Condon probabilities

	NO^- band[a]				$NO^+(X\,^1\Sigma^+)$	
v	"a"	"b"	"c"	"d"	Experimental	Theoretical
0	0.84	0.57	...	0.66	0.7	0.48
1	1	1	...	1	1	1
2	0.62	0.64	...	0.7	0.7	0.92
3	0.16	0.24	...	0.19	0.5	0.49

[a] "a", "b", "c", "d" represent designations of bands, which start at 5.04, 5.41, 5.46, and 6.44±0.05 eV, respectively.

APPENDIX VIII

Resonances in NO and their grandparents (12–18 eV) (Sanche and Schulz, 1972).

Resonance[a] NO^- energy eV	Grandparent NO^+ Designation	Energy eV	Binding eV
12.36(v=0)	$b\,^3\Pi$	16.56	4.20
12.57(v=1)			
12.73(s)			
12.94(s)			
14.19(v=0)	$A\,^1\Pi$	18.32	4.13
14.52(s)			
...	$C\,^3\Pi$	20.46	...
17.51(v=0)	$B\,^1\Pi$	21.72	4.21
17.94(s)			
5.04(v=0)	$X\,^1\Sigma^+$	9.27	4.23

[a] The features marked (v=0) are interpreted as the lowest states of core-excited Feshbach resonances. The features marked (s) are interpreted as core-excited shape resonances.

APPENDIX IX

Spacing of vibrational states of O_2^- $X(^2\Pi_g)$ in meV.[a]

Vibrational transition	Spence and Schulz (1970)	Linder and Schmidt (1971b)	Gray *et al.* (1971)
4⟶5	117	125	128
5⟶6	113	123	125
6⟶7	110	120	121
7⟶8	108	119	118
8–9	106	117	115
9–10		115	113
10–11		113	109
11–12		111	105
12–13		110	
13–14		107	
14–15		104	
15–16		103	
16–17		101	
17–18		99	
Extrapolated:			
0–1	135	135	140

[a] The state $v'=8$ is located near 569 meV (Linder and Schmidt, 1971b) and it is nearly coincident with the $v=3$ state of O_2 (Spence and Schulz, 1970).

APPENDIX X

Resonance energies of $O_2^-(X\,^2\Pi_g)$, widths of $O_2^-(X\,^2\Pi_g)$ and energy-integrated vibrational cross sections. [Energies and cross sections from Linder and Schmidt (1971b); widths from Koike and Watanabe (1973).]

v' [a]	4[h]	5	6	7	8	9	10	11	12	13	14	15	16	17	18
E [eV][b]	0.082	0.207	0.330	0.450	0.569	0.686	0.801	0.914	1.025	1.135	1.242	1.346	1.449	1.550	1.649
ΔE [meV][c]		125	123	120	119	117	115	113	111	110	107	104	103	101	99
Γ [meV]	0.004	0.036	0.12	0.26	0.46	0.74	1.1								
$\bar{Q}_v$ (in 10^{-20} cm$^2\times$eV)[e]															
$v=1$	x[g]	...	25	82	110	100	61	35	17	9	5	...	...	...	...
$v=2$	x	x	x	...	8.5	25	32	28	19	12	5.8	2.4	1.0	...	...
$v=3$	x	x	x	x	...	...	1.3	5.5	7.3	7.0	5.8	3.3	1.8	1.0	...
$v=4$	x	x	x	x	x	x	...	...	...	1.0	1.9	2.0	1.7	1.0	1.0

[a] v' is the vibrational quantum number of the $O_2^-(X\,^2\Pi_g)$ compound state.

[b] E is the energy of the compound state in the v' level (in eV).

[c] ΔE is the spacing of the vibrational levels (in meV) of the compound state.

[d] Γ is the width of the vibrational level v' (in meV).

[e] $\bar{Q}_v$ is the energy-integrated cross section to the final vibrational state, v, of $O_2(X\,^3\Sigma_g^-)$, which proceeds via $O_2^-(v')$ [in units of 10^{-20} cm$^2\times$eV].

[g] The symbol x indicates that the state is energetically inaccessible.

[h] Using a time-of-flight spectrometer, Land and Raith (1973) locate the center of the $v'=4$ state at 0.090 ± 0.004 eV, i.e., 8 meV above the value given in this table. The splitting of the $v'=4$ state of $O_2^-(X\,^2\Pi_g)$ is $\Delta E=22\pm2$ meV.

[f] v is the quantum number of vibrational states of $O_2(X\,^3\Sigma_g^-)$.

APPENDIX XI

Core-excited resonances in O_2 as observed in a transmission experiment (Sanche and Schulz, 1972).

1–1′	2	3–3′	4	5–5′
8.03–8.06	8.12	8.24–8.28	8.34	8.47–8.54
6–6′	7–7′	8–8′	9–9′	10–10′
8.71–8.78	8.90–8.98	9.08–9.11	9.16–9.23	9.36–9.44
11–11′	12	13–13′–13	14–14′	15–15′
9.53–9.61	9.73	9.86–9.92–9.98	10.43–10.48	10.55–10.61
16–16′	17–17′			
10.74–10.82	10.91–11.00			

Band "a"

11.81	11.93	12.05	12.17	12.29
$v=1$	$v=2$	$v=3$	$v=4$	$v=5$
12.40	12.51	12.62	12.73	12.84
$v=6$	$v=7$	$v=8$	$v=9$	$v-10$

Band "b"

14.27	14.43	14.58	14.72

*The writing of this review was supported by the National Bureau of Standards, Office of Standard Reference Data, as part of the National Standard Reference Data Program.

Abram, R. A., and A. Herzenberg, 1969, Chem. Phys. Lett. **3,** 187.
Badger, R. M., 1935, J. Chem. Phys. **3,** 710.
Bardsley, J. N., A. Herzenberg,, and F. Mandl, 1966a, Proc. Phys. Soc. Lond. **89,** 305.
Bardsley, J. N., A. Herzenberg, and F. Mandl, 1966b, Proc. Phys. Soc. Lond. **89,** 321.
Bardsley, J. N., and F. H. Read, 1968, Chem. Phys. Lett. **2,** 333.
Bardsley, J. N., and F. Mandl, 1968, Rep. Prog. Phys. **31,** 472.
Bates, D. R., and H. S. W. Massey, 1954, Philos. Mag. **45,** 111.
Berkowitz, J., W. A. Chupka, and D. Gutman, 1971, J. Chem. Phys. **55,** 2733.
Birtwistle, D. T., and A. Herzenberg, 1971, J. Phys. B **4,** 53.
Black, K. F., and N. F. Lane, 1971, in *Electronic and Atomic Collisions,* Abstracts of Papers of the VIIth International Conference on the Physics of Electronic and Atomic Collisions (North-Holland, Amsterdam), p. 332 (1971).
Blatt, J. M., and V. F. Weisskopf, 1952, *Theoretical Nuclear Physics* (Wiley, New York), p. 360 (1952).
Boness, M. J. W., and J. B. Hasted, 1966, Phys. Lett. **21,** 526.
Boness. M. J. W., J. B. Hasted, and I. W. Larkin, 1968, Proc. R. Soc. A**305.** 493.
Boness, M. J. W., and G. J. Schulz, 1970, Phys. Rev. A **2,** 2182.
Borst, W. L., and E. C. Zipf, 1971, Phys. Rev. A **3,** 979.
Breig, E. L., and C. C. Lin, 1965, J. Chem. Phys. **43,** 3839.
Brongersma, H. H., A. J. H. Boerboom, and J. Kistemaker, 1969, Physica (Utr.) **44,** 449.
Brongersma, H. H., and L. J. Oosterhoff, 1967, Chem. Phys. Lett. **1,** 169.
Browne, J. C., and A. Dalgarno, 1969, J. Phys. B **2,** 885.
Buchelnikova, I. S., 1959, Sov. Phys.-JETP **8,** 783.
Burke, P. G., and A. L. Sinfailam, 1970, J. Phys. B **3,** 641.
Burke, P. G., 1968, Adv. At. Mol. Phys. **4,** 173.
Burrow, P. D., 1973 (unpublished).
Burrow, P. D., and L. Sanche, 1972, Phys. Rev. Lett. **28,** 333.
Burrow, P. D., and G. J. Schulz, 1969, Phys. Rev. **187,** 97.
Celotta, R. J., R. A. Bennett, J. L. Hall, M. W. Siegel, and J. Levine, 1972, Phys. Rev. A **6,** 631.
Chang, E. S., and U. Fano, 1972, Phys. Rev. A **6,** 173.
Chanin, L. M., A. V. Phelps, and M. A. Biondi, 1962, Phys. Rev. **128,** 219.
Chantry, P. J., 1968, Phys. Rev. **172,** 125.
Chantry, P. J., 1971, J. Chem. Phys. **55,** 2746.
Chantry, P. J., and G. J. Schulz, 1967, Phys. Rev. **156,** 134.
Chen, J. C. Y., 1964a, J. Chem. Phys. **40,** 3507.
Chen, J. C. Y., 1964b, J. Chem. Phys. **40,** 3513.
Chen, J. C. Y., 1966a, J. Chem. Phys. **45,** 2710.
Chen, J. C. Y., 1966b, Phys. Rev. **146,** 61.
Chen, J. C. Y., 1969, Adv. Radiative Chem. **1,** 245.
Chen, J. C. Y., and J. L. Peacher, 1967, Phys. Rev. **163,** 103.
Chen, J. C. Y., and J. L. Peacher, 1968a, Phys. Rev. **167,** 30.
Chen, J. C. Y., and J. L. Peacher, 1968b, Phys. Rev. **168,** 56.
Christophorou, L. G., and R. N. Compton, G. J. Hurst, and P. W. Reinhardt, 1965, J. Chem. Phys. **43,** 4273.
Chutjian, A., D. G. Truhlar, W. Williams, and S. Trajmar, 1972, Phys. Rev. Lett. **29,** 1580.
Clampitt, R., and A. S. Newton, 1969, J. Chem. Phys. **50,** 1997.
Claydon, C. R., G. A. Segal, and H. S. Taylor, 1970, J. Chem. Phys. **52,** 3387.
Comer, J., and F. H. Read, 1971a, J. Phys. B **4,** 368.
Comer, J., and F. H. Read, 1971b, J. Phys. B **4,** 1055.
Comer, J., and F. H. Read, 1971c, J. Phys. B **4,** 1678.
Craggs, J. D., C. Thorburn, and B. A. Tozer, 1957, Proc. R. Soc. A **240,** 473.

Crawford, O. H., and A. Dalgarno, 1971, J. Phys. B **4,** 494.
Crompton, R. W., D. K. Gibson, and A. I. McIntosh, 1969, Aust. J. Phys. **22,** 715.
Crompton, R. W., D. K. Gibson, and A. G. Robertson, 1970, Phys. Rev. A **2,** 1386.
Crompton, R. W., and A. G. Robertson, 1971, Aust. J. Phys. **24,** 543.
Dalgarno, A., 1961, Ann. Geophys. **17,** 16.
Demkov, Yu. N., 1964, Zh. Eksp. Teor. Fiz. **46,** 1126. [Sov. Phys.-JETP **19,** 762.].
Demkov, Yu. N., 1965, Phys. Lett. **15,** 235.
Dowell, J. T., and T. E. Sharp, 1968, Phys. Rev. **167,** 124.
Dunn, G. H., 1962, Phys. Rev. Lett. **8,** 62.
Ehrhardt, H., 1969, *Physics of One- and Two-Electron Atoms*, edited by F. Bopp and H. Kleinpoppen (North-Holland, Amsterdam) (1969).
Ehrhardt, H., L. Langhans, F. Linder, and H. S. Taylor, 1968, Phys. Rev. **173,** 222.
Ehrhardt, H., and F. Linder, 1968, Phys. Rev. Lett. **21,** 419.
Ehrhardt, H., and A. Weingartshofer, 1969, Z. Phys. **226,** 33.
Ehrhardt, H., and K. Willmann, 1967, Z. Phys. **204,** 462.
Eliezer, I., H. S. Taylor, and J. K. Williams, 1967, J. Chem. Phys. **47,** 2165.
Englehardt, A. G., and A. V. Phelps, 1963, Phys. Rev. **131,** 2115.
Englehardt, A. G., A. V. Phelps, and C. G. Risk, 1964, Phys. Rev. **135,** A1566.
Faisal, F. H. M., and A. Temkin, 1972, Phys. Rev. Lett. **28,** 203.
Farragher, A. L., F. M. Page, and R. C. Wheeler, 1964, Discuss. Faraday Soc. **37,** 205.
Ferguson, E. E., 1968, Adv. Electron. Electron Phys. **24,** 1.
Ferguson, E. E., 1970, Acc. Chem. Res. **3,** 402.
Feshbach, H., 1958, Ann. Phys. (N.Y.) **5,** 357.
Feshbach, H., 1962, Ann. Phys. (N.Y.) **19,** 287.
Franck, J., and W. Grotrian, 1921, Z. Phys. **4,** 89.
Frommhold, L., 1968, Phys. Rev. **172,** 118. ; see also D. J. Kouri, W. N. Sams, and L. Frommhold, 1969, Phys. Rev. **184,** 252.
Gilmore, F. R., 1965, J. Quant. Spectrosc. Radiat. Transfer **5,** 369.
Golden, D. E., 1966, Phys. Rev. Lett. **17,** 847.
Golden, D. E., 1971, Phys. Rev. Lett. **27,** 227.
Golden, D. E., and H. W. Bandel, 1965, Phys. Rev. Lett. **14,** 1010.
Golden, D. E., H. W. Bandel, and J. A. Salerno, 1966, Phys. Rev. **146,** 40.
Golden, D. E., N. F. Lane, A. Temkin, and E. Gerjuoy, 1971, Rev. Mod. Phys. **43,** 642.
Golden, D. E., and H. Nakano, 1966, Phys. Rev. **144,** 71.
Gray, R. L., H. H. Haselton, D. Krause, Jr., and E. A. Soltysik, 1971, in *Electronic and Atomic Collisions*, Abstracts of Papers of the VIIth International Conference on the Physics of Electronic and Atomic Collisions (North-Holland Amsterdam), p. 347 (1971).
Haas, R., 1957, Z. Phys. **148,** 177.
Hake, R. D., and A. V. Phelps, 1967, Phys. Rev. **158,** 70.
Hall, R. I., M. Mazeau, J. Reinhardt, and C. Shermann, 1970, J. Phys. B **3,** 991.
Hara, S., 1969, J. Phys. Soc. Jap. **27,** 1592.
Hasted, J. B., and A. M. Awan, 1969, J. Phys. B **2,** 367.
Heideman, H. G. M., C. E. Kuyatt, and G. E. Chamberlain, 1966a, J. Chem. Phys. **44,** 355.
Heideman, H. G. M., C. E. Kuyatt. and G. E. Chamberlain, 1966b, J. Chem. Phys. **44,** 440.
Henderson, W. R., W. L. Fite, and R. T. Brackmann, 1969, Phys. Rev. **183,** 157.
Henry, R. J. W., 1970, Phys. Rev. A **2,** 1349.
Henry, R. J. W., and E. S. Chang, 1972, Phys. Rev. A **5,** 276.
Henry, R. J. W., and N. F. Lane, 1969, Phys. Rev. **183,** 221.
Herzberg, G., 1950, *The Spectra of Diatomic Molecules* (Van Nostrand, Princeton, N. J.) (1950)
Herzenberg, A., 1967, Phys. Rev. **160,** 80.
Herzenberg, A., 1968, J. Phys. B **1,** 548.
Herzenberg, A., 1969, J. Chem. Phys. **51,** 4992.
Herzenberg, A., 1970, *Methods and Problems of Theoretical Physics*, edited by J. E. Bowcock (North-Holland, Amsterdam), p. 131 (1970).
Herzenberg, A., 1971, Phys. Bull. Inst. Phys. Soc. Lond. **22,** 521.
Herzenberg, A., and F. Mandl, 1962, Proc. R. Soc. A **270,** 48.
Holzer, W., W. F. Murphy, H. J. Bernstein, and J. Rolfe, 1968, J. Mol. Spectrosc. **26,** 543.
Joyez, G., J. Comer, and F. H. Read, 1973, *Eighth International Conference on the Physics of Electronic and Atomic Collisions: Abstracts of Papers* (Belgrade, Yugoslavia). Paper to be published in J. Phys. B.
Julienne, P. S., and M. Krauss, 1972, J. Res. Natl. Bur. Stand. (U.S.) 76A, 661.
Kisker. E., 1972, Z. Phys. **257,** 51.
Koike, F., and T. Watanabe, 1973, J. Phys. Soc. Jap. 34 (1022).
Kolos, W., and L. Wolniewicz, 1965, J. Chem. Phys. **43,** 2429.
Kouri, D. J., 1968, J. Chem. Phys. **49,** 5205.
Krauss, M., and F. H. Mies, 1970, Phys. Rev. A **1,** 1592.
Krauss, M., and D. Neumann, 1972, Chem. Phys. Lett. **14,** 26.
Krauss, M., D. Neumann, A. C. Wahl, G. Das, and W. Zemke, 1973, Phys. Rev. A **7,** 69.
Kuyatt, C. E., S. R. Mielczarek, and J. A. Simpson, 1964, Phys. Rev. Lett. **12,** 293.
Kuyatt, C. E., J. A. Simpson, and S. R. Mielczarek, 1966, J. Chem. Phys. **44,** 437.
Lacmann, K., and D. R. Herschbach, 1970, Chem. Phys. Lett. **6,** 106.
Land, J. E., and W. Raith, 1973, Phys. Rev. Lett. **30,** 193.
Lane, N. F., and S. Geltman, 1967, Phys. Rev. **160,** 53.
Lawton, S. A., and F. M. J. Pichanick, 1973, Phys. Rev. A **7,** 1004.
Lassettre, E. N., A. Skerbele, M. A. Dillon, and K. J. Ross, 1968, J. Chem. Phys. **48,** 5066.
Linder, F., 1969, in *Sixth International Conference on the Physics of Electronic and Atomic Collisions: Abstracts of Papers* (North-Holland, Amsterdam), p. 141 (1969a).
Linder, F., and H. Schmidt, 1971a, Z. Naturforsch. **26a,** 1603.
Linder, F., and H. Schmidt, 1971b, Z. Naturforsch. **26a,** 1617.
Lineberger, W. C., and T. A. Patterson, 1972, Chem. Phys. Lett. **13,** 40.
Massey, H. S. W., and E. H. S. Burhop, 1969, *Electronic and Ionic Impact Phenomena* (Clarendon, Oxford), Vol. II. (1969).
Mauer, J. L., and G. J. Schulz, 1973, Phys. Rev. A **7,** 593.
Mazeau, J., F. Gresteau, G. Joyez, R. Reinhardt, and R. I. Hall, 1972a, J. Phys. B **5,** 1890.
Mazeau, J., R. I. Hall, G. Joyez, M. Landau, and J. Reinhardt, 1972b, private communication and J. Phys. B6, 873 (1973).
Mazeau, J., F. Gresteau, R. I. Hall, G. Joyez, and J. Reinhardt, 1972c, private communication and J. Phys. B6, 862 (1973).
McFarland, M., D. B. Dunkin, F. C. Fehsenfeld, A. L. Schmeltekopf, and E. E. Ferguson, 1972, J. Chem. Phys. **56,** 2358.
McGowan, J. W., and J. F. Williams, 1969, in *Sixth International Conference on the Physics of Electronic and Atomic Collisions*: Abstract of Papers (MIT, Cambridge, Mass.), p. 506 (1969).
Menendez, M. G., and H. K. Holt, 1966, J. Chem. Phys. **45,** 2743.
Michels, H. H., and F. E. Harris, 1971, in *Seventh International Conference on the Physics of Electronic and Atomic Collisions*: *Abstract of Papers*, (North-Holland, Amsterdam), Vol. II, p. 1170. (1971).

Moruzzi, J. L., J. W. Ekin, Jr., and A. V. Phelps, 1968, J. Chem. Phys. **48,** 3070.
Mulliken, R. S., 1957, in *The Threshold of Space*, edited by M. Zelikoff (Pergamon, New York) (1957).
Nalley, S. J., and R. N. Compton, 1971, Chem. Phys. Lett. **9,** 529.
Ogawa, M., and Y. Tanaka, 1962, Can. J. Phys. **40,** 1593.
Oksyuk, Yu. D., 1966, Sov. Phys.-JETP **22,** 873.
Olmsted, J., A. S. Newton, and K. Street, 1965, J. Chem. Phys. **42,** 2321.
O'Malley, T. F., 1967, Phys. Rev. **155,** 59.
O'Malley, T. F., and H. S. Taylor, 1968, Phys. Rev. **176,** 207.
Pack, J. L., and A. V. Phelps, 1966, J. Chem. Phys. **44,** 1870.
Paquet, C., P. Marchand, and P. Marmet, 1971, Can. J. Phys. **49,** 2013.
Pavlovic, Z., M. J. W. Boness, A. Herzenberg, and G. J. Schulz, 1972, Phys. Rev. A **6,** 676.
Pavlovic, Z., and M. J. W. Boness, 1973 (unpublished).
Phelps, A. V., 1968, Rev. Mod. Phys. **40,** 399.
Pichanick, F. M. J., S. A. Lawton, and R. D. Dubois, 1971, in *Electronic and Atomic Collisions*, Abstract of Papers of the VIIth International Conference on the Physics of Electronic and Atomic Collisions (North-Holland, Amsterdam), p. 339 (1971).
Raith, W., and J. E. Land, 1972, in *Third International Conference on Atomic Physics* (University of Colorado, Boulder)(1972). See Land and Raith, 1973.
Ramien, H., 1931, Z. Phys. **70,** 353.
Ramsauer, C., and R. Kollath, 1931, Ann. Phys. (Leipz.) **10,** 143.
Rapp, D. and D. D. Briglia, 1965, J. Chem. Phys. **43,** 1480.
Rapp, D., T. E. Sharp, and D. D. Briglia, 1965, Phys. Rev. Lett. **14,** 533.
Read, F. H., 1968, J. Phys. B **1,** 893.
Reinhardt, J., G. Joyez, J. Mazeau, and R. I. Hall, 1972, J. Phys. B **5,** 1884.
Rosen, B., 1970, *Spectroscopic Data Relative to Diatomic Molecules* (Pergamon, New York) (1970).
Sampson, D. H., and R. C. Mjolsness, 1965, Phys. Rev. **140,** A1466.
Sanche, L., Z. Pavlovic, M. J. W. Boness, and G. J. Schulz, 1971, in *Electronic and Atomic Collisions*, Abstracts of Papers of the VIIth International Conference on the Physics of Electronic and Atomic Collisions (North-Holland, Amsterdam), p. 350 (1971).
Sanche, L., and G. J. Schulz, 1971a, Phys. Rev. Lett. **26,** 943.
Sanche, L., and G. J. Schulz, 1971b, Phys. Rev. Lett. **27,** 1333.
Sanche, L., and G. J. Schulz, 1972, Phys. Rev. A **6,** 69. Note that the bands in the transmission spectrum of N_2 (their Fig. 10) are improperly labelled. The proper designation appears in the Erratum. Phys. Rev. A **6,** 2500 (1972)and also in Fig. 42 of the present text.
Schmeltekopf, A. L., F. C. Fehsenfeld, and E. E. Ferguson, 1967, Astrophys. J. **148,** L155.
Schulz, G. J., 1959a, Phys. Rev. **113,** 816.
Schulz, G. J., 1959b, Phys. Rev. **116,** 1141.
Schulz, G. J., 1962a, Phys. Rev. **125,** 229.
Schulz, G. J., 1962b, Phys. Rev. **128,** 178.
Schulz, G. J., 1964a, Phys. Rev. **135,** A988.
Schulz, G. J., 1964b, Phys. Rev. **136,** A650.
Schulz, G. J., and R. K. Asundi, 1967, Phys. Rev. **158,** 25.
Schulz, G. J., and J. T. Dowell, 1962, Phys. Rev. **128,** 174.
Schulz, G. J., and H. C. Koons, 1966, J. Chem. Phys. **44,** 1297.
Sharp, T. E., 1971, At. Data **2,** 119.
Siegel, M. W., R. J. Celotta, J. L. Hall, J. Levine, and R. A. Bennett, 1972, Phys. Rev. A **6,** 607.
Spence, D., and G. J. Schulz, 1970, Phys. Rev. A **2,** 1802.
Spence, D., and G. J. Schulz, 1971a, J. Chem. Phys. **54,** 5424.
Spence, D., and G. J. Schulz, 1971b, Phys. Rev. A **3,** 1968.
Spence, D., and G. J. Schulz, 1972, Phys. Rev. A **5,** 724.
Stamatovic, A., and G. J. Schulz, 1970, J. Chem. Phys. **53,** 2663.
Swanson, N., C. E. Kuyatt, J. W. Cooper, M. Krauss, 1972, Phys. Rev. Lett. **28,** 948.
Stockdale, J. A. D., R. N. Compton, G. S. Hurst, and P. W. Reinhardt, 1969, J. Chem. Phys. **50,** 2176.
Swanson, N., J. W. Cooper, and C. E. Kuyatt, 1971, in *Electronic and Atomic Collisions*, Abstracts of Papers of the VIIth International Conference on the Physics of Electronic and Atomic Collisions (North-Holland, Amsterdam), p. 344 (1971).
Takayanagi, K., and S. Geltman, 1965, Phys. Rev. **138,** A1003.
Takayanagi, K., and Y. Itikawa, 1970, Adv. At. Mol. Phys. **6,** 105.
Taylor, H. S., 1970, Adv. Chem. Phys. **18,** 91.
Taylor, H. S., G. V. Nazaroff, and A. Golebiewski, 1966, J. Chem. Phys. **45,** 2872.
Trajmar, S., D. C. Cartwright, and W. Williams, 1971, Phys. Rev. A **4,** 1482.
Trajmar, S., D. G. Truhlar, J. K. Rice, and A. Kuppermann, 1970. J. Chem. Phys. **52,** 4516.
Truhlar, D. G., S. Trajmar, and W. Williams, 1972, J. Chem. Phys. **57,** 3250.
Van Brunt, R. J., and L. J. Kieffer, 1970, Phys. Rev **A2,** 1899.
Weingartshofer, A., H. Ehrhardt, V. Hermann, and F. Linder, 1970, Phys. Rev. A **2,** 294.
Weiss, A. W., and M. Krauss, 1970, J. Chem. Phys. **52,** 4363.
Wong, S. F., M. J. W. Boness, and G. J. Schulz, 1973 (unpublished).

☆ U. S. GOVERNMENT PRINTING OFFICE : 1973—542-650/55

FORM NBS-114A (1-71)

U.S. DEPT. OF COMM. BIBLIOGRAPHIC DATA SHEET	1. PUBLICATION OR REPORT NO. NSRDS-NBS-50	2. Gov't Accession No.	3. Recipient's Accession No.

4. TITLE AND SUBTITLE

Resonances in Electron Impact on Atoms and Diatomic Molecules

5. Publication Date: **October 1973**

6. Performing Organization Code

7. AUTHOR(S): **George J. Schulz**

8. Performing Organization

9. PERFORMING ORGANIZATION NAME AND ADDRESS

NATIONAL BUREAU OF STANDARDS
DEPARTMENT OF COMMERCE
WASHINGTON, D.C. 20234

10. Project/Task/Work Unit No.

11. Contract/Grant No.

12. Sponsoring Organization Name and Address

Joint Institute for Laboratory Astrophysics, National Bureau of Standards, Boulder, Colorado 80302

13. Type of Report & Period Covered: **Final**

14. Sponsoring Agency Code

15. SUPPLEMENTARY NOTES

Reprinted from Reviews of Modern Physics, Vol. 45, 378-486, July 1973.

16. ABSTRACT (A 200-word or less factual summary of most significant information. If document includes a significant bibliography or literature survey, mention it here.)

Two reviews are presented on the energies, configuration and other properties of resonances in electron impact on atoms and diatomic molecules. Included are discussions of the experimental methods which are useful for studying resonances and of the results obtained by various investigations. Much of the information is presented in the form of tables and energy level diagrams.

17. KEY WORDS (Alphabetical order, separated by semicolons) **Atoms; compound states; cross-sections; diatomic molecules; electron impact; energy levels; resonances; temporary negative ions.**

18. AVAILABILITY STATEMENT

[X] UNLIMITED.

[ ] FOR OFFICIAL DISTRIBUTION. DO NOT RELEASE TO NTIS.

19. SECURITY CLASS (THIS REPORT): UNCLASSIFIED

21. NO. OF PAGES: 118

20. SECURITY CLASS (THIS PAGE): UNCLASSIFIED

22. Price: $1.35